Analysis, design, optimisation and testing of a gyroscopically stabilized platform

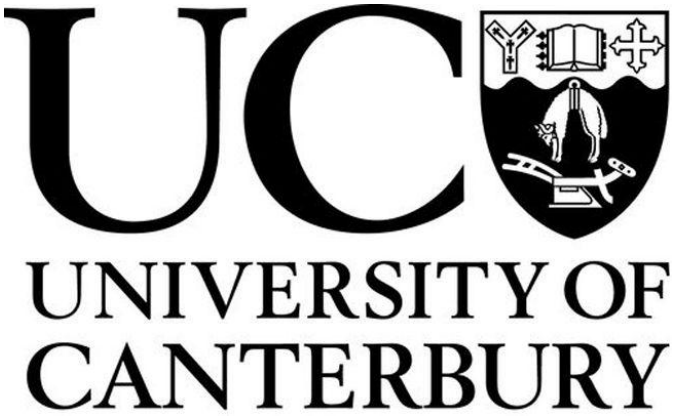

Doctorate of Philosophy Thesis

Mechanical Engineering

Ben Redwood

January 2014

“If I had asked people what they wanted,

they would have said faster horses.”

- Henry Ford

Acknowledgements

Firstly, I thank Dr Shayne Gooch for his help and support throughout this research project. The knowledge and guidance offered has been invaluable and I am truly grateful for his continued help and assistance throughout the entirety of this research.

I also thank John Matthews. Without support from people like John research projects such as this would not exist and for that I am forever indebted. His passion for this project and constant interest in progress were one of the main driving forces motivating me to succeed. I am deeply thankful for everything he has done for me.

I thank Dr Greg Townsend whose knowledge and passion for mathematics was invaluable. The two trips he made out to Christchurch to assist in the project were incredibly helpful and I am glad to now call him a friend.

I thank David Read from whom I learnt a great deal. His knowledge of manufacturing processes and eagerness to offer advice greatly increased my understanding of the complexities of a design and build project. I also wish to thank Garry Cotton for his patience and guidance in the workshop when manufacturing components myself.

Finally, I thank my fiancé Sjaan, whose support and understanding of the ups and downs of post graduate life gave me the drive to keep going. And to my parents for always giving me the opportunity to do whatever I was passionate about in life.

Abstract

Gyroscopic stabilization can be used to maintain an otherwise unstable body in an upright position. Devices equipped with gyroscopes can balance upon a small area or point without falling over when the gyroscopic stabilizing force is greater than a rotational force or moment from an out-of-balance load that causes the device to tip.

A new concept for a gyroscopically stabilized platform has been proposed in the form of a schematic diagram. The proposed system comprises of four interconnected gyroscopes that react to the tipping of an inherently unstable external body. The purpose of this research is to evolve a design for, and establish the feasibility of building the proposed stable platform using available materials and technology. If feasible, the gyroscopically stabilized platform will be made at the most practical and economic size.

Louis Brennan developed a 37 tonne monorail that was maintained in the upright position with two 3 tonne counter rotating gyroscopes. The Brennan monorail is analysed to better understand the behaviour of a similar coupled gyroscopic stabilization system. The reactions between the components that maintain the monorail in the stable position are studied and comparisons are made between the proposed stable platform and the Brennan system.

A mathematical analysis of the proposed system is presented. The equations of motion for the system are derived using the Lagrangian Formalism. The

characteristic equation of the system is then determined and from this a set of stability conditions imposed on the design of the physical parameters of the stable platform. The general solutions to the equations of motion are then derived. Expressions that model the behaviour of two of the variables that describe the motion of the stable platform are determined.

A systematic approach is adopted for establishing a new concept for the proposed system. Testing of the initial stable platform prototype (*Prototype A*) showed the system did not behave as intended. The platform was optimised further and this resulted in a second prototype, *Prototype B. Prototype B* exhibiting the desired oscillatory motion about the vertical of the platform.

Predictions made using the mathematical model are compared with empirical results. The mathematical model was found to be an accurate method for predicting the response of the stable platform.

Table of Contents

List of Figures

List of Tables

Nomenclature

A, B, C, D	represent simplifying substitutions used in the derivation of the systems stability conditions
a-b	the pivot axis of a gyroscope parallel to x'
$C(\omega_0)$	is the torque exerted by a gyroscope made to precess at a rate of ω_0 in the direction perpendicular to its axis of rotation when the structure deviates from the vertical
C_{ϕ_g}	a constant that we approximate as $4I\dot{\phi}_g$ (based upon θ_s being very small)
F	is the amplitude of the force associated with the driving of the motor that will oscillate the disc back and forth
F_{θ_s}	the non conservative generalised force associated with the variable θ_s
F_{ϕ_d}	the non conservative generalised force associated with the variable ϕ_d
F_{ϕ_g}	the non conservative generalised force associated with the variable ϕ_g
g	the acceleration due to gravity ($9.81ms^{-2}$)
h_d	is the height of O_d above O_s
h_s	the height of the external structure centre of mass above O_s
I	the moment of inertia of the gyroscopes in all directions
I_x, I_y, I_z	the moments of inertia of the gyroscope systems (gimbal frame, motor, and flywheel)

$I_x^d = I_y^d$	The moment of inertia of the disc about the x and y axes
I_z^d	The moment of inertia of the disc about the z axis
L_d	the Lagrangian associated with the disc
L_g	the Lagrangian associated with the gyroscopes
L_s	the Lagrangian associated with the external structure
L_{Total}	the Lagrangian associated with the overall system
M_d	the mass of the disc
$M_{g_1} = M_{g_2} = M_{g_3} = M_{g_4} = M_g$	the mass of the gyroscopes
m_k	the mass of the k^{th} particle in the rigid body
M_{max}	the maximum moment produced by the stable platform
M_s	the mass of the external structure
$M_{stability}$	the stability matrix of the system.
O_d	the origin and centre of mass of the disc
O_{g_m}	the origin and centre of mass of each of the gyroscopes
O_s	the origin of the external structure (also its pivot point)
r	the distance from the external centre of mass above the pivot
rad	the radial distance from O_d to O_g in the direction of y'
r_d	the radial distance the pivot point of the gyroscopes are from O_d
r_g	the distance from the gyroscopes pivot axis to the end of the contact arm

$\vec{r}_k$	is the location of the k[th] particle of the disc relative to O_d
T	the kinetic energy of the stable platform
T_d	the kinetic energy of the disc
T_g	the kinetic energy of the gyroscopes
T_s	the kinetic energy of the external structure point O_s
$v_{a-b}, v_{rad}, v_{\perp}$	The velocity $\vec{v}_{O_d}$ relative to the origin of the gyroscopes in the a-b,rad, $\perp$ axes
V_d	the potential energy of the disc
V_g	the potential energy of the gyroscopes
$\vec{v}_i^k$	the inertial space velocity of the k[th] particle in the rigid body relative to its body fixed axis with components $v_{i_x}^k, v_{i_y}^k, v_{i_z}^k$ and having mass m_k
$\vec{v}_{0_d}$	is the velocity of the origin of the body fixed axis attached to the disc relative to the inertial reference frame centred at the pivot point O_d written in terms of the body fixed axes associated with the disc
$\vec{v}_{O_{gm}(\text{relative to } O_d)}$	the velocity of the pivot point of a gyroscope O_{g_m} relative to the inertial frame centred at O_d written in terms of the body fixed axis associated with the m[th] gyroscope
$\vec{v}_{0_s}$	the velocity of the centre of mass of the external frame relative to the inertial reference frame at the pivot point O_s written in terms of the body fixed axis of the external structure
V_s	the potential energy of the external structure

v_x', v_y', v_z'	the components of $\vec{v}_{O_d}$ realtive to the body fixed frame of the gyroscopes
X, Y, Z	is the body fixed frame centred at the origin
X_1, Y_1, Z_1	the inertial reference frame
X', Y', Z'	the inertial frame parallel to X_1, Y_1, Z_1 but centred at origin O of the rigid body
γ	is the frequency the driving force, F, oscillates at
δ_m	to the angular position of each of the four gyroscopes (e.g. when $m = 1$, $\delta_m = 0$ or when $m = 3$, $\delta_m = \pi$) in the body fixed axis of the disc
$\delta\phi_d(t)$	represents small deviations in the variable $\phi_d(t)$
$\delta\theta_s(t)$	represents small deviations in the variable $\theta_s(t)$
$\theta_d(t), \psi_d(t), \phi_d(t)$	the Euler angles associated with location of the disc around the pivot point
θ_g	the gyroscopes pivot angle
$\dot{\theta}_g$	the rotation of the gyroscope/frame along the a-b axis through O_{g_m}
$\theta_m(t), \phi_m(t)$	the Euler angles associated with the location of the gyroscopes relative to their pivot point, $m = 1 \ldots 4$
$\theta_s(t)$	the angle of deviation of the external structure from the vertical
$\vec{\theta}_s$	the rotation of the external structure along $O_s - X_1$ axis
$\lambda_1, \lambda_2, \lambda_3$	the roots of the characteristic equation

μ	relates to the coefficient of friction the motor must overcome to initiate rotation of the disc (from bearings, gear backlash etc)
$\vec{\dot{\phi}}_{\mathrm{d}}$	the rotation of the disc along the $\mathrm{O_s} - \mathrm{Z_1}$ axis
ϕ_{g}	the gyroscopes rotation angle
$\dot{\phi}_{\mathrm{g}}$	the rotation of the gyroscope along $\mathrm{O_{g_m}} - \mathrm{Z}$
$\vec{\omega}$	the angular velocity of the body fixed axes X, Y, Z relative to the inertial axes X', Y', Z'
$\vec{\omega}_{\mathrm{d}}$	is the angular velocity of the body fixed axes associated with the disc relative to the inertial reference frame
$\vec{\omega}_{\mathrm{g_m}}$	the angular velocity of the body fixed axis of the gyroscope relative to the inertial frame entered at O_d written in terms of the body fixed axis associated with the m^{th} gyroscope
$\vec{\omega}_{\mathrm{s}}$	is the angular velocity of the body fixed axes associated with the external structure relative to the inertial reference frame
$\omega_{x_{\mathrm{d}}}, \omega_{y_{\mathrm{d}}}, \omega_{z_{\mathrm{d}}}$	the angular velocity components of the disc taken along X, Y, Z relative to the inertial reference frame
$\omega_x^{(\mathrm{m})}, \omega_y^{(\mathrm{m})}, \omega_z^{(\mathrm{m})}$	the angular velocities of the gyroscopes in their body fixed axes
$\perp$	the axis perpendicular to the disc in the direction of z'

1

Introduction

1.1 The purpose of this work

A new concept for a gyroscopically stabilized platform has been proposed in the form of a schematic diagram. The purpose of this thesis is to establish the feasibility of implementing this schematic concept using available technology. If feasible the gyroscopically stabilized platform will be made at the most practical and economic size.

The stable platform uses four interconnected gyroscopes that react to the tipping movement of an inherently unstable external body. In this system configuration, the gyroscopes act as actuators (commonly known as moment gyro's) and not as sensors, meaning they produce the torque that stabilizes the system. The proposed system has the gyroscopes arranged in such a way that it will stabilize an external body in the horizontal pitch and roll. Research has revealed that no such interconnected multi-gyroscopic system currently exists for stabilizing objects in both pitch and roll directions.

1.2 Historical background

The aim of this section is to discuss briefly the historical background of the project and give some insight into the nature of the task.

1.2.1 Basic gyroscope theory

The gyroscope was first constructed around 1810 (Bennett (1970)). A basic gyroscope comprises of a disc (or flywheel) attached to a shaft. The shaft is mounted in a gimbal frame which in ordinary applications allows the flywheel assembly the ability to move in any direction. When the flywheel rotates at a high speed it will take up a position from which a large force is required to move it from this orientation. Because the disc is typically mounted in a gimbal frame, any external torque is minimized resulting in the orientation of the wheel remaining fixed no matter how the platform that the system is attached to moves (Savet (1961)). Because of this, traditional applications for gyroscopes were devices used for measuring or maintaining orientation in planes and ships (Arnold, Maunder, & Roberson (1963)). More recently, gyroscopes are used in many advanced electronic devices for the same purpose of measuring orientation.

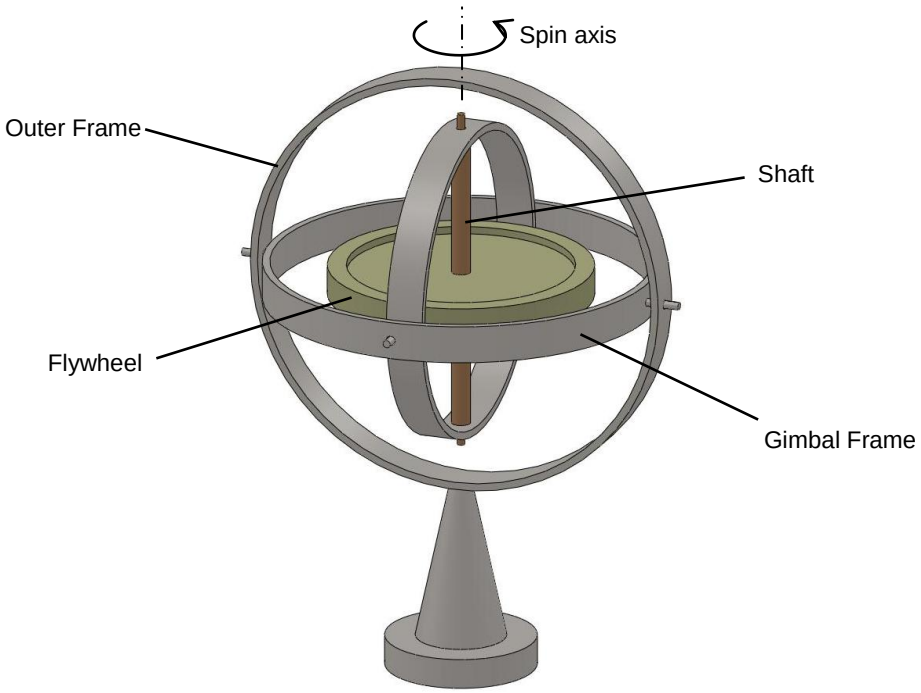

Figure 1.1 – Basic gyroscope arrangement

Figure 1.2 illustrates an example of a rotating gyroscope and the resulting direction of the output precession (reaction torques) as an external torque is applied to the system.

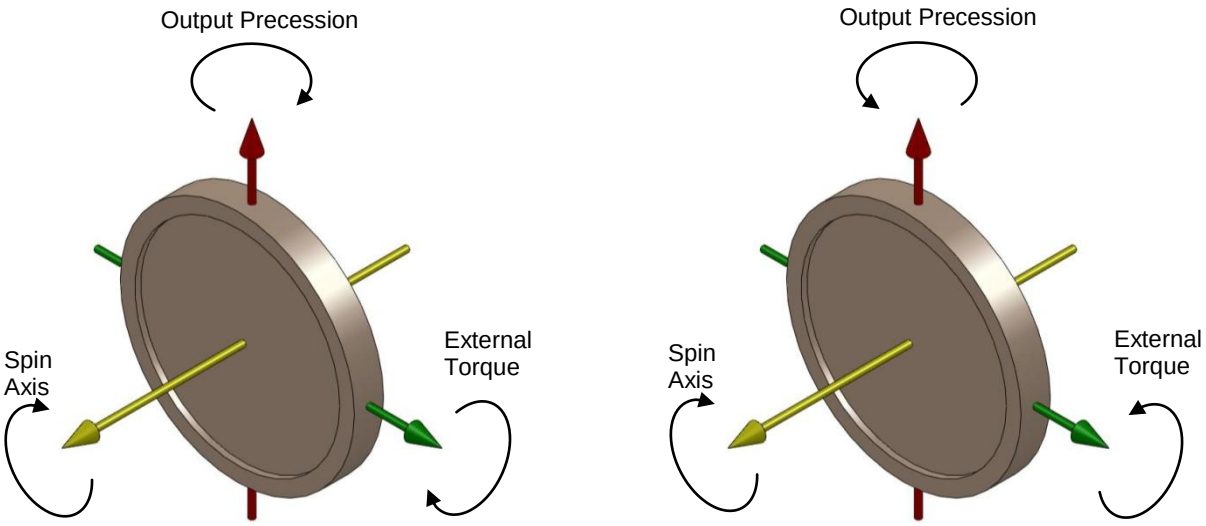

Figure 1.2 – Response of a simple gyroscope

Consider a simple gyroscope system like that shown in Figure 1.2. If the flywheel rotates at a constant angular velocity, $\dot{\phi}$, and posses an inertia, I, then the angular momentum of the system can be expressed as $I\dot{\phi}$ (represented by the line a-a_1).

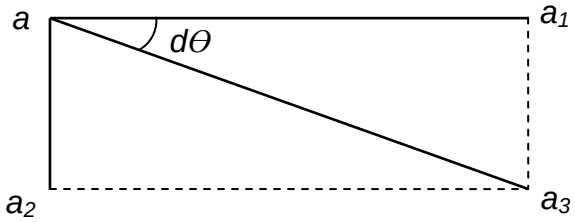

Figure 1.3 – Angular momentum of simple gyroscope system

If an external torque, T, is applied to the axle of the flywheel, the gyroscope will begin to precess at right angles to the axis of rotation of the flywheel and as a

consequence it generates angular momentum that is also perpendicular to the axis of rotation. This additional angular momentum is represented by the line *a-a2* in Figure 1.3. By completing the parallelogram, the resultant angular momentum of the system is the line *a-a3* in magnitude and direction (Davidson (1946)).

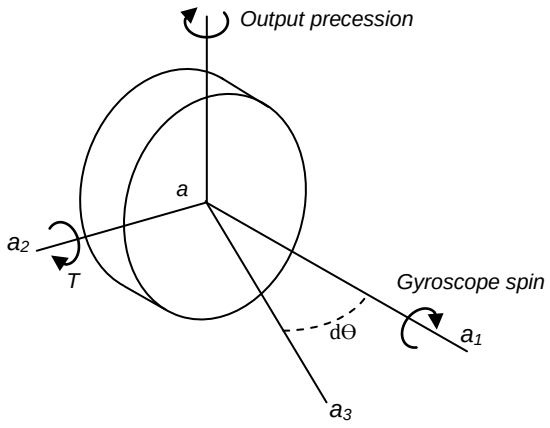

Figure 1.4 – Translation of Figure 1.3 into 3 dimensions

If the angle *a1-a3* is small (such that $\sin d\theta \approx d\theta$) and it takes dt for the wheel to move through this small angle then *a-a2* = *a1-a3* = *a-a3*.$d\theta$. If *a-a2* = Tdt, the added angular momentum in the system, and *a-a3* = $I\dot{\phi}$, the resultant angular momentum, then setting *a-a2*= *a-a3*.$d\theta$ yields

$$Tdt = I\dot{\phi}d\theta$$

$$T = I\dot{\phi}\frac{d\theta}{dt}$$

$$T = I\dot{\phi}\omega \qquad (1.1)$$

where ω is the angular velocity of the precession (which is equal to $\frac{d\theta}{dt}$).

Equation (1.1) is the fundamental equation that the motion of all gyroscopes is based upon. Using this equation it is possible to determine the magnitude of an external torque that is applied to a gyroscope if the inertia of the flywheel, the angular velocity of the flywheel and the precession rate are all known.

1.2.2 Gyroscopic stabilization

Gyroscopic stabilization is a popular and common stabilization method. Devices equipped with gyroscopes can balance upon a small area or point without falling over when the gyroscopic stabilizing force is greater than a rotational force tending to cause the device to tip.

Brennan (1905) was one of the first published examples of gyroscopic stabilization. Brennan's gyroscopic stabilization system used two coupled counter rotating gyroscopes to stabilize a body in one plane. Brennan's design proved very successful and set the foundations for the development of gyroscopic stabilization. Brennan's system is discussed in more detail in Chapter 2.

Similar patents to Brennan's design were then released by Schilovski (1909), Schilovski (1914) and Sperry (1908). Schilovski (1924) designed and developed a two-wheeled, narrow-body car with a 1,344 lb gyroscope located in the middle of the vehicle chassis that provided the stabilizing moment.

One of the most popular examples of a gyroscopically stabilized vehicle is the Gyro X car (Figure 1.5) developed by Alex Tremulis and Thomas O. Summers Jr. of Gyro Transport Systems Inc. This 840kg two wheel car was designed and built in 1963.

The gyroscope, located inside the car, consisted of a 22” diameter rotor weighing 11.3kg with a spindle speed of 4000-6000rpm (Joseph (1967)). While Tremulis and Summers proved successfully that it is possible to stabilize larger vehicles using a single rotating flywheel there were some critical issues with the design. The issues included the fact that the gyroscope took 3 minutes to get up to operating speed before the car could be driven. There were also some problems with the vehicle when it turned corners as it sometimes banked in the opposite direction.

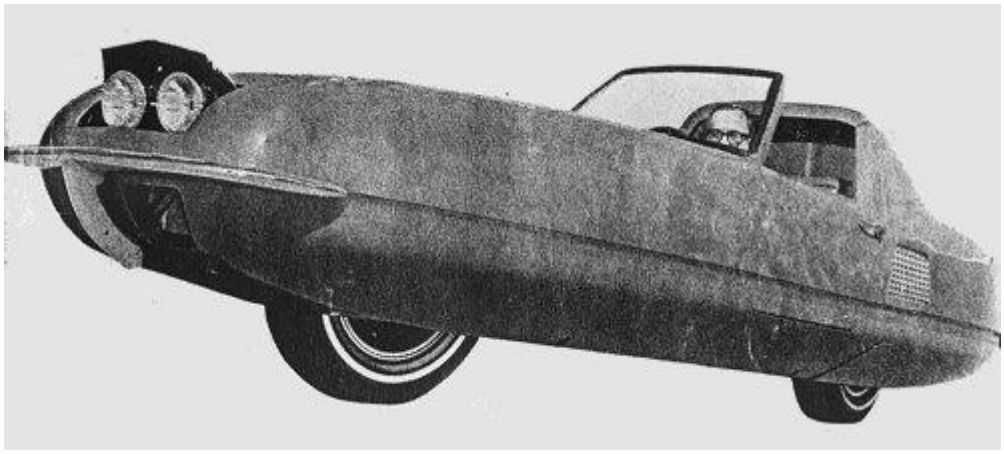

Figure 1.5 – Gyro X gyroscopically stabilized car from Joseph (1967)

1.2.3 Gyroscopic stabilization in literature

The following section looks at literature and publications applicable to this project. It should be noted that there is little relevant prior research on the subject of multi-gyroscope stabilization in the available literature.

This section of the literature review presents research into the mathematical analysis of gyroscopically stabilized systems and their research findings. An approach similar

to the research presented below was adopted in the mathematical analysis of gyroscopically stabilized system presented in this thesis.

Huseyin, Hagedorn, & Teschner (1983) studied the stability of linear conservative gyroscopic systems. Huseyin et al. (1983) investigated the conditions required for stability and instability of a gyroscopic system via an appropriate Lyapunov function. Kliem & Seyranian (1997) investigated the effects of stability, flutter (the self excitation of a gyroscope at certain speeds and orientations) and divergence (the tendency for mechanical gyroscopes to drift over extended periods of time) on gyroscopic systems. Kliem and Seyranian were able to produce graphs indicating when these phenomena occurred under specific stabilizations conditions with multiple gyroscopic stabilization systems each with varying degrees of freedom. Using the characteristic equation $\mathrm{M\ddot{z}} + 2\mathrm{G\dot{z}} + \mathrm{Kz} = 0$, Kliem and Seyrania were able to verify when stability, flutter and divergence occur for specific conditions based upon the roots of the gyroscopic systems characteristic equation.

Davyskib & Samsonov (1995) investigated the possibility of gyroscopic stabilization of spaceships in space. Due to the complex and varying geometry of the different objects in space, Davyskib focused on establishing a range of physical parameters in which gyroscope stabilization could be achieved. Davyskib analysis revealed that such geometric parameters do exist when external forces (friction, spring effects etc) are ignored and hypothesised on the effect these would have on the gyroscopic stabilization of rigid bodies in space.

Both Roitenberg (1960) and Matrosov (1960) reviewed both passive and active gyroscopic stabilizers in ships and planes. Though purely mathematical, both papers reviewed the equations of motion of systems based upon the general solution of the Kelvin theorem. By varying the parameters of the systems the resulting stability conditions were investigated by means of the roots of the characteristic equations.

This section of the literature review presents the use of Control Moment Gyroscopes (CMG's) to achieve stabilization. CMG's use a flywheel rotating at a constant speed, located in a mechanical gimbal, that can be manipulated to produce reaction torques in a desired direction (Brown & Peck (2008)). While a CMG was not considered for use in this research, the underlying theory and behaviour of the CMG's provided an excellent insight into how a gyroscopically stabilized system responds.

Most modern spacecraft require some form of active control to accomplish their mission objectives. This control may include regulating the altitude of the entire spacecraft, pointing some articulated payload, and vibration control (Bauer (2002)). Bauer studied the kinematics and dynamics of a novel double-gimballed CMG design used for these applications.

Karnopp (2002) implemented a single CMG into a motorcycle to obtain stability during loss of traction. Karnopp showed that a relatively simple control scheme can be used to achieve stability even on a very low traction surface as long as the vehicle is loaded symmetrically. He also investigated using the gyroscopes momentum to act with the drive train to supply or recover energy during braking and acceleration. Karnopp analysed the dynamics of such a system using Lagrange's

method and was able to determine the conditions that made the system stable. A control scheme was derived that would supply feedback control to the CMG to maintain stability of the motorcycle.

Lam (2011) further developed the work on bicycle stabilization with the use of CMG's. Lam's design used a single CMG located on a motorised gimbal. When the bicycle tipped, an integrated magnetic concentrator sensor detected the movement and commanded the gimbal motor to rotate such that a gyroscopic precessive torque was produced that restored the bicycle to an upright position.

This final section of the literature review presents research where a gyroscopically stabilized system has been designed, manufactured and tested. This section has particular relevance to this research as a similar approach to the verification of the performance of the proposed design was adopted.

Spry & Girard (2008) presented the case where the gyroscope acts as an actuator and not a sensor. In this regard the Spry and Girard study is similar to the dynamics investigated by Brennan and Schilovski. Using Lagrangian mechanics, Spry & Girar established a set the equations of motion for a pair of gyroscopes with opposite directions of rotation (and in turn opposite precessions). These results where then used to determine the conditions of stability for the system and analysed in Matlab. A scale model of the single gyroscope system was constructed to verify the theoretical results.

Beznos et al. (1998) produced a stabilisation unit that employed two coupled gyroscopes. Benzo's system consisted of a modified bicycle that had the steering tube mounted vertically with the front wheel lying directly below (contrary to typical bicycle designs). This made the bicycle inherently less stable. The stabilization system consisted of two interlinked, counter rotating gyroscopes located between the bicycle wheels. Benzos' bicycle measured the systems deviation from the horizontal through a series of sensors (measuring 3 degrees of freedom). A control system then precessed the gyroscopes restabilzing the bicycle.

A gyroscopic method of active ride control in marine vehicles was presented by Townsend et al. (2007). Two stabilization systems were proposed: an active system where feedback control is used to power a motor that precesses a rotating flywheel; and a passive system where the rotating flywheel was mounted on a set of bearings and left to precess by itself. The active system was selected as it produced the greater stabilizing moments. Townsend's results showed that the motion reduction achievable using the specified active system was in the range of 30 to 70%.

Ferreira, Tsai, Paredis, & Brown (2000) presented the findings of controlling a single wheel gyroscopically stabilized mobile robot named Gyrover invented at Carnegie Mellon University. A special extended Kalman Filter was used for sensor measurement and the experimental results were used to validate the theoretical model measuring the Gyrovers' deviation from the vertical as it travelled up and down a hallway. The dynamics of the Gyrover were described by a set of non-linear coupled differential equations and analysis showed that the dynamics could be linearized and simplified into two decoupled equations.

1.3 Previous work performed on platform

The aim of this section is to discuss past work that has been completed relating to the proposed gyroscopically stabilized system.

1.3.1 Townsend's feasibility analysis

Townsend (1983) was commissioned to investigate the behaviour of a proposed gyroscopic stabilization mechanism. The initial motivation for producing a gyroscopically stabilized platform at this time was for the stabilization of a mono-wheel vehicle.

Townsend focused on whether it was possible to achieve the desired reactions from the gyroscopes with the proposed arrangement and also investigated the impact of three sources of horizontal forces (wind pressure, centrifugal forces and deceleration) on the performance of the system.

Two initial conditions were placed upon Townsend's design:

i) The device must actively resist the applications of torques which are applied to it about two of the three axis associated with is rotational degrees of freedom.
ii) The device must be able to stabilize bodies which are normally unstable under the action of such torques.

Townsend never attempted to manufacture a working stabilizer. The reasons for this are discussed in more detail in Section 1.3.5.

Gooch (1998-1999) continued the work Townsend had begun. It was hoped that advances in flywheel technology would make the manufacture of the platform more feasible. Gooch's research focused on the use of off-the-shelf flywheels and the magnitudes of stabilizing moments that they were able to produce. Various applications for the gyroscopically stabilized platform were also investigated. The project was again abandoned due to technological constraints.

1.3.2 Townsend's purposed system layout

Townsend developed a series of schematic sketches indicating how the gyroscopically stabilized platform could potentially be arranged. A schematic sketch of the purposed system is shown in Figure 1.6. Further sketches of the proposed system configuration can be found in Appendix F.

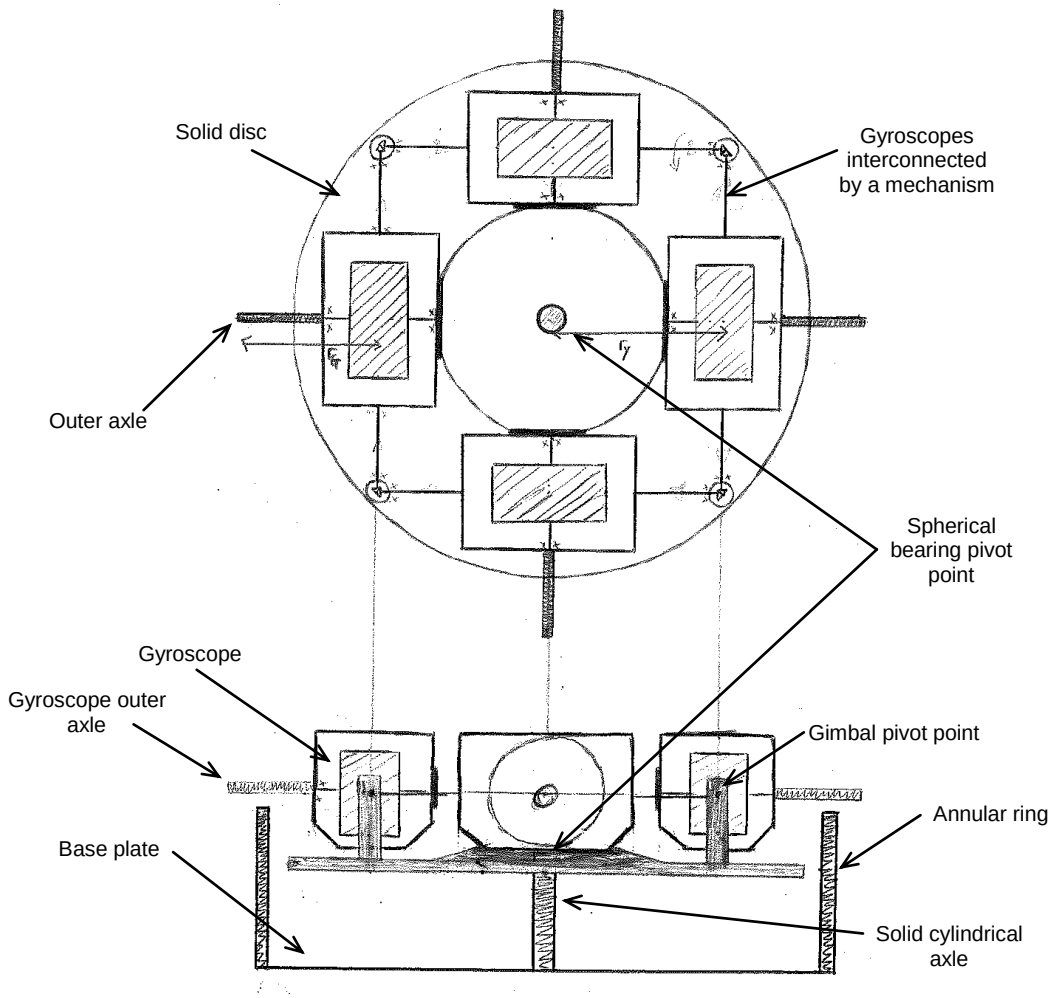

Figure 1.6 – Gyroscopically stabilized platform schematic sketch from Townsend (1983)

The proposed schematic system consisted of:

- A base plate attached to an annular cylinder

- A solid cylindrical axle attached to the base plate such that it was concentric with the annular cylinder. The axle must be lower than the height of the cylinder

- Attached to the axle by means of a spherical bearing is a solid disc whose centre of mass is below the pivot point of the spherical bearing.

- Mounted upon the disc are four self-contained gyroscopes positioned perpendicular to each other so that all four of their axes of rotation point towards the centre of the solid disc. The gyroscope systems are interconnected such that their angular displacement relative to the horizontal is always equal (bevel gears were a suggested solution). The four gyroscopes and the solid discs centre of mass are assumed to be below the spherical bearings pivot point.

- Attached to the gimbal frame of each of the gyroscopes, along the axis of rotation is an axle which extends out beyond the edge of the solid disc.

Townsend proposed that when the solid disc is rotating at a constant speed, with each of the gyroscopes also rotating at a speed equal to each other, under these conditions each of the gyroscopic systems will rotate downward about the gimbal pivot point until the gyroscope outer axle's contact with the edge of the annular cylinder. The four outer axles contact the annular ring applying an equal force such that no net torque is exerted upon the disc.

Assume an external torque is now applied to the system causing the base plate and annular cylinder to pivot upwards. Because the solid disc sits upon a spherical bearing, the solid disc/gyroscope assembly remains level. The annular cylinder presses up on the outer axles of the gyroscopes trying to rotate them upwards about

the gimbal pivot point. Due to the precession of the disc and the rotation of the gyroscopes, the system opposes the external torque tipping the base plate and annular cylinder maintaining the system level.

1.3.3 System constraints

Townsend imposed several conditions on the system to ensure a manufactured prototype functioned as expected. These were:

- That all four gyroscopes rotate at an equal speed
- That all four gyroscopes have equal moments of inertia
- All four gyroscopes have the same angular displacement from the horizontal when pivoted in their gimbal frames

1.3.4 Gooch's purposed system

Gooch (1998-1999) purposed a different variation on Townsend's four gyroscope system. The assembly incorporated three flywheel assemblies mounted in a rigid chassis as shown in the schematic diagram, Figure 1.7.

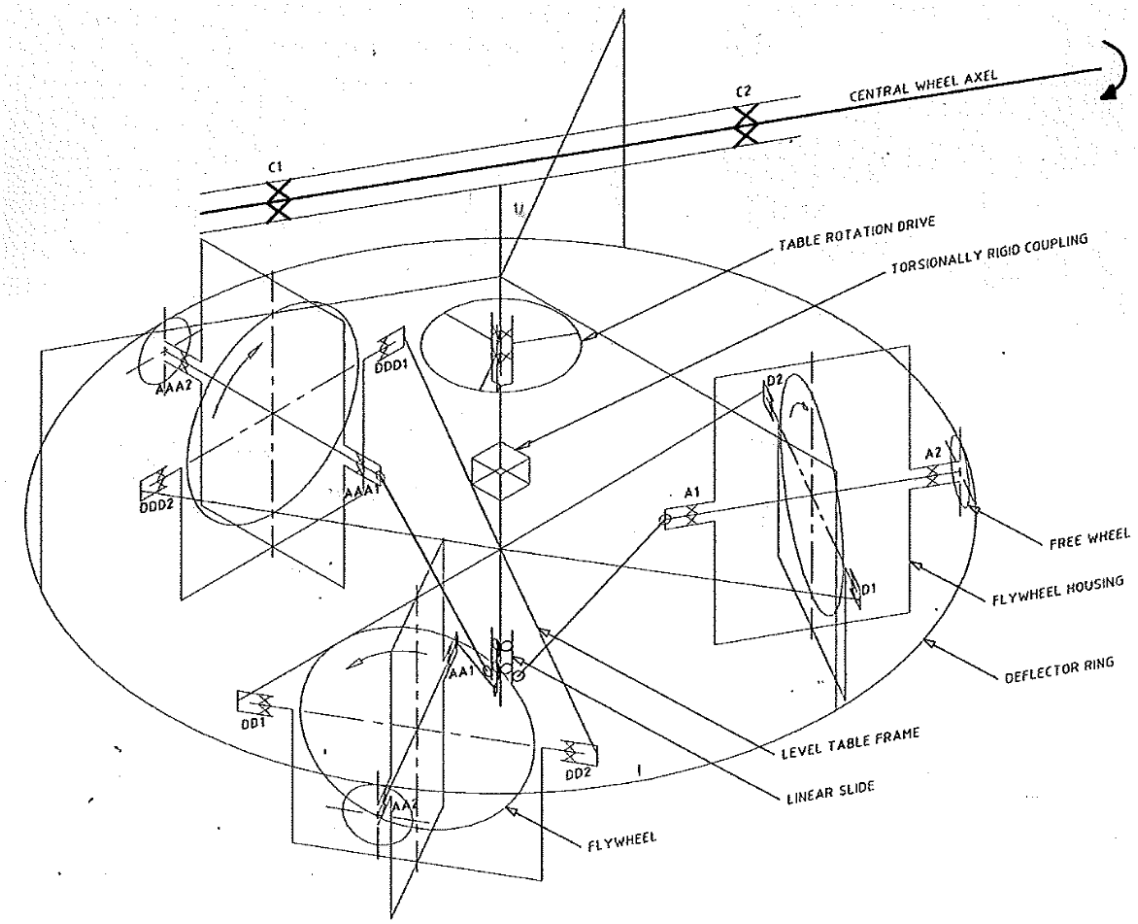

Figure 1.7 –Three gyroscope system schematic from Gooch (1998-1999)

Gooch's purposed system was also intended for the stabilization of a mono-wheel vehicle. The central wheel axle is fixed in the wheel hub (unstable external body). Forces are transmitted from the level table assembly to provide drive and control for accelerating/decelerating and cornering manoeuvres.

A support frame (not shown) provides the driving link between the level table and the wheel. The support frame incorporates a central stub shaft providing the central rotational axis of the stable platform. A gyroscope deflector ring then transmits the acceleration/deceleration and cornering forces from the wheel to the level table.

The deflector ring applies a force to the free wheel on the outboard end of one or more of the gyroscopes. This results in the table precessing about the central axis. In plan view the rotation will be in the anticlockwise direction. As the table precession rate accelerates up to speed or decelerates from constant speed to rest there is a slight angular displacement of the axis of rotation of the flywheel with respect to the horizontal. A table rotation drive is included to drive the precession of the level table and correct the level of the axis of rotation.

The three flywheel assemblies are connected using a central linkage. The central linkage incorporates a linear slide that runs on a central table axis. This linkage ensures that the axis of rotation of each flywheel is offset at the same angle with respect to the horizon. The central linkage also ensures that each flywheel does the same amount of work in transmitting the forces back to the central wheel axle.

1.3.5 Reason for not developing project further

While it was shown that theoretically the proposed gyroscopically stabilized platform would resist external unbalance forces, neither Townsend nor Gooch attempted to manufacture a working prototype. The main reason for this was technological restrictions relating to the type of electric motors that were available at the time. Most electric motors that could operate at the required speeds were of an impractical size and required large batteries. It was decided that the project would be placed on hold until advances in electric motor design and control allowed for a more elegant solution to the problem of powering the gyroscope flywheels.

1.4 The scope and structure of this thesis

The gyroscopically stabilized platform is a novel design that will allow inherently unstable bodies to remain in a stable position. The system can be adapted and applied to a vast range of applications. Research has identified no such system currently exists.

Hypothesis: *i) To determine the feasibility of implementing Townsend's proposed gyroscopically stabilized platform configuration using available materials, technology and manufacturing techniques.*

ii) To develop a mathematical model that accurate predicts the behaviour of the proposed system and use the findings of the mathematical analysis in the design of the gyroscopically stabilized platform to optimise the likelihood of stabilization being achieved.

The scope of this thesis is to mathematically derive a set of conditions under which the proposed gyroscopically stabilized platform configuration is stable and to develop a general solution that models the behaviour of the system. The mathematical results will then be used in the physical design of the gyroscopically stabilized platform to maximise the likelihood of the manufactured prototype remaining stable. Testing of the gyroscopically stabilized platform prototype will then be performed to validate the mathematical model.

Chapter 2 of this thesis investigates an early gyroscopically stabilized vehicle, the Brennan monorail. A free body diagram of the stabilizing system is produced and a step by step guide of the monorails operation is presented. The similarities between

the proposed system and the Brennan monorail help to establish fundamental theory regarding how gyroscopes react and behave when interconnected.

In Chapter 3 the Lagrangian equations of a general gyroscopically stabilized platform (referred to as the stable platform), based upon Townsend's proposed schematic, are derived by means of the Lagrangian formalism. The systems variables are established, a set of Euler angles defined, and from this the kinetic energy and potential energies of the system are derived. From these the total Lagrangian equation that describes the overall system is determined.

In Chapter 4 the equations of motion for the variables that govern the systems behaviour are formulated and a set of the stability conditions for the stable platform are established. From these stability conditions, an inequality is derived that describes the condition where the restoring moment produced by the stable platform overcomes the unbalance forces generated by the systems deviation from the vertical axis. This inequality is then used in the physical design of the system.

Chapter 5 uses the results from Chapter 4 to determine the general solutions to a homogeneous stable platform arrangement and a driven system.

Chapter 6 presents the design study relating to the manufacture of a working prototype. The system is considered as a number of sub-systems and the optimal design for each of these sub-systems is sought.

In Chapter 7 the design of the stable platform prototype is evolved further. The overall design of the system was developed as testing was taking place.

Chapter 8 reports the observations of the testing stages for the stable platform and looks to validate the mathematical model with the testing results.

Finally Chapter 9 presents on the key findings of the research and recommendations for future work on the project are made.

2

The Brennan Monorail

2.1 Introduction

Louis Brennan was a renowned mechanical engineer who lived from 1852 -1932. He is most notably known for his invention of the Brennan torpedo (a steerable torpedo that is guided from the shore by a set of counter rotating propellers). In 1903 he successfully patented the world's first gyroscopically stabilized monorail. At the 1910 Japan-British Exhibition Brennan showcased a full scale monorail upon which 50 people were transported around a circular track at 20mph. The Brennan monorail has significant relevance to this project due to the coupling of the gyroscopes used to maintain the monorail upright.

The objective of this chapter is to describe the stabilization mechanism used by Brennan to create a stable monorail.

While other multi gyroscope systems have since been manufactured, the simplicity and success of the Brennan monorail system make it an excellent reference point when considering gyroscopic stabilization of an unstable body.

2.2 Background information

The Brennan monorail is believed to be the first successfully patented example of the gyroscopic stabilization of a moving vehicle. Brennan's mechanism was novel

because if used interconnected gyroscopes that actively resisted the imbalance force created by the monorail as it tilted from the vertical axis. A diagram outlining the Brennan monorails components and how they are assembled together is shown in Figure 2.1.

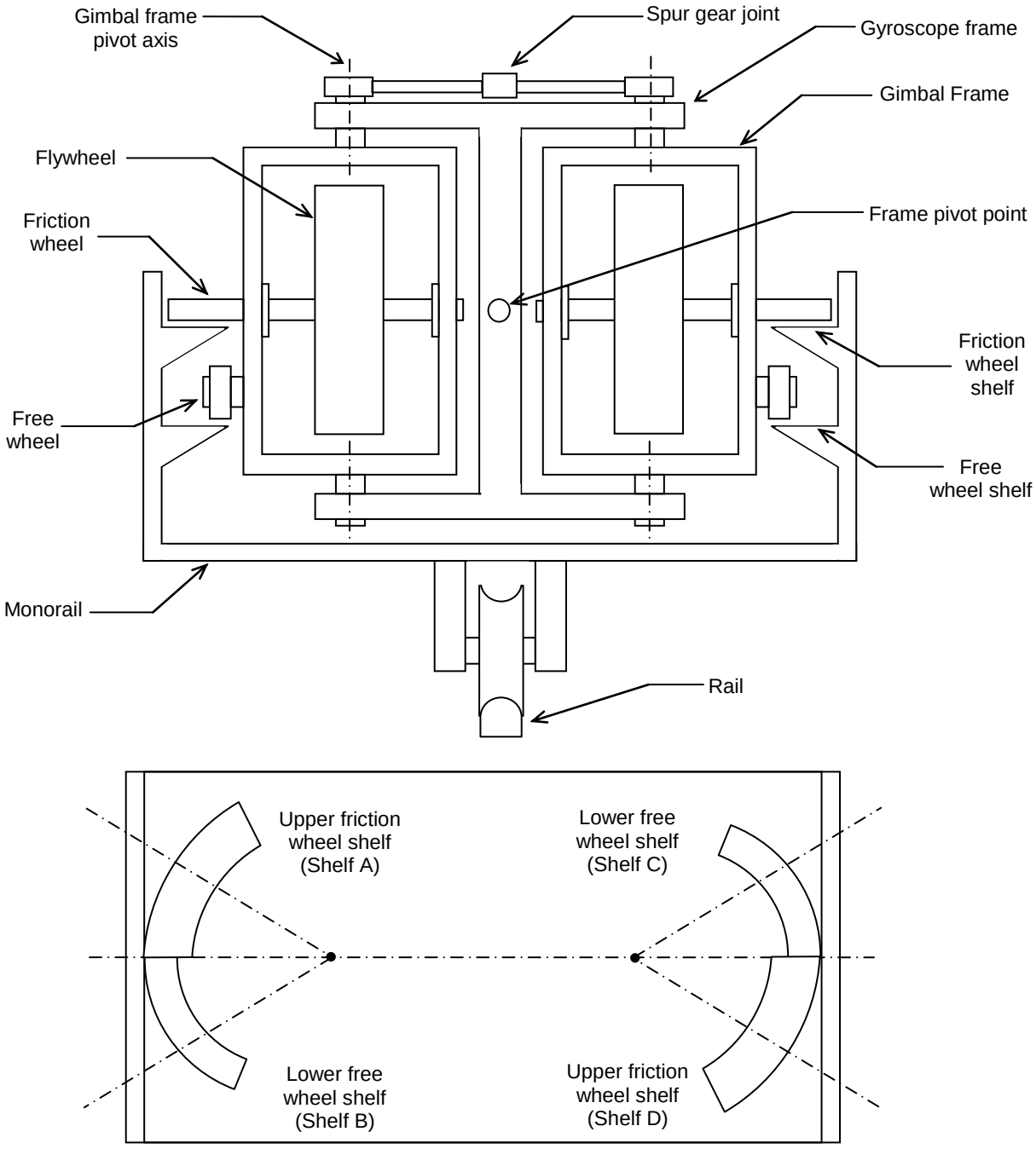

Figure 2.1 – Brennan monorail layout (top) and plan view of outer shelves (bottom)

The Brenna system incorporated two large flywheels counter rotating at a constant speed. The flywheels were mounted in two gimbal frames in a common gyroscope frame. When the monorail deviates from the vertical one of the friction wheels contacts the upper friction self. The friction wheels are fixed to the same shaft as the flywheels. This contact would cause the wheel to track along a curved upper shelf. This in turn would cause one of the gimbal frames that house a flywheel to pivot (or precess).

The two gimbal frames are connected together via a spur gear hence when an external load is applied to the free wheel both flywheels precess simultaneously in opposite directions. Due to the nature of gyroscopes this precession would cause a downwards restorative moment to be exerted on one of the outer shelves forcing the monorail back to level. The monorail would then tip over the equilibrium point and the process would be repeated on the opposite side of the mechanism resulting in the gyroscopes and monorail executing damped oscillatory motion (Franklin (1912)).

2.3 Advantages and disadvantages of the Brennan system

The main advantages of Brennan's monorail were rail lines could be installed at a lower cost (as only one rail was required for the monorail to run on) and production costs for producing the monorail were also greatly reduced. The monorail was also able to turn at much sharper angles compared to typical trains at the time. Figure 2.2 shows the monorail banking around a corner a conventional train would have struggled to negotiate.

The main issue with the design was that each monorail carriage needed its own rotating set of flywheels to keep stabilized rather than just the locomotive at the front. This meant there also had to be a motor running constantly to supply energy to the flywheels to keep them rotating to maintain the monorail in the desired upright position. This added a significant amount of weight to the overall monorail.

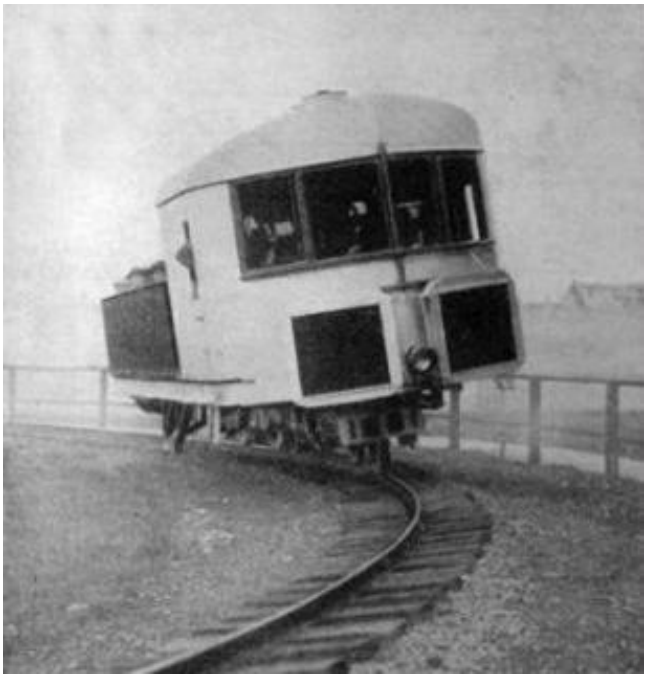

Figure 2.2 – The Brennan monorail (Photographer Unknown, 1927)

Although Brennan's system was shown to work very successfully, fears that the gyroscopes may fail prevented adoption of the system for widespread use (Eddy (1910)). To date no gyroscopically stabilized monorail has been developed past the prototype stage.

2.4 Relevance to this project

The Brennan Monorail has significant relevance to this project due to the coupling of the flywheels used in the stabilization system. Investigation of this system will give an understanding of the reactions that gyroscopes produce when moved in their gimbal frames and how this can be applied to stabilize an external unstable body in the proposed schematic design.

2.5 Brennan monorail parameters

In order to establish the size of the gyroscopically stabilized platform prototype it is useful to understand the parameters used for the design of the Brennan system. This information helps give a greater understanding of the magnitudes of the stabilizing moments that maintained the monorail in its upright position and potentially reveal relevant design solutions about how the proposed system could be assembled together.

The interactions between the components that make up the Brennan monorail are purely mechanical; similar to the connections and linkages that are suggested in the proposed schematic (Figure 1.6). Dickinson (1910) discussed several quantitative values that encompassed an early full sized car that Brennan had manufactured. The values are shown in Table 2.1 and Table 2.2.

Table 2.1– Brennan monorail parameters from Dickinson (1910)

Parameter	Value	Units
Monorail		
Length between buffers	12.2	m
Width	3.0	m
Height from rail level	4.0	m
Weight when empty	19958.1	kg
Maximum load	13607.8	kg
Total weight	33565.9	tons
Number of drive motors	2	
Total horsepower	100	hp
Maximum speed	56.3	kph
Maximum incline	1:13	
Distance between wheels	6.1	m
Wheel diameter	1.6	m

Table 2.2 – Brennan gyroscope parameters from Dickinson (1910)

Gyroscopes		
Number of flywheels	2	
Flywheel diameter	0.914	m
Flywheel weight	680.4	kg
Flywheel rotational speed	3000	rpm
	314.2	rads-1

During the course of this study no engineering drawings of the Brennan monorail were found. The only known dimensions relating to the arrangement of a Brennan stabilizing system were obtained from a drawing published by Moots (1911). Moots manufactured a working model Brennan monorail (Figure 2.3) in 1911 from Norway

pine as part of a thesis and successfully showcased the stabilization principles behind the system in a variety of tests.

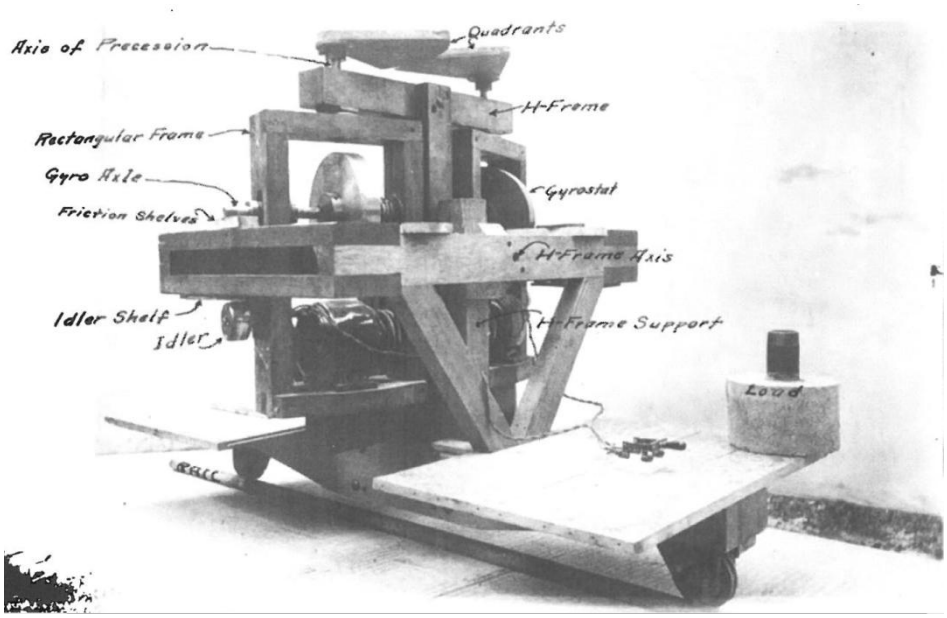

Figure 2.3 – Working model Brennan monorail from Moots (1911)

2.6 Free body analysis

This section presents the free body diagrams for the Brennan monorail system. Figure 2.4 shows a schematic representation of the Brennan system

While the proposed gyroscopically stabilized platform is more complex than the Brennan monorail, the interactions and reactions produced by the gyroscopes are similar. Understanding of the load paths and transmission of forces of Brennan's system will aid in the mechanical design of the proposed system.

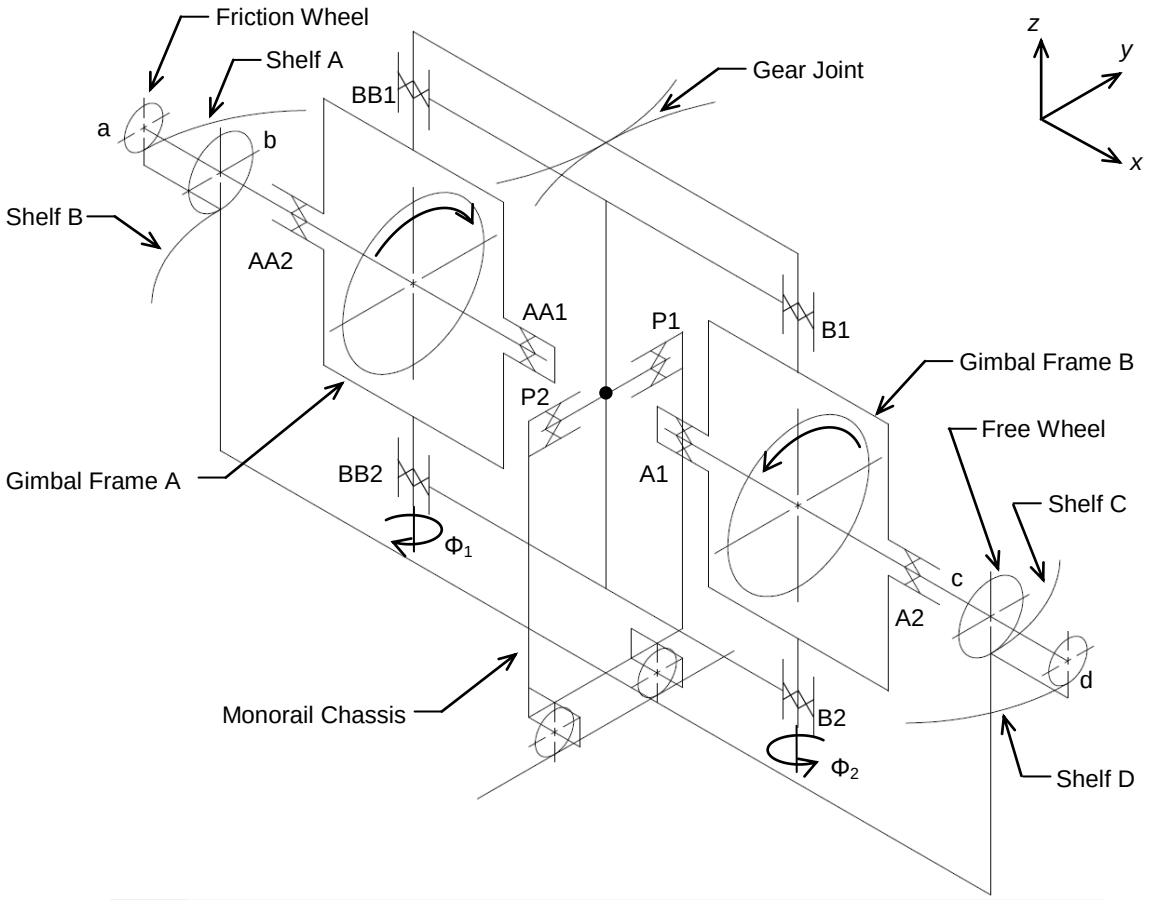

Figure 2.4 – Schematic of Brennan monorail

Consider the sequence of events after a disturbance of the system causes the monorail chassis to roll about the y axis. Figure 2.5 shows the reactions that occur for gimbal frame A when this tipping motion of the chassis occurs.

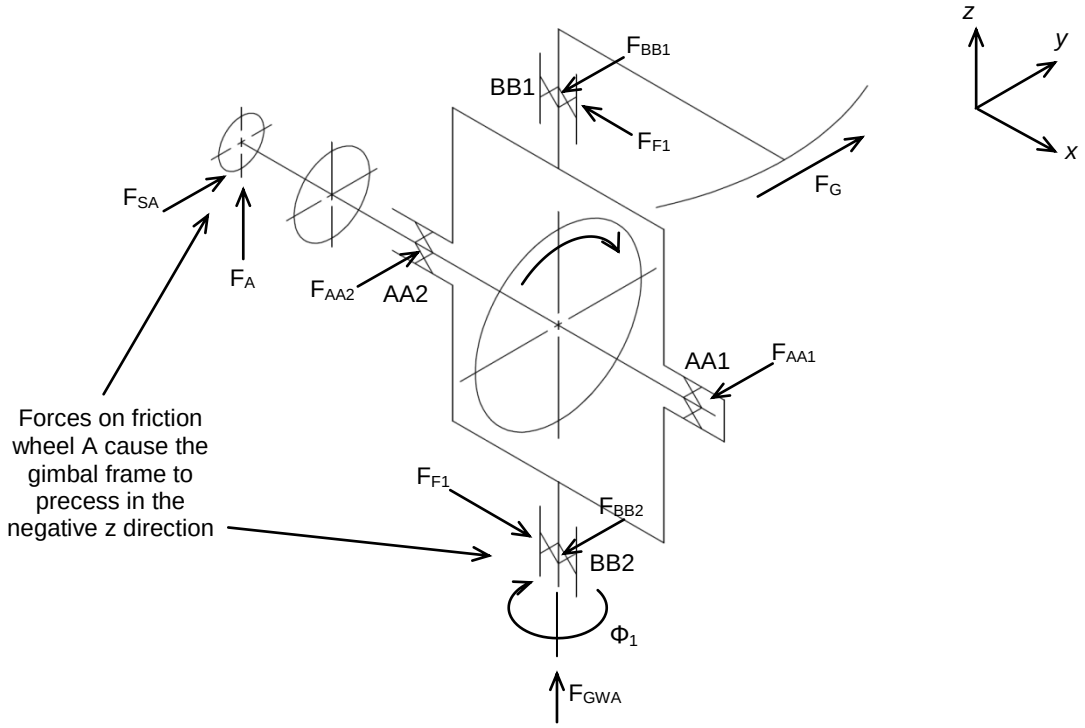

Figure 2.5 – Gimbal frame A of Brennan monorail

As the monorail tips the friction wheel ‘a’ comes in contact with shelf A. The friction force, F_{SA} will cause gimbal frame A to rotate about axis BB1-BB2 in the negative z direction (Φ_1).

The upward shelf reaction force, F_A will also cause gimbal frame A to rotate (precess) about BB1-BB2 in the negative z direction (Φ_1).

Figure 2.6 shows the reactions that occur on gimbal frame B.

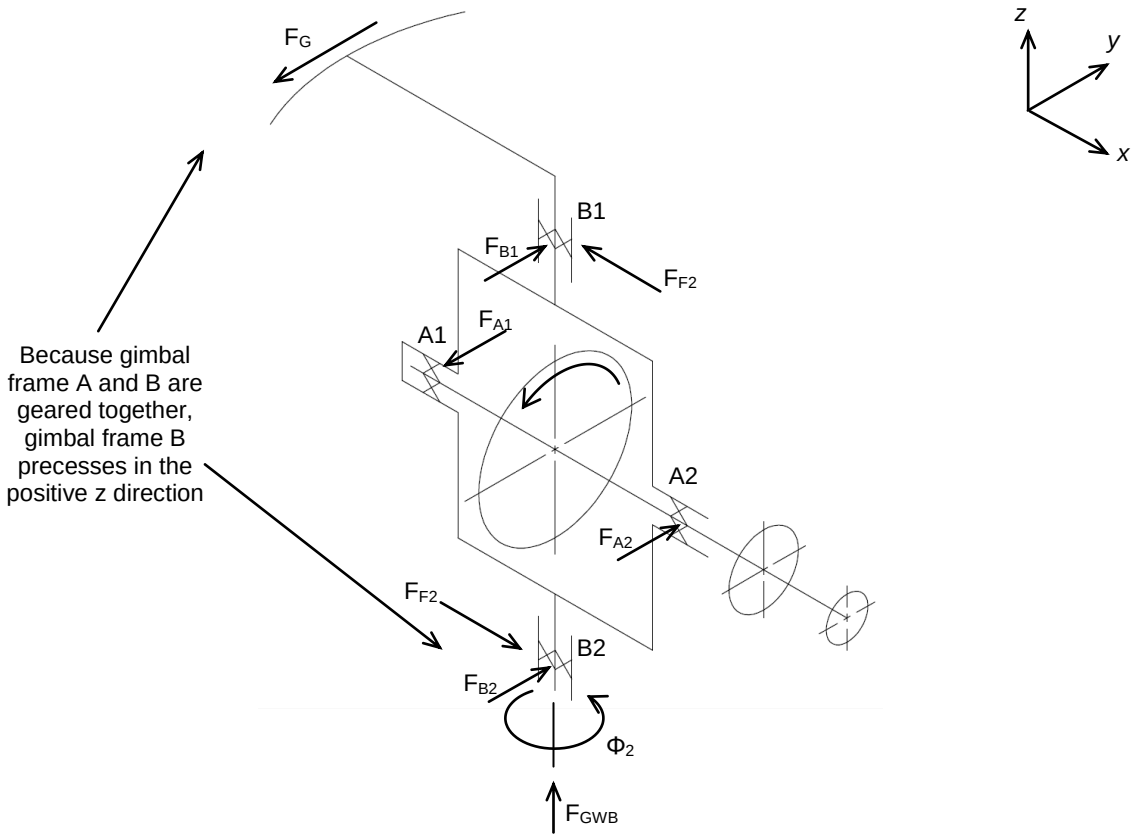

Figure 2.6 – Gimbal frame B

The gear force F_G causes gimbal frame B to precess about the axis B1-B2 in the positive z direction (Φ_2).

The forced precession of gimbal frame B results in a righting moment (forces F_{F2}) due to gyroscopic effects. The gimbal frame B gyroscope assists the gimbal frame A gyroscope in resisting the upward tipping force from shelf A (about axis P1-P2).

The forces on the frame of the Brennan monorail gimbal mounting frame (when wheel ‘a’ contacts shelf A) are shown in Figure 2.7.

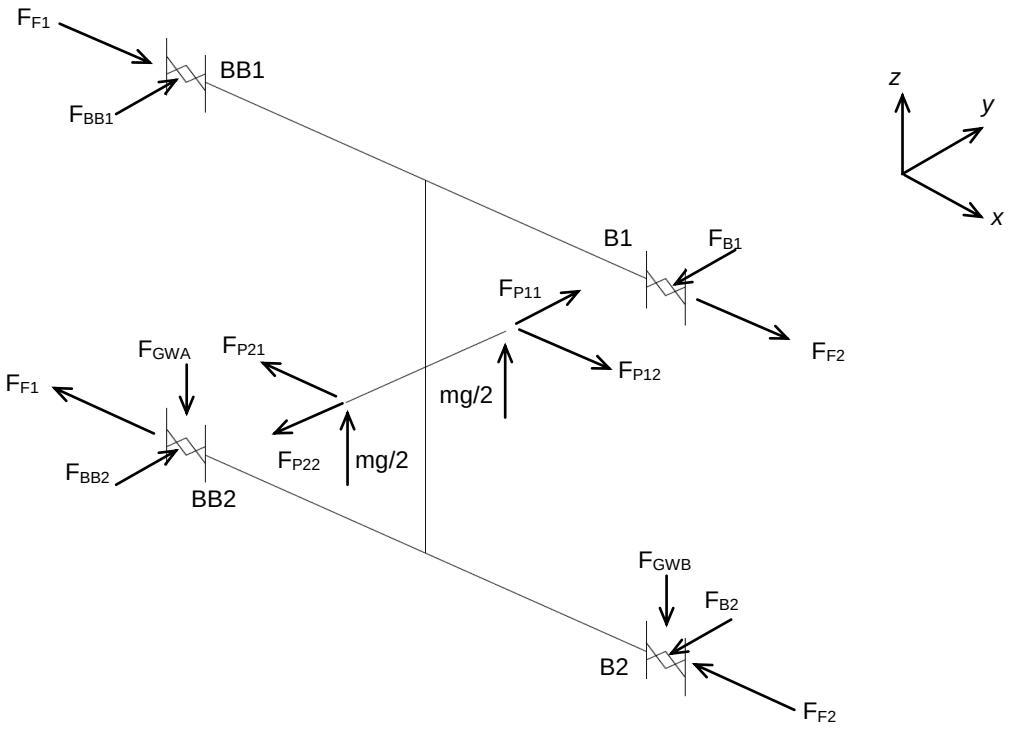

Figure 2.7 – Brennan monorail gimbal mounting frame

The forces on the monorail chassis (when wheel ‘a’ contacts shelf A) are shown in Figure 2.8.

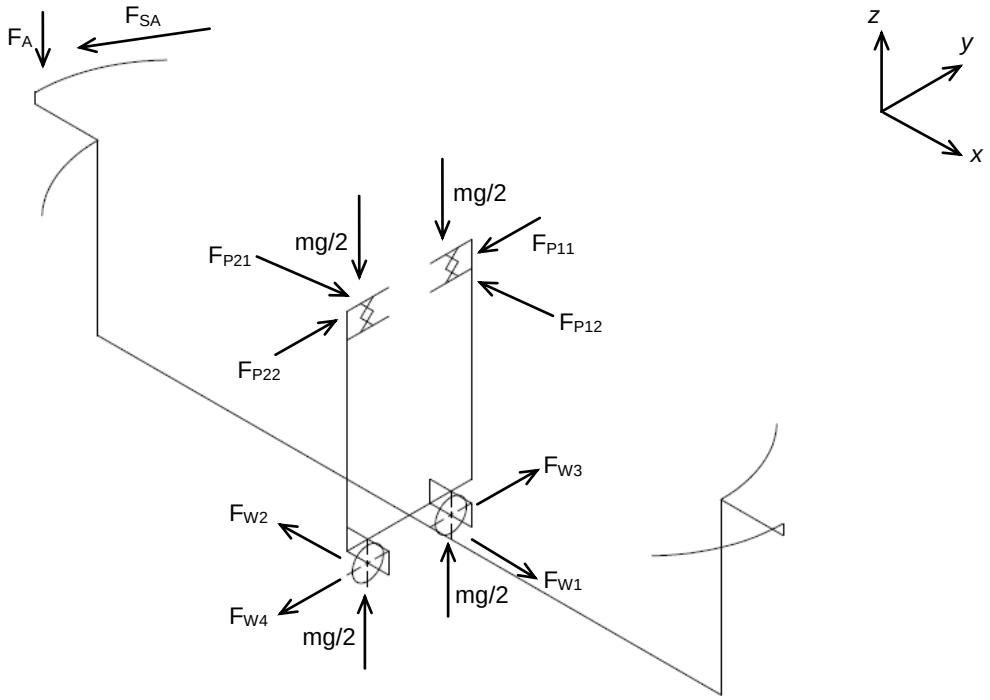

Figure 2.8 – Brennan monorail chassis

The applied righting moment down upon shelf A continues until the Brennan monorail chassis is tipped over the equilibrium point (axis P1-P2). The tipping motion continues until free wheel ‘c’ contacts shelf C (on the other side of the monorail).

Gimbal frame B of the Brennan monorail now becomes Figure 2.9.

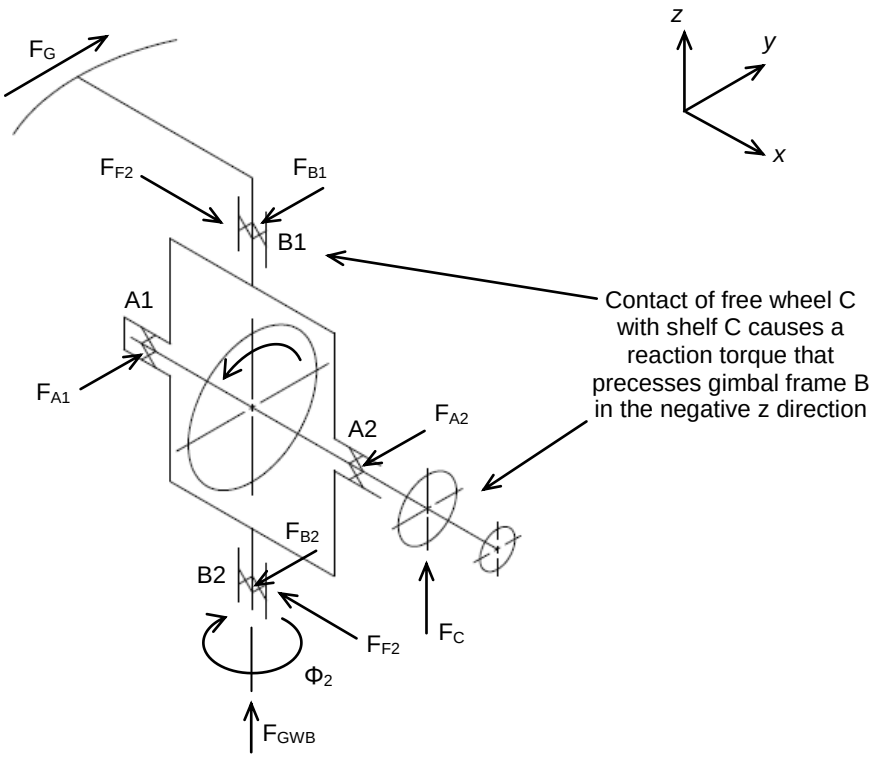

Figure 2.9 – Gimbal frame B

The tipping of the monorail over the equilibrium will cause a force to be applied to shelf ‘C’, F_C, by free wheel ‘c’ resulting in the precession of gimbal frame B about B1-B2 in the negative z direction (Φ_2). This precession continues until friction wheel ‘d’ comes in contact with shelf D. This contact causes the force precession of gimbal frame B, and due to the geared joint this also results in the forced precession of gimbal frame A.

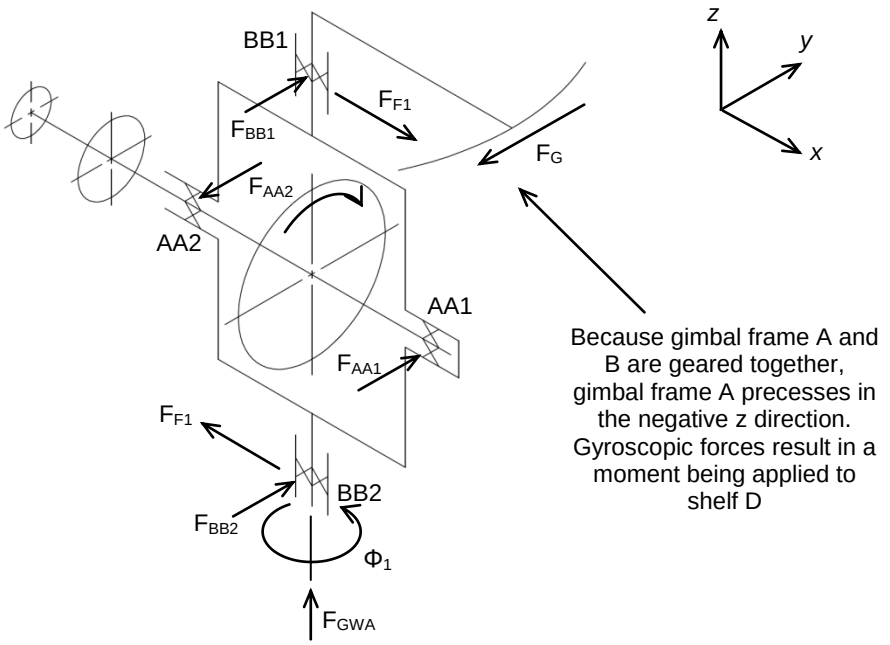

Figure 2.10 – Gimbal frame A

The gear force F_G causes the gimbal frame A to rotate about the axis BB1-BB2 in the positive z direction (Φ_1). The forced precession of gimbal frame A results in the righting moment (forces F_{F1}) due to gyroscopic effects.

This results in the application of a righting moment to shelf D (about axis P1-P2). This righting moment continues pushing upon shelf D until the monorail again tips over the equilibrium (about axis P1-P2) causing free wheel ‘b’ to come in contact with shelf B. The process is then repeated resulting in the monorail executing damped oscillatory motion about the equilibrium point.

The forces on the gimbal mounting frame of the monorail when wheel ‘c’ contacts shelf C are shown in Figure 2.11.

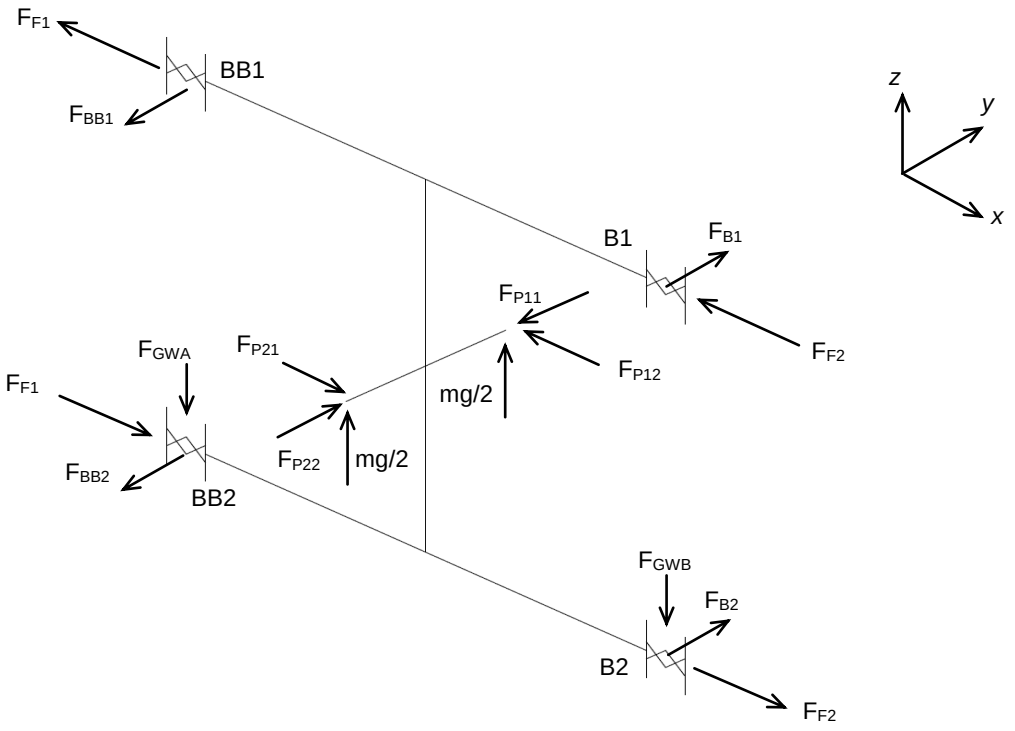

Figure 2.11 – Brennan monorail gimbal mounting frame

The forces on the monorail chassis (when wheel ‘c’ contacts shelf C) are shown in Figure 2.12.

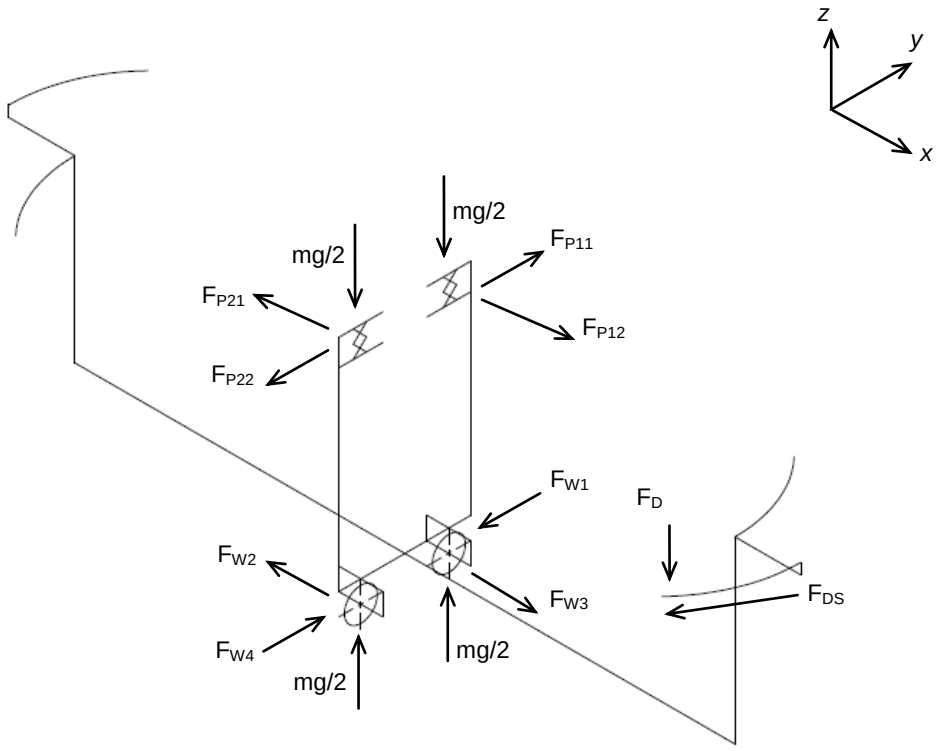

Figure 2.12 – Brennan monorail chassis

2.7 Main advantages of proposed system over Brennan monorail

There are several advantages of the proposed stable platform over the Brennan monorail. These are:

- While the Brennan monorail stabilized an external structure in one plane the proposed stable platform posses the ability to stabilize in the horizontal pitch and roll directions.
- Because the proposed gyroscopically stabilized platform precesses around a central axis the system is able to produce an equivalent restoring force in all directions. This feature makes the proposed system novel and adaptable to a large range of applications.

Advances in technology have allowed a stabilization system that achieves the same result as the Brennan monorail to be produced at a much smaller scale. High speed electric motors and lightweight batteries will greatly increase flywheel speed while significantly reducing the overall weight of the system. These technologies will be utilized in the design of the stable platform.

2.8 Concluding comments

The review of the Brennan monorail has shown how gyroscopes behave when coupled together and how this can be adapted to maintain an unstable body upright. This understanding of the reactions produced by gyroscopes when subjected to an external force along with the free body analysis of the Brennan monorail has revealed the critical load paths and important system interactions. This will aid in the design of the proposed gyroscopically stabilized platform.

3

Derivation of Lagrangian of Stable Platform

3.1 Introduction

The proposed gyroscopically stabilized platform will now be referred to as the stable platform. It is desirable to derive a set of equations that model the oscillatory motion of the stable platform. A Lagrangian energy approach is adopted with goal of obtaining a set of equations of motion for each of the variables that relate to the behaviour of the stable platform.

The objective of this chapter is to derive the Lagrangian of the stable platform system. The kinetic and potential energy for the stable platform subsystems (external structure, disc and gyroscopes) are derived and combined to obtain the required Lagrangian. This result will then be used to derive the equations of motion of the system.

3.2 System variables

The following variables are used to describe the motion of the stable platform during the stabilization process:

$$\theta_s(t), \theta_d(t), \psi_d(t), \phi_d(t), \theta_k(t), \phi_k(t)$$

The six variable are defined as

$\theta_s(t)$ = the location of the external structure from the vertical

$\theta_d(t), \psi_d(t), \phi_d(t)$ = the Euler angles associated with location of the disc around the pivot point

$\theta_m(t), \phi_m(t)$ = the Euler angles associated with the location of the gyroscopes relative to their pivot point, $m = 1 \ldots 4$

Figure 3.1 denotes how the system variables relate to the physical system.

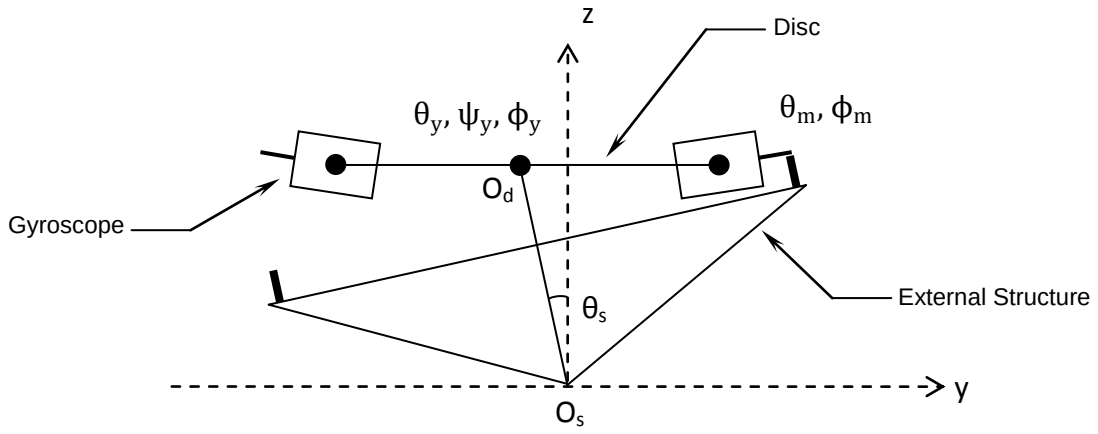

Figure 3.1 – Relationship of system variables to physical system

$\bar{\theta}(t)$ is defined as an Euler angle that measures deviations of the system from the horizontal, rather than the normal (like $\theta_s(t)$). It is thus related to $\theta(t)$ by the equation

$$\theta(t) = \frac{\pi}{2} - \bar{\theta}(t) \qquad (3.1)$$

such that $0 \leq \theta(t) \leq \pi \rightarrow \frac{-\pi}{2} \leq \bar{\theta}(t) \leq \frac{\pi}{2}$

3.3 Initial simplifying assumptions

Several simplifying assumptions are established. These assumptions will all be implemented in the physical design of the system so that it adheres to the mathematical analysis. The four key assumptions used in this mathematical analysis of the system are:

i) $\left.\begin{aligned} I_x{}^{(k)} &= I_x \\ I_y{}^{(k)} &= I_y \\ I_z{}^{(k)} &= I_z \end{aligned}\right\} \rightarrow k = 1 \ldots 4$ All four of the gyroscope systems (gimbal frame, motor, and gyroscope) have identical moments of inertia

ii) $\theta_m(t) = \bar{\theta}(t) \rightarrow m = 1 \ldots 4$ All the gyroscope systems have equal angular displacement ($\bar{\theta}(t)$) from the horizontal of the disc

iii) $\phi_m(t) = \phi(t) \rightarrow m = 1 \ldots 4$ All the gyroscopes have identical rotational speeds, $\phi(t)$, taken to be constant

iv) The torque produced by the external structure's deviation from the normal is applied to the gyroscopes only (the disc does not tip).

3.4 Lagrangian formalism

We derive the equations of motion for $\theta_s(t), \theta_d(t), \psi_d(t), \phi_d(t), \theta_k(t), \phi_k(t)$ by the means of the Lagrangian formalism.

The Lagrangian function, $L\{q_m(t), \dot{q}_m(t), t\}$ associated with a system described by $q_m(t)$, $(m = 1 \ldots n)$ independent variables, is defined as

$$L\{q_m(t), \dot{q}_m(t), t\} = T\left(\dot{q}_m(t)\right) - V\left(q_m(t)\right) \qquad (3.2)$$

where $T\left(\dot{q}_m(t)\right)$ = the kinetic energy of the energy of the system

$V\left(q_m(t), t\right)$ = the potential energy of the system

where the equations of motion of the system are given by

$$\frac{d}{dt}\left(\frac{\partial L}{\partial \dot{q}_m}\right) - \left(\frac{\partial L}{\partial q_m}\right) = F_{q_m} \qquad m=1\ldots n$$

where F_{q_m} = the generalised non conservative force affecting the motion of the $q_m{}^{th}$ co-ordinate (where applicable)

3.5 Approach to derivation of system Lagrangian

The procedure for deriving the Lagrangian of the stable platform requires the formulation of the kinetic and potential energies and the non-conservative forces of

the system in terms of suitable co-ordinates. This is completed for each of the three sub systems that comprise the stable platform (the external structure, the disc and the gyroscope) and then summed together so that

$$L_{Total} = L_s + L_d + L_g \qquad (3.3)$$

where L_s = the Lagrangian associated with the external structure

L_d = the Lagrangian associated with the disc

L_g = the Lagrangian associated with the gyroscopes

The most convenient co-ordinates for a rigid body (such as this system) are those associated with the body fixed axis with origin, O, attached to a specific point of the body (often the centre of mass) so the co-ordinate system has all the body's motion (Wells (1967)).

3.6 Derivation of kinetic energy terms

The required expression for the kinetic energy is obtained by rewriting the components of the inertial space velocity $\overrightarrow{v_I}$ in terms of the variables associated with the co-ordinate system used in the expression

$$T = \sum_k \frac{1}{2} m_k \left({v_{i_x}^k}^2 + {v_{i_y}^k}^2 + {v_{i_z}^k}^2 \right) \qquad (3.4)$$

where $\vec{v}_i^k$ = the inertial space velocity of the k^{th} particle in the rigid body relative to its body fixed axis with components $v_{i_x}^k, v_{i_y}^k, v_{i_z}^k$ and having mass m_k

and then simplifying this summation.

3.7 Reference frame relations

It is important to establish a set of reference frames that will describe how the system moves relative to a fixed point in space. The relationship between the reference frames used to describe the motion of the system is shown in Figure 3.2.

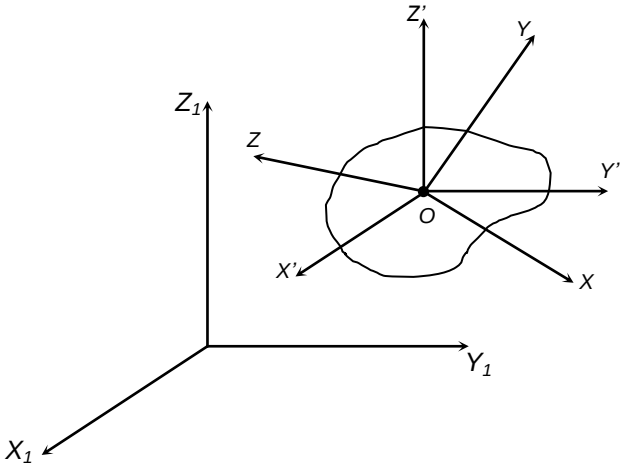

Figure 3.2 – Relationship between inertial reference frame, inertial frame centred at the origin of the body and the body fixed frame

where X_1, Y_1, Z_1 is the inertial reference frame

X', Y', Z' is the inertial frame parallel to X_1, Y_1, Z_1 but centred at origin O of the rigid body

X, Y, Z is the body fixed frame centred at the origin

If the origin O, has an inertial space velocity $\vec{v}_0$ with components $v_{0_x}, v_{0_y}, v_{0_z}$ along X, Y, Z, then the components v_x, v_y, v_z of the inertial space velocity of a particle at a location $\vec{r}$ from the origin in the X, Y, Z co-ordinate system with respect to this system are

$$\vec{v} = \vec{v}_0 + \vec{r} \times \vec{\omega} \tag{3.5}$$

where $\vec{\omega}$ = the angular velocity of the body fixed axes X, Y, Z relative to the inertial axes X', Y', Z'

So the kinetic energy of the stable platform system can be expressed as

$$T = \sum_k \frac{1}{2} m_k \left[\left(v_{0_x} + (\vec{r_k} \times \vec{\omega})_x \right)^2 + \left(v_{0_y} + (\vec{r_k} \times \vec{\omega})_y \right)^2 + \left(v_{0_z} + (\vec{r_k} \times \vec{\omega})_z \right)^2 \right] \tag{3.6}$$

3.8 Lagrangian of external structure

In this section the derivation of the Lagrangian of the external structure is presented. The Lagrangian, L_s depends upon the kinetic energy, T_s, and potential energy, V_s, of the external structure such that, $L_s = T_s - V_s$.

3.8.1 Kinetic energy of external structure

The external structure is assumed to be a point mass M_s with a centre of mass situated at a height h_s above the pivot point O_s.

Figure 3.3 illustrates the location of the centre of mass of the external structure relative to the pivot point.

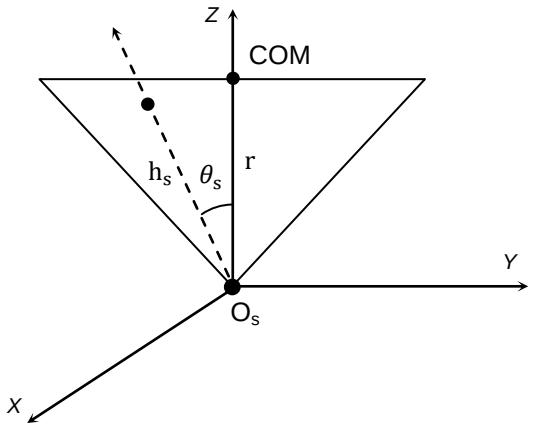

Figure 3.3 – Location of external structure centre of mass relative to origin

The kinetic energy of the external structure can be expressed as

$$T_s = \frac{1}{2}\sum_k m_k \vec{v}_{0_s}{}^2 \qquad (3.7)$$

where $\vec{v}_{0_s} = r \times \vec{\omega}_s$ the velocity of the centre of mass of the external frame relative to the inertial reference frame at the pivot point O_s written in terms of the body fixed axis of the external structure

By inspection it can be seen that

$$\mathrm{r} = \left(x_{0_s}, y_{0_s}, z_{0_s}\right) \tag{3.8}$$

where

$$x_{0_\mathrm{s}} = 0$$

$$y_{0_\mathrm{s}} = \mathrm{h_s}\cos\theta_\mathrm{s}$$

$$z_{0_\mathrm{s}} = \mathrm{h_s}\sin\theta_\mathrm{s}$$

and

$$\vec{\omega}_\mathrm{s} = \left(\omega_{x_s}, \omega_{y_s}, \omega_{z_s}\right) \tag{3.9}$$

where

$$\omega_{x_s} = \dot{\theta}_\mathrm{s}$$

$$\omega_{y_s} = 0$$

$$\omega_{z_s} = 0$$

Therefore, the kinetic energy of the external structure can be expressed as

$$\mathrm{T_s} = \frac{1}{2}\sum_\mathrm{k} \mathrm{m_k}\,\vec{\mathrm{v}}_{0_\mathrm{s}}{}^2$$

$$= \frac{1}{2}\sum_\mathrm{k} \mathrm{m_k}\,(\mathrm{r} \times \vec{\omega}_\mathrm{s})^2$$

$$= \frac{1}{2} M_s \left[\left((0)\dot{\theta}_s \right)^2 + \left(h_s \cos(\theta_s)\dot{\theta}_s \right)^2 + \left(h_s \sin(\theta_s)\dot{\theta}_s \right)^2 \right]$$

$$= \frac{1}{2} M_s \left[{h_s}^2 \cos^2(\theta_s) + {h_s}^2 \sin^2(\theta_s) \right] {\dot{\theta}_s}^2$$

$$= \frac{1}{2} M_s {h_s}^2 {\dot{\theta}_s}^2 \qquad (3.10)$$

where M_s is the mass of the external structure

3.8.2 Potential energy of the external structure

The potential energy of the external structure is determined from the mass of the external structure and the height of the centre of mass of the external structure above the origin O_S.

If we make the simplifying assumption that the external structure can be represented as a point mass, M_s, at its centre of mass h_s above O_S we obtain

$$V_s = M_s g h_s \cos\theta_s \qquad (3.11)$$

3.8.3 Lagrangian for the external structure

The Lagrangian for the external structure is therefore a combination of equations (3.10) and (3.11).

$$L_s = T_s - V_s$$

$$= \frac{1}{2} M_s {h_s}^2 \dot{\theta_s}^2 - M_s g h_s \cos\theta_s \qquad (3.12)$$

3.9 Lagrangian of disc

This section presents the derivation of the Lagrangian of the disc. The Lagrangian, L_d depends upon the kinetic energy, T_d and potential energy,V_d of the disc.

3.9.1 Kinetic energy of the disc

As with the external structure, the kinetic energy of the disc can be expressed in the form

$$T_d = \frac{1}{2} \sum_k m_k \vec{v}_k^{\,2} \qquad (3.13)$$

where $\vec{v}_k$ is the inertial space velocity of the k^{th} particle in the disc written in terms of the body fixed axes of the disc. These are taken to be along the principal axes of inertia of the disc.

We also make the assumption that the disc is symmetric about the z axis of the body fixed reference frame and O_d. The origin of this frame is at its centre of mass which is located in line with the systems pivot point.

The velocity of the k^{th} particle for the disc can be written in the form

$$\vec{v}_k = \vec{v}_{0_d} + \vec{r}_k \times \vec{\omega}_d \qquad (3.14)$$

where $\vec{v}_{0_d}$ is the velocity of the origin of the body fixed axis attached to the disc relative to the inertial reference frame centred at the pivot point O_d written in terms of the body fixed axes associated with the disc

$\vec{\omega}_d$ is the angular velocity of the body fixed axes associated with the disc relative to the inertial reference frame

$\vec{r}_k$ is the location of the k^{th} particle of the disc relative to O_d

Because the external structure and disc share a common origin, $\vec{v}_{0_d}$ can be written as

$$\vec{v}_{0_d} = \vec{v}_{0_s} = \left(0, h_d \cos(\theta_s)\dot{\theta}_s, -h_d \sin(\theta_s)\dot{\theta}_s\right) \qquad (3.15)$$

where h_d is the height of O_d above O_s

3.9.2 Euler angles

In order to describe the angular velocity of the disc we introduce a set of angular variables known as Euler angles. Euler angles θ, ψ, ϕ are commonly used to describe the behaviour of a rotating body (Wells, 1967).

For all applications performed in the following set of calculations X_1, Y_1, Z_1 will be taken as the fixed axes in space. If a rigid body (in this case the disc) is fixed at point O and is rotated about this point, let X, Y, Z denote the reference axis attached to this body (body fixed axis) (Kane (1983)). Each Euler angle, shown in Figure 3.4, are defined as

- Line 'ON' is defined as the intersection of the plane created by moving XY through the stationary X_1Y_1 plane
- ψ is defined as the angle between X_1 and 'ON'
- θ is defined as the angle between Z_1 and Z
- ϕ is defined as the angle between X and 'ON'

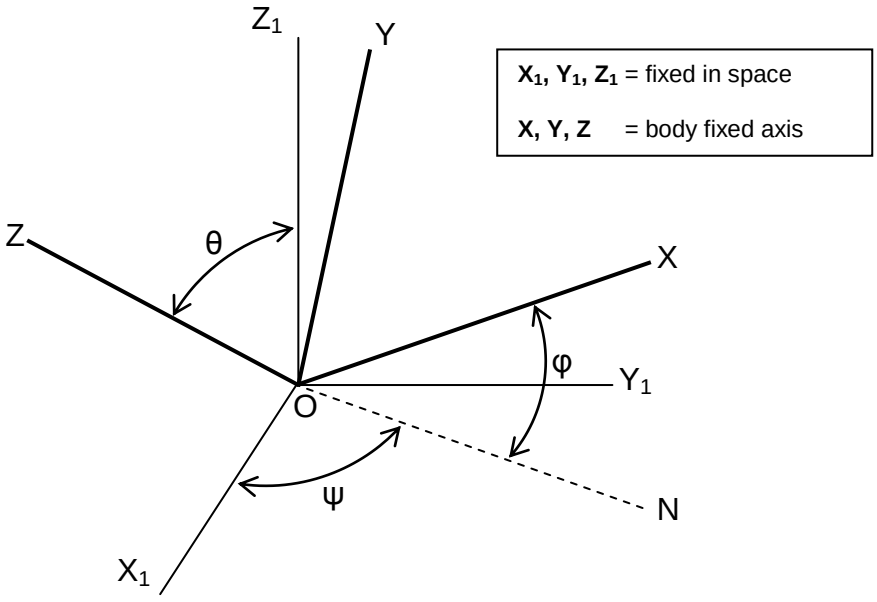

Figure 3.4 – Definition of Euler angles relative to inertial reference frame

3.9.3 Angular velocity of disc

Assuming that $\dot{\theta}$, $\dot{\phi}$, $\dot{\psi}$ are regarded as angular velocity vectors acting along ON, Z, Z_1 respectively, the total angular velocity, ω is the vector sum of these three quantities (Wells (1967)). This is illustrated in Figure 3.5.

For the purpose of this analysis it is useful to establish the components of this vector $\omega_{x_d}, \omega_{y_d}, \omega_{z_d}$ relative to the body fixed axes X, Y, Z.

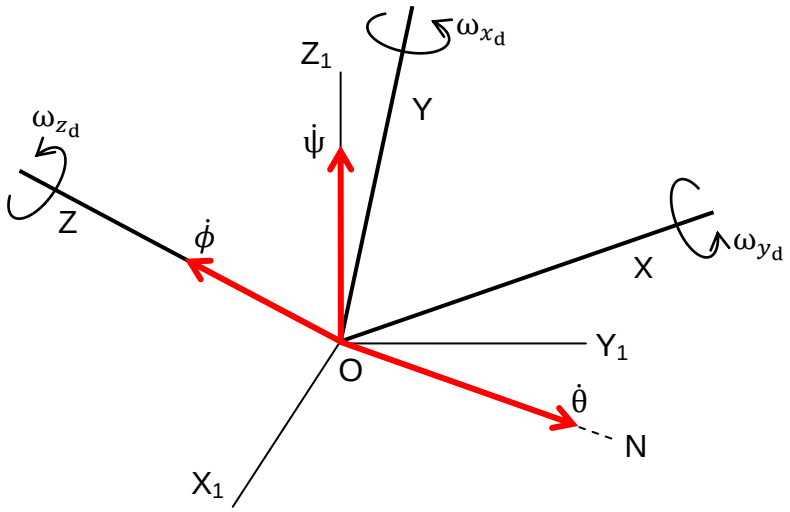

Figure 3.5 – Location of angular velocity vectors relative to reference frame

It is possible to derive a directional cosine table to translate the vectors that act along the body fixed axis onto the axes 'ON', Z, Z_1 (which in turn is related to the inertial reference frame).

The relationship between each of the angular velocity vectors is shown in Table 3.1.

Table 3.1 - Cosine of angles between X, Y, Z and Z1, ON

	X	Y	Z
Z_1	$\sin\theta\sin\phi$	$\sin\theta\cos\phi$	$\cos\theta$
ON	$\cos\phi$	$-\sin\phi$	0

An example of how one of the angles is derived follows.

Assume we wish to determine the direction cosines between the line ON and the axis X in the body fixed frame (that is, what would we need to multiply a vector along ON by to transform it into the X axis).

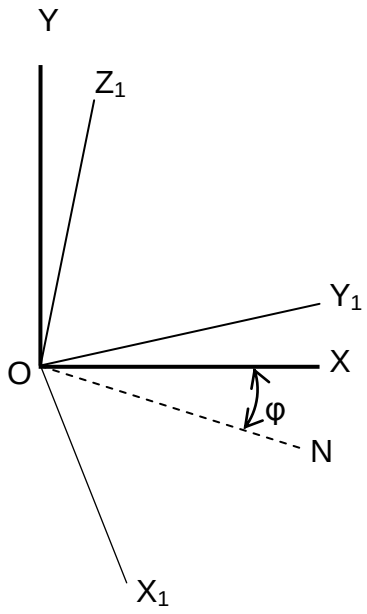

Figure 3.6 – Rotation of Figure 3.5 such that ON, X and Y all are on a common plane parallel to the page

Figure 3.5 is rotated so that 'ON', X and Y all lie on a common plane (that is parallel to the page) such that it is possible to see ϕ as a 'true angle' (Figure 3.6). If ON is a unit vector of length 1, X is equal to $\cos\phi$; this is the resulting direction cosine

relating to a transformation of 'ON' onto X. Using this method it is possible to determine the angles between each of the respective axes of rotation and complete the elements of Table 3.1.

By taking components $\dot{\theta}$, $\dot{\phi}$ and $\dot{\psi}$ the angular velocities of the disc acting along the body fixed with respect to 'ON', Z, Z1 the angular velocity components of the disc taken along X, Y, Z relative to the inertial reference frame are:

$$\omega_{x_d} = \dot{\psi}_d \sin\theta_d \sin\phi_d + \dot{\theta}_d \cos\phi_d \qquad (3.16)$$

$$\omega_{y_d} = \dot{\psi}_d \sin\theta_d \cos\phi_d - \dot{\theta}_d \sin\phi_d \qquad (3.17)$$

$$\omega_{z_d} = \dot{\phi}_d + \dot{\psi}_d \cos\theta_d \qquad (3.18)$$

Equations (3.16), (3.17) and (3.18) represent a transformation that puts the angular velocities into a common frame where all velocities (both angular and linear) can be summed together.

We also make the simplifying assumption that $I_x^d = I_y^d$ (the disc is symmetric about the z axis of the body fixed frame).

3.9.4 Total kinetic energy of the disc

The total kinetic energy of the disc can now be determined.

$$T_d = \frac{1}{2}\sum_k m_k \vec{v}_k^{\,2}$$

$$= \frac{1}{2}\sum_k m_k \left(\vec{v}_{0_d} + \vec{r}_k \times \vec{\omega}_d\right)^2 \qquad (3.19)$$

Since O_d is located at the centre of mass, this simplifies to

$$T_d = \frac{1}{2}\sum_k \left[m_k\left(\vec{v}_{0_d}\right)^2 + m_k(\vec{r}_k \times \vec{\omega}_d)^2\right]$$

$$= \frac{1}{2}M_d\left(\vec{v}_{0_d}\right)^2 + \frac{1}{2}I_x^{(d)}\left(\omega_{x_d} + \omega_{y_d}\right)^2 + \frac{1}{2}I_z^{(d)}\left(\omega_{z_d}\right)^2 \qquad (3.20)$$

where $M_d = \sum_k m_k$

This result can be obtained because O_d (the centre of mass of the disc) and the body fixed axes are taken along the principal axes of inertia of the disc and $I_x^d = I_y^d$. From Equation (3.15) we express $\vec{v}_{0_d}$ as

$$\vec{v}_{0_d}^{\,2} = v_{0_{d_x}}^{\,2} + v_{0_{d_y}}^{\,2} + v_{0_{d_z}}^{\,2}$$

$$= (0)^2 + \left(h_d\cos(\theta_s)\dot{\theta}_s\right)^2 + \left(h_d\sin(\theta_s)\dot{\theta}_s\right)^2 \qquad (3.21)$$

Substituting Equations (3.16), (3.17), (3.18) and (3.21) into Equation (3.19) we obtain the result

$$\begin{aligned} T_d &= \frac{1}{2}M_d\left(\left[(0)^2 + \left(h_d\cos(\theta_s)\dot{\theta}_s\right)^2 + \left(h_d\sin(\theta_s)\dot{\theta}_s\right)^2\right]\right)^2 \\ &\quad + \frac{1}{2}I_x^{(d)}\left(\left(\dot{\psi}_d\sin\theta_d\sin\phi_d + \dot{\theta}_d\cos\phi_d\right)^2 + \left(\dot{\psi}_d\sin\theta_d\cos\phi_d - \dot{\theta}_d\sin\phi_d\right)^2\right) \\ &\quad + \frac{1}{2}I_z^{(d)}\left(\dot{\phi}_d + \dot{\psi}_d\cos\theta_d\right)^2 \\ &= \frac{1}{2}M_d{h_s}^2{\dot{\theta}_s}^2 + \frac{1}{2}I_x^{(d)}\left({\dot{\theta}_d}^2 + {\dot{\psi}_d}^2\sin^2\theta_d\right) + \frac{1}{2}I_z^{(d)}\left(\dot{\phi}_d + \dot{\psi}_d\cos\theta_d\right)^2 \end{aligned} \qquad (3.22)$$

See Appendix A for the full simplification of the result

$$\left(\dot{\psi}_d\sin\theta_d\sin\phi_d + \dot{\theta}_d\cos\phi_d\right)^2 + \left(\dot{\psi}_d\sin\theta_d\cos\phi_d - \dot{\theta}_d\sin\phi_d\right)^2 = \left({\dot{\theta}_d}^2 + {\dot{\psi}_d}^2\sin^2\theta_d\right)$$

3.9.5 Potential energy of the disc

The potential energy of the disc is determined from the mass of the disc M_d and the height of the COM of the disc h_d above the origin O_s. Again we make the simplifying assumption that the disc can be represented as a point mass at its centre of mass. We therefore obtain

$$V_d = M_d g h_d \cos\theta_s \qquad (3.23)$$

3.9.6 Lagrangian for the disc

The Lagrangian for the disc can therefore be expressed as a combination of Equations (3.22) and (3.23).

$$L_d = T_d - V_d$$

$$= \frac{1}{2} M_d {h_s}^2 {\dot{\theta}_s}^2 + \frac{1}{2} I_x^{(d)} \left({\dot{\theta}_d}^2 + {\dot{\psi}_d}^2 \sin^2\theta_d \right) + \frac{1}{2} I_z^{(d)} \left(\dot{\phi}_d + \dot{\psi}_d \cos\theta_d \right)^2$$

$$- M_d g h_d \cos\theta_s \qquad (3.24)$$

This equation can further be simplified based on the assumption that the disc will always remain level as the centre of mass of the gyroscopes/disc is below the pivot point (the disc possess high gravitational stability). This leads to the assumption that

$$\psi_d = \theta_d = 0$$

$$\dot{\psi}_d = \dot{\theta}_d = 0$$

which when substituted into the equation for L_d yields

$$L_d = \frac{1}{2} M_d {h_d}^2 {\dot{\theta}_s}^2 + \frac{1}{2} I_z^{(d)} {\dot{\phi}_d}^2 - M_d g h_d \cos\theta_s \qquad (3.25)$$

3.10 Lagrangian of gyroscopes

The following sections look at the derivation of the Lagrangian of the gyroscopes. The Lagrangian, L_g, depends upon the kinetic energy, T_g, and potential energy,V_g, of the gyroscopes.

3.10.1 Kinetic energy of the gyroscopes

As with the external structure and the disc, the kinetic energy of the gyroscopes can be expressed in the form

$$T_g = \frac{1}{2}\sum_{\substack{gyros \\ m=1}}^{4}\left(\sum_{k} m_k \vec{v}_k{}^2\right) \qquad (3.26)$$

where $\vec{v}_k$ is the inertial space velocity of the k[th] particle in the gyroscope written in terms of the body fixed axes associated with each gyroscope (numbered 1 to 4). This is taken to be along the principle axis of inertia of the gyroscopes where m_k is the mass of this particle.

We also make the assumption that the mass of each gyroscope is symmetric about the z axis of its body fixed frame and O_{g_m} (the origin of the reference frame is its centre of mass). The velocity of the k[th] particle of the gyroscopes can be written in the form

$$\vec{v}_k = \vec{v}_{O_d} + \vec{v}_{O_{g_m}(\text{relative to } O_d)} + \vec{r}_k \times \vec{\omega}_{g_m} \qquad (3.27)$$

Where the components that comprise $\vec{v}_k$ are defined as

$\vec{v}_{O_d}$	the velocity of the pivot point of the disc (O_d) relative to the inertial reference frame centred at the origin O_s written in terms of the body fixed axis associated with the m[th] gyroscope
$\vec{v}_{O_{g_m}(\text{relative to } O_d)}$	the velocity of the pivot point of a gyroscope O_{g_m} relative to the inertial frame centred at O_d written in terms of the body fixed axis associated with the m[th] gyroscope
$\vec{\omega}_{g_m}$	the angular velocity of the body fixed axis of the m[th] gyroscope relative to the inertial frame entered at O_d written in terms of the body fixed axis associated with the m[th] gyroscope
$\vec{r}_k$	the location of the particle in the body fixed axes

While it would be useful to distinguish between the gyroscopes writing $\vec{v}_k$ and $\vec{r}_k$ respectively; since it is assumed that all gyroscopes have a similar design specification this notation does not add to the basic results.

Because O_{g_m} is the centre of mass of each gyroscope and the body fixed axes are taken along the principle axes of inertia of the gyroscopes, the expression for the kinetic energy of the gyroscopes reduces to

$$T_g = \frac{1}{2}\sum_m M_{g_m}\left(v_{O_{g_x}}^{(m)^2} + v_{O_{g_y}}^{(m)^2} + v_{O_{g_z}}^{(m)^2}\right) + \frac{1}{2}\sum_m \left(I\left(\omega_x^{(m)^2} + \omega_y^{(m)^2}\right) + I_z\omega_z^{(m)^2}\right) \quad (3.28)$$

It is also assumed that the gyroscopes are identical and are symmetric (that is that $I_x = I_y = I$) and $M_{g_m} = \sum_k m_k$.

3.10.2 Inertial space linear velocity of gyroscope pivot point O_{g_m}

The linear velocity of the gyroscopes depends upon the rotation of the disc. Because of this, we need to derive an expression for the velocity of the pivot point of the disc $\vec{v}_{O_d}$ (Equation (3.15)) relative to the body-fixed frame of the gyroscope. Consider a rotation of the disc through ϕ_d as shown in Figure 3.7.

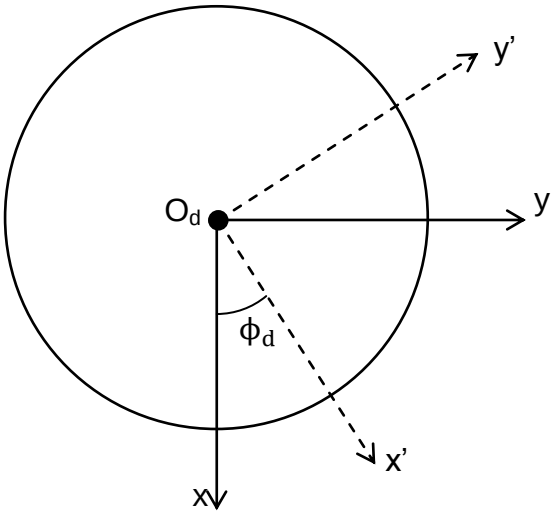

Figure 3.7 – Rotation of disc about O_d through angle ϕ_d

A transformation relative to the body-fixed axis attached to the disc but rotated an angle ϕ_d, relative to the above axis results in the following velocities (shown as a resultant of the sum of the x and y components).

$$\begin{aligned} v'_x &= v_x \cos(\phi_d) + v_y \sin(\phi_d) \\ v'_y &= -v_x \sin(\phi_d) + v_y \cos(\phi_d) \\ v'_z &= v_z \end{aligned} \qquad (3.29)$$

Substitution of the values from Equation (3.15) into Equation (3.29) means that for the components of $\vec{v}_{O_d}$ relative to this frame we obtain

$$\begin{aligned} v'_x &= (0)\cos(\phi_d) + \left(h_d \dot{\theta}_s \cos(\theta_s)\right) \sin(\phi_d) \\ &= h_d \dot{\theta}_s \cos(\theta_s) \sin(\phi_d) \end{aligned}$$

$$v'_y = -(0)\sin(\phi_d) + \left(h_d\dot{\theta}_s\cos(\theta_s)\right)\cos(\phi_d)$$

$$= h_d\dot{\theta}_s\cos(\theta_s)\cos(\phi_d)$$

$$v'_z = -h_d\dot{\theta}_s\sin(\theta_s) \qquad (3.30)$$

If we make the assumption that the origin of this axis is taken at O_{g_m} with each axes remaining parallel to its first position then we now introduce a transformation onto a new set of axes relative to the origin of the gyroscopes, O_{g_m}.

These axes are depicted in Figure 3.8 and are defined as:

- a-b - the pivot axis of a gyroscope parallel to x'
- rad - the radial distance from O_d to O_g in the direction of y'
- $\perp$ - the axis perpendicular to the disc in the direction of z'

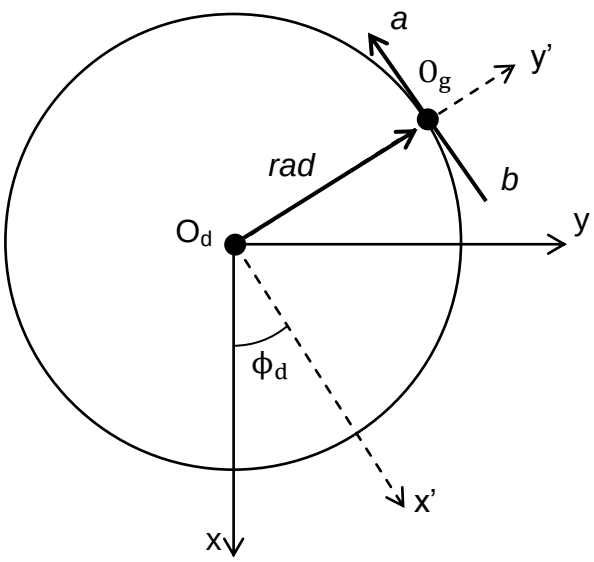

Figure 3.8 – Translation axes relative to body fixed axis

By direct substitution the velocity $\vec{v}_{O_d}$ relative to the origin of the gyroscopes has components in this set of axes defined as

$$v_{a-b} = h_d \dot{\theta}_s \cos(\theta_s)\sin(\phi_d)$$

$$v_{rad} = h_d \dot{\theta}_s \cos(\theta_s)\cos(\phi_d)$$

$$v_{\perp} = -h_d \dot{\theta}_s \sin(\theta_s) \qquad (3.31)$$

We also know that $\vec{v}_{O_{gm}(\text{relative to } O_d)}$ has been defined as the velocity of the pivot point of the gyroscopes relative to the origin of the disc. This velocity is directed along the *a-b* axis of each gyroscope (which lies along the gyroscope pivot axis). It is clear that

$$\vec{v}_{O_{gm}(\text{relative to } O_d)} = r_d \dot{\phi}_d \quad \text{(written in the form } v = \omega r\text{, along the } a\text{-}b \text{ axis)} \qquad (3.32)$$

where r_d = the radial distance the pivot point of the gyroscopes are from O_d

$\dot{\phi}_d$ = the angular velocity of the disc

Hence $\vec{v}_{O_{g_m}}$ has components

$$v_{a-b} = r_d\dot{\phi}_d + h_d\dot{\theta}_s\cos(\theta_s)\sin(\phi_d + \delta_m)$$
$$v_{rad} = h_d\dot{\theta}_s\cos(\theta_s)\cos(\phi_d + \delta_m)$$
$$v_{\perp} = -h_d\dot{\theta}_s\sin(\theta_s) \qquad (3.33)$$

where δ_m relates to the angular position of each of the four gyroscopes (e.g. when $m = 1,\ \delta_m = 0$ or when $m = 3,\ \delta_m = \pi$) in the body fixed axis of the disc.

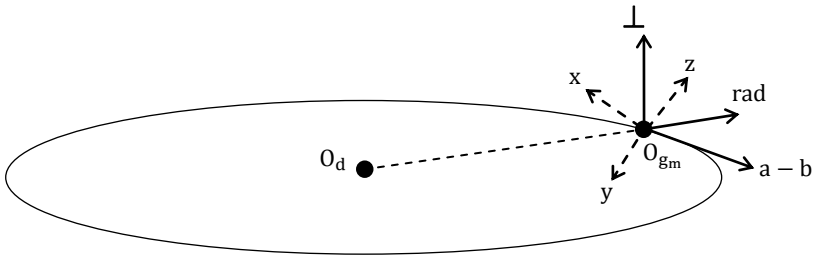

Figure 3.9 – Transformation axes relative to body fixed axis of gyroscope

The transformation

$$(a - b, rad, \perp) \longrightarrow (X, Y, Z)$$

where (X,Y,Z) is the body fixed axes associated with the gyroscope centred at O_{g_m}; is a rotation and under this type of transformation, even though the components along each axis change we obtain

$$(v_{a-b}, v_{rad}, v_{\perp}) \longrightarrow \left(v_{O_{g_x}}^{(m)}, v_{O_{g_y}}^{(m)}, v_{O_{g_z}}^{(m)}\right)$$

and from this we have

$$(v_{a-b}{}^2 + v_{rad}{}^2 + v_{\perp}{}^2) \longrightarrow \left(v_{O_{g_x}}^{(m)\,2} + v_{O_{g_y}}^{(m)\,2} + v_{O_{g_z}}^{(m)\,2}\right)$$

because any axis rotation preserves vector length.

Substituting in our previous results for $v_{a-b}, v_{rad}, v_{\perp}$ (Equation (3.33)) into $\left(v_{O_{g_x}}^{(m)\,2} + v_{O_{g_y}}^{(m)\,2} + v_{O_{g_z}}^{(m)\,2}\right)$ reveals

$$v_{O_{g_x}}^{(m)\,2} + v_{O_{g_y}}^{(m)\,2} + v_{O_{g_z}}^{(m)\,2} = \left[r_d\dot{\phi}_d + h_d\dot{\theta}_s\cos(\theta_s)\sin(\phi_d + \delta_m)\right]^2$$
$$+\left[h_d\dot{\theta}_s\cos(\theta_s)\cos(\phi_d + \delta_m)\right]^2 + \left[-h_d\dot{\theta}_s\sin(\theta_s)\right]^2$$

$$= r_d{}^2\dot{\phi}_d{}^2 + 2r_d\dot{\phi}_d h_d\dot{\theta}_s\cos(\theta_s)\sin(\phi_d + \delta_m)$$
$$+h_d{}^2\dot{\theta}_s{}^2\cos^2(\theta_s)\sin^2(\phi_d + \delta_m)$$
$$+h_d{}^2\dot{\theta}_s{}^2\cos^2(\theta_s)\cos^2(\phi_d + \delta_m) + h_d{}^2\dot{\theta}_s{}^2\sin^2(\theta_s)$$

$$= r_d{}^2\dot{\phi}_d{}^2 + 2r_d\dot{\phi}_d h_d\dot{\theta}_s\cos(\theta_s)\sin(\phi_d + \delta_m)$$
$$+h_d{}^2\dot{\theta}_s{}^2\cos^2(\theta_s)[\sin^2(\phi_d + \delta_m) + \cos^2(\phi_d + \delta_m)]$$
$$+h_d{}^2\dot{\theta}_s{}^2\sin^2(\theta_s)$$

$$= r_d{}^2\dot{\phi}_d{}^2 + 2r_d\dot{\phi}_d h_d\dot{\theta}_s\cos(\theta_s)\sin(\phi_d + \delta_m)$$
$$+h_d{}^2\dot{\theta}_s{}^2[\cos^2(\theta_s) + \sin^2(\theta_s)]$$

which when simplified reveals

$$v_{Og_x}^{(m)2} + v_{Og_y}^{(m)2} + v_{Og_z}^{(m)2} = r_d{}^2\dot{\phi}_d{}^2 + 2r_d\dot{\phi}_d h_d\dot{\theta}_s\cos(\theta_s)\sin(\phi_d + \delta_m) + h_d{}^2\dot{\theta}_s{}^2 \qquad (3.34)$$

At each location of the gyroscopes we can determine the value for δ_m and therefore the values for the linear velocities.

At $m = 1,\ \delta_m = 0 \quad \Rightarrow \quad \sin(\phi_d + 0) = \sin(\phi_d)$

$m = 2,\ \delta_m = \frac{\pi}{2} \quad \Rightarrow \quad \sin\left(\phi_d + \frac{\pi}{2}\right) = \cos(\phi_d)$

$m = 3,\ \delta_m = \pi \quad \Rightarrow \quad \sin(\phi_d + \pi) = -\sin(\phi_d)$

$m = 4,\ \delta_m = \frac{3\pi}{2} \quad \Rightarrow \quad \sin\left(\phi_d + \frac{3\pi}{2}\right) = -\cos(\phi_d) \qquad (3.35)$

Substituting Equations (3.34) and (3.35) into the linear velocity component of Equation (3.28) gives the linear velocity of the body fixed axis of the gyroscope as

$$\frac{1}{2}\sum_{m} M_{g_m}\left(v_{O_{g_x}}^{(m)^2} + v_{O_{g_y}}^{(m)^2} + v_{O_{g_z}}^{(m)^2}\right)$$

$$= \frac{1}{2}M_{g_1}\left[r_d{}^2\dot{\phi}_d{}^2 + 2r_d\dot{\phi}_d h_d\dot{\theta}_s\cos(\theta_s)\sin(\phi_d) + h_d{}^2\dot{\theta}_s{}^2\right]$$

$$+\frac{1}{2}M_{g_2}\left[r_d{}^2\dot{\phi}_d{}^2 + 2r_d\dot{\phi}_d h_d\dot{\theta}_s\cos(\theta_s)\cos(\phi_d) + h_d{}^2\dot{\theta}_s{}^2\right]$$

$$+\frac{1}{2}M_{g_3}\left[r_d{}^2\dot{\phi}_d{}^2 - 2r_d\dot{\phi}_d h_d\dot{\theta}_s\cos(\theta_s)\sin(\phi_d) + h_d{}^2\dot{\theta}_s{}^2\right]$$

$$+\frac{1}{2}M_{g_4}\left[r_d{}^2\dot{\phi}_d{}^2 - 2r_d\dot{\phi}_d h_d\dot{\theta}_s\cos(\theta_s)\cos(\phi_d) + h_d{}^2\dot{\theta}_s{}^2\right] \quad (3.36)$$

which can be simplified to

$$\frac{1}{2}\sum_{m} M_{g_m}\left(v_{O_{g_x}}^{(m)^2} + v_{O_{g_y}}^{(m)^2} + v_{O_{g_z}}^{(m)^2}\right) = \frac{1}{2}\left[4M_g\left(r_d{}^2\dot{\phi}_d{}^2 + h_d{}^2\dot{\theta}_s{}^2\right)\right]$$

$$= 2M_g\left(r_d{}^2\dot{\phi}_d{}^2 + h_d{}^2\dot{\theta}_s{}^2\right) \quad (3.37)$$

based on the assumption that $M_{g_1} = M_{g_2} = M_{g_3} = M_{g_4} = M_g$.

3.10.3 Angular velocity of body fixed axis $\vec{\omega}_{g_m}$

The total angular velocity of the gyroscopes is

$$\vec{\omega}_{g_m} = \vec{\dot{\phi}}_d + \vec{\dot{\theta}}_s + \vec{\dot{\theta}}_g + \vec{\dot{\phi}}_g \quad (3.38)$$

where $\vec{\dot{\phi}}_d$ the rotation of the disc along the $O_s - Z_1$ axis

$\vec{\theta}_s$ the rotation of the external structure along $O_s - X_1$ axis

$\dot{\theta}_g$ the rotation of the gyroscope/frame along the a-b axis through O_{g_m}

$\dot{\phi}_g$ the rotation of the gyroscope along $O_{g_m} - Z$

To describe the angular velocity of the gyroscope, the components of $\vec{\omega}_{g_m}$ in the body fixed axis of the gyroscope centred at O_{g_m} must be determined.

Figure 3.10 shows the location of each of the critical pivot points and axes of the system.

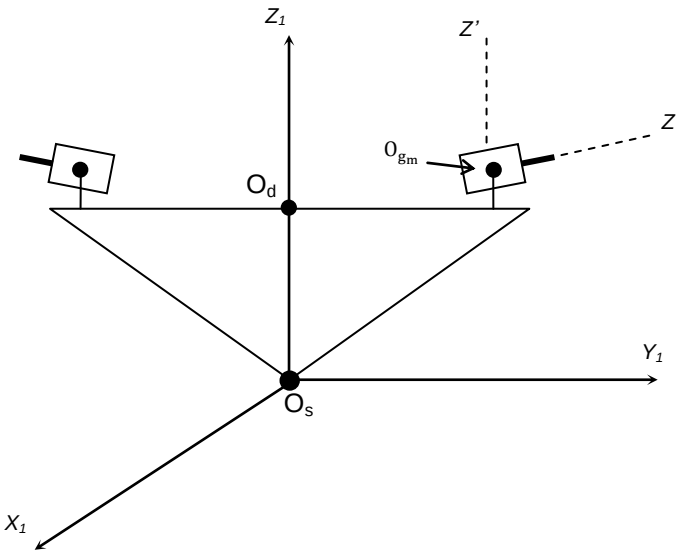

Figure 3.10 – Pivot point and axes locations

In order to determine the angular velocities of the gyroscopes we must transform all angular velocities that the gyroscope depends upon $(\dot{\phi}_d,\ \dot{\theta}_s,\ \dot{\theta}_g,\ \dot{\phi}_g)$, into the same

reference frame. In this case, we chose the origin of the gyroscopes O_{g_m} as our common origin and establish a set of axes that relate to this point.

Located at O_{g_m} we establish a set of axes such that the

- z axis is parallel to $O_s - Z_1$
- y axis is radially outward from O_d
- x axis is along $O_{g_m} - a$ (the pivot axis of the gyroscope/frame)

To see where these axes lie in relation to the system refer to Figure 3.9 and Figure 3.10.

The set of axes are rotated at an angle ϕ_d (rotation of the disc) to the inertial reference frame parallel to X_1, Y_1, Z_1 but centred at O_d.

The direction of each of the associated angular velocities after this transformation is described as:

- $\dot{\theta}_s$ (consisting of two components, one parallel to the x axis of the body fixed axes of the disc along the line $O_{g_m} - a$, and one parallel to the y axis radically outwards from O_d)

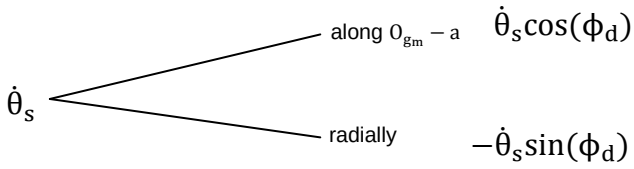

- $\dot{\theta}_{g_m}$ along $O_{g_m} - a$

- $\dot{\phi}_{g_m}$ along the $O_{g_m} - Z$

The location of the angles ϕ_{g_m} and θ_{g_m} are shown in Figure 3.11.

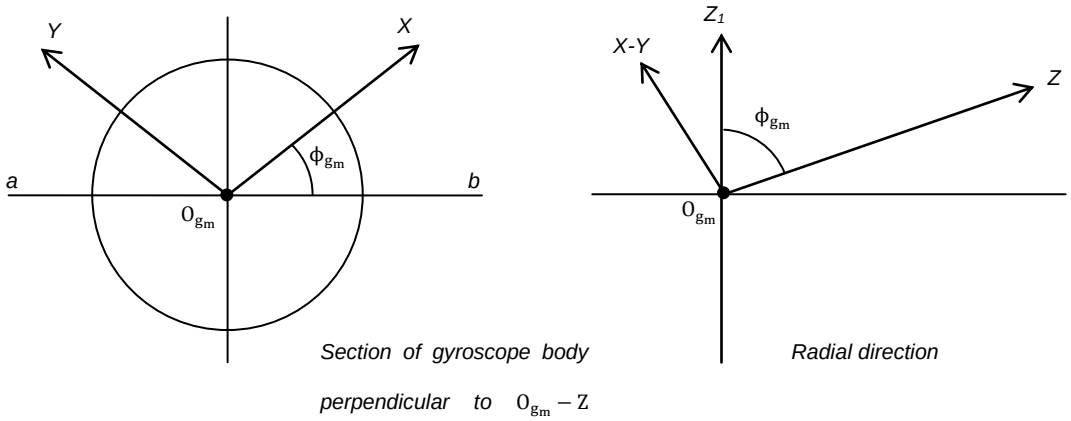

Figure 3.11 – Location of gyroscope body fixed axes centred at 0_{g_m} and associated angles

Figure 3.11 illustrates how this new set of axes relates to the body fixed axes of the gyroscopes.

The relative variables that need to be transformed and the axes relating to the frame with which we wish to transform them onto have been established. It is now possible

to derive expressions that describe $\dot{\phi}_d$, $\dot{\theta}_s$, $\dot{\theta}_g$, $\dot{\phi}_g$ in terms of $\omega_x, \omega_y, \omega_z$ (the angular velocities that relate to the gyroscope) in the body fixed axes centred at O_{g_m} (Gutschmidt (2005)).

Table 3.2 outlines all the transformations of $\dot{\theta}_s$, $\dot{\phi}_d, \dot{\theta}_{g_m}, \dot{\phi}_{g_m}$ into the O_{g_m} frame.

As an example, the derivation of the first term of Table 3.2 will be shown.

Let us consider the $O_{g_m} - a$ component of the variable $\dot{\theta}_s$. We have defined a transformation of this component from the frame centred at O_s into the frame centred at O_d as $\dot{\theta}_s cos(\phi_d)$.

We required this component to be transformed into the O_{g_m} frame. This component of $\dot{\theta}_s$ consists of two components in the O_{g_m} frame; one along the x axis and one along the y axis of the body fixed axes we previously established.

The x axis component of the $\dot{\theta}_s cos(\phi_d)$ term in the O_{g_m} frame can therefore be described as $-\dot{\theta}_s cos(\phi_d) cos(\phi_{g_m})$.

Table 3.2 – Transformations of angular velocities into the body fixed frame centred at 0_{g_m}

Variable in O_s frame	Variable in O_d frame	Variable in O_{g_m} frame
$\dot{\theta}_s$		
A transformation along $O_{g_m} - a$ into the O_d frame	$\dot{\theta}_s cos(\phi_d)$	
	A transformation into the O_{g_m} frame	$\omega_x = -\dot{\theta}_s cos(\phi_d) cos(\phi_{g_m})$
	A transformation into the O_{g_m} frame	$\omega_y = \dot{\theta}_s cos(\phi_d) sin(\phi_{g_m})$
A transformation radially into the O_d frame	$-\dot{\theta}_s sin(\phi_d)$	
	A transformation into the O_{g_m} frame	$\omega_z = -\dot{\theta}_s sin(\phi_d) sin(\theta_{g_m})$
	A transformation into the O_{g_m} frame	$\omega_{x-y} = \dot{\theta}_s sin(\phi_d) cos(\theta_{g_m})$
	A transformation from the x-y plane into the x and y axes	$\omega_x = \dot{\theta}_s sin(\phi_d) cos(\theta_g) sin(\phi_{g_m})$
	A transformation from the x-y plane into the x and y axes	$\omega_y = \dot{\theta}_s sin(\phi_d) cos(\theta_g) cos(\phi_{g_m})$
	$\dot{\phi}_d$	
	A transformation into the O_{g_m} frame	$\omega_z = \dot{\phi}_d cos(\theta_{g_m})$
	A transformation into the O_{g_m} frame	$\omega_{x-y} = \dot{\theta}_s sin(\phi_d) cos(\theta_{g_m})$
	A transformation from the x-y plane into the x and y axes	$\omega_x = \dot{\theta}_s sin(\phi_d) cos(\theta_g) sin(\phi_{g_m})$
	A transformation from the x-y plane into the x and y axes	$\omega_y = \dot{\theta}_s sin(\phi_d) cos(\theta_g) cos(\phi_{g_m})$
		$\dot{\theta}_{g_m}$
	Has a x component along $O_{g_m} - a$	$\omega_x = -\dot{\theta}_{g_m} cos(\phi_{g_m})$
	Has a y component along $O_{g_m} - a$	$\omega_y = \dot{\theta}_{g_m} sin(\phi_{g_m})$
		$\dot{\phi}_{g_m}$
	Has a z component along $O_{g_m} - z$	$\omega_z = \dot{\phi}_{g_m}$

Collecting the various contributions to $\omega_x, \omega_y, \omega_z$ we obtain the following expressions for the angular velocities of the gyroscopes in their body fixed axes

$$\omega_x^{(\mathrm{m})} = -\dot{\theta}_\mathrm{s}\cos(\phi_\mathrm{d} + \delta_\mathrm{m})\cos(\phi_{\mathrm{g_m}}) + \dot{\theta}_\mathrm{s}\sin(\phi_\mathrm{d} + \delta_\mathrm{m})\cos(\theta_{\mathrm{g_m}})\sin(\phi_{\mathrm{g_m}}) + \dot{\phi}_\mathrm{d}\sin(\theta_{\mathrm{g_m}})\sin(\phi_{\mathrm{g_m}}) - \dot{\theta}_{\mathrm{g_m}}\cos(\phi_{\mathrm{g_m}}) \quad (3.39)$$

$$\omega_y^{(\mathrm{m})} = \dot{\theta}_\mathrm{s}\cos(\phi_\mathrm{d} + \delta_\mathrm{m})\sin(\phi_{\mathrm{g_m}}) + \dot{\theta}_\mathrm{s}\sin(\phi_\mathrm{d} + \delta_\mathrm{m})\cos(\theta_{\mathrm{g_m}})\cos(\phi_{\mathrm{g_m}}) + \dot{\phi}_\mathrm{d}\sin(\theta_{\mathrm{g_m}})\cos(\phi_{\mathrm{g_m}}) + \dot{\theta}_{\mathrm{g_m}}\sin(\phi_{\mathrm{g_m}}) \quad (3.40)$$

$$\omega_z^{(\mathrm{m})} = -\dot{\theta}_\mathrm{s}\sin(\phi_\mathrm{d} + \delta_\mathrm{m})\sin(\theta_{\mathrm{g_m}}) + \dot{\phi}_\mathrm{d}\cos(\theta_{\mathrm{g_m}}) + \dot{\phi}_{\mathrm{g_m}} \quad (3.41)$$

where δ_m relates to the angular position of each of the four gyroscopes eg. when $m = 1,\ \delta_\mathrm{m} = 0$ or when $m = 3,\ \delta_\mathrm{m} = \pi$ etc

From Equation (3.28) we required $\left(\omega_\mathrm{x}^{(\mathrm{m})^2} + \omega_\mathrm{y}^{(\mathrm{m})^2}\right)$ and $\omega_\mathrm{z}^{(\mathrm{m})^2}$. Combining Equations (3.39) and (3.40) results in

$$\begin{aligned}\omega_\mathrm{x}^{(\mathrm{m})^2} + \omega_\mathrm{y}^{(\mathrm{m})^2} = {} & \big[-\dot{\theta}_\mathrm{s}\cos(\phi_\mathrm{d} + \delta_\mathrm{m})\cos(\phi_{\mathrm{g_m}}) \\ & + \dot{\theta}_\mathrm{s}\sin(\phi_\mathrm{d} + \delta_\mathrm{m})\cos(\theta_{\mathrm{g_m}})\sin(\phi_{\mathrm{g_m}}) \\ & + \dot{\phi}_\mathrm{d}\sin(\theta_{\mathrm{g_m}})\sin(\phi_{\mathrm{g_m}}) - \dot{\theta}_{\mathrm{g_m}}\cos(\phi_{\mathrm{g_m}})\big]^2 \\ & + \big[\dot{\theta}_\mathrm{s}\cos(\phi_\mathrm{d} + \delta_\mathrm{m})\sin(\phi_{\mathrm{g_m}}) \\ & + \dot{\theta}_\mathrm{s}\sin(\phi_\mathrm{d} + \delta_\mathrm{m})\cos(\theta_{\mathrm{g_m}})\cos(\phi_{\mathrm{g_m}}) \\ & + \dot{\phi}_\mathrm{d}\sin(\theta_{\mathrm{g_m}})\cos(\phi_{\mathrm{g_m}}) + \dot{\theta}_{\mathrm{g_m}}\sin(\phi_{\mathrm{g_m}})\big]^2\end{aligned}$$

$$\omega_x^{(m)^2} + \omega_y^{(m)^2} = \left(\dot{\theta}_s \cos(\phi_d + \delta_m) + \dot{\theta}_{g_m}\right)^2 + \left(\dot{\theta}_s \sin(\phi_d + \delta_m)\cos\left(\theta_{g_m}\right) + \dot{\phi}_d \sin\left(\theta_{g_m}\right)\right)^2 \quad (3.42)$$

See Appendix A for the full working of this simplification.

We therefore have

$$\sum_m I\left(\omega_x^{(m)^2} + \omega_y^{(m)^2}\right) = I\sum_m \left[\left(\dot{\theta}_s \cos(\phi_d + \delta_m) + \dot{\theta}_{g_m}\right)^2 + \left(\dot{\theta}_s \sin(\phi_d + \delta_m)\cos\left(\theta_{g_m}\right) + \dot{\phi}_d \sin\left(\theta_{g_m}\right)\right)^2\right] \quad (3.43)$$

Substitution of Equation (3.35) along with the solutions

$$\begin{aligned} m = 1,\ \delta_m = 0 \quad &\Rightarrow \quad \cos(\phi_d + 0) = \cos(\phi_d) \\ m = 2,\ \delta_m = \frac{\pi}{2} \quad &\Rightarrow \quad \cos\left(\phi_d + \frac{\pi}{2}\right) = -\sin(\phi_d) \\ m = 3,\ \delta_m = \pi \quad &\Rightarrow \quad \cos(\phi_d + \pi) = -\cos(\phi_d) \\ m = 4,\ \delta_m = \frac{3\pi}{2} \quad &\Rightarrow \quad \cos\left(\phi_d + \frac{3\pi}{2}\right) = \sin(\phi_d) \end{aligned} \quad (3.44)$$

from which the following simplification can be derived

$$\dot{\theta}_s{}^2 \cos^2(\phi_d) + \dot{\theta}_s{}^2 \cos^2\left(\phi_d + \frac{\pi}{2}\right) + \dot{\theta}_s{}^2 \cos^2(\phi_d + \pi) + \dot{\theta}_s{}^2 \cos^2\left(\phi_d + \frac{3\pi}{2}\right) = 2\dot{\theta}_s{}^2 \quad (3.45)$$

into Equation (3.43) produces the result

$$\sum_{m} I\left(\omega_x^{(m)^2} + \omega_y^{(m)^2}\right) = 2I\left(\dot{\theta}_s{}^2 + 2\dot{\theta}_g{}^2 + \dot{\theta}_s{}^2\cos^2(\theta_g) + 2\dot{\phi}_d{}^2\sin^2(\theta_g)\right) \quad (3.46)$$

Note that we also assume

$\theta_{g_1} = \theta_{g_2} = \theta_{g_3} = \theta_{g_4} = \theta_g$ (all gyros pivot at an equal angle)

$\phi_{g_1} = \phi_{g_2} = \phi_{g_3} = \phi_{g_4} = \phi_g$ (all gyros have equal rotational speed)

We also require the $\omega_z^{(m)}$ component in Equation (3.28). Substitution of Equation (3.35) into Equation (3.41) results in

$$\sum_{m} I_z\left(\omega_z^{(m)^2}\right) = 2I_z\left[\dot{\theta}_s{}^2\sin^2(\theta_g) + 2\left(\dot{\phi}_g + \dot{\phi}_d\cos(\theta_g)\right)^2\right] \quad (3.47)$$

The total kinetic energy of the gyroscopes is therefore

$$\begin{aligned}&\sum_{m}\left(I\left(\omega_x^{(m)^2} + \omega_y^{(m)^2}\right) + I_z\omega_z^{(m)^2}\right)\\ &= 2I\left[\dot{\theta}_s{}^2 + 2\dot{\theta}_g{}^2 + \dot{\theta}_s{}^2\cos^2(\theta_g) + 2\dot{\phi}_d{}^2\sin^2(\theta_g)\right]\\ &\quad + 2I_z\left[\dot{\theta}_s{}^2\sin^2(\theta_g) + 2\left(\dot{\phi}_g + \dot{\phi}_d\cos(\theta_g)\right)^2\right]\end{aligned} \quad (3.48)$$

We make the simplifying assumption that $I = I_z$ and obtain

$$\sum_m I\left(\omega_x^{(m)^2} + \omega_y^{(m)^2}\right) + I\omega_z^{(m)^2}$$

$$= 2I\dot{\theta}_s{}^2 + 4I\dot{\theta}_g{}^2 + 2I\dot{\theta}_s{}^2\cos^2(\theta_g) + 4I\dot{\phi}_d{}^2\sin^2(\theta_g)$$

$$+2I\dot{\theta}_s{}^2\sin^2(\theta_g) + 4I\left(\dot{\phi}_g + \dot{\phi}_d\cos(\theta_g)\right)^2$$

$$= 2I\dot{\theta}_s{}^2 + 4I\dot{\theta}_g{}^2 + \left[2I\dot{\theta}_s{}^2\cos^2(\theta_g) + 2I\dot{\theta}_s{}^2\sin^2(\theta_g)\right]$$

$$+4I\dot{\phi}_d{}^2\sin^2(\theta_g) + 4I\left(\dot{\phi}_g + \dot{\phi}_d\cos(\theta_g)\right)^2$$

$$= 2I\dot{\theta}_s{}^2 + 4I\dot{\theta}_g{}^2 + 2I\dot{\theta}_s{}^2 + 4I\dot{\phi}_d{}^2\sin^2(\theta_g) + 4I\left(\dot{\phi}_g + \dot{\phi}_d\cos(\theta_g)\right)^2$$

$$= 4I\left[\dot{\theta}_s{}^2 + \dot{\theta}_g{}^2 + \dot{\theta}_s{}^2 + \dot{\phi}_d{}^2\sin^2(\theta_g)\right] + 4I\left(\dot{\phi}_g + \dot{\phi}_d\cos(\theta_g)\right)^2 \qquad \textit{(3.49)}$$

We can make one final simplifying substitution based upon $\theta_g = \frac{\pi}{2} - \theta_s$ and the equation for the angular velocity of the gyroscopes reduces to

$$\frac{1}{2}\sum_m I\left(\omega_x^{(m)^2} + \omega_y^{(m)^2}\right) + I\omega_z^{(m)^2}$$

$$= 2I\left[2\dot{\theta}_s{}^2 + \dot{\phi}_d{}^2\cos^2(\theta_s)\right] + 2I\left(\dot{\phi}_g + \dot{\phi}_d\sin(\theta_s)\right)^2 \qquad \textit{(3.50)}$$

3.10.4 Total kinetic energy of gyroscopes

The total kinetic energy of the gyroscopes can now be determined. Substituting Equations (3.37) and (3.50) into Equation (3.28) results in

$$T_g = \frac{1}{2}\sum_m M_{g_m}\left(v_{O_{g_x}}^{(m)^2} + v_{O_{g_y}}^{(m)^2} + v_{O_{g_z}}^{(m)^2}\right)$$

$$+\frac{1}{2}\sum_m \left(I\left(\omega_x^{(m)^2} + \omega_y^{(m)^2}\right) + I_z\omega_z^{(m)^2}\right)$$

$$= 2M_g\left(r_d{}^2\dot{\phi}_d{}^2 + h_d{}^2\dot{\theta}_s{}^2\right) + 2I\left[2\dot{\theta}_s{}^2 + \dot{\phi}_d{}^2\cos^2(\theta_s)\right]$$

$$+2I\left(\dot{\phi}_g + \dot{\phi}_d\sin(\theta_s)\right)^2 \qquad (3.51)$$

3.10.5 Potential energy of gyroscopes

The potential energy of the gyroscopes is determined from their mass M_g and the height of the COM of the disc h_d above the origin O_s.

Again we make the simplifying assumption that the gyroscopes can be represented as four point masses at their centre of mass and obtain

$$V_g = 4M_g g h_d \cos\theta_s \qquad (3.52)$$

3.10.6 Lagrangian for the gyroscopes

The Lagrangian for the gyroscopes is therefore a combination of Equations (3.51) and (3.52)

$$L_g = T_g - V_g$$

$$\begin{aligned} &= 2M_g\left(r_d{}^2\dot{\phi}_d{}^2 + h_d{}^2\dot{\theta}_s{}^2\right) + 2I\left[2\dot{\theta}_s{}^2 + \dot{\phi}_d{}^2\cos^2(\theta_s)\right] \\ &+2I\left(\dot{\phi}_g + \dot{\phi}_d\sin(\theta_s)\right)^2 - 4M_g g h_d\cos\theta_s \end{aligned} \qquad (3.53)$$

3.11 Lagrangian for the stable platform system

The total Lagrangian for the system can now be expressed as a combination of Equations (3.12), (3.24) and (3.53).

$$L_{Total} = L_s + L_d + L_g$$

$$\begin{aligned} &= \frac{1}{2}M_s h_s{}^2\dot{\theta}_s{}^2 - M_s g h_s\cos\theta_s + \frac{1}{2}M_d h_d{}^2\dot{\theta}_s{}^2 + \frac{1}{2}I_z^{(d)}\dot{\phi}_d{}^2 - M_d g h_d\cos\theta_s \\ &+2M_g\left(r_d{}^2\dot{\phi}_d{}^2 + h_d{}^2\dot{\theta}_s{}^2\right) + 2I\left[2\dot{\theta}_s{}^2 + \dot{\phi}_d{}^2\cos^2(\theta_s)\right] \\ &+2I\left(\dot{\phi}_g + \dot{\phi}_d\sin(\theta_s)\right)^2 - 4M_g g h_d\cos\theta_s \end{aligned}$$

$$= \frac{1}{2} M_s {h_s}^2 {\dot{\theta}_s}^2 + \frac{1}{2} M_d {h_d}^2 {\dot{\theta}_s}^2 + \frac{1}{2} I_z^{(d)} {\dot{\phi}_d}^2 + 2M_g \left({r_d}^2 {\dot{\phi}_d}^2 + {h_d}^2 {\dot{\theta}_s}^2 \right)$$
$$+ 2I \left[2{\dot{\theta}_s}^2 + {\dot{\phi}_d}^2 \cos^2(\theta_s) \right] + 2I \left(\dot{\phi}_g + \dot{\phi}_d \sin(\theta_s) \right)^2$$
$$- M_s g h_s \cos\theta_s - \left(M_d + 4M_g \right) g h_d \cos\theta_s$$

$$= \frac{1}{2} \left(M_s {h_s}^2 + \left(M_d + 4M_g \right) {h_d}^2 + 8I \right) {\dot{\theta}_s}^2 + \frac{1}{2} \left(I_z^{(d)} + 4M_g {r_d}^2 \right) {\dot{\phi}_d}^2$$
$$+ 2I \left[{\dot{\phi}_d}^2 \cos^2(\theta_s) \right] + 2I \left(\dot{\phi}_g + \dot{\phi}_d \sin(\theta_s) \right)^2$$
$$- \left(M_s h_s + \left(M_d + 4M_g \right) h_d \right) g \cos\theta_s$$

$$= \frac{1}{2} \left(M_s {h_s}^2 + \left(M_d + 4M_g \right) {h_d}^2 + 8I \right) {\dot{\theta}_s}^2$$
$$+ \frac{1}{2} \left(I_z^{(d)} + 4M_g {r_d}^2 + 4I\cos^2(\theta_s) \right) {\dot{\phi}_d}^2$$
$$+ 2I \left(\dot{\phi}_g + \dot{\phi}_d \sin(\theta_s) \right)^2$$
$$- \left(M_s h_s + \left(M_d + 4M_g \right) h_d \right) g \cos\theta_s \qquad (3.54)$$

3.12 Concluding comments

The Lagrangian for the stable platform has been derived (Equation (3.54)) and reduced to its simplest form. This equation will be used to derive the equations of motion of the system which in turn will be used to determine the behaviour of the system as it stabilizes an external structure. Conditions upon the behaviour will then be stipulated and used in the physical design of the system.

4

Derivation of Equations of Motion and Stability Conditions

4.1 Introduction

Having established the Lagrangian equation for the stable platform system in Chapter 3, the equations of motion that describe the systems behaviour can be determined. The equations of motion can then be used to derive stability conditions that will be used in the design of the stable platform.

The objective of this chapter is to derive a set of equations of motion from the Lagrangian that relate to the behaviour of the stable platform. This set of equations will then be used to derive an inequality condition that will govern the response of the stable platform during operation. This inequality will also be used in the physical design of the system to optimise the stabilizing moment it is able to produce.

The process used in the derivation of the equations of motions and inequality is adopted from Cousins (1913).

4.2 Lagrangian formalism for platform system

From Chapter 3, Equation (3.54), the Lagrangian of the system is described as

$$\begin{aligned} L_{Total} = {} & \frac{1}{2}\left(M_s {h_s}^2 + \left(M_d + 4M_g\right){h_d}^2 + 8I\right){\dot{\theta}_s}^2 \\ & + \frac{1}{2}\left(I_z^{(d)} + 4M_g {r_d}^2 + 4I\cos^2(\theta_s)\right){\dot{\phi}_d}^2 \\ & + 2I\left(\dot{\phi}_g + \dot{\phi}_d \sin(\theta_s)\right)^2 \\ & - \left(M_s h_s + \left(M_d + 4M_g\right)h_d\right)g\cos\theta_s \end{aligned} \qquad (3.54)$$

4.2.1 Lagrangian formalisation

The equations of motion for each variable are given by the Lagrangian equation

$$\frac{d}{dt}\left(\frac{\partial L}{\partial \dot{q}_m}\right) - \left(\frac{\partial L}{\partial q_m}\right) = F_{q_m} \qquad m=1\ldots4$$

where F_{q_m} is the non conservative generalised force associated with q_m.

4.2.2 Equation of motion for ϕ_g

The following calculations relate to the derivation of the EOM for the rotational motion of the gyroscopes (ϕ_g). There is no generalised force acting on this body. Therefore

$$F_{\phi_g} = 0 \tag{4.1}$$

$$\frac{\partial \mathrm{L}}{\partial \phi_g} = 0 \tag{4.2}$$

$$\frac{\partial \mathrm{L}}{\partial \dot{\phi}_g} = 4\mathrm{I}\left(\dot{\phi}_\mathrm{g} + \dot{\phi}_\mathrm{d}\sin(\theta_\mathrm{s})\right) \tag{4.3}$$

Combining Equations (4.1), (4.2) and (4.3) results in the equation of motion for ϕ_g as

$$\frac{\mathrm{d}}{\mathrm{dt}}\left(4\mathrm{I}\left(\dot{\phi}_\mathrm{g} + \dot{\phi}_\mathrm{d}\sin(\theta_\mathrm{s})\right)\right) - 0 = 0 \tag{4.4}$$

Resolving Equation (4.4) gives

$$4\mathrm{I}\left(\dot{\phi}_\mathrm{g} + \dot{\phi}_\mathrm{d}\sin(\theta_\mathrm{s})\right) = \mathrm{C}_{\phi_g} \tag{4.5}$$

where C_{ϕ_g} is a constant that we approximate as $4\mathrm{I}\dot{\phi}_\mathrm{g}$ (based upon θ_s being very small such that $\sin(\theta_\mathrm{s}) = 0$)

4.2.3 Equation of motion for ϕ_d

The following calculations relate to the derivation of the EOM for the rotational motion of the main disc as it precesses back and forth (ϕ_d). There is a non conservative force present which physically acts to change the rotation of the disc (i.e. a motor).

The force F_{ϕ_d} can be expressed as

$$F_{\phi_d} = -\mu\dot{\phi}_d + C(\omega_0)\sin(\theta_s) \qquad (4.6)$$

where μ relates to the coefficient of friction the motor must overcome to initiate rotation of the disc (from bearings, gear backlash etc)

$C(\omega_0)$ is the torque exerted by a gyroscope made to precess at a rate of ω_0 in the direction perpendicular to its axis of rotation when the structure deviates from the vertical.

Note that at high speeds we may take

$$C(\omega_0) = \mathrm{C}\omega_0 \text{ where } \mathrm{C} = \mathrm{I}\dot{\phi}_\mathrm{g}\left(\frac{\mathrm{r_g}+\mathrm{r_d}}{\mathrm{r_g}}\right) \qquad (4.7)$$

where $\mathrm{r_g}$ is the distance from the gyroscope gimbal frame pivot to the end of the outer contact arm

$\mathrm{r_d}$ is the distance from the disc central pivot axis to the gyroscope gimbal frame pivot

such that $\left(\frac{\mathrm{r_g}+\mathrm{r_d}}{\mathrm{r_g}}\right)$ is the transformation of the moment $\mathrm{I}\dot{\phi}_\mathrm{g}\omega_0$ produced by the gimbal frame at its pivot point to the disc central pivot point.

We are able to make the assumption $C(\omega_0) = \mathrm{C}\omega_0$ as the function $C(\omega_0)$ has a dependence upon the rotational speeds of the gyroscopes. Because the rotational speed of the gyroscopes is so much higher than the rotational speed of the disc, variations in the speed of the disc are negligible. Because of this we can approximate the function as a constant.

$$\frac{\partial \mathrm{L}}{\partial \phi_d} = 0 \tag{4.8}$$

$$\frac{\partial \mathrm{L}}{\partial \dot{\phi}_d} = \left(\mathrm{I}_{\mathrm{z}}^{(\mathrm{d})} + 4\mathrm{M}_{\mathrm{g}}{\mathrm{r}_{\mathrm{d}}}^2 + 4\mathrm{I}\cos^2(\theta_{\mathrm{s}})\right)\dot{\phi}_{\mathrm{d}} + \mathrm{C}_{\phi_g}\sin(\theta_{\mathrm{s}}) \tag{4.9}$$

Combining Equations (4.6), (4.8) and (4.9) results in the equation of motion for ϕ_d as

$$\frac{\mathrm{d}}{\mathrm{dt}}\left[\left(\mathrm{I}_{\mathrm{z}}^{(\mathrm{d})} + 4\mathrm{M}_{\mathrm{g}}{\mathrm{r}_{\mathrm{d}}}^2 + 4\mathrm{I}\cos^2(\theta_{\mathrm{s}})\right)\dot{\phi}_{\mathrm{d}} + \mathrm{C}_{\phi_g}\sin(\theta_{\mathrm{s}})\right] - 0$$
$$= -\mu\dot{\phi}_{\mathrm{d}} + \mathrm{C}\omega_0\sin(\theta_{\mathrm{s}}) \tag{4.10}$$

Differentiating Equation (4.10) yields

$$\left(\mathrm{I}_{\mathrm{z}}^{(\mathrm{d})} + 4\mathrm{M}_{\mathrm{g}}{\mathrm{r}_{\mathrm{d}}}^2 + 4\mathrm{I}\cos^2(\theta_{\mathrm{s}})\right)\ddot{\phi}_{\mathrm{d}} + 8\mathrm{I}\cos(\theta_{\mathrm{s}})\sin(\theta_{\mathrm{s}})\dot{\theta}_{\mathrm{s}} + \mathrm{C}_{\phi_g}\cos(\theta_{\mathrm{s}})\dot{\theta}_{\mathrm{s}}$$
$$= \mu\dot{\phi}_{\mathrm{d}} + \mathrm{C}\omega_0\sin(\theta_{\mathrm{s}}) \tag{4.11}$$

4.2.4 Equation of motion for θ_s

The following calculations relate to the derivation of the EOM for the tipping motion of the external structure as it deviates from the vertical (θ_s). There is no generalised force acting on this body.

$$F_{\theta_s} = 0 \tag{4.12}$$

$$\frac{\partial \mathrm{L}}{\partial \theta_s} = 4\mathrm{I}\cos(\theta_\mathrm{s})\sin(\theta_\mathrm{s})\dot{\phi}_\mathrm{d}{}^2 + \mathrm{C}_{\phi_g}\dot{\phi}_\mathrm{d}\cos(\theta_\mathrm{s}) + \left(\mathrm{M_s h_s} + \left(\mathrm{M_d} + 4\mathrm{M_g}\right)\mathrm{h_d}\right)\mathrm{g}\sin(\theta_\mathrm{s}) \tag{4.13}$$

$$\frac{\partial \mathrm{L}}{\partial \dot{\theta}_s} = \left(\mathrm{M_s h_s}^2 + \left(\mathrm{M_d} + 4\mathrm{M_g}\right)\mathrm{h_d}^2 + 8\mathrm{I}\right)\dot{\theta}_\mathrm{s} \tag{4.14}$$

Combining Equations (4.12), (4.13) and (4.14) results in the equation of motion for θ_s as

$$\frac{\mathrm{d}}{\mathrm{dt}}\left[\left(\mathrm{M_s h_s}^2 + \left(\mathrm{M_d} + 4\mathrm{M_g}\right)\mathrm{h_d}^2 + 8\mathrm{I}\right)\dot{\theta}_\mathrm{s}\right] + 4\mathrm{I}\cos(\theta_\mathrm{s})\sin(\theta_\mathrm{s})\dot{\phi}_\mathrm{d}{}^2 - \left[\mathrm{C}_{\phi_g}\dot{\phi}_\mathrm{d}\cos(\theta_\mathrm{s}) + \left(\mathrm{M_s h_s} + \left(\mathrm{M_d} + 4\mathrm{M_g}\right)\mathrm{h_d}\right)\mathrm{g}\sin(\theta_\mathrm{s})\right] = 0 \tag{4.15}$$

which when differentiated and simplified results in

$$\left(\mathrm{M_s h_s}^2 + \left(\mathrm{M_d} + 4\mathrm{M_g}\right)\mathrm{h_d}^2 + 8\mathrm{I}\right)\ddot{\theta}_\mathrm{s} + 4\mathrm{I}\cos(\theta_\mathrm{s})\sin(\theta_\mathrm{s})\dot{\phi}_\mathrm{d}{}^2 - \mathrm{C}_{\phi_g}\dot{\phi}_\mathrm{d}\cos(\theta_\mathrm{s}) - \left(\mathrm{M_s h_s} + \left(\mathrm{M_d} + 4\mathrm{M_g}\right)\mathrm{h_d}\right)\mathrm{g}\sin(\theta_\mathrm{s}) = 0 \tag{4.16}$$

4.2.5 Final equations of motion for stable platform

Based on our initial simplifying assumptions the motion of the system can be described by: ϕ_g, the rotation of gyroscopes; ϕ_d, the rotation of the disc; and θ_s, the deviation of the external structure from the vertical. Therefore, the three equations that describe the motion of the system are:

For ϕ_g,

$$C_{\phi_g} = 4I\dot{\phi}_g \tag{4.5}$$

For ϕ_d,

$$\left(I_z^{(d)} + 4M_g {r_d}^2 + 4I\cos^2(\theta_s)\right)\ddot{\phi}_d + 8I\cos(\theta_s)\sin(\theta_s)\dot{\theta}_s + C_{\phi_g}\cos(\theta_s)\dot{\theta}_s = -\mu\dot{\phi}_d + C\omega_0\sin(\theta_s) \tag{4.11}$$

For θ_s,

$$\left(M_s {h_s}^2 + \left(M_d + 4M_g\right){h_d}^2 + 8I\right)\ddot{\theta}_s + 2I\sin(2\theta_s){\dot{\phi}_d}^2 - C_{\phi_g}\dot{\phi}_d\cos(\theta_s) - \left(M_s h_s + \left(M_d + 4M_g\right)h_d\right)g\sin(\theta_s) = 0 \tag{4.16}$$

4.3 Derivation of system stability conditions

Having established the equations of motion of the stable platform system it is desirable to derive a set of stability conditions that will govern the system's

behaviour. Manipulation of the values in these stability conditions will govern the type of motion the system will exhibit.

4.3.1 Position of equilibrium

To be able to derive the conditions for stability, the position of equilibrium must be determined. This is described as the position the system would take if there were no changes to its position (that is, all accelerations and relevant velocities are equal to zero).

We look for conditions that allow us to have

$$\ddot{\phi}_d, \ddot{\theta}_s = 0$$

Inspection of Equations (4.11) and (4.16) reveals that for the above condition to be satisfied we require several of the system variables to be equal to zero. The conditions established for the position of equilibrium are therefore defined as

$$\theta_s = 0$$

$$\dot{\phi}_d = \dot{\theta}_s = 0 \qquad (4.17)$$

4.3.2 Conditions of stability

To determine the nature of the equilibrium position we look at the nature of small deviations from it. We obtain a general solution for the system by writing an equation

that includes the nature of small deviations from the equilibrium of each of the variables that define the motion of the system. It is therefore assumed that

$$\phi_d(t) = 0 + \delta\phi_d(t)$$

$$\theta_s(t) = 0 + \delta\theta_s(t) \qquad (4.18)$$

where $\delta\phi_d(t)$ represents small deviations in the variable $\phi_d(t)$ and $\delta\theta_s(t)$ represents small deviations in the variable $\theta_s(t)$.

Equations (4.11) and (4.16) govern the behaviour of the system about the equilibrium point. Substituting in Equations (4.17) and (4.18) into Equations (4.11) and (4.16) and retaining only first order terms yields a set of two equations with two degrees of freedom

$$\left(I_z^{(d)} + 4M_g {r_d}^2 + 4I\right)\delta\ddot{\phi}_d + C_{\phi_g}\delta\dot{\theta}_s = -\mu\delta\dot{\phi}_d + C\omega_0\delta\theta_s \qquad (4.19)$$

$$\left(M_s {h_s}^2 + \left(M_d + 4M_g\right){h_d}^2 + 8I\right)\delta\ddot{\theta}_s - C_{\phi_g}\delta\dot{\phi}_d$$
$$-\left(M_s h_s + \left(M_d + 4M_g\right)h_d\right)\delta\theta_s = 0 \qquad (4.20)$$

Note we use the small angle approximation to the trigonometric functions based on Taylor's expansion (in the form of radians rather than degrees)

$$\sin(x) \approx x$$

$$\cos(x) \approx 1$$

4.3.3 Derivation of general solution to first order equations

Assuming that solutions to equations (4.19) and (4.20) are of the form

$$\delta\phi_d(t) = \phi_d^0 e^{\lambda t}$$

$$\delta\theta_s(t) = \theta_s^0 e^{\lambda t} \qquad (4.21)$$

the general equations of motion of the system for small deviations from the equilibrium position become

$$\left(I_z^{(d)} + 4M_g {r_d}^2 + 4I\right)\lambda^2\phi_d^0 + C_{\phi_g}\lambda\theta_s^0 = -\mu\lambda\phi_d^0 + C\omega_0\theta_s^0 \qquad (4.22)$$

$$\left(M_s {h_s}^2 + \left(M_d + 4M_g\right){h_d}^2 + 8I\right)\lambda^2\theta_s^0 - C_{\phi_g}\lambda\phi_d^0$$
$$-\left(M_s h_s + \left(M_d + 4M_g\right)h_d\right)g\theta_s^0 = 0 \qquad (4.23)$$

which can be simplified to

$$\left[\left(I_z^{(d)} + 4M_g {r_d}^2 + 4I\right)\lambda^2 - \mu\lambda\right]\phi_d^0 + \left[C_{\phi_g}\lambda - C\omega_0\right]\theta_s^0 = 0 \qquad (4.24)$$

$$\left[\left(M_s {h_s}^2 + \left(M_d + 4M_g\right){h_d}^2 + 8I\right)\lambda^2 - \left(M_s h_s + \left(M_d + 4M_g\right)h_d\right)g\right]\theta_s^0$$
$$-C_{\phi_g}\lambda\phi_d^0 = 0 \qquad (4.25)$$

4.3.4 Stability matrix

Substitution of the above assumptions about the form of $\delta\phi_d(t)$ and $\delta\theta_s(t)$ yields the matrix system:

$$\begin{bmatrix} \left(I_z^{(d)} + 4M_g {r_d}^2 + 4I\right)\lambda^2 - \mu\lambda & C_{\phi_g}\lambda - C\omega_0 \\ -C_{\phi_g}\lambda & \left(M_s {h_s}^2 + \left(M_d + 4M_g\right){h_d}^2 + 8I\right)\lambda^2 - \left(M_s h_s + \left(M_d + 4M_g\right)h_d\right) \end{bmatrix} \begin{bmatrix} \phi_d^0 \\ \theta_s^0 \end{bmatrix} = 0$$

For the purpose of simplification, the following substitutions are made

$$A = \left(I_z^{(d)} + 4M_g {r_d}^2 + 4I\right) \tag{4.26}$$

$$B = \left(M_s {h_s}^2 + \left(M_d + 4M_g\right){h_d}^2 + 8I\right) \tag{4.27}$$

$$D = \left(M_s h_s + \left(M_d + 4M_g\right)h_d\right)g \tag{4.28}$$

And the matrix becomes

$$M_{stability} = \begin{bmatrix} A\lambda^2 - \mu\lambda & C_{\phi_g}\lambda - C\omega_0 \\ -C_{\phi_g}\lambda & B\lambda^2 - D \end{bmatrix} \tag{4.29}$$

which is known as the stability matrix of the system (Luong, (1996)).

4.3.5 System characteristic equation

The characteristic equation of the system is defined as the determinant of the stability matrix ($M_{stability}$) and must be equal to zero for a non trivial solution to exist.

The characteristic equation for this system is the 4th order polynomial shown below

$$\begin{aligned}\det\left(M_{stability}\right) &= (\mathrm{A}\lambda^2 - \mu\lambda)(\mathrm{B}\lambda^2 - \mathrm{D}) - \left(\mathrm{C}_{\phi_g}\lambda - \mathrm{C}\omega_0\right)\left(-\mathrm{C}_{\phi_g}\lambda\right) \\ &= \mathrm{AB}\lambda^4 - \mathrm{AD}\lambda^2 - \mu B\lambda^3 + \mu\mathrm{D}\lambda + {\mathrm{C}_{\phi_g}}^2\lambda^2 - \mathrm{C}_{\phi_g}\mathrm{C}\omega_0\lambda \\ &= \lambda\left[\mathrm{AB}\lambda^3 - \mu B\lambda^2 - (\mathrm{AD} - {\mathrm{C}_{\phi_g}}^2)\lambda + \left(\mu\mathrm{D} - \mathrm{C}\omega_0\mathrm{C}_{\phi_g}\right)\right]\end{aligned} \qquad (4.30)$$

and so we need to solve $\det\left(M_{stability}\right) = 0$ to determine the nature of the stability of the equilibrium position (by investigation of its roots).

4.3.6 Behaviour of system from characteristic equation

For the system that is being investigated we required damped oscillations about the equilibrium position. To satisfy this condition we require that the characteristic equation has complex roots whose real parts are negative. It is clear the Equation (4.30) has one root $\lambda = 0$. We now investigate the remaining 3rd order cubic polynomial

$$\mathrm{AB}\lambda^3 - \mu B\lambda^2 - \left(\mathrm{AD} - {\mathrm{C}_{\phi_g}}^2\right)\lambda + \left(\mu\mathrm{D} - \mathrm{C}\omega_0\mathrm{C}_{\phi_g}\right) = 0 \qquad (4.31)$$

(Cousins,1913) states that any 3rd order polynomial in the form

$$\lambda^3 - c_1\lambda^2 + c_2\lambda + c_3 = 0 \tag{4.32}$$

must have roots of the form

$$\lambda_1 = b$$
$$\lambda_2 = a + id$$
$$\lambda_3 = a - id \tag{4.33}$$

This satisfies the conditions we have imposed on the behaviour of the system. We therefore continue to investigate this behaviour of our system based upon the above results. Firstly, we write our 3rd order polynomial in the form of Equation (4.32)

$$\lambda^3 - \frac{\mu}{A}\lambda^2 - \frac{(AD - C_{\phi_g}{}^2)}{AB}\lambda + \frac{\left(\mu D - C\omega_0 C_{\phi_g}\right)}{AB} \tag{4.34}$$

which results in

$$c_1 = \frac{\mu}{A} \tag{4.35}$$

$$c_2 = -\frac{(AD - C_{\phi_g}{}^2)}{AB} \tag{4.36}$$

$$c_3 = \frac{\left(\mu D - C\omega_0 C_{\phi_g}\right)}{AB} \tag{4.37}$$

As we are only concerned with the case where the roots of characteristic equation has complex conjugate roots (oscillatory damped behaviour) let us assume that Equation (4.43) has roots $b, a + id, a - id$ then

$$(\lambda - b)\big(\lambda - (a + id)\big)\big(\lambda - (a + id)\big)$$

$$= (\lambda - b)(\lambda^2 - (a + id)\lambda) - (a + id)\lambda + (a^2 + d^2)$$

$$= (\lambda - b)(\lambda^2 - 2a\lambda + (a^2 + d^2))$$

$$= (\lambda^3 - 2a\lambda^2 + (a^2 + d^2)\lambda - b\lambda^2 + 2ab\lambda - (a^2 + d^2)b)$$

$$= \lambda^3 - (2a + b)\lambda^2 + \big((a^2 + d^2) + 2ab\big)\lambda - (a^2 + d^2)b \tag{4.38}$$

which now written in the form of Equation (4.32) results in

$$c_1 = 2a + b \tag{4.39}$$

$$c_2 = (a^2 + d^2) + 2ab \tag{4.40}$$

$$c_3 = -(a^2 + d^2)b \tag{4.41}$$

Equating Equation (4.35) to Equation (4.39), Equation (4.36) to (4.40) and Equation (4.37) to (4.41) (that is $c_1 = c_1$, $c_2 = c_2$ and $c_3 = c_3$) we obtain the results

$$2a + b = \frac{\mu}{A} \tag{4.42}$$

$$(a^2 + d^2) + 2ab = -\frac{(AD - C_{\phi_g}{}^2)}{AB} \tag{4.43}$$

$$-(a^2 + d^2)b = \frac{\left(\mu D - C\omega_0 C_{\phi_g}\right)}{AB} \tag{4.44}$$

Based upon our desired damped oscillatory behaviour we know that we require b to always be positive (the real root is positive) and a to always be negative (the real part of our complex conjugates are negative) in Equations (4.42), (4.43) and (4.44).

Investigating Equation (4.44) reveals

$$-(a^2 + d^2) = \frac{\left(\mu D - C\omega_0 C_{\phi_g}\right)}{ABb} \tag{4.45}$$

From physical values for A and B we know they must always be positive (as A and B depend upon physical parameters like dimensions or speeds), therefore for the above condition to hold true we require

$$\left(\mu D - C\omega_0 C_{\phi_g}\right) < 0$$

or

$$\mu D < C\omega_0 C_{\phi_g} \tag{4.46}$$

Substituting in our values for D (Equation (4.28)), C (Equation (4.7)) and C_{ϕ_g} (Equation (4.5)) results in the condition (for the system to experience the desired damped oscillatory behaviour) being

$$\mu\left[\left(M_s h_s + (M_d + 4M_g)h_d\right)g\right] < \left[I\dot{\phi}_g\left(\frac{r_g + r_d}{r_g}\right)\right]\omega_0\left(4I\left(\dot{\phi}_g\right)\right)$$

which simplifies to

$$\left(M_s h_s + (M_d + 4M_g)h_d\right)g\mu < 4(I)^2\left(\dot{\phi}_g\right)^2\omega_0\left(\frac{r_g + r_d}{r_g}\right) \tag{4.47}$$

We also investigate Equation (4.43). From Equation (4.45) and Equation (4.40) we obtain

$$(a^2 + d^2) = -\frac{\left(C\omega_0 C_{\phi_g} - \mu D\right)}{ABb} = -\frac{(AD - {C_{\phi_g}}^2)}{AB} - 2ab$$

$$-\frac{\left(C\omega_0 C_{\phi_g} - \mu D\right)}{ABb} = -\frac{\left(AD - {C_{\phi_g}}^2\right)}{AB} - 2ab$$

$$2a = -\frac{\left(AD - C_{\phi_g}{}^2\right)}{ABb} - \frac{\left(C\omega_0 C_{\phi_g} - \mu D\right)}{ABb^2} \qquad (4.48)$$

We know that b must always be positive (the real part of our complex conjugates must always be positive for the system to exhibit damped oscillatory behaviour) and $\mu D < C\omega_0 C_{\phi_g}$. Therefore for a to always remain negative we require

$$AD - C_{\phi_g}{}^2 > 0$$

$$-C_{\phi_g}{}^2 > -AD$$

$$C_{\phi_g}{}^2 > AD \qquad (4.49)$$

Substitution of our values for A (Equation (4.26)), D (Equation (4.28)) and $C_{\phi_g}{}^2$ (Equation (4.5)) results in the condition

$$\left(4I\dot{\phi}_g\right)^2 > \left(I_z^{(d)} + 4M_g r_d{}^2 + 4I\right)\left(M_s h_s + \left(M_d + 4M_g\right)h_d\right)g$$

Which simplifies to

$$16I^2\left(\dot{\phi}_g\right)^2 > \left(I_z^{(d)} + 4M_g r_d{}^2 + 4I\right)\left(M_s h_s + \left(M_d + 4M_g\right)h_d\right)g \qquad (4.50)$$

4.4 Concluding comments

The investigation into the behaviour of the system has revealed two conditions on the physical design of the system in order for it to exhibit damped oscillations about the equilibrium point. These are Equations (4.47) and (4.50) repeated here:

$$\left(M_s h_s + (M_d + 4M_g) h_d\right) g\mu < 4(I)^2 \left(\dot{\phi}_g\right)^2 \omega_0 \left(\frac{r_g + r_d}{r_g}\right) \qquad (4.47)$$

$$16I^2 \left(\dot{\phi}_g\right)^2 > \left(I_z^{(d)} + 4M_g {r_d}^2 + 4I\right)\left(M_s h_s + \left(M_d + 4M_g\right) h_d\right) g \qquad (4.50)$$

These conditions will be used in the physical design of the stable platform system. Equation (4.47) is of particular interest as it is a combination of the imbalance torque produced by the mass of the system moving off the vertical (left side of the equation) and the total restoring moment that the stable platform is able to produce (right side of the equation).

5

Investigation of Stable Platform Behaviour

5.1 Introduction

The characteristic equation for the stable platform system has been derived in Chapter 4 (Equation (4.34)). From this, a general solution can be determined that describes the oscillatory motion of the stable platform. Two system conditions will be investigated:

i) Homogeneous system behaviour: this investigation will look at the general solutions that relates to the system when the disc and gyroscope assembly is precessed around only when contact occurs with the tipping of the external structure. As the external structure moves off the horizontal, a switching mechanism will activate the precession. This effectively makes the stabilization process “active”, that is that the precession of the disc depends upon the tipping of the external structure

ii) Driven system behaviour: this investigation will look at the general solutions that relate to the system when the disc and gyroscope assembly is precessed by a drive motor that oscillates the assembly back and forth at a constant frequency, γ. The oscillation frequency is calculated via the general solution and is set to match the natural frequency of the external structure.

The objective of this chapter is to derive the general solutions of the homogeneous and driven systems based upon their associated characteristic equations.

5.2 Homogeneous system

This section presents the derivation of the general solutions to the homogeneous system arrangement.

5.2.1 Characteristic equation

The characteristic equation for the homogeneous system (Equation (4.34)) has been derived in Chapter 4.

$$\lambda^3 - \frac{\mu}{A}\lambda^2 - \frac{(AD - C_{\phi_g}{}^2)}{AB}\lambda + \frac{\left(\mu D - C\omega_0 C_{\phi_g}\right)}{AB} \qquad (4.34)$$

For a general cubic in the form

$$a\lambda^3 + b\lambda^2 + c\lambda + d = 0$$

the general formula for the roots, in terms of the coefficients are expressed in Equations (5.1) - (5.6) (Blinn (2006)).

$$\lambda_k = -\frac{1}{3a}\left(b + u_k C + \frac{\Delta_0}{u_k C}\right) \qquad k \in \{1,2,3\} \qquad (5.1)$$

where

$$u_1 = 1,\ u_2 = \frac{-1 + i\sqrt{3}}{2},\ u_3 = \frac{-1 - i\sqrt{3}}{2} \tag{5.2}$$

$$C = \sqrt[3]{\frac{\Delta_1 + \sqrt{{\Delta_1}^2 - 4{\Delta_0}^3}}{2}} \tag{5.3}$$

$$\Delta_0 = b^2 - 3ac \tag{5.4}$$

$$\Delta_1 = 2b^3 - 9abc + 27a^2d \tag{5.5}$$

Note that the discriminant for a cubic in the above form is

$$\Delta = 18abcd - 4b^3d + b^2c^2 - 4ac^3 - 27a^2d^2 \tag{5.6}$$

and its properties determine the nature of the roots. If $\Delta < 0$ the characteristic equation has positive root and a pair of complex conjugates.

For the system being considered

$$a = AB \tag{5.7}$$

$$b = -\mu B \tag{5.8}$$

$$c = -\left(AD - {C_{\phi_g}}^2\right) \tag{5.9}$$

$$d = \left(\mu D - C\omega_0 C_{\phi_g}\right) \tag{5.10}$$

where Equations (4.5), (4.7), (4.26), (4.27) and (4.28) relate to $C_{\phi_g}, C, A, B \text{ and } D$ respectively.

Using this result it is possible to determine the response of the physical system based upon the physical values selected for the constants in A, B, C, C_{ϕ_g}, D and μ.

5.2.2 Homogeneous system general solutions

Investigation into the general solution of Equation (4.24)

$$[A\lambda^2 - \mu\lambda]\phi_d^0 + \left[C_{\phi_g}\lambda - C\omega_0\right]\theta_s^0 = 0 \tag{4.24}$$

yields the result

$$\theta_s^0 = \left(\frac{C_{\phi_g}\lambda - C\omega_0}{A\lambda^2 - \mu\lambda}\right)\phi_d^0 \tag{5.11}$$

As we require damped oscillations we only consider the complex roots of our characteristic equation (McCallion (1973)). Equation (5.11) will always be in the form

$$\theta_s^0 = (m \pm in)\phi_d^0 \qquad (5.12)$$

We can convert the complex number into polar form such that

$$\theta_s^0 = re^{i\theta}\theta_d^0 \qquad (5.13)$$

where $r = \sqrt{|m|^2 + |n|^2}$

$\tan\theta = \frac{n}{m}$ such that $\theta = \tan^{-1}\left(\frac{n}{m}\right)$

The two general solutions that describe the oscillatory motion of the precession of the disc and deviation from the vertical of the external structure can therefore be written in the form

$$\delta\phi_d(t) = Q_{\phi_d}e^{bt} + e^{-mt}(M_{\phi_d}\cos(nt) + N_{\phi_d}\sin(nt)) \qquad (5.14)$$

$$\delta\theta_s(t) = Q_{\theta_s}e^{bt} + re^{-mt}(M_{\theta_s}\cos(nt + \theta) + N_{\theta_s}\sin(nt + \theta)) \qquad (5.15)$$

Note we have used Euler's formula

$$e^{i\theta} = \cos(\theta) + i\sin(\theta)) \tag{5.16}$$

to write the complex exponential terms in terms of trigonometric functions.

where $M_{\phi_d} = \frac{\phi_d^{0(m+in)} + \phi_d^{0(m-in)}}{2}$

$N_{\phi_d} = \frac{\phi_d^{0(m+in)} - \phi_d^{0(m-in)}}{2i}$

and $M_{\theta_s} = \frac{\theta_s^{0(m+in)} + \theta_s^{0(m-in)}}{2}$

$N_{\theta_s} = \frac{\theta_s^{0(m+in)} - \theta_s^{0(m-in)}}{2i}$

The variable Q can be set as zero eliminating this term from the general solution. Q relates to an initial excitation of the system which is does not occur in the arrangement of the stable platform that is being investigated.

The resulting two general solutions that describe the oscillatory motion of the system are

$$\delta\phi_d(t) = e^{-mt}(M_{\phi_d}\cos(nt) + N_{\phi_d}\sin(nt)) \tag{5.17}$$

$$\delta\theta_s(t) = re^{-mt}(M_{\theta_s}\cos(nt + \theta) + N_{\theta_s}\sin(nt + \theta)) \tag{5.18}$$

5.3 Driven System

Having investigated the response of the system when the precession of the disc responds to the tilt of the system (through a switching contact that initiates the drive motor; for a detailed description as to how this system was implemented refer to Section 7.3.10.), it is useful to know how the system will behave when the disc is oscillated back and forth at a constant frequency by means of an external force.

It should be noted that the system that is driven at a constant oscillating frequency shall be referred to as the driven system. The main motivation for investigating the driven system is that it is a much simpler arrangement to design, manufacture and control.

5.3.1 Advantages of driven system

There are several advantages associated with oscillating the disc at a constant frequency.

- The rotation is much simpler to control (the oscillatory frequency of the motor can easily be adjusted and set at a constant value).

- The precession of the disc through driven oscillations is much more reliable. The precession no longer depends upon contact between the external structure and the disc to begin rotation of the disc.

The main concern with oscillating the disc back and forth is that the stabilizing moment may not always be applied where it is most required. This issue will be eliminated by oscillating the disc at a high frequency.

5.3.2 Updated equations of motion

The addition of a driving force that oscillates the disc back and forth during operation results in a change to the equations of motion. The only body that is affected by this change is ϕ_d, the motion associated with the rotation of the disc. The initial equation of motion that described this rotation of the disc was stated in Equation (4.11).

A driving force term is added to Equation (4.11) which then becomes

$$\left(\mathrm{I_z^{(d)}} + 4\mathrm{M_g r_d}^2 + 4\mathrm{I}\cos^2(\theta_s)\right)\ddot{\phi}_\mathrm{d} + 8\mathrm{I}\cos(\theta_s)\sin(\theta_s)\dot{\theta}_s + \mathrm{C}_{\phi_g}\cos(\theta_s)\dot{\theta}_s = \mu\dot{\phi}_d + \mathrm{C}\omega_0\sin(\theta_s) + \mathrm{F}\cos(\gamma t) \quad \textit{(5.19)}$$

where F is the amplitude of the force associated with the driving of the motor that will oscillate the disc back and forth

γ is the frequency that the driving force oscillates at

5.3.3 Position of equilibrium

As with the homogeneous system, the position of equilibrium must be investigated.

We look for conditions that allow us to have

$$\ddot{\phi}_d, \ddot{\theta}_s = 0$$

Inspection of Equations (5.19) and (4.16)

$$\left(M_s {h_s}^2 + \left(M_d + 4M_g\right){h_d}^2 + 8I\right)\ddot{\theta}_s + 4I\cos(\theta_s)\sin(\theta_s){\dot{\phi}_d}^2$$
$$-C_{\phi_g}\dot{\phi}_d\cos(\theta_s) - \left(M_s h_s + \left(M_d + 4M_g\right)h_d\right)g\sin(\theta_s) = 0 \qquad (4.16)$$

reveals that at $t = 0$ for the above condition to be satisfied we require

$$\theta_s = 0$$

$$\dot{\phi}_d = \dot{\theta}_s = 0$$

These are the same results obtained for the homogeneous system.

5.3.4 Conditions of stability

The general solution to the homogeneous system was written in the form

$$\phi_d(t) = 0 + \delta\phi_d(t)$$

$$\theta_s(t) = 0 + \delta\theta_s(t) \qquad (5.20)$$

where $\delta\phi_d(t)$ represents small deviations in the variable $\phi_d(t)$ and $\delta\phi_s(t)$ represents small deviations in the variable $\phi_s(t)$.

Now that we have added another scenario (oscillating the disc back and forth by external means), the general solution to the overall system becomes

$$\phi_d(t) = \delta\phi_d^0(t) + \delta\phi_d^1(t)$$

$$\theta_s(t) = \delta\theta_s^0(t) + \delta\theta_s^1(t) \qquad (5.21)$$

where $\delta\phi_d^0(t), \delta\theta_s^0(t)$ are the general solutions to the homogenous system (determined in Section 5.2.2) and $\delta\phi_d^1(t), \delta\theta_s^1(t)$ are the particular integrals of Equations (5.19) and (4.16). Since the general solutions to the homogeneous system decay the essential long term behaviour of the driven system is governed by the particular integrals $\delta\phi_d^1(t)$ and $\delta\theta_s^1(t)$.

The first order equations that govern the behaviour of the driven system about the equilibrium point are therefore

$$\left(I_z^{(d)} + 4M_g{r_d}^2 + 4I\right)\delta\ddot{\phi}_d + C_{\phi_g}\delta\dot{\theta}_s = -\mu\delta\dot{\phi}_d + C\omega_0\delta\theta_s + F\cos(\gamma t) \qquad (5.22)$$

where Equation (5.22) is effectively Equation (5.19) with the driving force term added.

$$\left(M_s {h_s}^2 + \left(M_d + 4M_g\right){h_d}^2 + 8I\right)\delta\ddot{\theta}_s - C_{\phi_g}\delta\dot{\phi}_d$$
$$-\left(M_s h_s + \left(M_d + 4M_g\right)h_d\right)g\delta\theta_s = 0 \qquad (5.23)$$

Note we again use the small angle approximation to the trigonometric functions based on Taylor's expansion.

The driving force term in the equation of motion of ϕ_g can be more conveniently written in complex form as

$$F\cos(\gamma t) = Fe^{i\gamma t}$$

In this form it allows easy manipulation of the equations. As we are only interested in the real parts of the term associated with the driving force, and since the equations are linear, we can find the solution by considering the real parts of the resulting solutions.

This result means that the two equations of motion that describe the behaviour of the driven system are

$$\left(I_z^{(d)} + 4M_g {r_d}^2 + 4I\right)\delta\ddot{\phi}_d + C_{\phi_g}\delta\dot{\theta}_s + \mu\delta\dot{\phi}_d - C\omega_0\delta\theta_s) = Fe^{i\gamma t} \qquad (5.24)$$

$$\left(M_s {h_s}^2 + \left(M_d + 4M_g\right){h_d}^2 + 8I\right)\delta\ddot{\theta}_s - C_{\phi_g}\delta\dot{\phi}_d$$
$$-\left(M_s h_s + \left(M_d + 4M_g\right)h_d\right)g\delta\theta_s = 0 \qquad (5.25)$$

5.3.5 Derivation of particular integral of driven system

If the solutions to Equations (5.24) and (5.25) take the form

$$\delta\phi_d{}'(t) = \phi_d^1 e^{i\gamma t} \tag{5.26}$$

$$\delta\theta_s{}'(t) = \theta_s^1 e^{i\gamma t} \tag{5.27}$$

Then a solution to the equations of motion for small deviations from the equilibrium position for the driven system is

$$\left(I_z^{(d)} + 4M_g {r_d}^2 + 4I\right)\gamma^2\phi_d^1 + C_{\phi_g}\gamma\theta_s^1 + \mu\gamma\phi_d^1 - C\omega_0\theta_s^1 = Fe^{i\gamma t} \tag{5.28}$$

$$\left(M_s {h_s}^2 + \left(M_d + 4M_g\right){h_d}^2 + 8I\right)\gamma^2\theta_s^1 - C_{\phi_g}\gamma\phi_d^1$$
$$-\left(M_s h_s + \left(M_d + 4M_g\right)h_d\right)g\theta_s^1 = 0 \tag{5.29}$$

which can be factorised to

$$\left[\left(I_z^{(d)} + 4M_g {r_d}^2 + 4I\right)\gamma^2 + \mu\gamma\right]\phi_d^1 + \left[C_{\phi_g}\gamma - C\omega_0\right]\theta_s^1 = Fe^{i\gamma t} \tag{5.30}$$

$$\left[\left(M_s {h_s}^2 + \left(M_d + 4M_g\right){h_d}^2 + 8I\right)\gamma^2 - \left(M_s h_s + \left(M_d + 4M_g\right)h_d\right)g\right]\theta_s^1$$
$$-C_{\phi_g}\gamma\phi_d^1 = 0 \tag{5.31}$$

Substitution of the above assumptions about the form $\delta\phi_d(t) = \phi_d^1 e^{i\gamma t}, \delta\theta_s(t) = \theta_s^1 e^{i\gamma t}$ yields the matrix system

$$\begin{bmatrix} -\left(I_z^{(d)} + 4M_g {r_d}^2 + 4I\right)\gamma^2 - i\mu\gamma & C_{\phi_g} i\gamma - C\omega_0 \\ -C_{\phi_g} i\gamma & -\left(M_s {h_s}^2 + \left(M_d + 4M_g\right){h_d}^2 + 8I\right)\gamma^2 - \left(M_s h_s + \left(M_d + 4M_g\right)h_d\right)g \end{bmatrix} \begin{bmatrix} \phi_d^1 \\ \theta_s^1 \end{bmatrix} = \begin{bmatrix} F \\ 0 \end{bmatrix}$$

As we did with the homogeneous system, for the purpose of simplification, we substitute in A, B and D from Equations (4.26), (4.27) and (4.28) and the matrix system becomes

$$\begin{bmatrix} -A\gamma^2 - i\mu\gamma & -(C_{\phi_g} i\gamma - C\omega_0) \\ C_{\phi_g} i\gamma & -B\gamma^2 - D \end{bmatrix} \begin{bmatrix} \phi_d^1 \\ \theta_s^1 \end{bmatrix} = \begin{bmatrix} F \\ 0 \end{bmatrix}$$

Cramer's rule allows us determine the solutions to a matrix (Klein, 1990) in the form

$$\begin{bmatrix} a & b \\ c & d \end{bmatrix} \begin{bmatrix} x \\ y \end{bmatrix} = \begin{bmatrix} e \\ f \end{bmatrix}$$

as

$$x = \frac{ed - bf}{ad - cd}$$

$$y = \frac{af - ec}{ad - cd} \qquad (5.32)$$

For the driven system

$$a = -\mathrm{A}\gamma^2 - \mathrm{i}\mu\gamma$$

$$b = -(\mathrm{C}_{\phi_g}\mathrm{i}\gamma - \mathrm{C}\omega_0)$$

$$c = \mathrm{C}_{\phi_g}\mathrm{i}\gamma$$

$$d = -\mathrm{B}\gamma^2 - \mathrm{D}$$

$$e = \mathrm{F}$$

$$f = 0 \qquad (5.33)$$

The solutions for ϕ_d^1 and θ_s^1 can be determined by substitution of Equations (5.33) into Equations (5.32). We therefore obtain

$$\phi_d^1 = \frac{\mathrm{F}(-\mathrm{B}\gamma^2 - \mathrm{D}) - (-)(\mathrm{C}_{\phi_g}\mathrm{i}\gamma - \mathrm{C}\omega_0)(0)}{(-\mathrm{A}\gamma^2 - \mathrm{i}\mu\gamma)(-\mathrm{B}\gamma^2 - \mathrm{D}) - -\left(\mathrm{C}_{\phi_g}\mathrm{i}\gamma\right)(\mathrm{C}_{\phi_g}\mathrm{i}\gamma - \mathrm{C}\omega_0)}$$

$$= \frac{-\mathrm{F}(\mathrm{B}\gamma^2 + \mathrm{D})}{(\mathrm{A}\gamma^2 + \mathrm{i}\mu\gamma)(\mathrm{B}\gamma^2 + \mathrm{D}) + \left(\mathrm{C}_{\phi_g}\mathrm{i}\gamma\right)(\mathrm{C}_{\phi_g}\mathrm{i}\gamma - \mathrm{C}\omega_0)} \qquad (5.34)$$

and

$$\theta_s^1 = \frac{(-\mathrm{A}\gamma^2 - \mathrm{i}\mu\gamma)(0) - (\mathrm{F})(\mathrm{C}_{\phi_g}\mathrm{i}\gamma)}{(-\mathrm{A}\gamma^2 - \mathrm{i}\mu\gamma)(-\mathrm{B}\gamma^2 - \mathrm{D}) - -\left(\mathrm{C}_{\phi_g}\mathrm{i}\gamma\right)(\mathrm{C}_{\phi_g}\mathrm{i}\gamma - \mathrm{C}\omega_0)}$$

$$= \frac{-\mathrm{i}\mathrm{F}\mathrm{C}_{\phi_g}\gamma}{(\mathrm{A}\gamma^2 + \mathrm{i}\mu\gamma)(\mathrm{B}\gamma^2 + \mathrm{D}) + \left(\mathrm{C}_{\phi_g}\mathrm{i}\gamma\right)(\mathrm{C}_{\phi_g}\mathrm{i}\gamma - \mathrm{C}\omega_0)} \qquad (5.35)$$

It is known that all the constants in Equations (5.34) and (5.35) are real and positive; therefore these solutions will reduce to two complex numbers.

$$\phi_d^1 = m + ni \tag{5.36}$$

$$\theta_s^1 = p + qi \tag{5.37}$$

where m, n, p and q are determined by substitution of the constants A, B and D (Equations (4.26), (4.27) and (4.28)). These complex numbers can be converted into polar form so that Equations (5.36) and (5.37) become

$$\phi_d^1 = m + ni = {b_d}^1 e^{i\delta_d} \tag{5.38}$$

$$\theta_s^1 = p + qi = {b_s}^1 e^{i\delta_s} \tag{5.39}$$

where $${b_d}^1 = \sqrt{|m|^2 + |n|^2}, {b_s}^1 = \sqrt{|p|^2 + |q|^2}$$

$$\tan\delta_d = \frac{n}{m}, \tan\delta_s = \frac{q}{p}$$

The oscillatory motion that describes the behaviour of the variables ϕ_d^1 and θ_s^1 is therefore

$$\begin{aligned}\delta\phi_d{}'(t) &= \mathrm{Re}\left[\phi_d^1 e^{i\gamma t}\right] \\ &= \mathrm{Re}\left[{b_d}^1 e^{i(\gamma t+\delta_d)}\right] \\ &= {b_d}^1 \cos(\gamma t+\delta_d)\end{aligned} \qquad (5.40)$$

$$\begin{aligned}\delta\theta_s{}'(t) &= \mathrm{Re}\left[\theta_s^1 e^{i\gamma t}\right] \\ &= \mathrm{Re}\left[{b_s}^1 e^{i(\gamma t+\delta_s)}\right] \\ &= {b_s}^1 \cos(\gamma t+\delta_s)\end{aligned} \qquad (5.41)$$

The overall response of the total system is therefore a combination of Equations (5.17) and (5.40) and Equations (5.18) and (5.41). From this we obtain

$$\phi_d(t) = \delta\phi_d^0(t) + \delta\phi_d{}'(t)$$

$$\phi_d(t) = e^{-mt}\left(M_{\phi_d}\cos(nt) + N_{\phi_d}\sin(nt)\right) + {b_d}^1\cos(\gamma t+\delta_d) \qquad (5.42)$$

and

$$\theta_s(t) = \delta\theta_s^0(t) + \delta\theta_s{}'(t)$$

$$\theta_s(t) = re^{-mt}\left(M_{\theta_s}\cos(nt+\theta) + N_{\theta_s}\sin(nt+\theta)\right) + {b_s}^1\cos(\gamma t+\delta_s) \qquad (5.43)$$

Note again that the long term behaviour of the system is governed by the particular integrals (5.40) and (5.41).

5.4 Concluding comments

The general solutions for the homogeneous system (Equations (5.17) and (5.18)) and the driven system (Equations (5.42) and (5.43)) have been derived. These equations will be used to investigate the behaviour of the stable platform system once a set of physical parameters have been establish through the systematic design of the experimental prototype (Chapter 6).

A set of plots modelling the behaviour of the system will be produced in Matlab based upon the prototype stable platforms physical parameters. The theoretical response will then be compared to data obtained via testing of the prototype stable platform to validate the predicted behaviour of the system. Once validated, the model can then be used to investigate the optimal design parameters for the stable platform for a range of applications (that is, stabilizing a range of different external structures by varying the physical parameters of the system).

6

Design of the gyroscopically stabilized platform

6.1 Introduction

The approach to the design of the gyroscopically stabilized platform was to establish a solution that implements the concept presented in the schematic diagram (Figure 1.6) that could be manufactured at the most feasibly economic scale using existing mechanical components. While proof of concept was the driving factor behind this research, it needed to be established whether it was even possible to manufacture the stable platform in the configuration proposed by Townsend (1983) and obtain the desired interactions between the subsystems that would make the system function as intended.

The mathematical analysis of the system revealed a set of conditions that must be satisfied in order for the stable platform to maintain an external structure level.

> ***The objective of this study is to establish the feasibility of constructing Townsend's proposed schematic, as represented in the schematic diagram, Figure 1.6, using available engineering components. Furthermore, the study will investigate the most practical and economic scale at which a prototype can be built.***

The design will be evolved in a systematic way applying the approach adopted by Pahl & Beitz (1984) and Hales & Gooch (2004).

6.2 Task clarification

This section defines the problem for which solutions for the design of the stable platform will be established. The following problem statement was formulated to identify the design task.

Problem statement: *To manufacture a working stable platform to be built on campus at the University of Canterbury Mechanical Engineering Workshop. The stable platform is to stabilize an inherently unstable external structure.*

6.2.1 The design requirements specification

Although several constraints were placed upon the performance of the stable platform, neither the size of the system or the magnitudes of the restoring moments were ever addressed. Townsend stated that the system must actively resist the applications of a tipping force and thus must be able to stabilize bodies which are normally unstable under the action of such loads.

To help establish a practical approach to the experimental prototype design and to aid in restricting the design to an economically feasible scale, a set of requirements were formulated as a list of demands and wishes (Table 6.1) in accordance with the design procedure of Pahl & Beitz (1984). The main focus of these requirements can

be categorised as functional, economic, ergonomic, ecological and life cycle (Hales & Gooch (2004)).

Table 6.1 - Demands & wishes list

Demand Wish	**Stable Platform design requirement specification (requirements under each heading are in order of importance**
Functional requirements for the stable platform mechanisms	
D	must produce a righting moment to restore assembly from 20˚offset
D	the mechanical components and mechanisms are to have sufficient strength and rigidity to withstand the loads produced by the gyroscopes
D	the overall system weight will be minimised to reduce the restoring torque the system must produce to overcome imbalances forces caused by the system moving off the equilibrium
D	be as symmetric and balanced as possible to reduce moments produced by imbalanced mass
D	gimbal frame linkage must maintain gyroscope frames at the same angles with respect to the disc to within 2˚
D	disc to rotate on central pivot joint that maintains constant velocity at tip angles up to 20˚
D	distance between disc centre of mass and pivot point to be maximised such that gravitational stability maintains disc level during operation
W	system to be easily integrated into any type of unstable external structure
W	must limit energy loses due to vibrations
W	must be able to adjust the angle the of the contact arms to ensure they all rest in the horizontal position to within 2˚

Table 6.1 - Demands & wishes list cont.

W	gyroscope rotational speed to exceed 5000rpm $(\dot{\phi} > 5000rpm)$
Functional requirements for control of stable platform	
D	have a simple method of accurately controlling the speeds of the gyroscopes and disc
D	use readily available electric motors to power gyroscopes and disc
D	safely house gyroscope motor batteries
W	control the rotational speed of the gyroscope to within $\pm$ 10rpm of each other
W	easy method of measuring flywheel and disc speeds
Safety requirements	
D	testing area must contain system should catastrophic failure occur
W	design must reduce potential pinch and jamming points
W	include an emergency stop button to isolate power in event of an emergency (positioned in a clearly identified location)
Quality requirements	
D	all manufactured components to be inspected to comply with tolerances specified on manufacturing drawings
D	all drawings to be approved by supervisor (Dr Shayne Gooch)
D	all wiring to be done by certified electrical technician who is familiar with the project
D	all electrical components and connections to be checked and verified by certified electrical technician

Table 6.1 - Demands & wishes list cont.

D	each subsystem components to be tested (where applicable) to ensure safe operation before installation into top level system assembly
W	design life for system components > 5 years
Manufacturing requirements	
D	be predominately manufactured in University of Canterbury Mechanical Engineering Workshop
D	ensure all components can be assembled/disassembled by an individual using readily available hand tools
Ergonomic requirements	
D	be of an ergonomic scale (easily operated by one person)
D	overall system must be able to be manipulated by one person and safely rest in the equilibrium position
W	simple speed control of rotating components
W	allow easy assembly/disassembly of individual subsystems for alterations/modifications
W	check that operation of stable platform does not cause discomfort to viewers e.g. strobe effect, noise levels
Timing requirements	
D	coordinate manufacture of components with University of Canterbury Mechanical Engineering Workshop timetable frequently corresponding with Workshop Manager
W	component checklist will be used to track manufacturing of parts to ensure schedule is maintained (to be accessible by Workshop Technicians)

Table 6.1 - Demands & wishes list cont.

Ecological requirements	
W	have an operation noise level of < 90dB
Life cycle requirements	
D	service stable platform after every 10 tests (check for loose components, bearing noise etc)
D	regularly check battery life and maintain battery charge

6.2.2 Stable platform subsystems

Given the design requirements specifications listed in Table 6.1, coupled with the procedure of mechanical design outlined in (Pahl & Beitz (1984)), the stable platform system may be considered as a set of 6 sub-systems represented in the organisation chart, Figure 6.1.

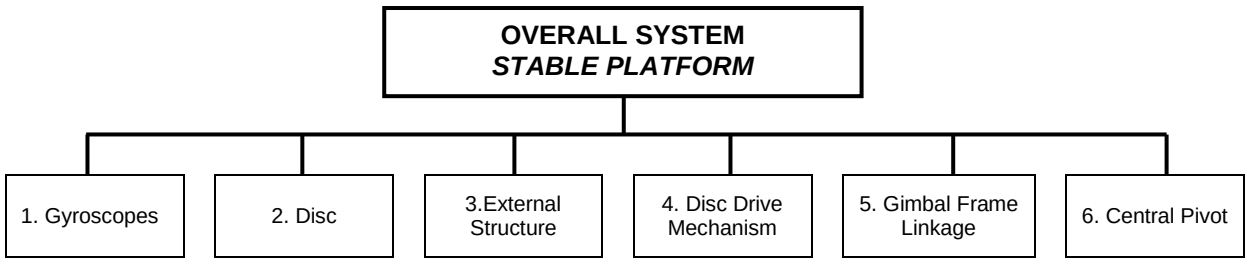

Figure 6.1 - Sub-systems for which design solutions have to be created for the stable platform

The functions of each of the subsystems are outlined below. The process used to design each of the subsystems focuses primarily on their function within the overall system rather than their form (Ullman (1992)).

1. Gyroscopes

The gyroscope assembly is considered in four sections; the motor, the flywheel, the gimbal frame and the outer contact arm. The flywheel gives the system its angular momentum so it is able to produce a restoring torque. The gimbal frame houses the motor and flywheel and pivots when an external torque is applied. The outer contact arm pushes down upon the outer ring returning the external structure back to the horizontal. The gyroscopes are interconnected via the gimbal frame linkage.

2. Disc

The majority of the sub-systems that compose the stable platform are mounted upon or connected to the disc. The gyroscopes sit symmetrically upon the disc equally spaced at 90˚ angles. The disc is also the central connection for the gimbal frame linkage and the central pivot joint. As per the assumption in the mathematical analysis of the system, the disc remains level during operation due to its high gravitational stability.

3. External Structure

The external structure is defined as the unstable mass that the stable platform is attempting to stabilize. The structure must contain an outer

contact ring with which the contact arms attached to the gyroscopes push down on to return the structure to the horizontal position. The structure will be designed to be inherently unstable.

4. Disc Drive Mechanism

The disc drive mechanism is fixed to the external structure. The drive is coupled to the disc via a central pivot joint (torsionally rigid coupling) and transmits drive to the disc resulting in precession of the gyroscopes. This mechanism contributes to the mass that the stable platform stabilizes. Ease of assembly will be an important factor in the design of this subsystem.

5. Gimbal Frame Linkage

The gyroscopes are located upon the disc and are all interconnected via the gimbal frame linkage. The linkage ensures that all the gimbal frame assemblies rest and pivot at an equal angle relative to the disc.

6. Central Pivot

The disc and gyroscopes all mount upon the central pivot joint. This pivot transmits the drive from the disc drive mechanism to the disc and allows the disc to remain level at all times during operation.

6.2.3 System schematic

It is desirable to produce a schematic layout of the system to clearly show how the various subsystems that comprise the design are connected and how they interact (Molian (1997)). Figure 6.2 indicates where each of the subsystems that have been defined in Figure 6.1 are located.

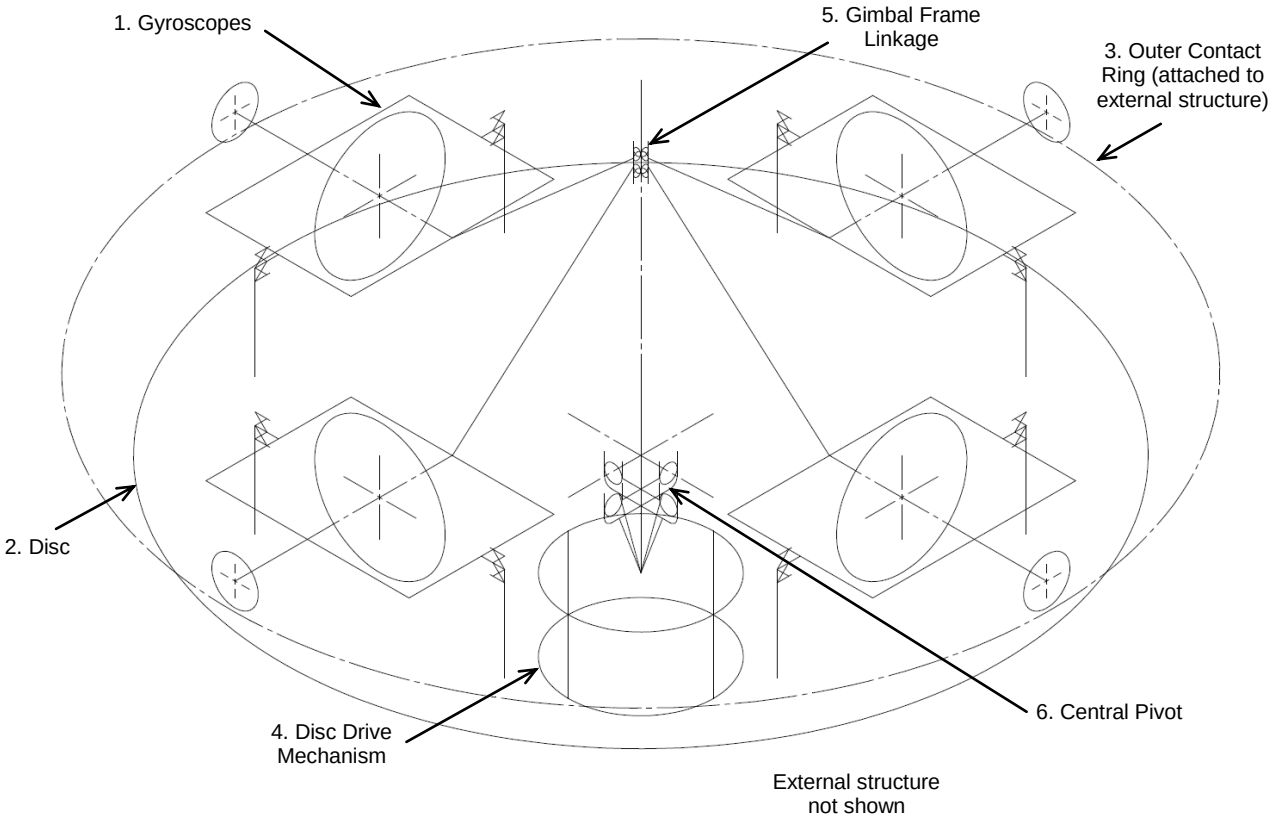

Figure 6.2 - Stable platform schematic layout

It should be noted that while the above schematic demonstrates system function it is not a representation of the final layout design.

6.2.4 Dependence of each subsystem on derived inequality

In order optimise the design of the stable platform and to increase the likelihood of stabilization occurring we include (Equation (4.47)) derived in Chapter 4 into the design process. This inequality must be satisfied in order for the stable platform to exhibit the desired oscillatory motion. Equation (4.47) has been defined as

$$\mu\left(M_s h_s + (M_d + 4M_g)h_d\right)g < 4(I)^2\left(\dot{\phi}_g\right)^2\omega_0\left(\frac{r_g + r_d}{r_g}\right) \qquad (4.47)$$

This equation is made up of 12 constants that will govern the design of the stable platform. A set of assumptions have been made based upon the variables in Equation (4.47)

- μ relates to the friction in the disc drive motor and is approximated as 0.5.

- $\dot{\phi}_g$ is assumed to be the maximum rotational speed of the flywheels.

- Due to the oscillatory motion of the disc, ω_0 is taken as the maximum disc precession speed.

Having categorised the stable platform as six sub-systems we now investigate each subsystem's dependence upon the values in Equation (4.47). The results are shown in Table 6.2.

Table 6.2 - Subsystem dependence upon Equation (4.47)

Subsystem	Dependent Variables	Variable Description
1. Gyroscopes		
	I	moment of inertia of gyroscope (kgm2)
	$\dot{\phi}_g$	rotational speed of gyroscope (rads-1)
	M_g	mass of a gyroscope (kg)
2. Disc		
	h_d	height of disc pivot point (m)
	$\left(\frac{r_g+r_d}{r_g}\right)$	ratio of distance from central disc axis to the end of the outer contact arm
	M_d	mass of the disc (kg)
3. External Structure		
	h_s	height of external structure COM (m)
	M_s	mass of external structure (kg)
4. Disc Drive Mechanism		
	μ	Friction in drive motor
	M_s	mass of external structure (kg)
5. Gimbal Frame Linkage		
	M_d	mass of the disc (kg)
6. Central Pivot		
	h_d	height of disc pivot point
	M_s	mass of external structure (kg)

Table 6.2 and Equation (4.47) reveal conditions that will aid in the derivation of conceptual solutions to the stable platform subsystems (Waldron & Waldron (1996)). These are:

- the mass of the disc (M_d) and the external structure (M_s) must be minimised. This does not apply to the mass of gyroscopes (M_g) as these will be maximised to obtain the largest possible moment of inertia (I).

- the height of the external structures centre of mass (h_s) needs to be designed to be as low as possible.

- the distance between the external structures centre of mass (h_s) and the centre of mass of the disc (h_d) must be as small as possible.

- the rotational speed of the flywheels will be maximised to the greatest feasible speed $(\dot{\phi}_g)$.

- the ratio $\left(\frac{r_g+r_d}{r_g}\right)$ must be made as large as possible. This results in the distance from the gyroscopes pivot point to the end of the outer contact arm (r_g) needing to be much smaller than the distance from the central axis of the disc to the gyroscopes pivot point (r_d).

- the rotational speed of the disc will be maximised to the highest possible speed (ω_0).

6.3 Conceptual design of stable platform

After breaking the overall stable platform into sub-systems represented in the organisation chart, Figure 6.1, a conceptual design solution for each of the six sub-

systems will be sought. The first four sub-systems (the gyroscopes, disc, external structure and disc drive mechanism) are classified as the critical sub-systems. The remaining two sub-systems (the gimbal frame linkage and central pivot) concept generation will depend upon the selected configurations of the four critical sub-systems as their interaction with these systems is important.

The approach taken is to divide each of the sub-systems into sub-functions and to build a morphological matrix using schematic diagrams of the solution principles considered. The solution principles for each sub-function in the morphological matrix are selected using concept selection charts adopted from (Pahl & Beitz (1984)). Cells that are greyed represent the selected conceptual sub-functions.

6.3.1 Gyroscopes

The gyroscope assemblies are the most integral part of the stable platform. The function of the gyroscope assemblies is to house the motor and flywheel and produce the restorative torque through the outer contact wheel and onto the external structure.

The working principles considered in the development of the gyroscopes are illustrated in the morphological matrix, Figure 6.3.

Two options were considered for the placement of the gyroscopes upon the disc (*solution A1 and A2*). Mounting the frame upon legs (*solution A1*) allowed more room for wiring to the motor and would make assembly of the system much simpler. Although this solution required more components to be manufactured this was

regarded as a preferable option compared to the complex machining required for the recessed design in *solution A2*.

Three concepts were considered for the motor mount arrangement. Mounting the flywheel over the top of the flywheel outer casing (*solution B1*), having the flywheel mount directly off the motor axle (*solution B2*) or driving the flywheel by a belt and having the motor mounted beside the arrangement (*solution B3*). *Solution B1* was selected as it is the simplest to manufacture. This solution keeps the centre of gravity of the flywheel and the motor in approximately the same place. *Solution B1* also eliminates the need for complex bearing arrangements and reduces the number of fasteners needed to hold the assembly in place.

The inertia of the flywheel coupled with its rotational speed is what governs the size of the restoring torque that the stable platform is able to produce. Three concepts were considered for the flywheel; a solid wheel that is fabricated from a single piece of material (*solution C1*), an airfoil design to encourage the flow of air into the motor to maintain a low operating temperature (*solution C2*), and an assembly where the flywheel is made up of two components (a face mount plate and the flywheel mass) fastened together (*solution C3*). *Solution C2* requires complex machining and initial testing of the motor verified that the temperature of the motor during operation is not an issue. One of the most important features of the flywheel is that it is machined to a high tolerance so that the assembly is dynamically balanced. This is much harder to achieve when two components are assemble.

An accurate method of fabricating the flywheel out of a single piece of material while keeping it balanced and concentric needs to be determined.

Morphological matrix. Subsystem 1 Gyroscopes				
Solution / Sub-system Sub-functions		1	2	3
A	Gimbal Frame - houses motor, flywheel and contact arm	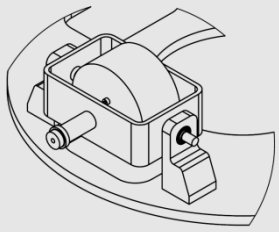 On legs	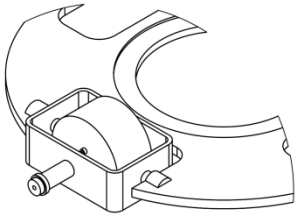 Recessed in disc	
B	Motor Mount Arrangement - drives flywheel	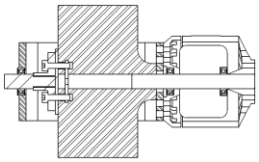 Flywheel mounts on motor	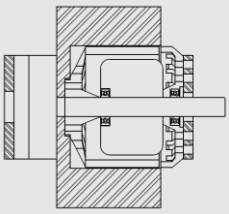 Flywheel on motor casing	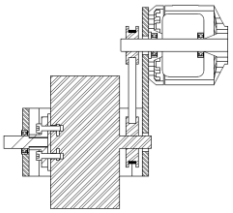 Flywheel belt/chain drive
C	Flywheel - inertia produces restoring torque	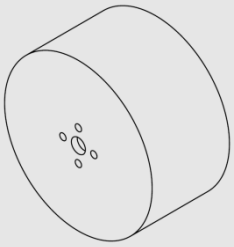 Solid	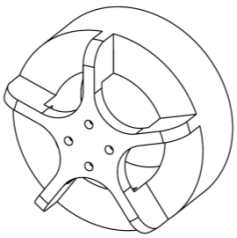 Air foil	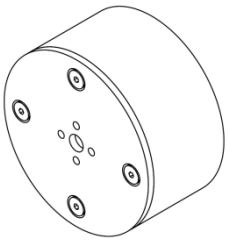 Assembly

Figure 6.3 - Solution forms considered for the gyroscopes

6.3.2 Disc

The function of the disc is to provide the main mounting platform for the gyroscopes (Figure 6.2) and batteries. The disc pivots in all directions about a central point. Several design constraints have been placed on the conceptual design of the disc:

- The pivot of the gimbal frame arrangement and the pivot of disc must be in line.
- The centre of mass of the disc and gimbal frame arrangement must be below the centre of the disc pivot point.
- The disc must have high gravitational stability.

The working principles considered in the development of the disc are illustrated in the morphological matrix, Figure 6.4.

Due to geometric constraints for the centre section of the disc a cone shape was required. This would allow the central pivot to be located up within the cavity of the cone, keeping the centre of mass of the disc below the pivot point. Machining the cone and disc as a solid piece (*solution D1*) would help ensure concentricity of the design but was considered too expensive. *Solution D2* required machining the cone and disc separately and then welding them together. *Solution D3* considers fastening the cone and disc sections together to allow for disassembly should the design need to be altered. *Solution D3* was selected.

Only two options were established for the mounting of the batteries that drive the motors and flywheels; above the disc (*solution E*1) or below the disc (*solution E2*).

Solution E2 was chosen as the lower the centre of mass of the disc the more gravitationally stable it would be. A slip ring design was also considered but was abandoned due to complexity and the high currents involved in driving the motors (in excess of 30A).

Solution F1 requires machining the legs that mount the gyroscopes out of solid aluminium. These would provide sufficient strength and an ideal cavity for mounting bearings. *Solution F2* presents the mount legs bent into the desired geometry from aluminium plate. The design would significantly reduce the weight of the disc assembly. Welding the legs to the disc was also considered (*solution F3*). *Solution F1* was selected as the legs are a load path for all restoring torques that the flywheels.

One of the critical requirements specified in Table 6.1 is that the disc and gyroscope assembly is as symmetric as possible. *Solution G1* uses dowel pins to ensure the gimbal frame legs are assembled in the exact same location each time. *Solution G2* achieves the same result but with a machined recess that locates on the edges of the gimbal frame legs. The final solution (*solution G3*) considers using locating tabs mounted on top of the disc to position the gimbal frame legs. *Solution G1* was selected.

Morphological matrix. Subsystem 2 Disc				
Sub-system Sub-functions / Solution		1	2	3
D	Disc geometry – mount for gyroscopes	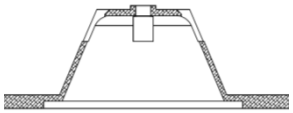 Machine from solid	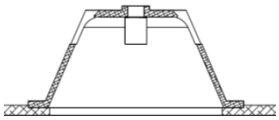 Fabricate	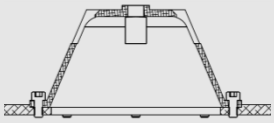 Fasten
E	Battery mounts – holds batteries that power flywheels	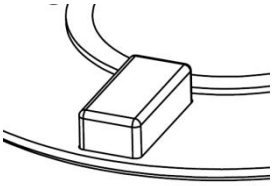 Above disc	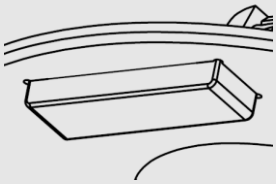 Below disc	
F	Gimbal frame legs – used to mount the main shaft of the gimbal frame allowing it to pivot	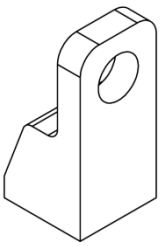 Milled from solid	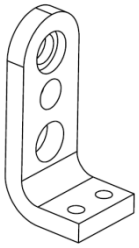 Bent	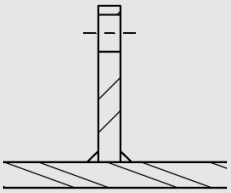 Fabricate
G	Locating frame legs – accurate method for locating gimbal frame in position	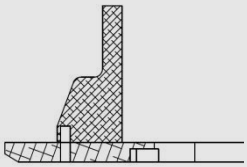 Dowel pins	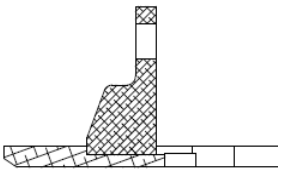 Machine recess	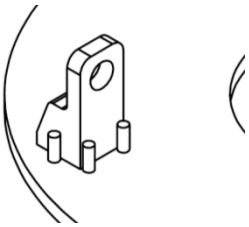 Location pins

Figure 6.4 - Solution forms considered for the disc

6.3.3 External structure

The function of the external structure is to act as the unstable body that the system will be mounted upon for testing. The external structure will be of the form of an inverted pendulum. The stable platform will work continuously to maintain it at an upright position. One critical component of the external structure is the inclusion of an outer ring; a circular surface that the outer contact arms can transmit a restoring force upon.

The working principles considered in the development of the external structure are illustrated in the morphological matrix, Figure 6.5.

Solutions H1-H3 consider what type of unstable attachment will be used at the base of the external structure. *Solution H1* (mounting the system upon a universal joint) and *solution H2* (a single shaft that can pivot in one plane) both require a significant amount of machining and are high in cost. Using a wooden sphere turned in the CNC lathe is a quick, cheap and lightweight solution (*solution H3*) and should demonstrate the desired restoring action.

It is critical that the outer ring is set at a predetermined height to maximise the magnitude of the restoring moment that the gyroscopes are producing. *Solution I1* uses two nuts either side of a plate to accurately set the desired height of the ring. *Solution I2* incorporates holes through the frame legs coupled with a pin that retains the ring at the desired height. *Solution I3* looks at fixing the length eliminating the adjustability but decreasing cost and complexity. *Solution I1* was selected as the preferred option.

Morphological matrix. Subsystem 3 External Structure				
Sub-system Sub-functions / Solution		1	2	3
H	External structure base – unstable attachment	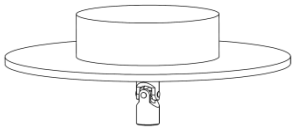 Universal Joint	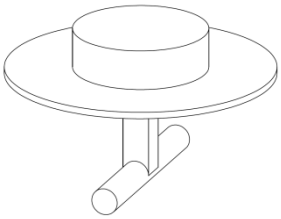 1 plane pivot	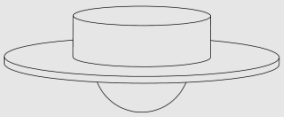 Hemi-spherical body
I	Outer ring height – method for adjusting ring height	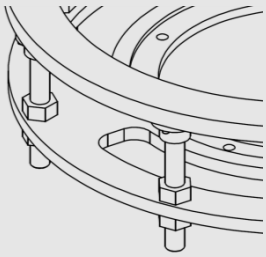 Adjust with thread	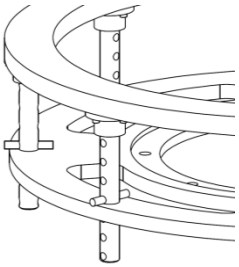 Locating pins	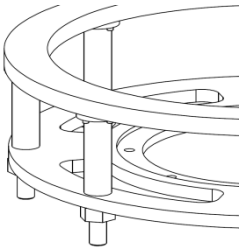 Fixed height

Figure 6.5 - Solution forms considered for the external structure

6.3.4 Disc drive mechanism

The function of the disc drive mechanism is to provide sufficient torque to precess the disc around, altering the angular momentum of the gyroscopes resulting in them pushing down on the external structure and returning it to its equilibrium position.

The working principles considered in the development of the disc drive mechanism are illustrated in the morphological matrix, Figure 6.6

The most important issue in the conceptual design of the disc drive mechanism is the type of motor that will be used to precess the disc. Three motor options were considered. *Solution J1* is 12V DC motor with a worm drive reduction. These motors are commonly used as window wiper motors in automotive applications. Worm drive gear arrangements transmit high torques and are compact. A straight drive DC motor with a gearbox axially is shown as *solution J2*. Although this solution would be heavy and expensive, the robustness of the motor-gearbox configuration would make it ideal for any backlash that the system experiences. *Solution J3* uses a stepper motor. Stepper motors give very accurate control but the control systems required and speed and torque limitations restrict easy adaption of the motor should the parameters of the system alter. *Solution J1* is selected as the favoured solution.

Solutions K1, K2 and *K3* were considered for transmitting drive from the external structure to the disc. An inline drive arrangement is compact and machining and assembly time is fast. *Solution K2* and *K3* use a helical gear or a belt/chain drive arrangement to rotate the disc. Extra components and alignment/tolerance requirements make them less desirable. *Solution K1* was selected as the preferred option.

Due to the probable small motor output shaft size a machine key was not considered as an option for securing the motor output shaft to the central drive shaft. *Solution L1* uses a dowel pin pressed in through both the drive shaft and motor shaft to transmit drive. *Solution L2* uses a clamped flexible coupling whose properties will be determined in the embodiment design section. This solution allows for misalignment

between shafts during assembly and helps reduce the backlash load on the motor and is the preferred solution.

The final sub-section relating to the disc drive mechanism is how the drive shaft is attached to the disc. A machine key assembly was considered (*solution M1*) however the preferred option of tightening a nut down onto a spacer and clamping the disc in place was selected. The simplicity of manufacturing and assembling this design made it more desirable.

Morphological matrix. Subsystem 4 Disc Drive Mechanism				
Sub-system Sub-functions / Solution		1	2	3
J	Drive motor – type of motor used to precess disc	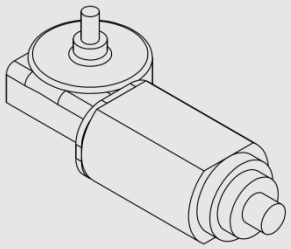 Window wiper	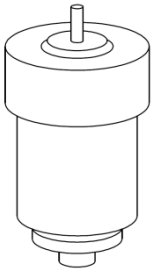 DC with gearbox	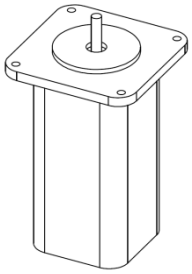 Stepper
K	Motor mounting – location of drive motor relative to shaft	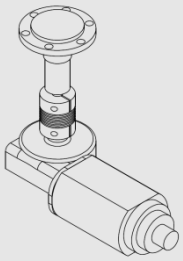 Inline	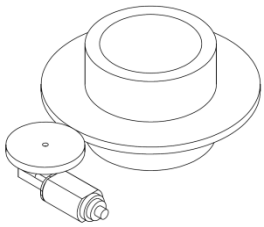 Geared	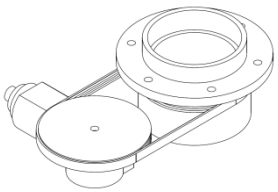 Belt or chain drive
L	Shaft connection – how is the motor connected to the drive shaft	 Dowel pins	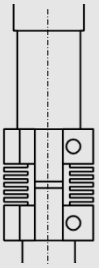 Flexible coupling	
M	Disc connection – method for transmitting drive from motor shaft to disc	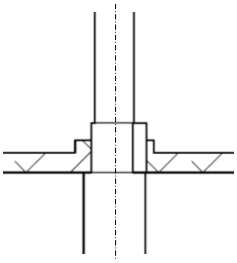 Machine key	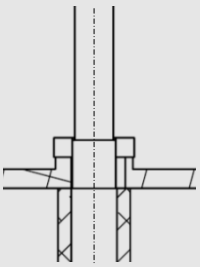 Threaded clamp	

Figure 6.6 - Solution forms considered for the disc drive mechanism

With all the critical conceptual subsystem functions selected the solutions for the gimbal frame linkage and central pivot concepts were determined.

6.3.5 Gimbal frame linkage

The function of the gimbal frame linkage is to constrain the gyroscopes so they all pivot with an equivalent angle relative to the disc. The gimbal frame linkage also acts as the load path for the restoring torque that the gyroscopes produce, transmitting the moment from all four gyroscopes through a single outer contact arm.

The working principles considered in the development of the gimbal frame linkage are illustrated in the morphological matrix, Figure 6.7.

Townsend (1983) suggested that the gimbal frames be connected by bevel gears (*solution N1*). The complexity and cost associated with designing and manufacturing custom gears meant that other solutions were considered. The use of universal joints was another option that was investigated (*solution N2*). *Solution N3* uses linkage arms connected to the gimbal frames and attached to a sliding connection on a central shaft. *Solution N3* was the chosen design of this sub function. This solution will require a central shaft to be incorporated into the design of the system to suit the linear slide linkage.

Sub-functions *O* and *P* relate to the central gimbal frame linkage and associated linear slide. A linear bearing (*solution O3*) was selected as the sliding element for the linear slide. The ability of linear bearings to deal with high radial loads while maintaining axial alignment make them ideal for this type of application. A fixed

length rigid connection arm (*solution P1*) was the preferred option for sub-function *P* as this component will be subjected to high loads.

Morphological matrix. Subsystem 5 Gimbal Frame Linkage				
Sub-system / Sub-functions \ Solution		1	2	3
N	Gimbal frame connection – type of connection used	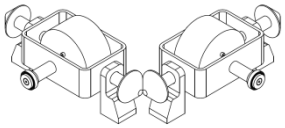 Bevel gears	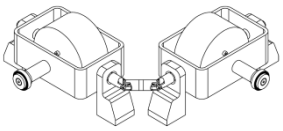 Universal joints	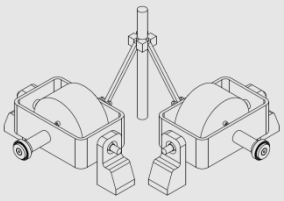 Linear slide
O	Sliding element – type of low friction element used on shaft	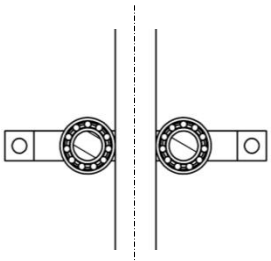 Single row	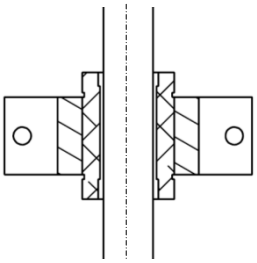 Nylon bush	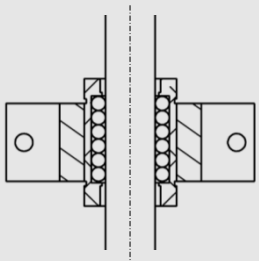 Linear
P	Connecting arms – type of connection arms used	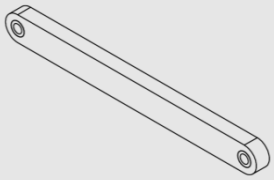 Fixed length	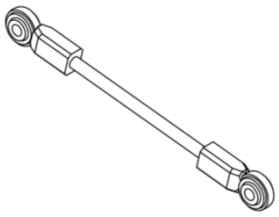 Adjustable rod ends	

Figure 6.7 - Solution forms considered for the gimbal frame linkage

6.3.6 Central pivot

The function of the central pivot is to support the weight of the disc and to allow the disc to pivot in the horizontal pitch and roll directions. This condition comes from the initial mathematical assumptions stated in Chapter 3. The disc must remain level as it precesses around no matter what angle the external structure has tipped to.

The working principles considered in the development of the central pivot are illustrated in the morphological matrix, Figure 6.8.

Three solutions were considered for sub-function *Q*. A universal joint does not provide constant velocity. *Solution Q2* (spherical bearing) would only perform as required at small angles. Constant velocity joints are very good at dealing with radial loads and provide a constant velocity no matter what angle the output shaft is tilted at. *Solution Q3* was selected for this sub-function.

Morphological matrix. Subsystem 6 Central Pivot				
Solution / Sub-system Sub-functions		1	2	3
Q	Central pivot – type of central pivot	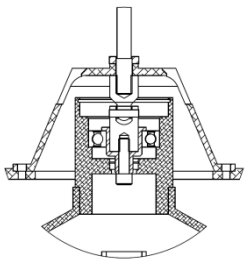 Universal joint	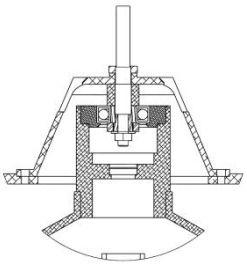 Spherical bearing	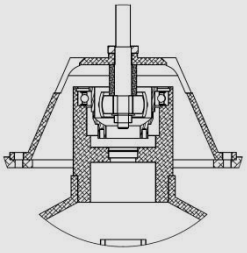 Constant velocity joint

Figure 6.8 - Solution forms considered for the central pivot

6.3.7 The final concept selected for the stable platform system

The attributes of each of the solutions considered for the sub-system sub-functions shown schematically in Figure 6.3 - Figure 6.8 were evaluated in terms of the design requirements specification from Table 6.1.

The concept selection process is summarised by the concept selection charts, Figures B1 to B6, where the requirement categories (functional, safety, quality, manufacturing, timing, economic, ergonomic, ecological, aesthetic and life cycle) were scored in terms of meeting the design requirements specifications. Two further categories were included in the concept selection process ‘can it be made to work’ and ‘information’ (i.e. whether the relevant expertise and experience are available).

The selected concepts for each sub-system were assembled to give a working concept for the stable platform system. The selected sub-functions are summarized in Table 6.3. The resulting concept for the overall system is shown in Figure 6.9. Note that no detailed design features are included in this figure (bearing housings, fasteners, weight reducing cut outs, radii etc). This figure is simply an assembly of the determined sub-functions grouped together.

Table 6.3 – Sub-function selection overview

Subsystem	Sub function	Selected Outcome
1. Gyroscope	A: Gimbal frame	On legs
	B: Motor mount	Flywheel on motor casing
	C: Flywheel	Solid
2. Disc	D: Disc geometry	Assemble
	E: Battery mounts	Below disc
	F: Gimbal frame legs	Milled from solid
	G: Locating frame legs	Dowel pins
3. External Structure	H: Degrees of freedom	Hemi-spherical body
	I: Outer ring height	Adjust with thread
4. Disc Drive Mechanism	J: Drive motor	Window wiper motor
	K: Motor mounting	Inline
	L: Shaft connection	Flexible coupling
	M: Disc connection	Threaded clamp
5. Gimbal frame connection	N: Gimbal frame connection	Linear slide
	O: Bearing arrangement	Linear
	P: Connecting arms	Fixed length
6. Central pivot	Q: Central pivot	Constant velocity joint

The stable platform conceptual layout was reviewed using a conceptual design worksheet, Figure B7 from Hales & Gooch (2004).The conceptual design work sheet shows a good confidence level for the systems function and it was decided to proceed to the embodiment design where further development was expected to improve the overall arrangement in terms of meeting manufacturing, economic and performance requirements.

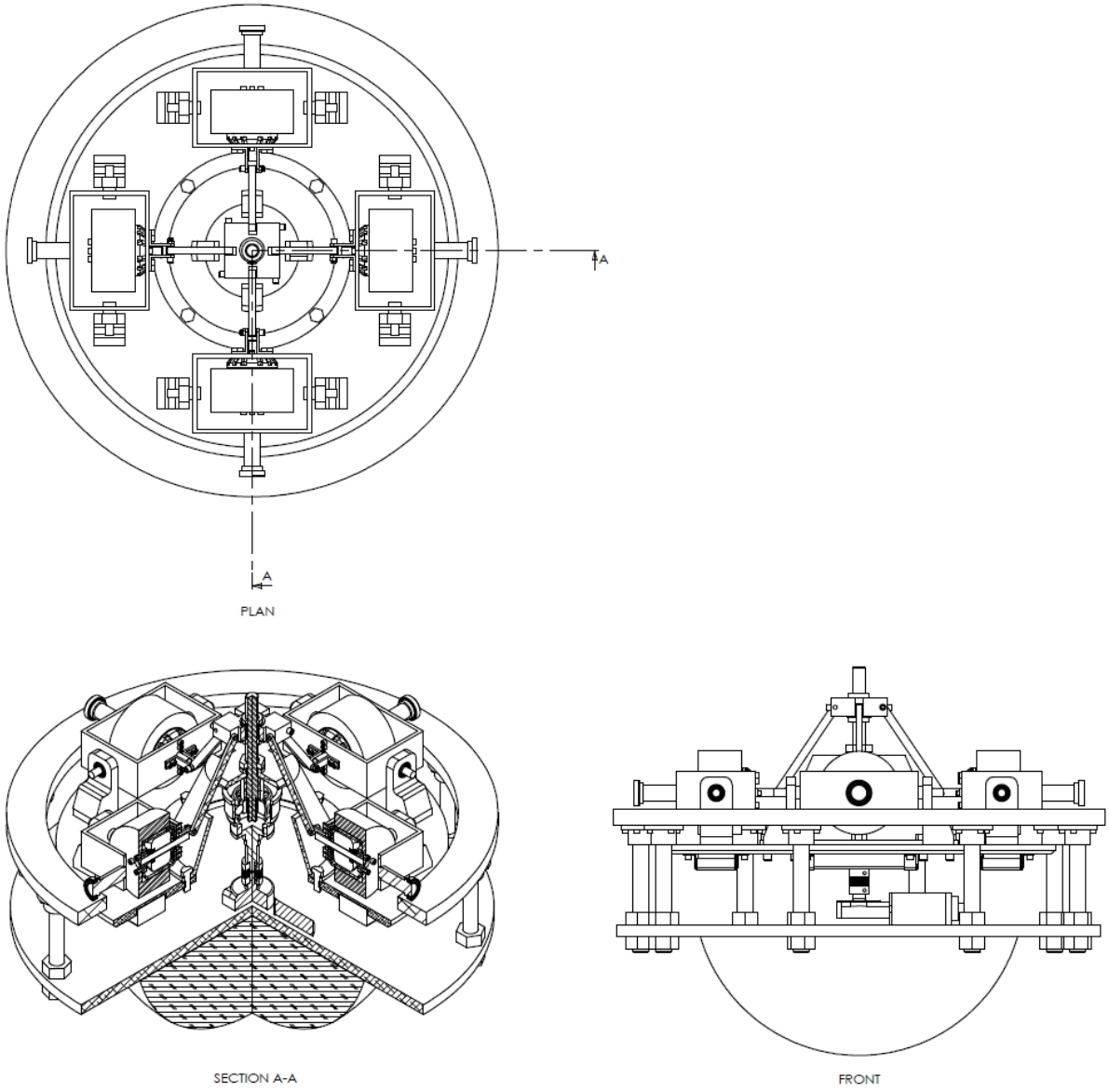

Figure 6.9 – Principal concept for stable platform system using a combination of sub-functions from Figure 6.3 to Figure 6.8

6.4 Establishment of platform scale

One of the most critical steps in the conceptual design of the stable platform is determining the scale to which the system will be designed and built. Initially, the goal of the project was to produce a stable platform that could stabilize a mono-wheel vehicle. After concept generation it was decided that the manufacture of the system was more complex than initially expected. Because of this, the motivation for the build of the project shifted from an application specific design and build to a broader proof of concept approach.

This shift increased the range of the sizes that the prototype stable platform could be built at. The availability of electric motors was established as the governing factor in determining the size of the prototype.

The flywheel electric motors were chosen to define the scale of the stable platform because:

- the size of the motor casing and shaft will govern the size of the flywheels that can be used. The inertia of the flywheel determines the size of the restoring torque the platform can produce.

- for this application the torque that the motor is able to produce is not critical. As the flywheels will not be under any load, they will be aided by momentum once they reach their desired speed.

6.4.1 Electric motor selection

Four different types of electric motors were considered for the flywheel drive motor. These were: induction motors; wound field “universal” motors; permanent magnet motors and brushless permanent magnet motors. Each of these motors are summarised in Table 6.4.

Table 6.4 - Types of Electric Motors

Motor Type	**DC or AC**	**Applications**
1. Induction	AC	Mains electric power applications
2. Wound Field “universal”	AC and DC	Power tools, and domestic appliances
3. Permanent Magnet	DC	Air pumps, golf carts, wheelchairs
4. Brushless Permanent Magnet	DC	Segway, model planes/helicopters, portable power tools

For the stable platform design, it is desirable that the flywheels run on a separate power supply. This will make the system applicable to situations where mains power is unavailable. Because of this, induction motors can be eliminated as a drive option. The remaining motors are evaluated in Table 6.5.

Table 6.5 - Motor evaluation chart

Motor Type	Functional (geometry, control, load paths, motion) /5	Information (cooperation, expertise, experience) /5	Manufacturing, quality (production, ease of purchase) /5	Can be made to work (potential, confidence) /5	*Comments*	Score /20
2	2	4	5	2	*Pros* – most common type of motor, cheap, constant speed under load *Cons* – poor efficiency at high speeds, speed not easily controlled	13
3	3	3	5	4	*Pros* – solid construction, high starting torque, sealed bearings *Cons* - poor ability to accelerate inertial loads, high voltage sensitivity	15
4	4	5	4	5	*Pros* – low maintenance, high operating speeds, easy to set up *Cons* – expensive, requires ESC, high power needed to stop motor	**18**

Table 6.5 shows that of the three available electric motor options for driving the gyroscope flywheels, brushless DC motors were found to be best suited to this application.

6.4.2 Brushless DC motors

Brushless DC motors come in a range sizes. They are commonly used in model aircraft applications to drive helicopter and plane propellers. The main advantages of using these types of motors to drive the flywheels in the stable platform are:

- The external casing of the motor rotates as well as the shaft. This means that the flywheel can be mounted over the casing aligning the motor and flywheels centre of mass.

- The motors have a large number of mount points on them. These are usually used for attaching aircraft propellers yet this will help aid in assembling the motors into the gyroscope assembly.

- Due to the use of brushless DC motors in the model industry, there is a vast amount of information available regarding setting up the motors and controlling their speed. Because most of the consumers who use the motors are hobbyists, the motors and their associated control systems are very simple to use.

6.4.3 Selection of motor/scale of stable platform

The main governing factor that will determine that size of the brushless motors used will be the load the bearings and main shaft are subjected to. To accommodate for the largest possible load the largest available motor shaft diameter was selected (Ø10mm).

To satisfy the conditions established in the design specification requirements (Table 6.1), the motor must have a rotational speed of at least 5000rpm and be as lightweight as possible.

Research into brushless motors and their associated specifications revealed an Exceed RC Brushless DC Motor (MP160) as the most appropriate motor to drive the gyroscopes. A summary of the MP160 motors specifications is available in the CD insert associated with this thesis under "*Purchased Project Components*".

Brushless DC motors maximum speed is related to the associated Kv rating (not to be confused with kilovolts) and the voltage that it receives from the batteries. In this case, the motor has a 245Kv rating. This results in the motor rotating at 245 rpm per 1 volt it receives from a battery. By connecting this motor up to a 22.2V Li-Po battery, the top speed this motor is able to achieve is approximately 5390rpm.

6.5 Embodiment design of stable platform system

The purpose of this section is to present the proposed solution developed for the overall stable platform system. The system is designed to maintain the external structure in an upright position with the goal of optimising the size of the restoring torque the gyroscopes produce, minimizing the losses due to friction through the connections and reducing the overall weight of the system.

6.5.1 Gyroscopes

Two main objectives in the development of the gyroscopes, shown in Figure 6.10, were established. To optimise the size of the torque produced when the gyroscopes are precessed and to develop the layout of the assembly such that the centre of mass is in line with the gimbal pivot point (so no mass imbalance torques were acting on the flywheel).

The gimbal frame is made from 100mm x 150mm x 5mm 350 grade RHS. This is a low cost material that will provide sufficient strength under the system loads. The flywheel motor is attached to the frame via eight cap screws. Clearance holes were drilled in the frame on a PCD that matched the threaded holes in the motor. Two aluminium brackets are attached to the back of the frame (via cap screws) for connecting the gimbal frame linkage assembly to the frame.

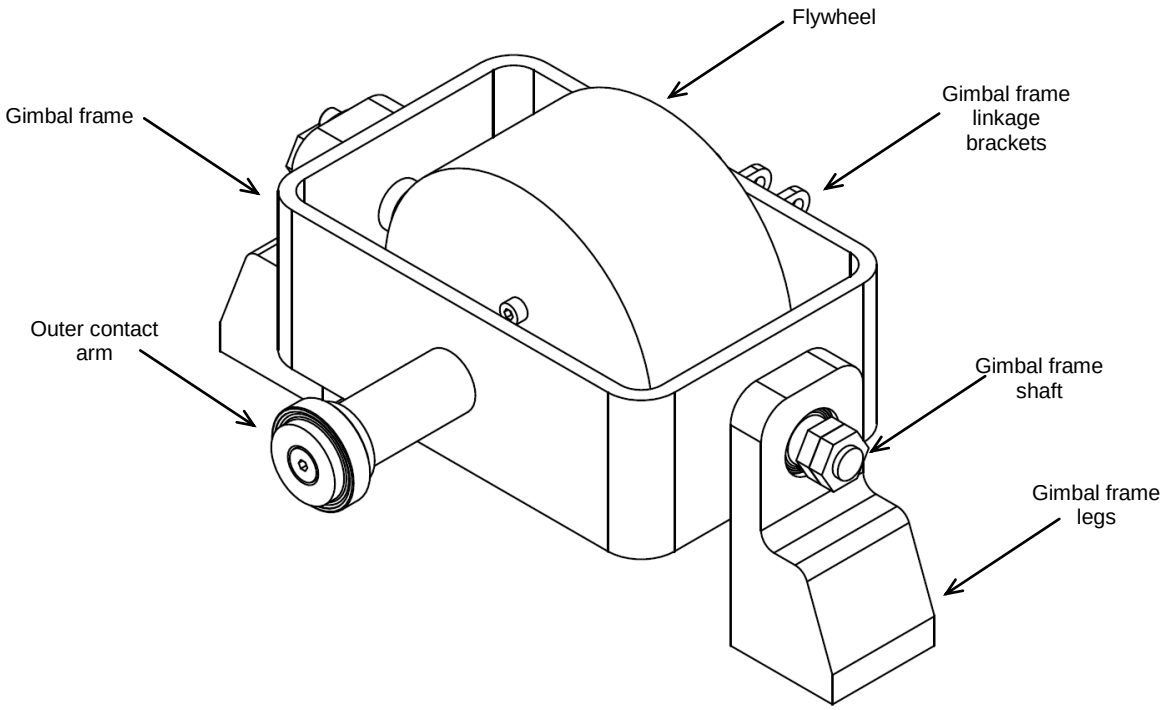

Figure 6.10 – Embodiment of gyroscope

The flywheel is manufactured from AISI 1040 round bar. This material provides significant mass to maximise the moment of inertia of the flywheel. The final flywheel dimensions are Ø110mm by 55mm deep. A cavity is machined in the flywheel equivalent to the diameter of the outer casing of the motor. The flywheel is attached to the motor via four cap screws on a 22mm PCD.

The gimbal frame shafts are manufactured from AISI 4140 alloy steel. Both ends of a single bar are machined and threaded prior to being placed in the gimbal frame. This will ensure concentricity post fabrication. The full length shaft is then braised in place and the unneeded centre section cut away. Large braising fillets are used to reduce stress at the connection (Shigley (2011)).

The gimbal frame legs are to be wire cut from 7075 aluminium plate. The overall thickness and depth of the gimbal frame legs was increased and large radii included to help reduce stress. Two Ø4mm dowel holes are drilled and then reamed in the base for accurate attachment to the disc and two M6 holes are also to be tapped in the base for securing the legs once in position. A toleranced Ø20mm hole is machined in the legs for the gimbal frame shaft bearing.

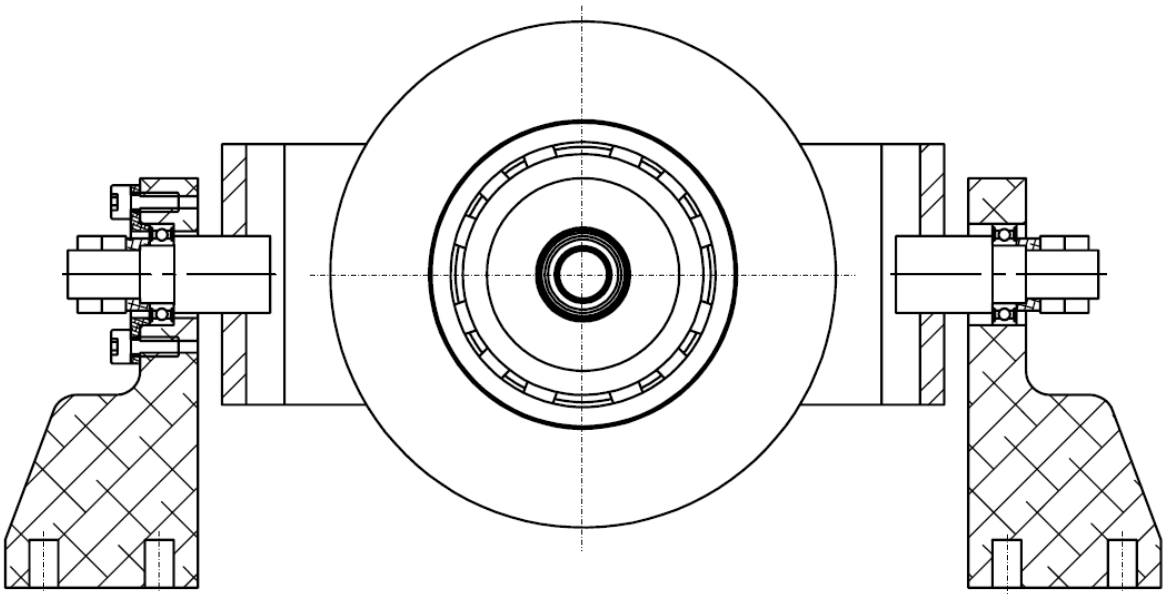

Figure 6.11 – Section of gyroscope assembly showing bearing retention design

The gimbal frame pivots on two Ø12mm single row deep groove bearings as shown in Figure 6.11. One bearing is fixed in place on the shaft while the other is left to float as to not over constrain the design and to aid in assembly. The fixed bearing is held in place with a collar that is secured to the gimbal frame legs with four cap screws. The bearings and shaft are then secured in place with two M10 half nuts tightened up against one another.

The outer contact arm is machined from AISI 4140 alloy steel. A bearing surface is machined on the shaft and a tapped hole is machined in the end face. Once the bearing is fitted on the shaft a washer is placed on the end in conjunction with a cap screw to secure the bearing in place. The final centre of mass of the gimbal frame aligns with the pivot point as intended. Multiple attachment points are available on the gimbal frame should any extra weight need to be added to aid in balancing the assembly.

6.5.2 Disc

Objectives in the development of the disc, shown in Figure 6.12, are: to reduce the overall weight of the assembly; to determine how to mount the batteries underneath the assembly; and optimise the shape of the central cone section to allow for assembly of other sub systems beneath it without interference.

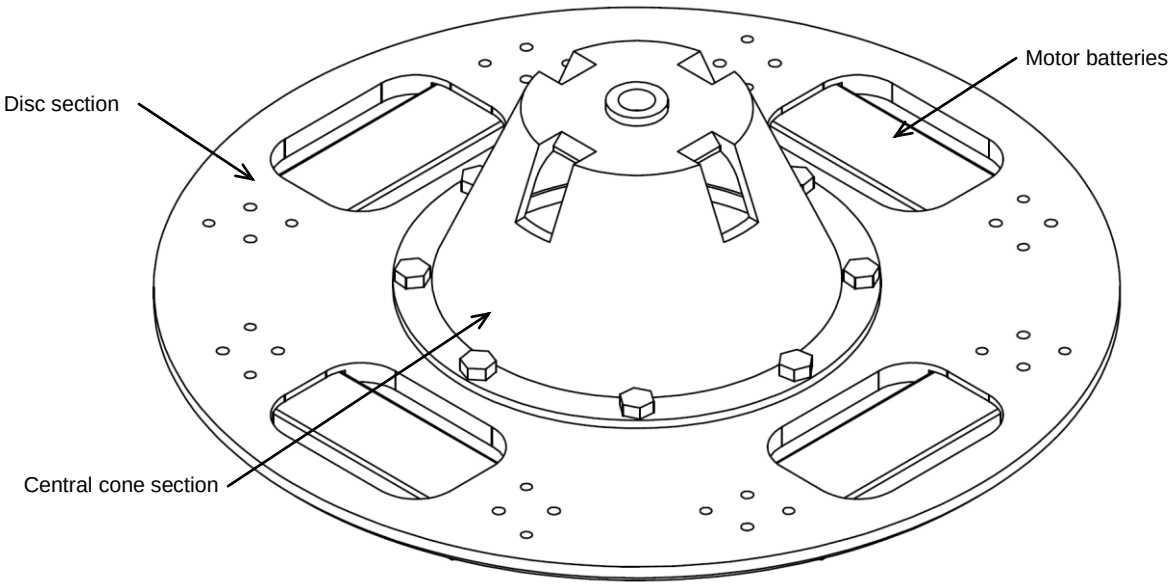

Figure 6.12 - Embodiment of disc

The central cone section is machined from a block of solid 5052 aluminium round bar in the CNC lathe. Aluminium is used to reduce the overall weight of the sub system. Development of the shape within SolidWorks allowed for the optimal wall angle and thickness to be determined. Figure 6.13 shows a section view of the disc assembly.

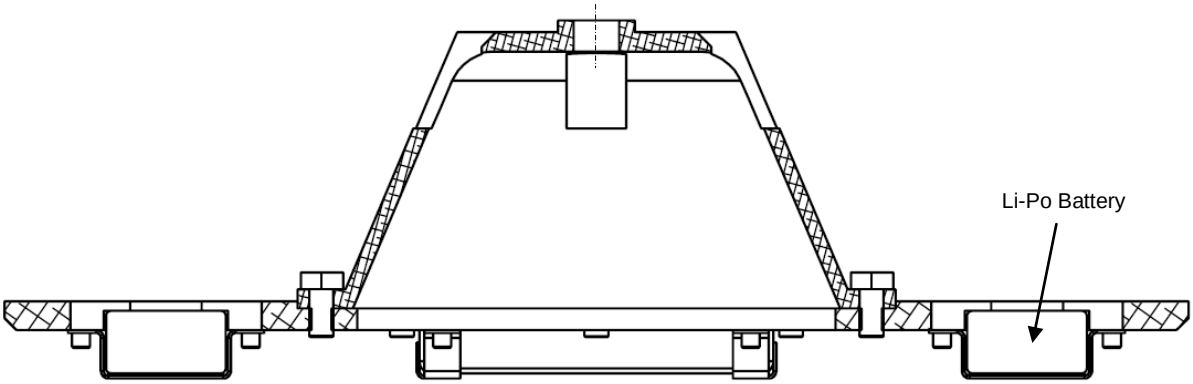

Figure 6.13 – Section of disc assembly showing battery location and central cone cross section geometry

The central cone is attached to the disc section using eight bolts. Cut outs are included at the top of the cone to provide clearance for the linear slide linkage arms. These also contribute to a reduction in the cone weight.

The disc is to be water jet cut from 16mm 7075 aluminium plate. The plate will then be skimmed to ensure flatness and machined to the final dimensions (an outside diameter of 500mm and overall thickness of 14mm). Flatness of the plate is vital as the gyroscope assemblies are all mounted upon this surface. Alignment of their centre of masses and symmetricity are all critical to the function of the overall system as stipulated in Table 6.1. Two Ø4mm dowel holes and two Ø6.5mm clearance holes are machined in the disc to mount the gyroscope mount legs in place. A recess is

added in the disc plate to ensure correct alignment when assembling with the central cone as seen in Figure 6.13. Four large weight reducing cut outs are added to reduce overall weight and give additional clearance should the flywheel size need to be increased.

The batteries selected for the brushless DC motors are 22.2V, 6 cell lithium polymer (Li-Po) batteries. Li-Po batteries are selected as they are lightweight and designed to be used in conjunction with the chosen flywheel motors. These coupled with the 245Kv rating on the motors give a top speed of approximately 5400rpm (meeting the requirement set in Table 6.1). To mount the batteries, 5mm recesses are milled under the disc (see Figure 6.13). The batteries are inserted into these and held in place with two 1mm mild steel brackets that are bent into shape. Each bracket is secured with two cap screws. Positioning the batteries below the disc helps contribute to its gravitational stability,

The embodiment design of the disc resulted in a much lighter assembly that met all the requirements specified at the start of the development phase.

6.5.3 External structure

Objectives in the development of the external structure, shown in Figure 6.14 were to reduce the overall weight of the assembly and to optimise the design such that it was easily integrated with the other sub systems that make up the stable platform.

The outer ring is to be water jet cut from 7075 aluminium plate. The outer ring has a maximum diameter of 620mm. Attached to the outer ring are 8 outer ring mount legs.

The use of eight legs should accommodate for any size restoring force the system subjects the ring to and will also ensure it is held rigidly in position. The legs hold the ring at a predetermined height and are adjustable (by moving M20 nuts located on either side of the outer ring mount plate). The overall length of each leg is 160mm. Each leg is secured to the outer ring by four cap screws. The legs are manufactured from 5025 aluminium and turned in a CNC lathe.

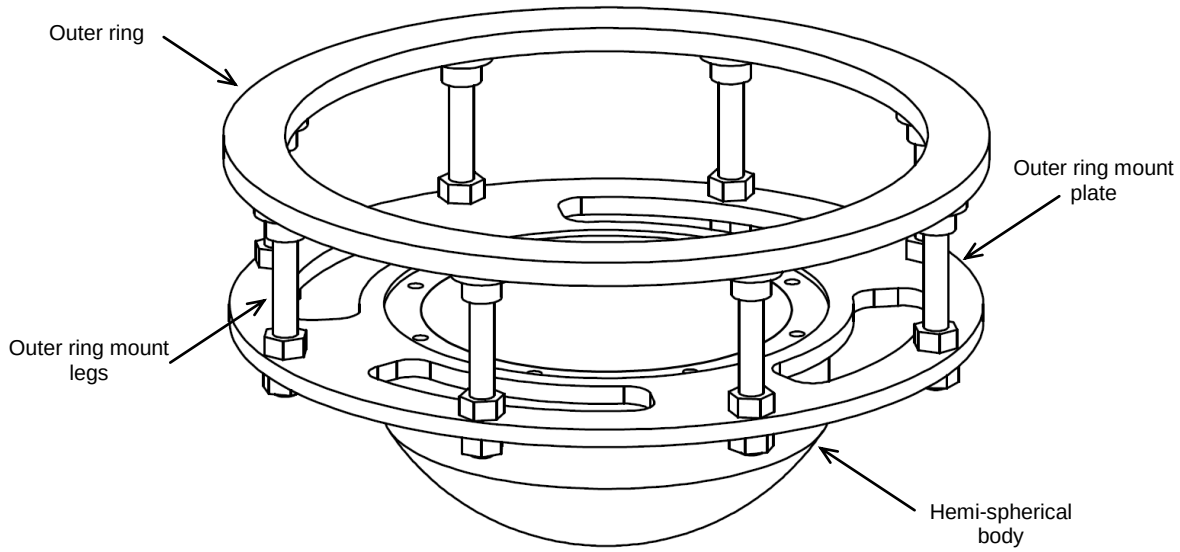

Figure 6.14 – Embodiment of external structure

The outer ring mount plate is made of 7075 aluminium plate. This plate is to be water jet cut oversize and then machined to the final dimensions (outside diameter to match the outer ring diameter). Weight reduction cut outs have been added along with a set of clearance holes on a 330mm PCD and a machined recess to allow for the mounting and alignment of the disc drive assembly.

The hemi-spherical body is to be made of model board. Several layers of the board will be glued together and then the final shape cut in a CNC lathe. Model board has excellent machining properties and good strength. The bottom of the body will be coated with a thin layer of fibre glass to increase wear resistance and reduce friction between the body and the floor. Holes are to be drilled and tapped and then coated with super glue to give a hardened set of threads on a 330mm PCD that the disc drive mechanism will bolt down to.

The embodiment phase of the external structure has achieved all set requirements. The assembly is symmetric as per the requirement in Table 6.1 and weight has been kept to a minimum. The structure is able to move in every plane and the outer ring height is adjustable.

6.5.4 Disc drive mechanism and central pivot

Objectives in the development of the disc drive mechanism, shown in Figure 6.15 were to develop a solution for housing all rotating components and to integrate the assembly into the overall system while providing adequate strength and minimum weight. The disc drive mechanism must also remain clear of the disc as it tips back and forth.

The bearing housing is developed to house the 12V DC motor, drive shaft, flexible coupling and CV joint assembly. The housing is made from two sections of 5083 aluminium (a top bearing housing section and a bottom cone shaped section) heat shrunk together as shown in Figure 6.17. The geometry of this bearing housing has been optimised in SolidWorks such that the 12V DC motor is able to fit inside

avoiding contact when the disc tipped at its maximum angle. The mass has also been minimised. The housing is designed to accommodate two bearings for the CV joint to rotate on; one Ø70mm internal deep groove single row bearing and one Ø20mm internal deep groove single row bearing. The bearings are then retained in the housing with internal circlips. The bearing housing mounts down onto the external structure and is secured in place via eight cap screws.

The motor is attached to the housing on a mount plate with a profile specific to the 12V DC motor machined onto it. This is discussed in more detail in Section 6.6. This mount then locks into place at the base of the bearing housing slotting into three machined grooves.

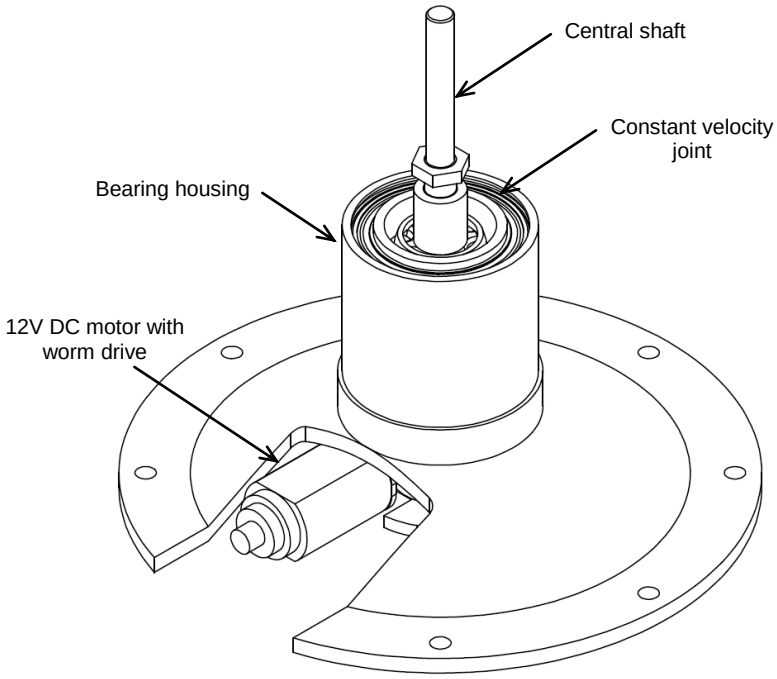

Figure 6.15 – Embodiment of disc drive mechanism

The CV joint assembly from Figure 6.17 was adapted from a Suzuki Alto drive shaft. The CV joint is attached via six bolts to a motor coupling shaft manufactured from

AISI 4140 alloy steel. The CV joint is disassembled and the outer housing machined to produce two bearing surfaces (Figure 6.16). This assembly slides into the top of the bearing housing and attaches to the flexible coupling that is connected to the 12V DC motor.

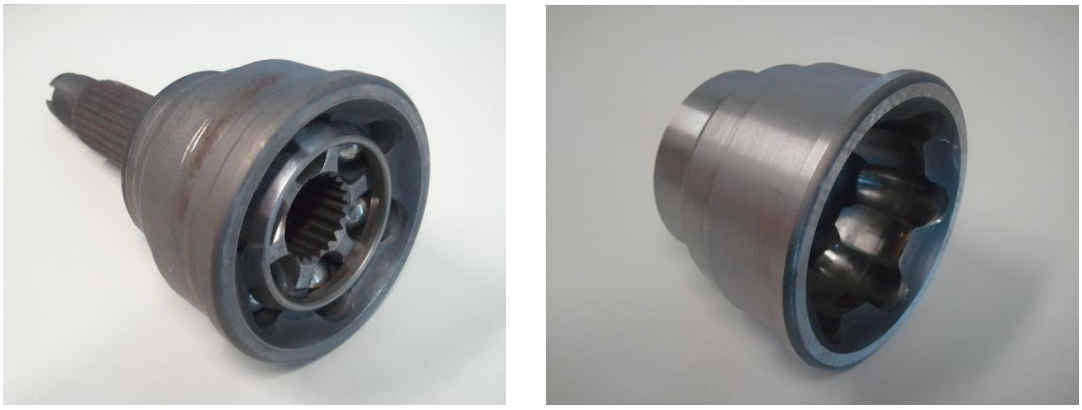

a) b)

Figure 6.16 – a) initial CV joint, b) CV joint machined to suit disc drive mechanism bearing housing

The drive shaft is attached to the CV joint via a spline. The spline is cut from an automotive shaft that is matched to the CV joint and machined to be heat shrunk onto the central shaft. This provides an excellent fit between the shaft and the CV joint with no backlash.

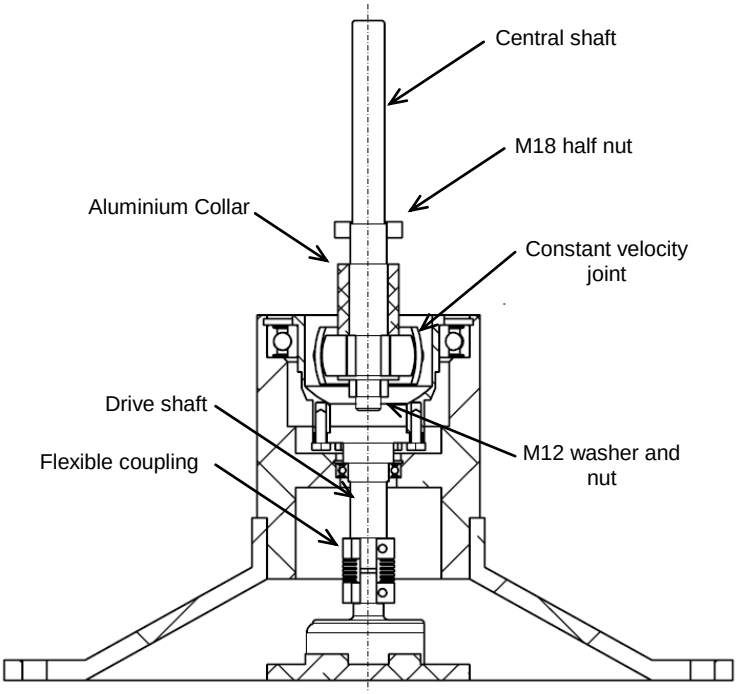

Figure 6.17 – Section of disc drive mechanism showing bearing location and CV joint

An increase in diameter of the central shaft retains it at the top of the CV joint while a threaded section at the bottom allows a washer and M12 bolt to be tightened securing the central shaft in place. An aluminium collar is placed between the shaft and the disc. The disc is assembled in place over the shaft and locked in place with an M18 half nut. The top section of the central shaft is ground to suit the tolerance specified for a Ø16mm linear bearing and allow for a smooth sliding fit. The length of this shaft is greater than required in case any alterations are made to the design during the testing phase.

The embodiment of the disc drive mechanism has resulted in a solution that is easily integrated into the other sub systems of the stable platform.

6.5.5 Gimbal frame linkage

Objectives in the development of the gimbal frame linkage, shown in Figure 6.18 were to: develop the assembly to reduce overall weight; to ensure friction between joints is kept at a minimum; and ensure the strength of each linkage member is sufficient to withstand the loads they are subjected to.

Although the rigid fixed length connection arm (Figure 6.7) was selected in Section 6.3.5, the design is altered so that only one of the fixed length connections is used. This fixed length rigid arm will act as the alignment member constraining the rotation of the linear bearing assembly.

The other three connecting arms will be assembled from rod ends attached to a threaded rod. The threaded sections of the rod ends on the connecting arms are opposite hand to allow for the overall length to be adjusted without disassembly. This adjustment will mean the angle of each of gyroscope gimbal frames can be altered individually to ensure they are all equal and level. The spherical bearing in the rod ends will also help when assembling the connections into place.

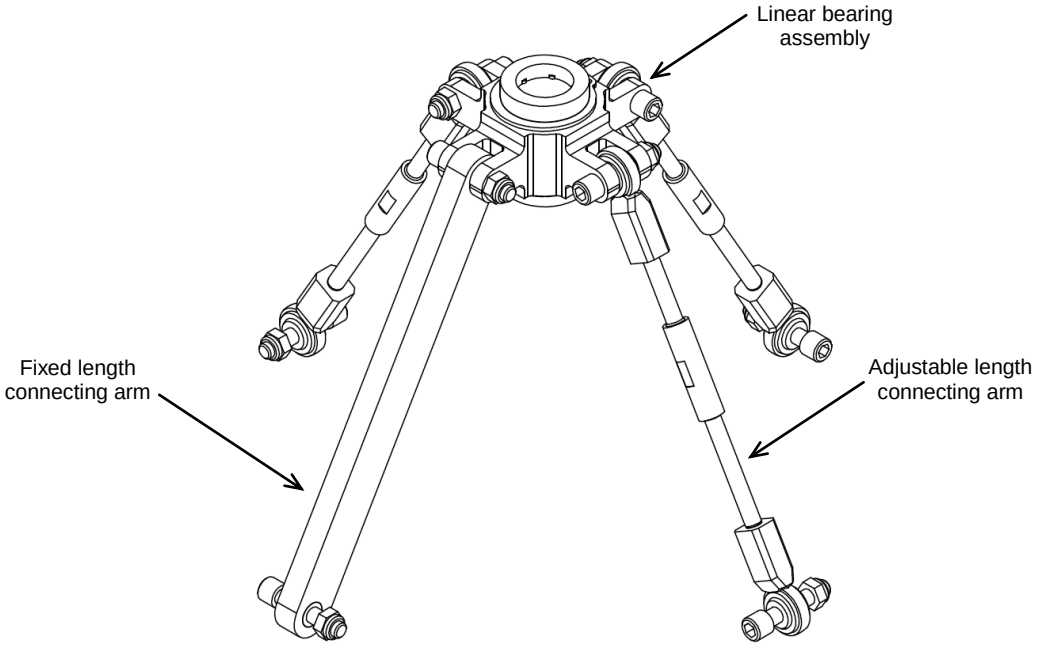

Figure 6.18 – Embodiment of gimbal frame linkage

The top and bottom of the connecting arms are attached to the gyroscopes via a cap screw and secured with a nyloc nut. The linear bearing attachment is wire cut from 7075 aluminium. Its shape has been optimised in SolidWorks to reduce weight. Large radii have been added to reduce stress. The attachment is placed over a Ø16mm linear bearing and secured in place with two 26mm external circlips to form the linear bearing assembly.

6.5.6 The general assembly

The general arrangement of the sub-systems discussed in Sections 6.5.1 to 6.5.5 is shown in Figure 6.19. This figure includes the embodiment design features discussed in the previous section.

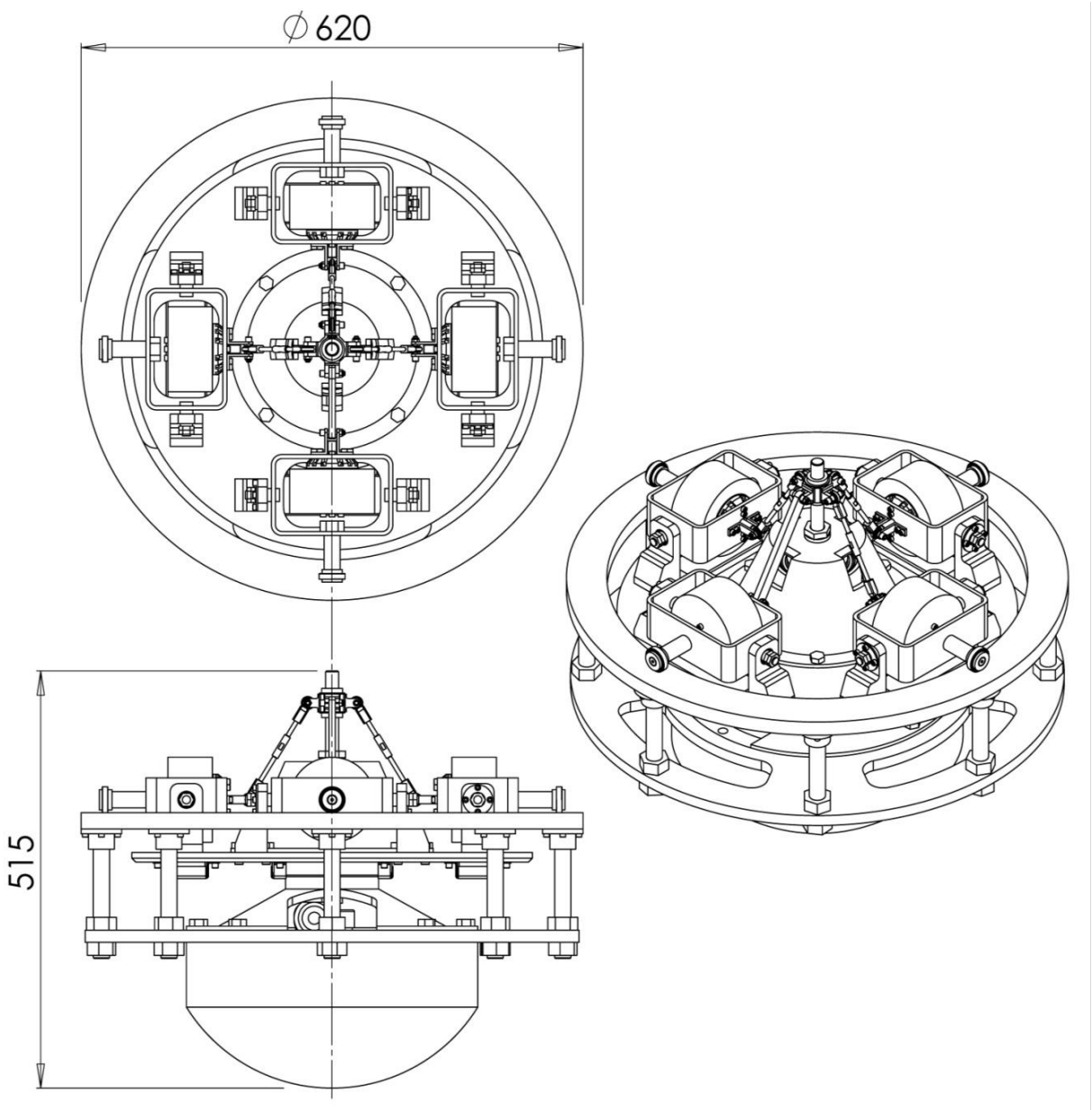

Figure 6.19 – Orthographic and isometric views showing the embodiment design for the stable platform

6.5.7 Assessment of embodiment design stage

The embodiment design stage was assessed using the embodiment design checklist, Figure B8, from Hales & Gooch (2004).

Figure B.8 shows confidence in meeting the functional requirements for the system. Several areas of concern are:

- the precession drive motor power supply has not been considered. This will need to come from an external source off the stable platform system. As the motor is DC, a variable power supply should be sufficient for testing to determine the optimal operating speeds.

- The brushless DC motors require electronic speed controllers (ESC) and a receiver to operate. They must be located within the vicinity of the motors and batteries as they connect up to both of them. The mass of a single ESC is approximately 30 grams.

- a large number of wires from the motors, batteries and ESC's will be located around the system. These will all be rotating with the disc. A safe method of securing and routing these connecting wires will be implemented with the electrical technicians at the University of Canterbury Mechanical Engineering Department.

6.6 Detailed design

The general assembly for the overall stable platform system following the detailed design stage is illustrated in Figure 6.20.

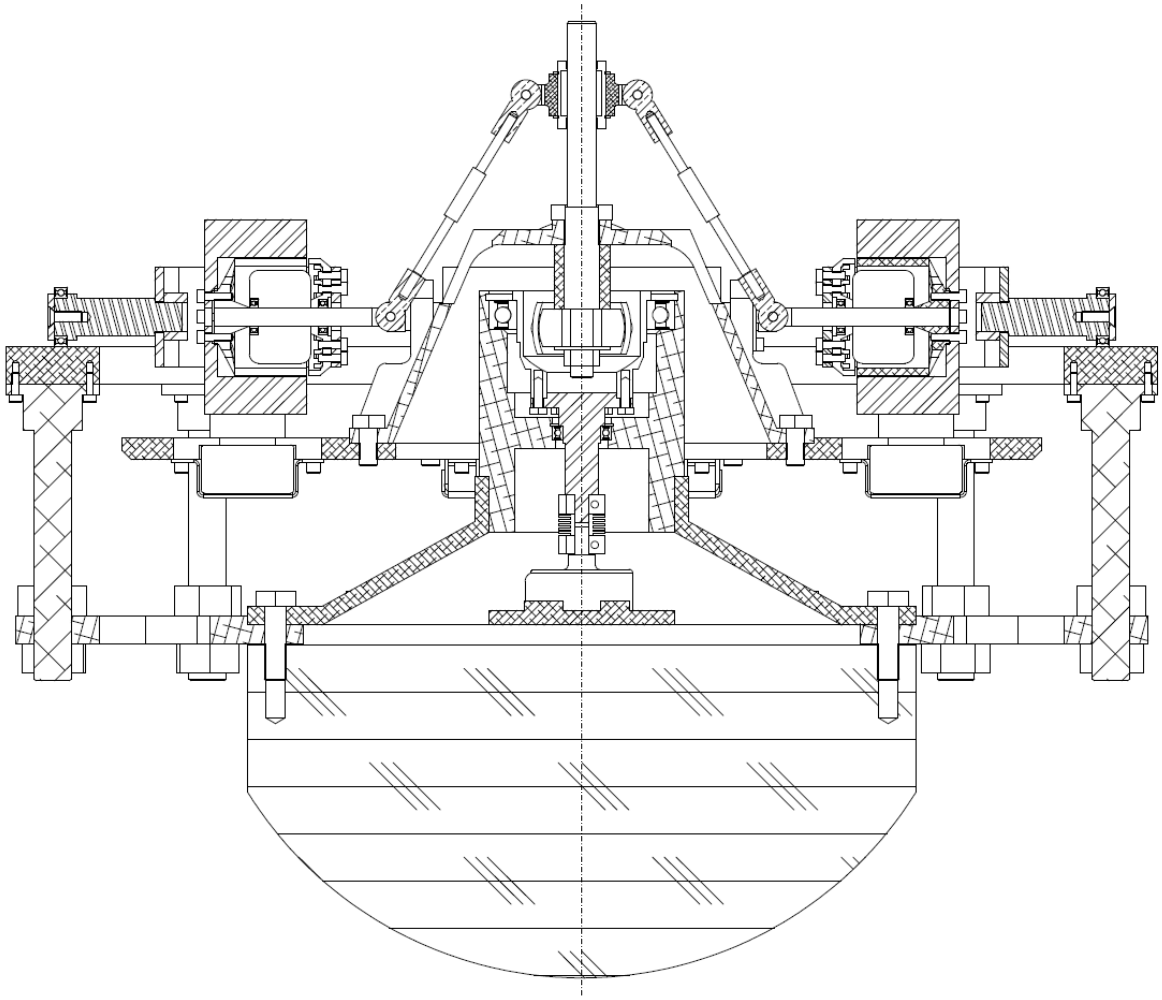

Figure 6.20 – Cross section view of the general assembly for the final stable platform conceptual design

All components were to be designed so that they could be manufactured with the equipment available to the University of Canterbury Mechanical Engineering Department Workshop. Suggestions for machining procedures have been included on manufacturing drawings where appropriate.

The DC drive motor is mounted in place onto a profile cut on the CNC mill. Due to the lack of mounting points on the motor this was the most ideal method to retain it in place. To accurately establish the dimensions of this profile ensuring a good fit the

profile was determined using a coordinate measurement machine (CMM) (Figure 6.21). This information was then transferred into SolidWorks where a profile for the CNC mill was generated.

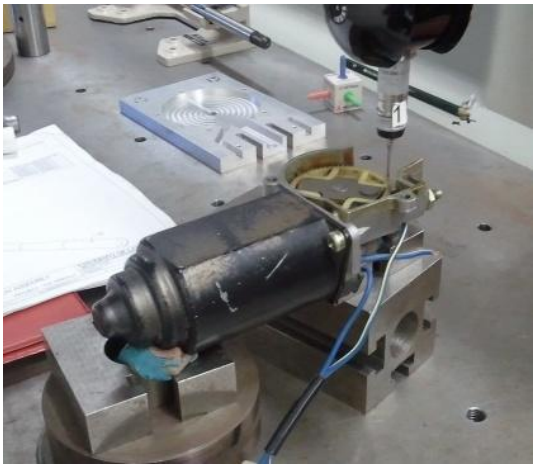

Figure 6.21 – Determining the DC drive motor profile using the CMM

Control of the flywheel was achieved using a 6 channel radio transmitter. A test rig was set up to ensure the motors operated as predicted and the maximum speed was measured using a tachometer to ensure it was equivalent to the predicted theoretical speed. The radio controller allows the stable platform to be operated from a safe distance.

In several locations on the assembly small cut outs and windows were added to the designs to allow access for an Allen key so cap screws could be tightened up to the required torque.

The detailed design stage was assessed using the detailed design checklist, Figure B.9. This critical stage in the evaluation of the design process suggests a high level

of confidence that the final prototype design will perform as intended. Review of the tables in Appendix B shows continued improvement of the design over the conceptual, embodiment and detailed design phases. This is a desirable outcome showcasing the advancement of the design to the final prototype solution

6.7 Stability conditions inequality

Having established the parameters and geometry for the prototype stable platform we are able to check that the stability conditions of the inequality derived in Chapter 4

$$\mu\left(M_s h_s + (M_d + 4M_g)h_d\right)g < 4(I)^2\left(\dot{\phi}_g\right)^2\omega_0\left(\frac{r_g + r_d}{r_g}\right) \qquad (4.47)$$

are satisfied.

Substitution of the known values of the prototype parameters into the inequality derived in Chapter 4 show that is has been satisfied (72 < 261). The stable platform prototype should exhibit oscillatory motion as it stabilizes the external structure.

6.8 Manufacture and testing of stable platform prototype

All components were manufactured in the University of Canterbury Mechanical Engineering Workshop and assembled in a secure testing container. No issues were encountered during the manufacture and assembly stages.

Testing of the prototype took place in a shipping container behind a clear polycarbonate wall to ensure the safety of the operator had a failure of the system occurred.

The testing procedure for the stable platform prototype involved turning on all the flywheel motors and the disc drive mechanism so that the disc assembly was precessed at a constant speed. The speeds of the two sub-systems were then varied and the behaviour of the system observed. The size of the moment produced by the system was only measured when the system was shown to remain stable. Due to the nature of the system, the highest stabilizing moment was known to occur at the highest flywheel and disc precession speeds. Subsequently most testing took place at these values.

Testing of the stable platform prototype revealed that the system was not stabilizing as intended.

6.8.1 Issues with initial stable platform prototype

It was desirable to identify where the main issues in the design of the prototype were and determine solutions to rectify these.

After extensive testing the issues with the initial stable platform prototype were established as:

- precession of disc – initial testing revealed that while the precession of the disc resulted in the gyroscopes pushing downward, the driving arrangement

meant that all four gyroscopes could push down at the same time on the outer ring (an occurrence that was undesirable). Other methods for precessing the disc needed to be considered.

- disc position – the disc was not remaining level during operation. As the external structure tipped the disc tipped with it. This is directly related to the height of the pivot point of the disc above the centre of mass of the disc assembly.

- angular momentum from gyroscopes – it is desirable to further increase the angular momentum of the system to enhance the restorative torque produced by the flywheel. Investigation into increasing flywheel speed and inertia was required.

- system weight – the overall weight of the stable platform prototype was considered too high reducing the responsiveness of the system. A further reduction in all areas of the system was required.

- external structure – an external structure that allowed a means for measuring the restoring torques produced by the system is required.

The optimisation and development phase that addresses these issues is described in detail in Chapter 7.

6.9 Concluding comments

The systematic approach adopted for the design of the stable platform system has resulted in the manufacture, assembly and testing of a preliminary prototype. This chapter has shown that a working mechanical configuration of the proposed stable platform schematic model can be manufactured at an economically feasible size. Further testing and development of the prototype configuration is required to obtain the desired oscillatory response.

7

Development of Prototype A

7.1 Introduction

We will define the first prototype stable platform designed in Chapter 6 as "*Prototype A*". Having shown that the proposed schematic design for the stable platform is manufacturable within the resources of the overall research project, several modifications were required to improve the performance of the system. These modifications took place over the duration of this research. The required modifications were revealed after significant testing had been performed on *Prototype A*.

A systematic approach was adopted for the development of *Prototype A*. The main issues in performance have been identified (Section 6.8.1) and solutions then generated based upon their expected impact on the overall stabilization process. This would ensure that time was spent efficiently developing the prototype with the aim of significant changes taking priority and being completed first. The physical changes to *Prototype A* were then substituted numerically into Equation (4.47) to gauge how effective their development had been.

The purpose of this chapter is to develop Prototype A so that it actively stabilizes an imbalanced mass caused by the external structure moving off the vertical. While all sub-systems currently

function as intended, development of the system would lead to the stable platform exhibiting the desired oscillatory behaviour. Each development will be assessed, implemented and then evaluated to validate its impact on the overall performance of the system. Pictures have been included where relevant.

7.2 Expected impact of changes

In order to quantify the expected impact of the changes to *Prototype A,* a ranking system was established based upon three governing factors. Each of these factors is given a score to measure the overall impact the development will have on the performance of the system. Table 7.1 shows how the ranking points are distributed.

Table 7.1 – Development ranking system

Time to complete	Ease of Integration	Overall impact on performance	Total
/5 5 = quick to complete 1 = long completion time	/5 5 = simple to integrate into existing system 1 = integration will be complex	/10 10 = large impact on overall system performance 1 = little effect on stable platform performance	/20

The overall impact on the system has been multiplied by a double weighting factor as this is the most critical outcome of the optimisation process.

We establish a set of conditions that will predict how effective the proposed change will be and whether or not to implement it into the system. These are:

Total < 10 development will not be implemented into *Prototype A*

Total ≥ 10 ≤ 15 development will have a positive impact on the performance of *Prototype A*. Implementation of development will depend upon time required and ease of integration.

Total > 15 ≤ 20 development will have a significant impact on the performance of *Prototype A*. Change will definitely be implemented.

7.3 Implemented developments

The following section describes the changes that were implemented to *Prototype A* to improve the systems performance.

7.3.1 Increased battery voltage and battery relocation

The initial batteries used in the prototype gave the flywheels a top speed of approximately 5400rpm. An increase in battery voltage would increase the magnitude of the stabilizing moment.

Table 7.2 – Increase in battery voltage and relocation

Time to complete	Ease of Integration	Overall impact on performance	Total
4/5	3/5	7/10	**14/20**

The battery voltage was increased from 22.2V to 44.4V (the maximum voltage the ESC's were able to manage). This doubled the top speed of the flywheels to approximately 11000rpm.

The batteries were relocated from the bottom of the disc to the top due to geometric constraints. Had larger batteries been placed underneath the disc the tilt angle of the disc/gyroscope assembly would have been restricted by contact with the external structure.

Figure 7.1 shows the proposed location of the batteries up on top on the disc adjacent to the gyroscopes. Mounting the batteries below the disc would have contributed to lowering the centre of mass of the disc assembly however adding extra batteries and having their COM sitting below the pivot point still had a positive impact on the stability of the disc.

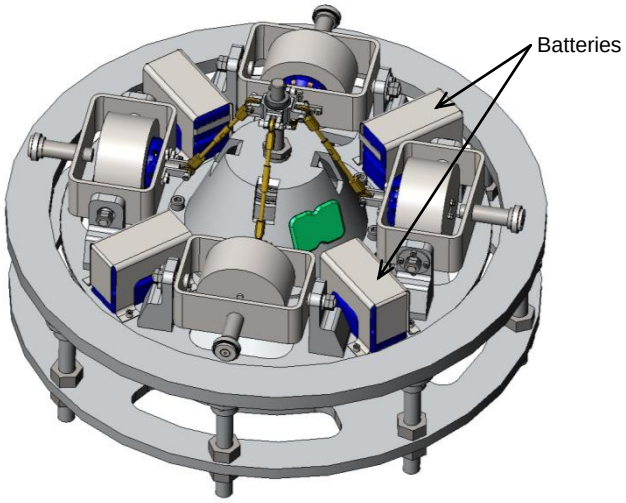

Figure 7.1 – Proposed increased battery voltage layout

Sheet metal covers were fabricated to secure the batteries in place. A 5mm recess was also machined in the disc for the batteries to locate in before the cover was placed over the top.

Increasing the battery size had a positive impact on *Prototype A*. The higher battery voltage has increased the top speed of the flywheels resulting in a greater stabilizing moment being produced and increased the gravitational stability of the disc.

> ***Outcome:*** *The increased battery voltage improved the overall stabilizing moment produced by Prototype A.*

7.3.2 New external structure

Testing of *Prototype A* revealed that the hemi-spherical external structure behaved too erratically to accurately quantify the performance of the system. This arrangement would be an excellent method of demonstrating the stabilizing ability of system once it has been shown to perform as intended but for testing a new design was required.

Table 7.3 – New external structure for testing

Time to complete	Ease of Integration	Overall impact on performance	Total
3/5	4/5	4/10	**11/20**

Figure 7.2 *a)* shows the proposed SolidWorks model for the new external structure. The outer ring and ring mount plate were mounted upon a base plate. The new external structure is only able to pivot in one plane. Due to the symmetry of the system, if the stable platform is able to maintain stability in one plane, it will also maintain stability in three planes.

Figure 7.2 *b)* shows the new external structure assembled into the system. The frame pivots through a single shaft mounted on two Ø35mm pillow blocks. A 415mm

lever arm is used to control the tilt angle of the external structure. By measuring the force at the end of this lever arm the size of the restoring moment that the system produces can be determined. A safety stop was added at the back of the test frame so that the system was unable to tip over backwards.

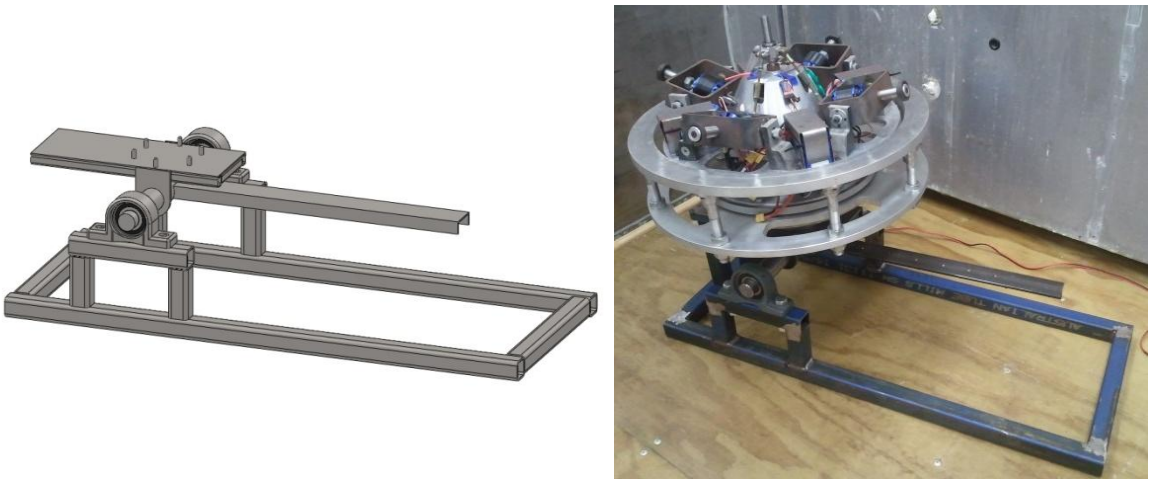

a) b)

Figure 7.2 – a) Proposed external structure, b) external structure assembled into system for testing

The design also allows for accurate measurement of the height of pivot points and other critical features above the origin (tilt frame pivot point). Accurately measuring these values is critical to the theoretical and experimental comparison of the system.

The new external structure improved control of the system allowing a more accurate method of measuring the magnitude of the restoring moment. As the system is symmetric, and therefore will behave the same in every direction, only being able to pivot in one plane does not affect the verification of the stable platform design.

Securing the structure to the floor reduced vibrations of the system when testing.

Outcome: *The new external structure allows the system to be accurately controlled for testing.*

7.3.3 Optimisation of flywheel geometry

Having increased the speed of the flywheels (increased battery capacity) an increase in the inertia of the flywheel was also investigated.

Table 7.4 – Optimisation of flywheel geometry

Time to complete	Ease of Integration	Overall impact on performance	Total
3/5	5/5	7/10	**15/20**

Table 7.5 outlines a series of flywheel iterations performed on Excel and verified in SolidWorks. Each iteration altered the dimensions of the flywheel with the aim of obtaining the optimum geometry to produce the largest angular momentum in the available space.

The main aim of this process was to optimise flywheel inertia while minimizing mass. All masses and moments of inertia have been calculated using plain carbon steel (density = 7800kgm^3).

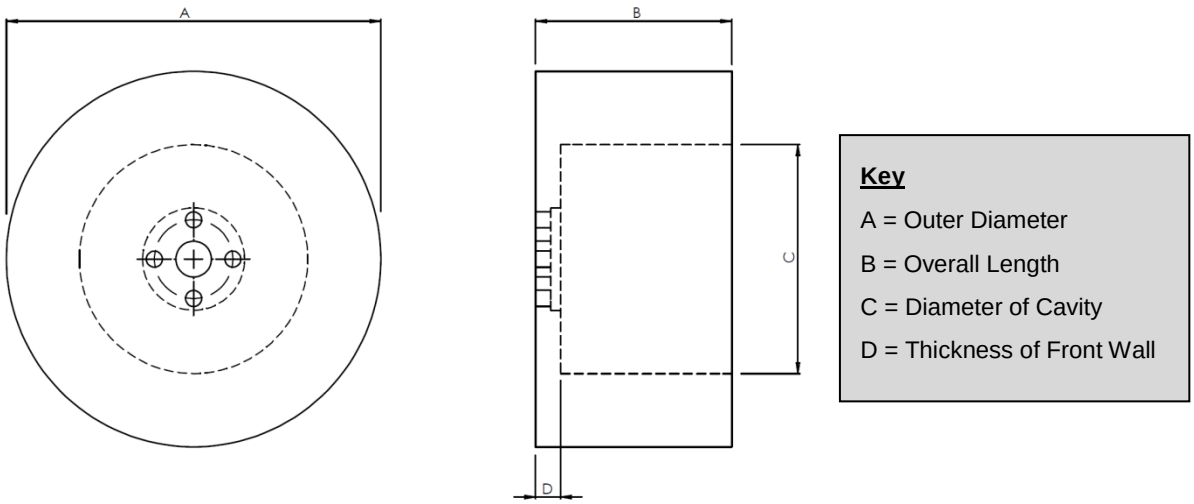

Figure 7.3 – Optimisation of flywheel geometry key

Based on the equation for inertia it is unnecessary to adjust dimension A. Setting this dimension at a maximum value will ensure inertia is always at its largest possible value. Dimension A is only restricted by the size of the gimbal frame. SolidWorks revealed that dimension D is optimised when it at its minimum possible value i.e. the minimum value that provides the required strength and stiffness. The only dimensions that needed to be varied in the iterative process were the depth of the flywheel (dimension B) and the diameter of the centre cavity (dimension C).

Table 7.5 - Variation in flywheel dimensions

Flywheel revision.	A	B	C	D	Mass (kg)	Moment of Inertia (kgm2)
Initial prototype flywheel	105	55	90	7	1.314	0.002706
Max. centre cavity value	130	55	64	5	4.423	0.01139
Min. centre cavity value	130	55	120	5	1.267	0.004088
Max. flywheel depth value	130	55	64	5	4.423	0.01139
Min. flywheel depth value	130	25	64	5	2.070	0.005209

Table 7.5 shows the maximum and minimum dimensions (in millimetres) and the mass and moments of inertia obtained by varying dimensions B and C.

Figure 7.4 shows a plot of mass versus the moment of inertia of the flywheel obtained by varying dimensions B and C by 1mm per iteration.

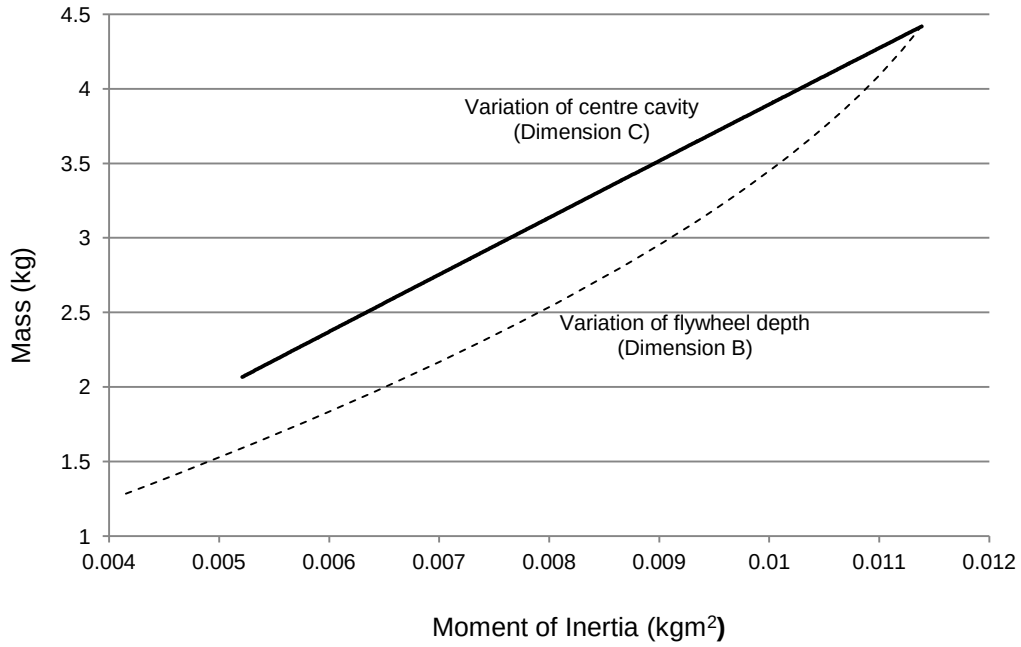

Figure 7.4 - Variation of centre cavity diameter (solid) and flywheel depth (dashed)

Figure 7.4 shows that varying the centre cavity or the flywheel depth both had a similar impact on the change in mass and moment of inertia. The cavity diameter was selected as the best dimension to alter as it did not shift the centre of mass of the flywheel relative to the motor centre of mass (a critical design requirement). A flywheel of mass less than 2kg was desirable to limit the weight of the stable platform. The dimensions of the optimised flywheel are summarised in Table 7.6.

Table 7.6 – Optimised flywheel geometry

Flywheel No.	A	B	C	D	Mass (kg)	Moment of Inertia (kgm2)
Optimised flywheel	130	55	130	5	1.836	0.006001

Figure 7.5 a) and b) shows the initial flywheel used on *Prototype A* and the optimised flywheel.

a) b)

Figure 7.5 – a) flywheel used in the initial prototype (ø110mm), b) optimised flywheel geometry (ø130mm)

To balance the flywheel so that vibrations are minimised during operation, the mounting face of the brushless DC motors were machined to help obtain a true flat surface for accurate flywheel location (Figure 7.6). The flywheel mounting face was then machined to equivalent dimensions. This accurate method of machining both surfaces to be identical resulted in a large decrease in axial deviation when the flywheels were rotating and greatly reduced vibrations created by misalignment of

the flywheels during operation. This allowed the system to be run at higher speeds for an extended period of time.

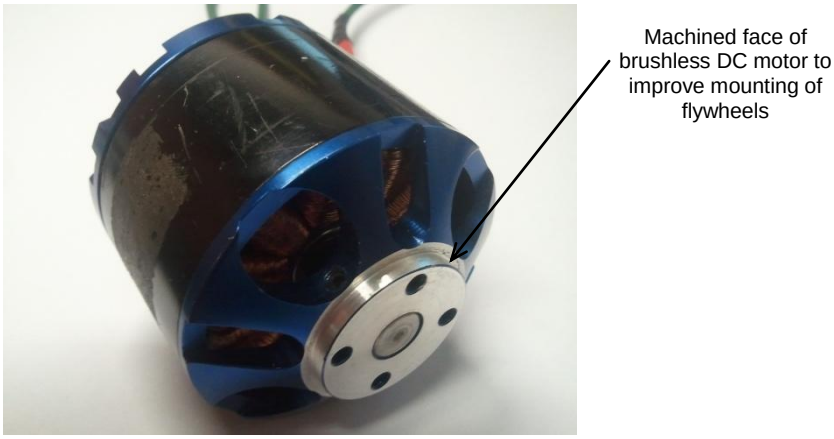

Figure 7.6 – Brushless DC motor showing machined mount face for mounting of flywheels

The resulting flywheel has been optimised through an iterative process to determine the best mass to moment of inertia ratio. The final flywheel is easily integrated into the existing system. An accurate method of machining both the flywheel and motor to fit one another has greatly reduced vibrations. These changes resulted in an overall increase in size of stabilizing moment the system is able to produce.

> ***Outcome:*** *The optimised flywheel geometry has significantly enhanced the restoring moment produced by the system*

7.3.4 Driving the outer ring

When the disc is precessed in one direction at a constant speed one of the gyroscopes pushes down on the outer ring. This downward force re-orientates the disc so that it is parallel with the outer ring resulting in all four gyroscopes pushing

down at the same time. When this occurs there is no possibility of stabilizing the external structure.

To overcome this problem, the disc must always be accelerating or decelerating (velocity is constantly changing). Two solutions were determined to solve this issue.

- Setting up a control system that constantly varies the speed of the disc drive motor.
- Remove the motor allowing the disc to rotate freely and drive the outer ring. In this case, when the structure deviates from the vertical, the outer contact arms contact the outer ring and friction accelerates the disc assembly around.

Driving the outer ring was selected as the preferred option. The main advantage of this design is that the disc remains stationary until contact with the outer ring occurs. This will make the system more responsive to the tipping of the external structure.

Table 7.7 – Driving the outer ring

Time to complete	Ease of Integration	Overall impact on performance	Total
2/5	2/5	7/10	**11/20**

The 12V DC motor is connected to a 1:1 pulley arrangement with drive being transferred to the outer ring via a poly v-belt. The drive arrangement is mounted upon the external structure frame. A fixed centre pillar is bolted to the frame and a threaded section on top of the shaft allows the disc bearing housing to be screwed down and fixed in place. An outer rotating shaft is fitted over the fixed centre pillar

and located on two bearings. The outer rotating shaft attaches to the outer ring bottom mount plate. Figure 7.7 shows the proposed outer ring drive arrangement.

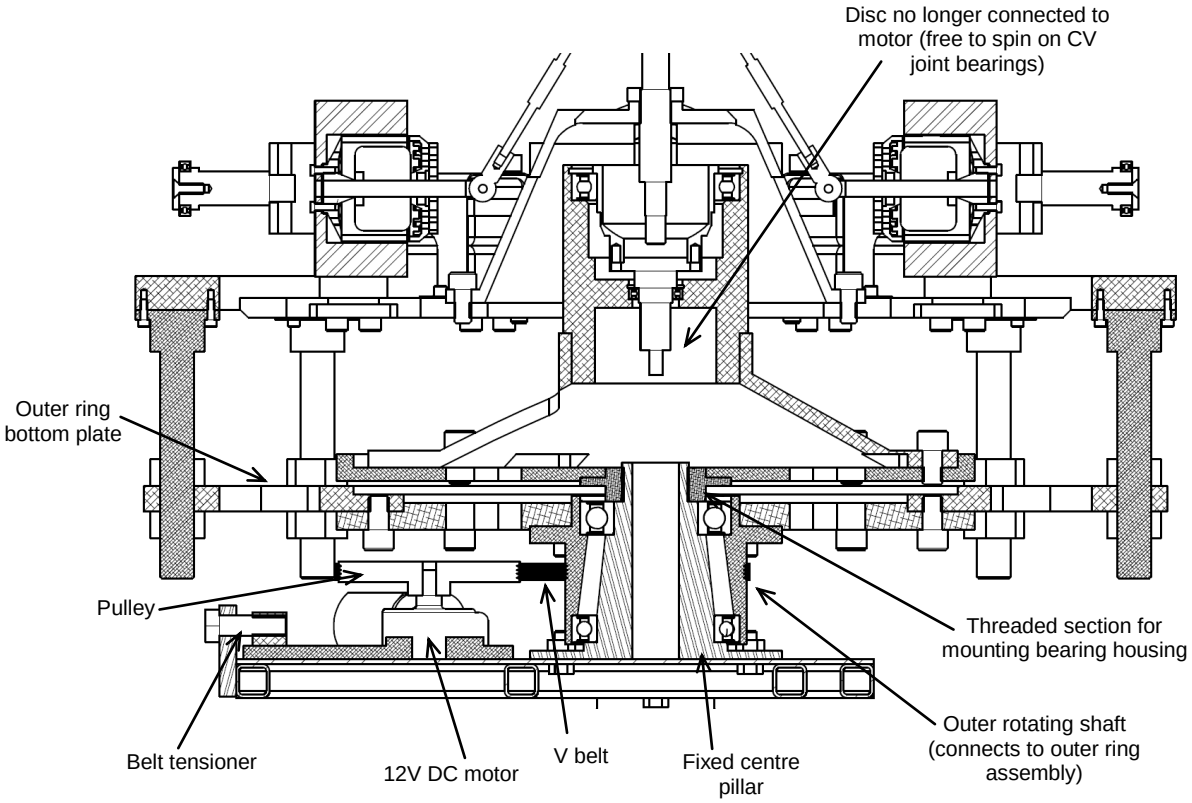

Figure 7.7 – Proposed outer ring drive assembly

Figure 7.8 shows the outer ring drive mechanism assembled into the system. The system behaved as intended. The addition of friction wheels instead of bearings on the end of the outer contact arms meant the disc was accelerated around when contact with the outer ring occurred (similar to the Brennan monorail).

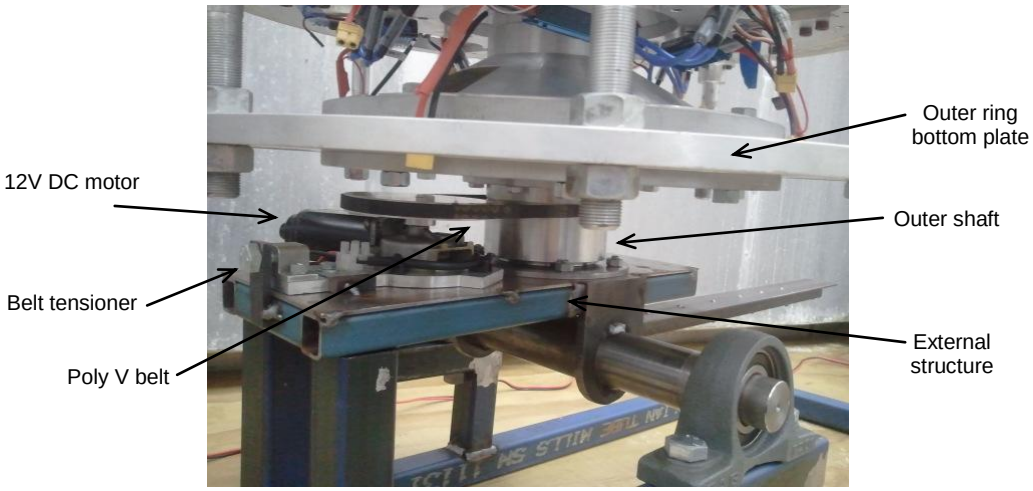

Figure 7.8 – Outer ring drive arrangement assembled into stable platform system

Outcome: *The outer ring drive arrangement means the disc is no longer precessed at a constant velocity*

7.3.5 Implementation of universal joint as central pivot

Testing revealed that the CV joint did not move as freely as intended and as a result the disc assembly did not pivot into the level position as the external structure moved off the horizontal. The axial loading from the weight of the disc assembly on the bearings inside the CV joint caused them to bind.

The CV joint arrangement was replaced by a universal joint design.

Table 7.8 – Implementation of universal joint

Time to complete	Ease of Integration	Overall impact on performance	Total
4/5	4/5	8/10	**16/20**

A Ø32mm steel universal joint was used. Holes were tapped in each end of the universal joint; one end for the disc central shaft to screw into and one for a cap screw that retained a universal joint adaptor coupling. The universal joint arrangement rotates on two bearings assembled into the existing bearing housing.

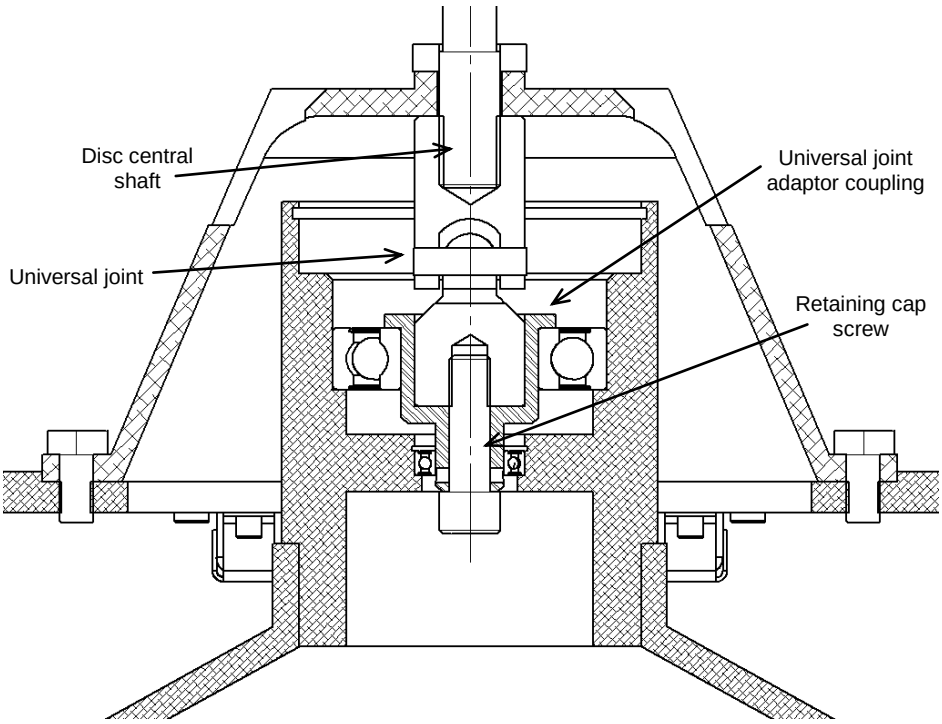

Figure 7.9 – Section view of universal joint pivot assembly

Figure 7.10 shows the manufactured universal joint assembled with the adaptor coupling and disc main shaft. The new design achieved the objective of lowering the tipping resistance of the disc assembly. The design was easily adapted into the existing system. Although universal joints produce a non uniform angular velocity, calculations showed that at the speed the disc precesses and angles the joint tips at these variances are negligible. The universal joint design also increased the distance

between the centre of mass of the disc and the disc pivot point enhancing the gravitational stability of the disc.

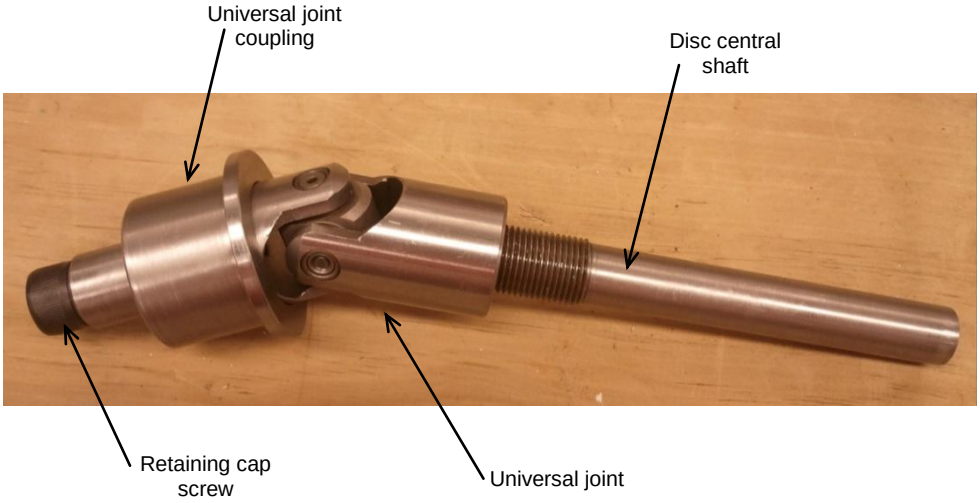

Figure 7.10 – Universal joint, coupling and main shaft assembly

Outcome: *The universal joint assembly has resulted in the disc maintaining a level orientation when the external structure tips off the horizontal*

7.3.6 Weight reduction

Weight was removed from the system via weight reducing cut outs. Several large steel components were also replaced with aluminium equivalents. Alternative materials (carbon fibre) were not considered due to time constraints on the project.

Table 7.9 – Reduction of weight of system

Time to complete	Ease of Integration	Overall impact on performance	Total
2/5	3/5	6/10	**11/20**

Figure 7.11 shows the weight reduced gimbal frame. The frame height was reduced from 50mm to 20mm and weight-reducing holes were drilled throughout the remaining section to further lower the frames mass.

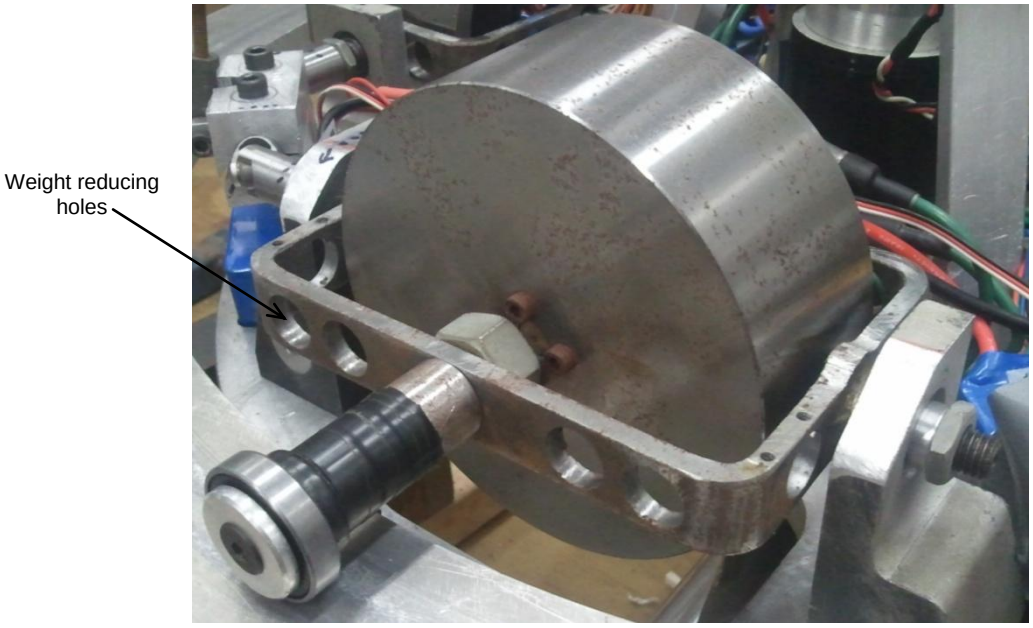

Figure 7.11 – Reduced weight gimbal frame

Outcome: *A reduction of approximately 6% of the overall stable platform weight was achieved resulting in a more responsive system.*

7.3.7 Spider counter weight

Testing revealed that the disc was not remaining level during operation. A counter weight frame was proposed to see if the reactions from the gyroscopes were causing precession of the disc in the desired directions. The counterweight allowed the centre of mass of the disc to be shifted well below its pivot point significantly enhancing its gravitational stability. Tests could then be run to verify that when the

outer ring contacted the outer contact arms, the gimbal frames pivoted and precession of the disc occurred.

Table 7.10 – Spider counterweight

Time to complete	Ease of Integration	Overall impact on performance	Total
4/5	5/5	7/10	**16/20**

The counter weight mounted upon the stable platform is shown in Figure 7.12. A set of four Ø100mm steel weights are hung equally spaced around the system as to not interfere with any rotation that occurs. The weights were attached to a spider frame via threaded rod sections. This also allowed more weight to be added to the frame if required.

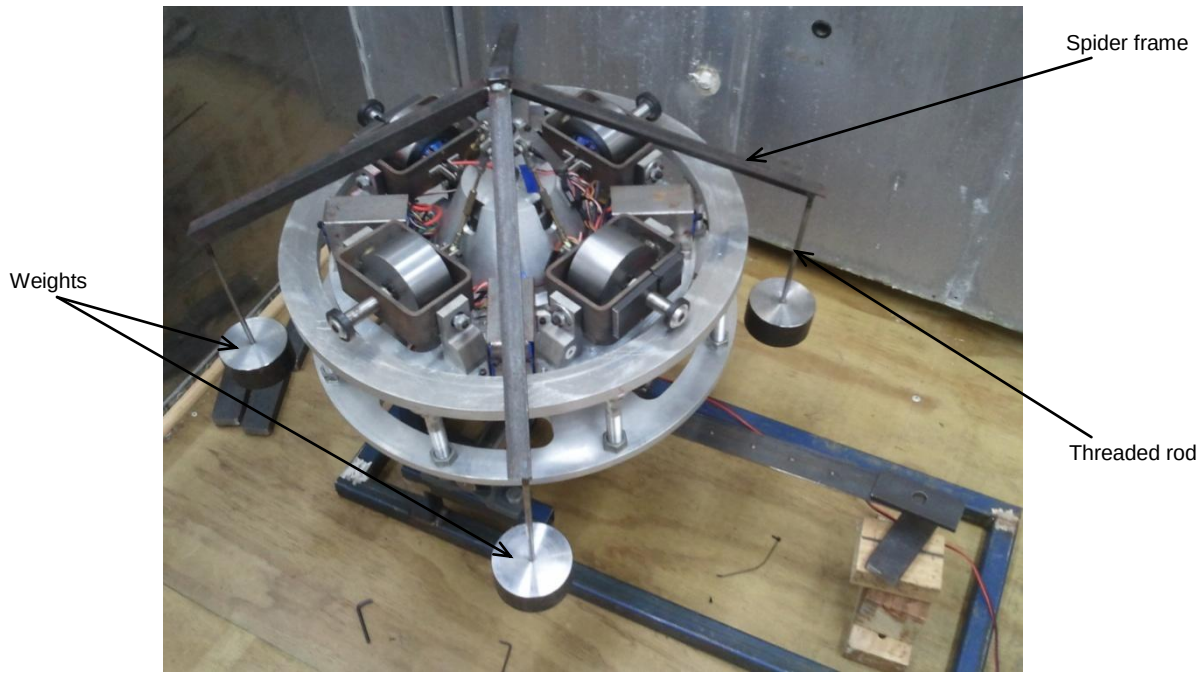

Figure 7.12 – Spider counter weight mounted upon stable platform

The design successfully proved that when the gyroscopes are run up to constant speed and the external structure is tipped off the equilibrium, contact between the outer ring and the contact arms cause the disc to precess around. This development showed that system was producing the desired reactions.

Although the counter weight proved that the stable platform reacted as intended, including it in the system was impractical. It greatly increased the rotational inertia of the disc and overall weight of the system.

> ***Outcome:*** *The addition of a large counterweight proved that the system was producing reactions in the intended directions when subject to a tipping force.*

7.3.8 Increase central pivot

Having shown the system was behaving as intended with the spider counter weight attached, other methods for increasing the gravitational stability of the disc were considered. The preferred solution was to increase the distance between the pivot point of the disc and centre of mass of the disc assembly.

Table 7.11 – Optimisation of flywheel geometry

Time to complete	Ease of Integration	Overall impact on performance	Total
2/5	5/5	8/10	**15/20**

A new centre cone design was produced in SolidWorks. The design looked to reduce the rotational inertia of the disc assembly (making it more responsive to precession) while increasing the distance between the pivot point of the disc and its centre of

mass. The mass, pivot point distance and rotational inertia of three configurations were compared in SolidWorks to gauge the impact the new centre cone design would have on the performance of the stable platform. The three configurations compared were:

- the disc arrangement of *Prototype A* that had been used for all testing of the system so far.
- *Prototype A* with the counterweight from Section 7.3.7.
- a new centre cone design fabricated out of aluminium that raised the height of the pivot point while reducing the overall weight of the disc assembly

The results of the comparison are shown in Table 7.12.

Table 7.12 – Central pivot comparison

	Weight (kg)	**Centre of mass to pivot distance (mm)**	**Rotational inertia (kgm^2)**
Initial prototype	23.18	11.25	0.6723
Initial prototype with counter weight	50.03	87.09	5.249
Raised pivot point	19.42	102.6	0.4144

The new disc centre section reduced the weight of the disc assembly by 16.2%, raised the pivot point by 91.4mm and reduced the resistance to rotation by 38.4%. The design maintained all the mount points of the original centre cone section. A new lightweight bearing housing arrangement was also designed and introduced in conjunction with the new centre cone.

Figure 7.13 a) and b) illustrates the comparison between the initial disc assembly and the increased pivot point design.

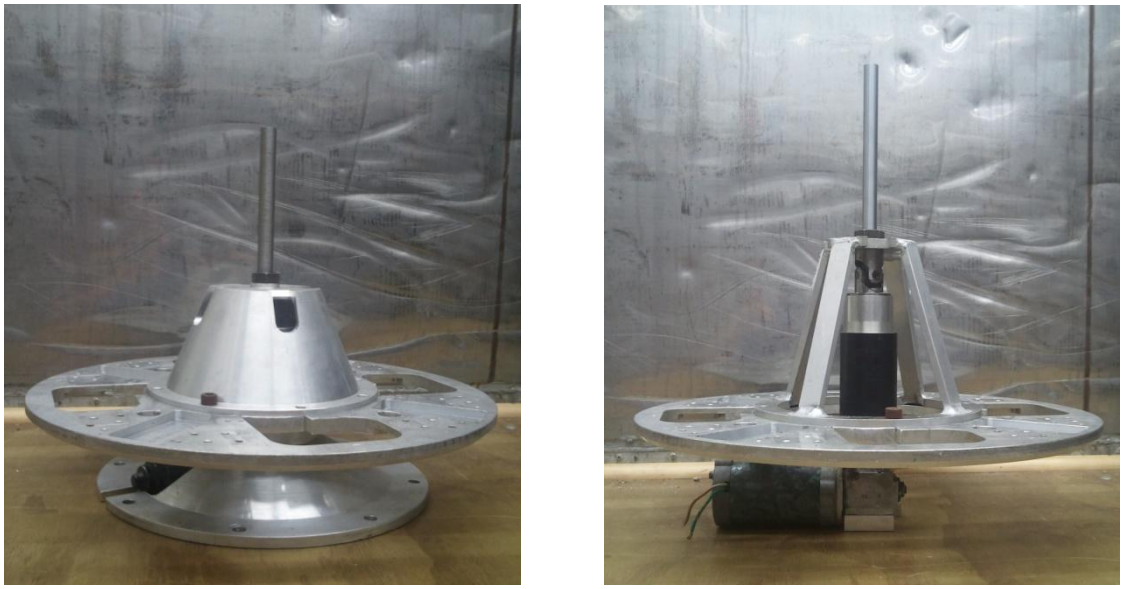

a) b)

Figure 7.13 – a) initial disc assembly and bearing housing, b) raised pivot point design

Outcome: *The new disc centre section increased the gravitational stability of the disc assembly and reduced the overall weight of the system*

7.3.9 Diametrically opposite gyroscope arrangement

Testing of *Prototype A* showed that performance of the system could further be improved by arranging the gyroscopes in diametrically opposite pairs. This would result in improved oscillatory motion of the disc. This arrangement required each pair of diametrically opposite gyroscopes to be rotate in the opposite sense to one another.

Table 7.13 – Diametrically opposite gyroscope arrangement

Time to complete	Ease of Integration	Overall impact on performance	Total
3/5	3/5	8/10	**14/20**

By coupling the gyroscopes together, when one pair of gyroscopes pivot downward the other pair would pivot up. As the disc precessed round, the upward pointing gyroscope outer contact arms would contact the outer ring and reverse the precession direction of the disc. This would occur at a high frequency resulting in the disc constantly oscillating back and forth about an equilibrium point (similar to the system Brennan developed). Two new linear slide linkage arms were needed to pivot two of the gyroscope assemblies from the front. Figure 7.14 shows the front pivoting gyroscope arrangement assembled into the system.

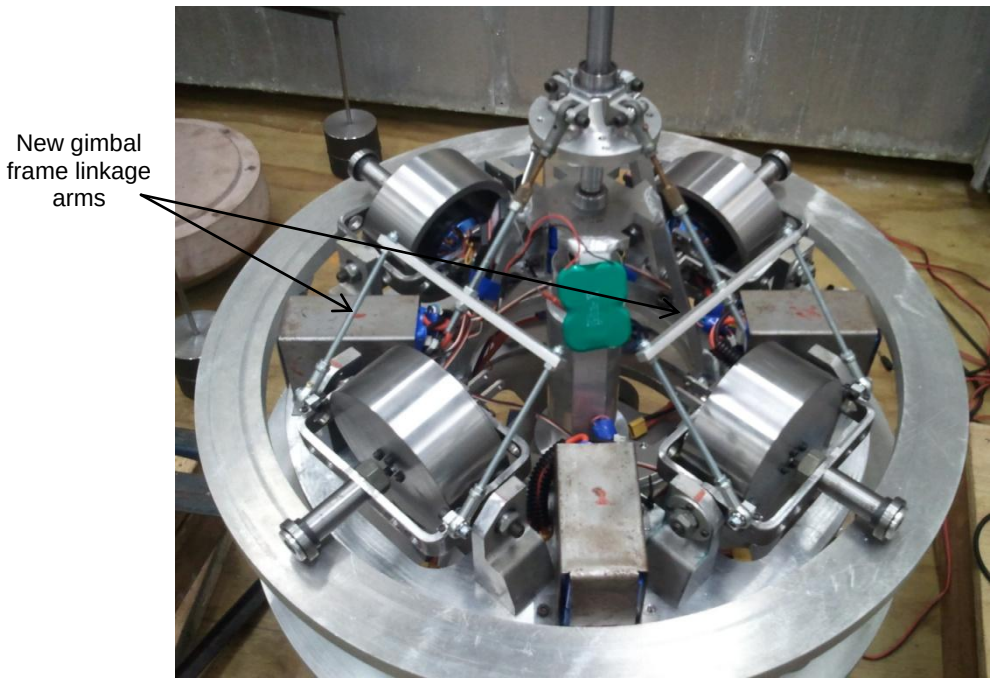

Figure 7.14 – Diametrically opposite gyroscope arrangement showing front pivoting gyroscopes

Initial testing of the diametrically opposite gyroscope arrangement showed the system performed as intended. One issue with the design was the unequal angles the gimbal frames pivoted at due to the connecting arms attaching at different points on the gimbal frame. This resulted in the outer contact arms contacting the outer ring at different angular positions.

An iterative process was used in SolidWorks and Excel to optimise the location of the front pivot to ensure the gyroscopes tipped at equal angles.

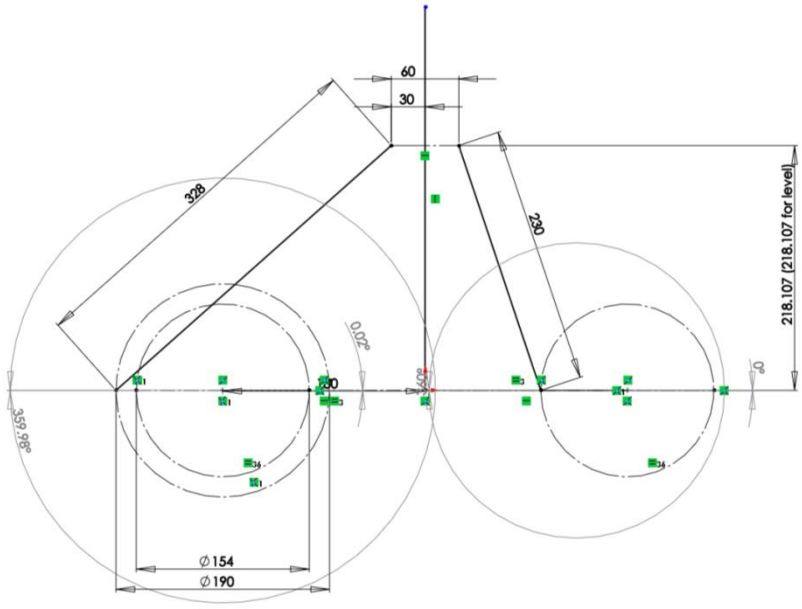

Figure 7.15 – Skeleton used in SolidWorks for iterative process in optimisation of front pivot location

The iterative process resulted in the maximum variation between the front and rear pivoting gyroscopes being reduced from 15 degrees to just 3 degrees. This discrepancy was taken as acceptable due to the variations present in the

manufacture and assembly of this type of system. Figure 7.16 a) and b) shows the comparison between the initial front pivot location and the final optimise location.

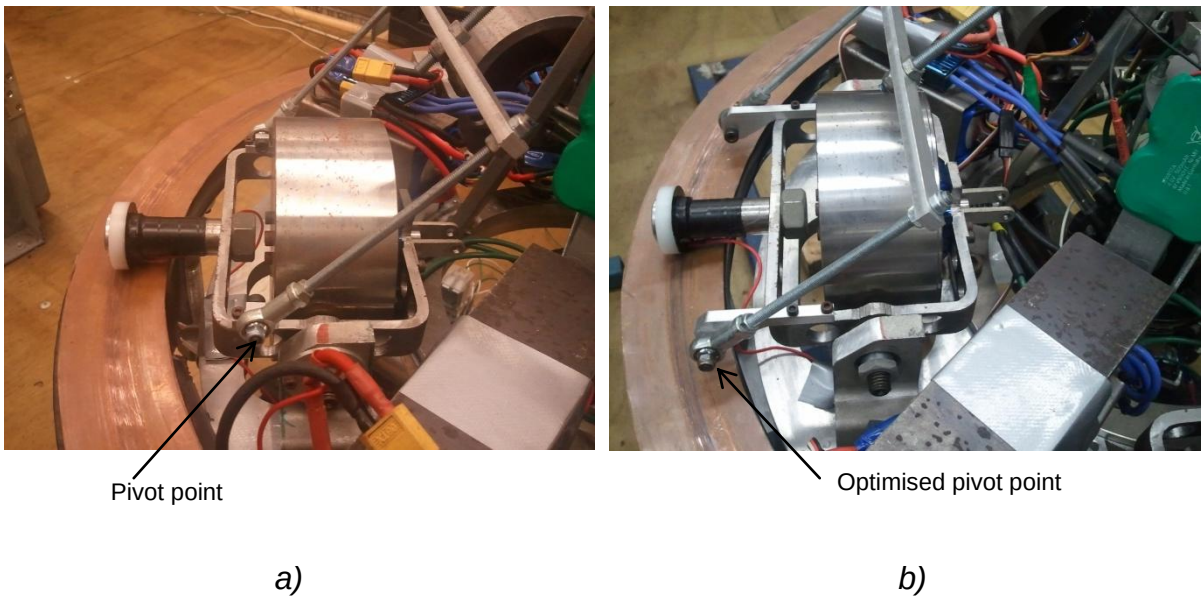

Figure 7.16 – a) initial front pivot location, b) optimised pivot location

The diametrically opposite arrangement improved the oscillatory motion of the system resulting in it exhibiting behaviour similar to the Brennan monorail stabilizer. The design was adapted into the existing prototype without any difficulty.

> ***Outcome:*** *The diametrically opposite arrangement resulted in improved oscillatory motion of the disc.*

7.3.10 Main disc drive arrangement and slip ring design

Further testing revealed the outer ring drive system was not making the stabilization process behave as intended. The option of driving the main disc was revisited.

Instead of driving the disc around at a constant velocity in a single direction two solutions were investigated to further enhance the oscillatory motion of the disc.

i) using a signal generator to switch the voltage the DC motor receives, constantly altering the direction the disc is precessed
ii) developing a switching system that changes the direction of precession of the disc when each of the outer contact arms contact the outer ring

Although solution ii) was much more complex to integrate into the existing prototype and manufacture, this solution meant that the system would responded actively to the tipping of the external structure.

Table 7.14 – New disc drive arrangement

Time to complete	Ease of Integration	Overall impact on performance	Total
2/5	2/5	7/10	**11/20**

The final design used a slip ring arrangement (Figure 7.17). The initial DC motor used to drive the disc was adapted into a new bearing assembly. The new assembly reduced the weight of the drive arrangement by 3kg and was easily integrated into the existing system. The universal joint, universal joint coupling, bearings and drive shaft were all reused in the design and the external structure did not need to be modified for mounting the new system. A schematic wiring diagram for the slip ring arrangement can be found in Appendix E.

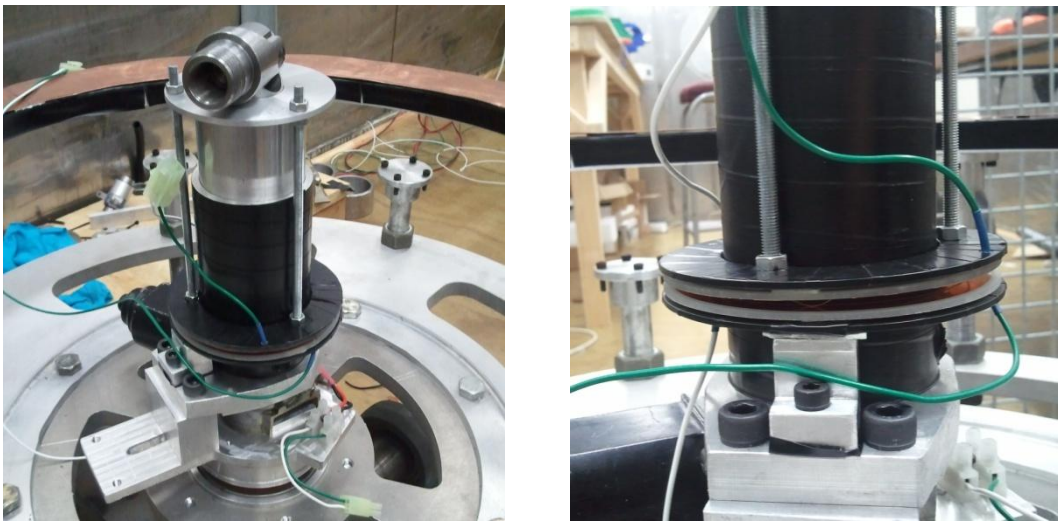

a) b)

Figure 7.17 – a) slip ring drive arrangement assembled into external structure, b) slip ring plates

As the external structure tips off the vertical it comes in contact with the outer contact arms and closes an electrical circuit.

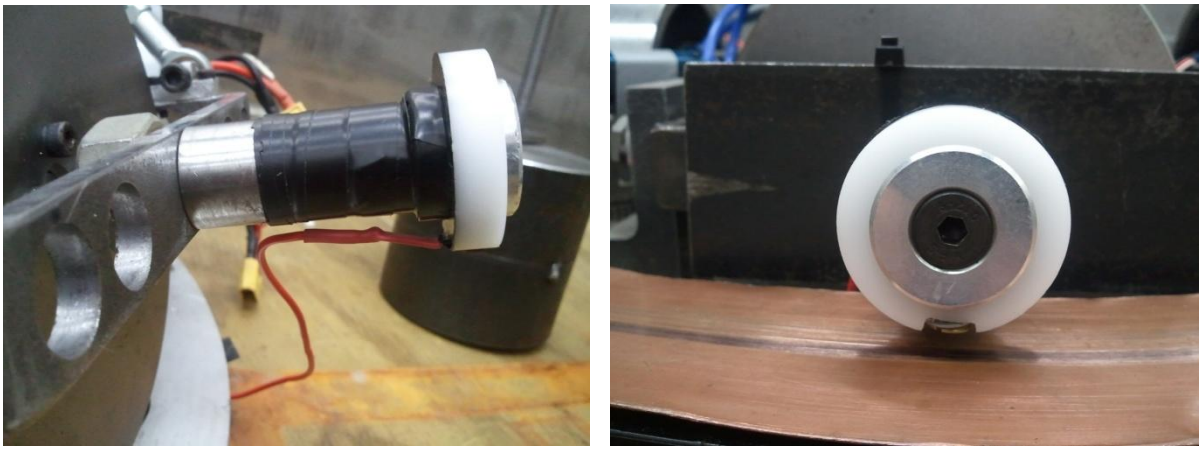

a) b)

Figure 7.18 – a) modified contact arms with wire connected, b) nylon bush and brass screw on contact arm

The outer contact arms were redesigned to include a nylon bush with a tapped hole in the bottom. A brass screw was fitted in the hole with a connecting wire running back to the drive motor via the slip ring arrangement (Figure 7.18). The contact arms were wired together to match their diametrically opposite pairing arrangement. When the circuit was closed by the contact of the outer ring and the contact arms, a set of relay switches (Figure 7.19 a)) turn on and drive the disc and gyroscopes around in one direction. This causes one pair of the gyroscopes to push down on the outer ring forcing the external structure back to the level position until it tips over the horizontal. The contact arms of the opposite pair of gyroscopes now come in contact with the other side of the outer ring, closing the circuit and switching the motor to drive the disc in the opposite direction. This process continues at a high frequency and maintains the external structure level by rocking it back and forth about the vertical.

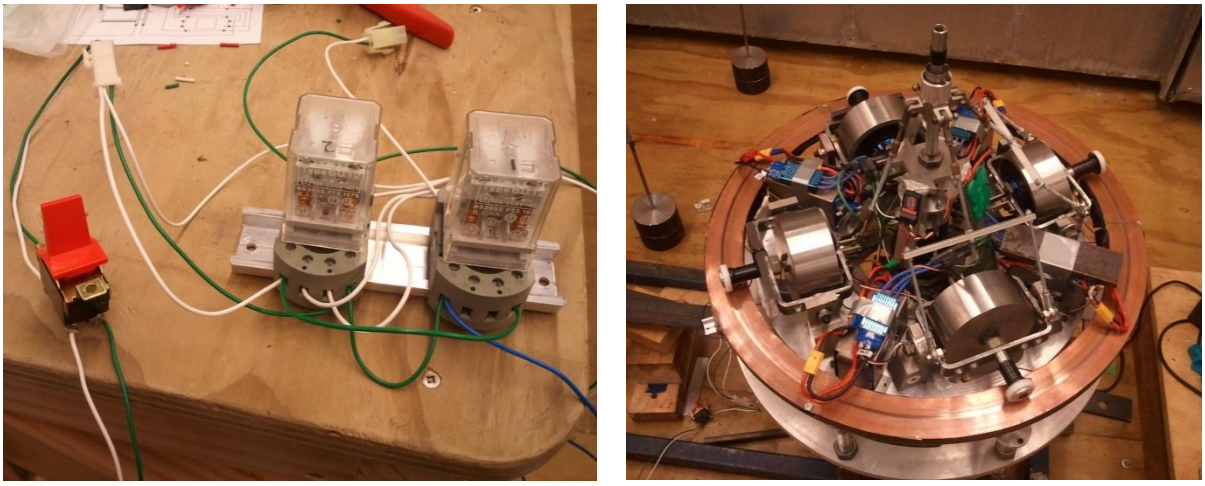

a) b)

Figure 7.19 – a) relay switches used to alternate voltage to disc drive motor, b) slip ring drive arrangement assembled together showing copper plating on outer ring

Figure 7.19 b) shows the slip ring drive mechanism assembled into the system. A thin copper ring was attached to the top of the outer ring to improve conductivity between it and the contact arms. The slip ring drive mechanism performed as intended driving the disc and oscillating it back and forth resulting in the gyroscopes pivoting up and down.

> ***Outcome:*** *The switching system further improved the oscillatory motion of the disc rocking the external structure about the equilibrium point.*

7.3.11 Low weight external structure

The external structure was redesigned to reduce the mass the system was attempting to stabilize.

Table 7.15 – Low weight external structure

Time to complete	Ease of Integration	Overall impact on performance	Total
4/5	5/5	8/10	**17/20**

The new design reduced the overall weight of the external structure from 30.6kg to 8.8kg. A comparison is illustrated in Figure 7.20. Constructed entirely of aluminium the new structure consisted of a central shaft (equivalent in dimension to the old shaft) with two brackets to support four outer ring mounting legs. All mounting points and connections were kept in the same location and the height of the outer ring remained adjustable.

a) b)

Figure 7.20 – a) Comparison of old external structure (top) and new light weight external structure (bottom), b) the lightweight external structure assembled into the test frame

Outcome: *The significant weight reduction of the external structure resulted in a more responsive system.*

7.3.12 Improved motor control

The implementation of the slip ring drive arrangement showed that the system could be made to oscillate about an equilibrium point. Testing revealed control of the frequency and amplitude of the oscillations would allow for a better understanding of the response produced by the system.

Table 7.16 – Improved motor control

Time to complete	Ease of Integration	Overall impact on performance	Total
3/5	5/5	7/10	**15/20**

A simple switching circuit consisting of a relay switch and a square wave signal generator were introduced to drive the 12V DC motor in place of the complex slip

ring drive arrangement. This meant that the oscillations of the motor and therefore the precession of the disc could be set to the desired frequency. Integration of the new oscillating motor arrangement required no major design changes to the system.

Figure 7.21 – Signal generator (left), flywheel speed controller (bottom middle), disc drive motor (bottom right) and relay switch power supplies (top right),

The oscillating motor control system used in the stable platform is shown in Figure 7.21. One power supply is used to drive the 12V DC motor and control the motor speed while another supplies voltage to the relay switch circuit to alternate the voltage polarity. The signal generator allows the voltage, duty cycle and frequency of the signal the motor receives to be adjusted.

Outcome: *Control of the frequency and amplitude of the oscillatory motion of the precession of the disc.*

7.3.13 Increased disc drive motor size

Torque restrictions meant the 12V DC motor had difficulty achieving the desired disc precession at higher frequencies. To eliminate this problem a larger disc drive motor was required that could operate at the desired frequencies and produced the required torques.

Table 7.17 – Increase disc drive motor size

Time to complete	Ease of Integration	Overall impact on performance	Total
3/5	5/5	7/10	**15/20**

A variety of different motor types were considered to replace the existing disc drive motor. A larger DC motor with a connected worm gear was selected as the new disc drive motor. The maximum input voltage of the disc drive motor was increased from 12V to 24V. A comparison is shown in Figure 7.22. The motor had multiple mount points and was easily integrated into the system.

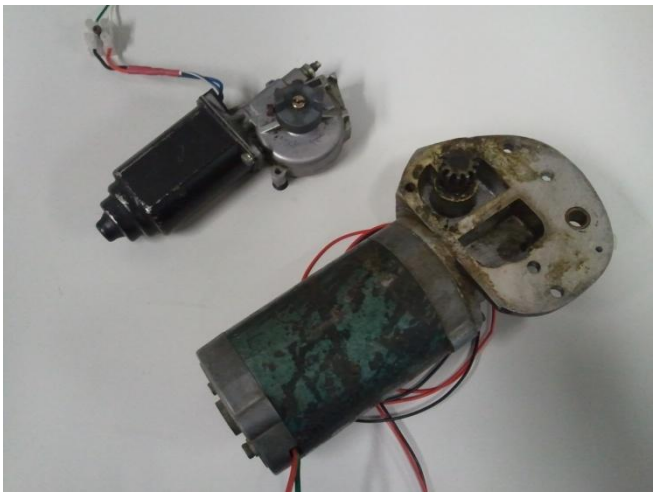

Figure 7.22 – Disc drive motor comparison showing Prototype A drive motor (top) and larger Prototype B drive motor (bottom).

The new drive motor showed a significant improvement in precessing the disc at high frequencies. The smaller motor overheated and stopped functioning after a short period of testing. The larger motor proved much more robust.

Outcome: *The increased disc drive motor improved both the range of speeds the disc could be precessed at and eliminated overheating during testing.*

7.3.14 New gyroscope pivot arrangement

At higher frequencies the discrepancies between the contact angles of the gimbal frames was still affecting the performance of the stable platform. An improved method for ensuring the gimbal frames pivoted at equivalent angles was needed

Table 7.18 – New gyroscope pivot arrangement

Time to complete	Ease of Integration	Overall impact on performance	Total
3/5	4/5	6/10	**13/20**

Solutions to pivoting the gimbal frames at equal angels were reviewed in sub-function Q in Section 6.3.5. Bevel gears were not selected due to cost and the complex machining and assembly required (Kamm, 1993). Universal joint connections were selected as the preferred option to replace the linear slide design.

A universal joint was attached to the gyroscope pivot shaft and interconnected via a clamping bracket. A linkage that attached to the front of one clamping bracket and to the back of the other meant that the coupled gimbal frames pivoted in opposite

directions. Figure 7.23 shows the new gyroscope pivoting arrangement assembled into the stable platform.

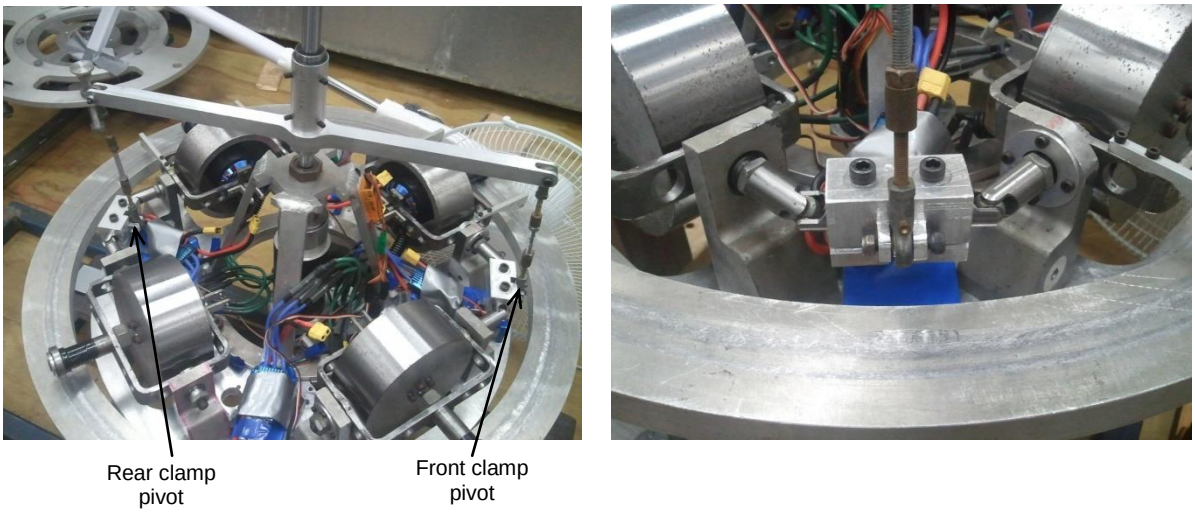

Figure 7.23 – a) New gyroscope pivot arrangement, b) universal joints and clamping bracket

Outcome: *The universal joint pivots are interconnected via an overhead slide arm that tracked on a linear bearing. This pivoted each diametrically opposite gyroscope pair at an equal angle.*

7.4 Final design

The final design of the stable platform exhibits oscillatory motion about the vertical with the stabilizing moment being transmitted at the desired points as the external structure tips back and forth. The final design is shown in Figure 7.24. This design shall be referred to as *Prototype B*.

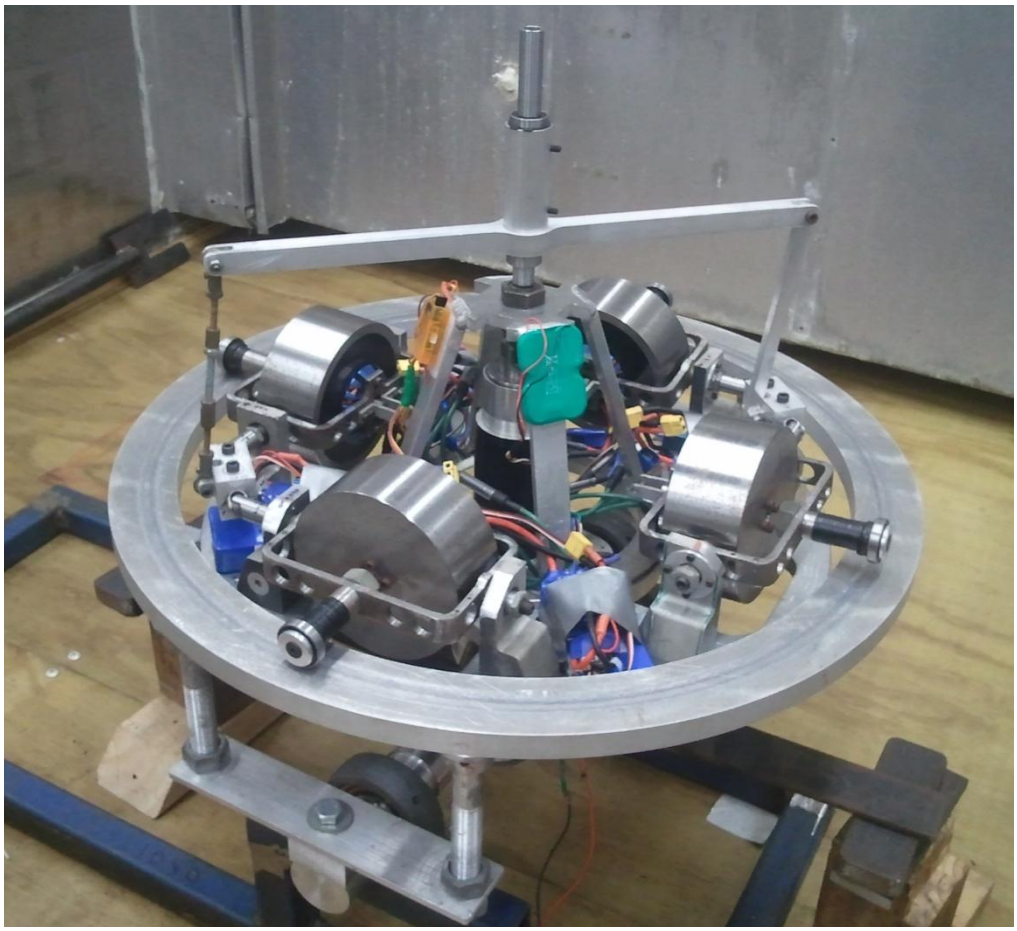

Figure 7.24 – Final stable platform (Prototype B)

7.5 Discussion

This section looks at the key findings of the optimisation and development phase. It concludes with a numerical comparison between *Prototype A* and the final improved design (*Prototype B*) via Equation (4.47).

The optimisation stage has shown that there is a clear relationship between the angular momentum produced by the stable platform and the mass it is required to balance. The total mass and angular momentum of *Prototype A* based upon the initial physical parameters of the system are compared in Table 7.19. Testing verified

that as the mass of the system was reduced and the inertia and speed of the gyroscopes increased the responsiveness of the system improved and the likelihood of achieving stabilization increased.

In order to quantify this result we consider a system that has been demonstrated to work. The physical parameters of the Brennan monorail were investigated in Table 2.1 and Table 2.2. Knowing the mass of the Brennan monorail and the dimensions and speeds of the gyroscopes we are able to calculate a ratio of the angular momentum versus the weight of the system. As can be seen in Table 7.19, the Brennan monorail has a ratio 7.5 times greater than the *Prototype A*.

The development phase has lead to the new system (*Prototype B*) having a ratio approximately 4 times better than *Prototype A* yet still only half as good as the Brennan monorail ratio.

Table 7.19 – Angular momentum and total mass ratio

System	Total mass (kg)	Angular momentum (kgm2)	Ratio
Prototype A	57.1	10.42	0.180
Brennan Monorail	33600	44680	1.33
Prototype B	37.7	28.00	0.743

This ratio, when used in conjunction with the stability inequality, gives yet another method for helping quantify the likelihood of a gyroscopically stabilized platform successfully achieving stabilization.

Several important design requirements were identified in the development phase of the Prototype A. It is critical that an equal pivot angle for the diametrically opposite gyroscopes gimbal frames is maintained. Due to the oscillatory motion of the system, this will ensure that an equivalent restoring torque is transmitted to the external structure in all planes as the system pivots about the equilibrium. This is essential in achieving the desired symmetric system response. Having the gyroscope gimbal frames rest in the equilibrium position (flywheel axes are horizontal) when the system is not turned on also contributes to achieving the desired response as there is no external torque from unbalanced masses present. Maintaining a symmetrically balanced design of the disc/gyroscopes assembly will also ensure that the system is not subjected to any mass imbalance torques.

Development of *Prototype A* also revealed that the distance between the pivot point and centre of mass of the disc needs to be maximised to increase the gravitational stability of the disc. The stability of the disc governs how effectively the gyroscopes are able to transmit the torque they produce to the external structure. If the disc remains level and does not tip, all of the torque produced by the precession of the flywheels is applied to the outer ring improving the likelihood of achieving stabilization.

Having established the parameters and geometry for the final design of the system (*Prototype B*) we are able to check how the optimisation process has affected the inequality (Equation (4.47)). Substitution of the values of the physical parameters of *Prototype B* results in the inequality being expressed numerically in Table 7.20.

Table 7.20 – Inequality for stable platform prototype

Left hand side of inequality	**29.5**
Right hand side of inequality	**574.8**

Table 7.20 shows that the ratio between the left and right hand sides of the equation has further been improved when compared to *Prototype A*.

7.6 Concluding comments

The changes implemented in the development of *Prototype A* have increased the right hand side of the inequality (Equation (4.47)) by 121% and a reduction in the left hand side of 41%. Having satisfied and enhanced the inequality derived in Chapter 4, *Prototype B* has been shown to exhibit improved oscillatory motion about the equilibrium point as it stabilizes the external structure. A bill of materials and set of manufacturing assembly drawings for *Prototype B* can be found in Appendix C. A full set of drawings for all the components and assemblies that comprise *Prototype B* can be found on the CD associated with this thesis.

8

Testing of Prototype B and theoretical comparison

8.1 Introduction

Prototype B was found to exhibit the desired oscillatory motion about the equilibrium. Substitution of the physical parameters of *Prototype B* allow for investigation of the theoretical model derived in Chapter 5. The magnitude and frequency of the restoring torque produced by the *Prototype B* will be measured. The frequency and shape of this response can then be plotted and compared with the theoretical results.

The purpose of this chapter is to compare the results obtained via the theoretical model and experimental testing of Prototype B. The outcome of this comparison is to validate the theoretical model such that it can be used in the future development of the system to further optimise its performance.

8.1.1 Outcome of theoretical and experimental comparison

It should be noted that the general solutions for the driven system (Equations (5.42) and (5.43)) calculate the angular displacement of the disc and external structure as they oscillate about their equilibrium positions. The load cell used in the experimental testing measures force (and as the location of the load cell relative to the pivot point is known, a moment can to be calculated). The main motivation behind this

comparison is to check that the theoretical and experimental results output responses that have the same shape and frequency. The largest magnitude of the restorative torque produced by the system obtained via experimental testing can be compared to the value obtained by substitution of the physical parameters of *Prototype B* into the inequality derived in the investigation of the stability conditions from Chapter 4 (Equation (4.47)).

8.2 Theoretical results from driven system

As the disc and gyroscope assembly is driven by a motor we investigate the behaviour of the general solution to the driven system (Equations (5.42) and (5.43)). We are only interested in the long term behaviour of the system so our equations become:

$$\phi_d(t) = {b_d}^1 \cos(\gamma t + \delta_d) \qquad (8.1)$$

and

$$\theta_s(t) = {b_s}^1 \cos(\gamma t + \delta_s) \qquad (8.2)$$

Substitution of the physical parameters of *Prototype B* into Equations (8.1) and (8.2) yields the results shown in Equations (8.3) and (8.4).

$$\phi_d(t) = (0.4065)\cos(5t + 0.103) \quad (8.3)$$

and

$$\theta_s(t) = (0.1999)\cos(5t + 1.468) \quad (8.4)$$

Note that to obtain the above results a coefficient of friction of 0.5 and a torque of 30N have been used as the physical conditions inside the 24V DC motor during operation. These values are based upon the constants used in the initial design of the system and testing of the motor to justify it was capable of producing the required torques to precess the disc.

Plotting the responses from Equations (8.3) and (8.4) in Matlab over a period of 20 seconds we obtain the graph shown in Figure 8.1. We plot both of the responses of the disc and the external structure on the same figure to help illustrate the variations in angular displacement (the disc travels through an angle 2 times greater than the external structure). Figure 8.1 also illustrates how the response of the disc and external structure are out of phase. This type of response must also be viewed in the experimental results.

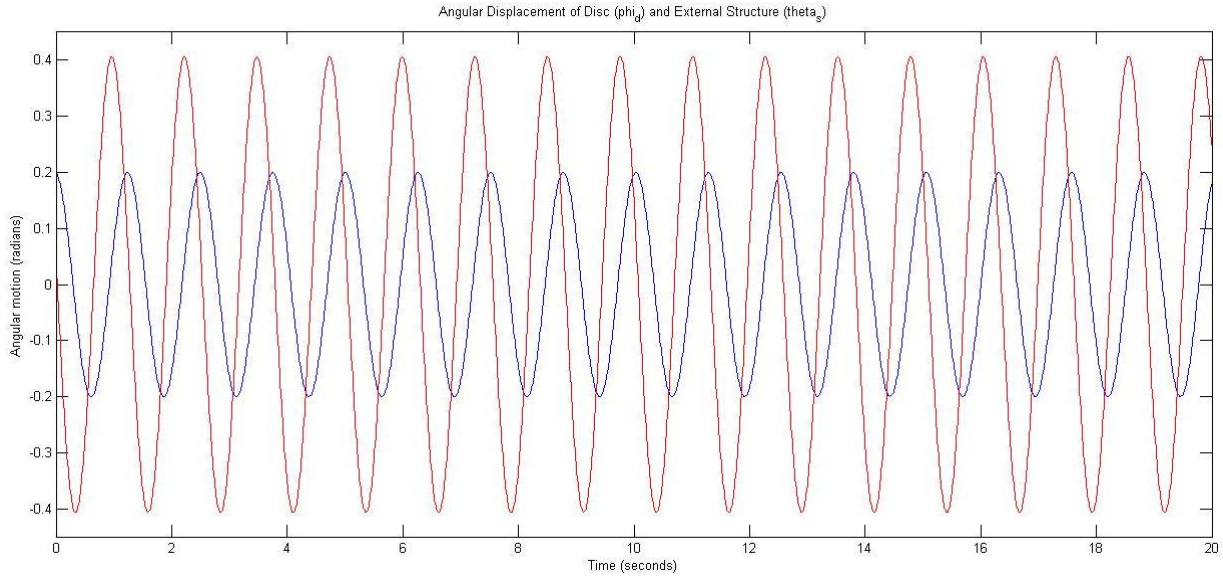

Figure 8.1 - Theoretical response of stable platform showing angular displacement over time of external structure (blue) and disc (red)

8.3 Driven system experimental results

The experimental testing of *Prototype B* comprised of a load cell attached to the existing test frame. The load cell was used to measure the magnitude of the restoring torque produced as well as the frequency response of the physical system.

8.3.1 Experiment arrangement

An adjustable bracket was manufactured to hold the load cell rigidly in place during testing. This bracket was fixed in place via two bolts that tightened up against the testing frame. Figure 8.2 shows the location of the testing rig relative to *Prototype B*.

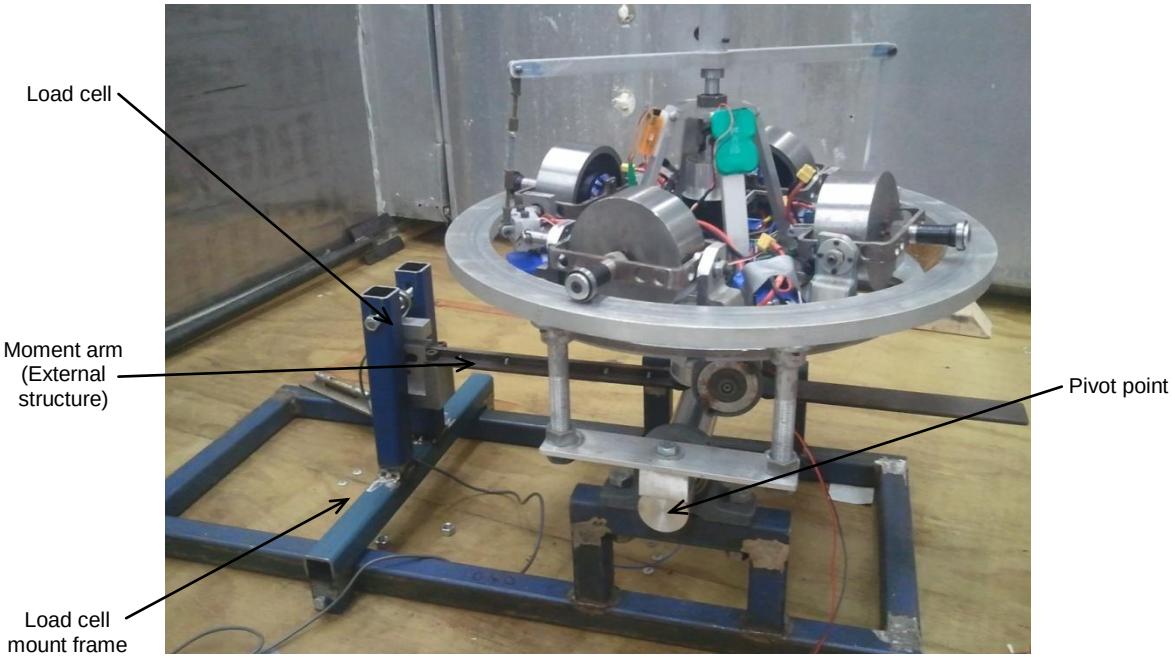

Figure 8.2 – Load cell test rig assembled into Prototype B

The load cell was fixed to the end of the moment arm of the external structure. The centre of the load cell was located 412.5mm from the systems pivot point. This distance in conjunction with the force exerted upon the load cell allows the total restorative torque produced by the platform to be measured.

The load cell is secured to the mount frame via a Ø12mm rod end. The use of a rod end and slotted holes allows for adjustment of the location of the load cell. An aluminium section was manufactured to connect the load cell to the moment arm and ensure it was accurately located in the required position. Figure 8.3 illustrates the load cell mounted in position.

Figure 8.3 – Mounting location of load cell in testing rig arrangement

An S-type AST1000 load cell was used for all testing. The load cell was connected to a laptop via a USB controller and all data was measured and processed in Labview 2012.

8.3.2 Experimental testing results

The oscillatory frequency of the theoretical system was determined via Figure 8.1 and *Prototype B* was set to precess back and forth at an equivalent frequency. The magnitude of the largest moment produced by the experimental response is then compared to the magnitude predicted by the theoretical model by substitution of the systems physical parameters.

The results obtained from the testing of the *Prototype B* are shown in Figure 8.4.

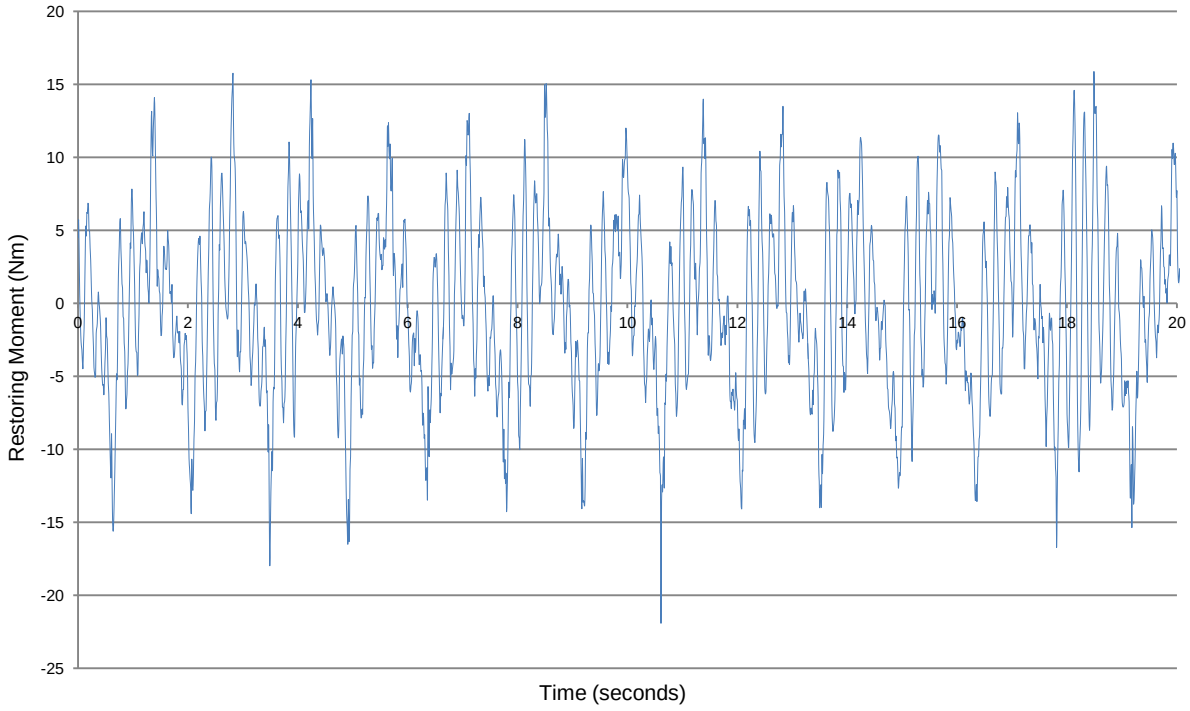

Figure 8.4 – Experimental response of stable platform Prototype B

8.4 Discussion of results

The theoretical results shown in Figure 8.1 illustrate oscillatory motion of the stable platform. The amplitude of the angular displacement of the disc (0.4065 rads) is approximately twice that of the external structure (0.1999 rads). This motion is desirable as it indicates that as the disc precesses through large angles the external structure only moves through angles half the size. This variation in the angular displacement results in small oscillations of the structure about the equilibrium.

Figure 8.1 also shows that the theoretical response of the disc and external structure are out of phase. This is the desired response of the system. If the disc and external structure were oscillated in phase then no stabilization would occur. This is because the equations of motion involve both accelerations and velocities. Looking at the

derivation of the equations of motion for the driven case, the presence of the velocities introduces complex terms as it is only the first derivative with respect to time, whereas the accelerations introduce real terms because it is the second derivative. A similar phenomenon occurs in the case of the Driven Damped Simple Harmonic Oscillator.

Prototype B was shown to exhibit the desired oscillatory motion. Figure 8.4 is overlaid with the optimal theoretical torque output response curve. The result is illustrated in Figure 8.5. This figure shows that the oscillatory response of the stable platform closely follows the theoretical response shown in Figure 8.1.

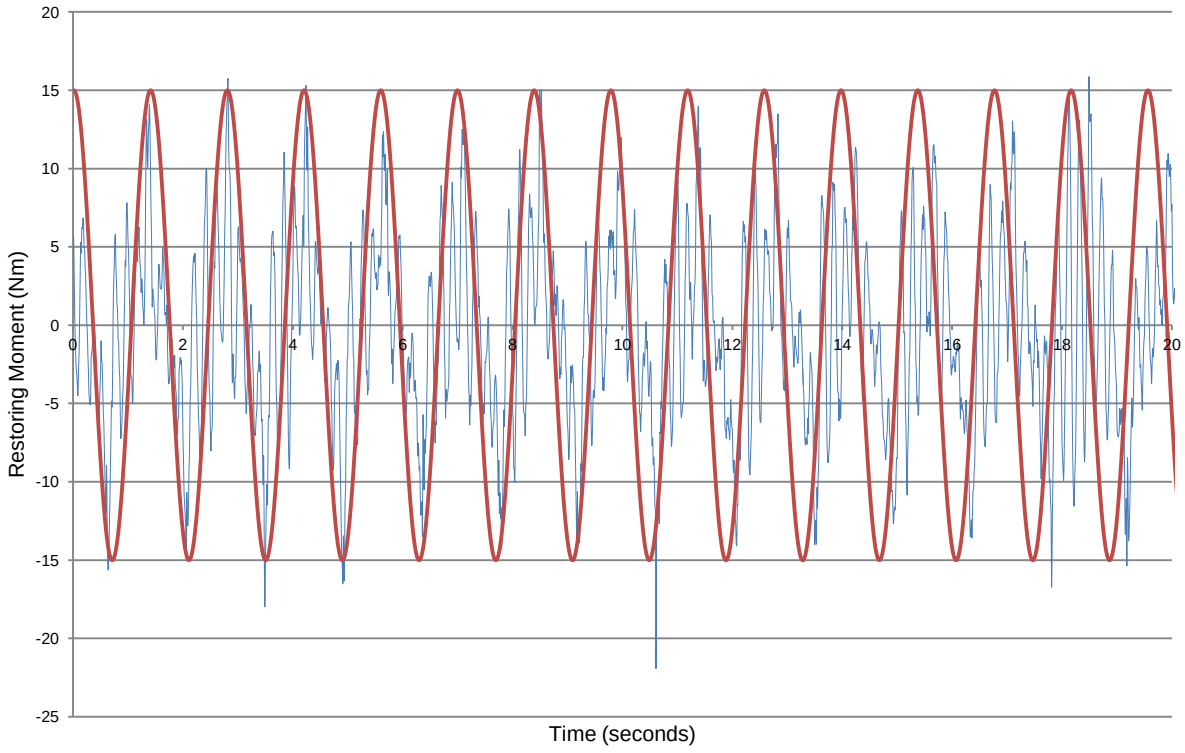

Figure 8.5 – Experimental response (blue) overlaid with an optimal torque response (red)

It is difficult to compare the magnitude of the theoretical and experimental responses. Testing has shown that the force applied by the system is directly proportional to the angle at which the disc precesses through (as the disc precess further the magnitude of the force applied to the external structure increases). This suggests that both the angular displacement of the disc and the restoring torque should exhibit equal oscillatory motion. The frequency responses shown in Figure 8.1 and Figure 8.5 suggest that this is occurring.

The optimal response from the testing of the *Prototype B* would be a smooth sinusoidal curve. Inconsistencies in the results when comparing the experimental and theoretical responses can be attributed to:

- the lack of rigidity of several connections. This meant that the motion of the connections between sub-systems was not as smooth as desired. This can be remedied by more accurate machining methods being used when manufacturing the systems components and more rigid load paths being established.

- a bouncing effect occurring as the outer contact arms contact the outer ring of the external structure. Metal on metal contact made this unavoidable. This issue can be remedied by placing a rubber or nylon covering on the outer ring to absorb the impact forces as the outer contact arms push down restoring the external structure back to the equilibrium position.

- the main disc not remaining perfectly level during operation

A summary of the theoretical and experimental values compared in testing are shown in Table 8.1. Note that the maximum theoretical moment is derived via the equation

$$M_{max} = 4(I)(\dot{\phi}_g)\omega_0\left(\frac{r_g + r_d}{r_g}\right) \qquad (8.5)$$

where $I = 0.006078\ \text{kgm}^2$

$\dot{\phi}_g = 314.2\ \text{rads}$

$\omega_0 = 1.047\ \text{rads}$

$\frac{r_g + r_d}{r_g} = 2.8$

Table 8.1 – Theoretical vs. experimental comparison

Variable	Theoretical Value	Experimental Value	Units	% Deviation
External structure frequency	1.365	1.5	s	+11
	0.7326	0.666	Hz	-9
Disc frequency	1.365	1.5	s	+11
	0.7320	0.666	Hz	-9
Disc deviation per period	0.8130	N/A	radians	-
	46.58	N/A	degrees	-
External structure deviation per period	0.3998	N/A	radians	-
	22.92	N/A	degrees	-
Maximum moment produced	22.40	18	Nm	-24

The discrepancy in the theoretical and experimental maximum moment produced by *Prototype B* can be attributed to loses through friction, vibrations and the main disc not remaining level during the stabilization process.

From these results we have observed that the theoretical response and experimental response of *Prototype B* have produced similar waveforms. This suggests that the theoretical model can be used to predict the oscillatory motion of the stable platform. By combining the responses of Equations (8.1) and (8.2) with the maximum theoretical moment produced by the system (Equation (8.5)) we are able to generate Figure 8.4. From this we are able to predict the oscillatory response that the system will produce as the physical parameters that make up the stable platform are varied.

8.5 Concluding comments

The theoretical and experimental responses of the system have been compared by substituting the physical conditions of the *Prototype B* into the relevant equations and plotting the resulting waveform. Investigation of the results has shown that the derived mathematical model is a suitable method for predicting the response of the system as well as determining the maximum restorative moment produced by the stable platform. By combining this information a figure of the theoretical response is able to be produced that will model the oscillatory behaviour of the system.

9

Conclusions and recommendations

This study has investigated the feasibility of producing a gyroscopically stabilized platform based upon a schematic diagram proposed by Townsend (1983). This chapter summarises the research activities, the results of this study and makes recommendations for future work.

9.1 Summary of research activities

A review of existing gyroscopically stabilized systems in the available literature was undertaken. This gave a sound understanding as to where the current and available technology relating to the project was in industry. All previous work completed on the project by Townsend (1983) and Gooch (1998-199) was reviewed and the proposed schematic layout of the gyroscopically stabilized platform was introduced.

The Brennan monorail was investigated due to its similarities with the proposed system. A free body diagram of the stabilizing system was developed and a step by step guide of the operation of the platform was presented. A review of the Brennan stabilizer helped to establish fundamental theory regarding how gyroscopes react and behave when interconnected.

The Lagrangian of a general gyroscopically stabilized platform (referred to as the stable platform) based upon the proposed schematic was derived by means of the

Lagrangian formalism. The variables that defined the motion of the system were established and from this a set of a set of Euler angles were determined. The kinetic energy and potential energy of each of the sub-systems that comprise the stable platform were then derived. This allowed the Lagrangian for the overall system to be determined.

The equations of motion of the system were derived and from this a set of stability conditions were established. From these stability conditions, an inequality was derived that described the situation where the restoring moment produced by the stable platform is greater than the imbalance forces generated by the unstable body's deviation from the vertical. This inequality was then used to impose conditions upon the physical design of the system. The equations of motion were used to derive general solutions to a homogeneous stable platform arrangement and a driven system.

A set of design requirement specifications were established for the design of the stable platform following the method of Pahl and Beitz (1984). The stable platform system was divided into 6 sub-systems (gyroscopes, disc, external structure, disc drive mechanism, gimbal frame linkage and central pivot) and a set of concepts based upon each of the sub-systems functions were derived. The embodiment design was developed and a detailed final design of the stable platform was established. This design was referred to as *Prototype A*.

Prototype A was manufactured at in the University of Canterbury Mechanical Engineering workshop. Testing of *Prototype A* revealed that it did not perform as

intended. An extensive set of design developments and modifications were undertaken to improve the performance of *Prototype A*. The developed system demonstrated the desired behaviour during testing and is referred to as *Prototype B*. *Prototype B* was shown to exhibit the desired oscillatory motion about an equilibrium point.

Finally, *Prototype B* was tested and the restorative torque produced by the system measured via a load cell. This data was then used to validate the mathematical model. The theoretical and experimental responses were shown to be similar confirming the mathematical model as an accurate method for predicting the behaviour of the system.

9.2 Conclusions of this study

A schematic of a gyroscopic stabilizer was proposed by Townsend. Early research by Townsend revealed that no multi-gyroscope interconnected stabilization system that could balance an unstable body in all directions existed at the time. Technological constraints on electric motors and batteries meant that the system could not be built to the desired scale. The project was placed on hold until such time as a proof of concept prototype could be manufactured at an economic size. Gooch (1998-1999) continued the work that Townsend had begun. Developments in brushless DC motors and Li-Po batteries have allowed the project to be revisited.

A theoretical mathematical analysis of the proposed system was under taken. The key variables that define the motion of the stable platform were established as a set of Euler angles. From these, expressions for the kinetic and potential energy of the

three critical sections that encompass the stable platform (external structure, disc and gyroscopes) were derived. The Lagrangian for each of the sections were then determined. Several key assumptions were established to assist in simplifying the overall mathematical problem. These were:

- The disc will remain horizontal during the stabilization process.
- The gyroscopes have equal moments of inertia about the x, y and z axes.
- All gyroscopes will rotate with equal speed.
- The angles of deviation of all of the gyroscopes gimbal frames from the horizontal will all be equal.

Investigation revealed that only three variables were required to describe the behaviour of the stable platform (several of the variables were shown to be equivalent or set as constants). These three variables were

ϕ_g relates to the rotation of the gyroscopes

ϕ_d defines the position of the main disc as it precesses round

θ_s defines the derivation of the system from the vertical

The equations of motion for the system in each of these directions were derived. A set of stability conditions were imposed upon the system by means of the characteristic equation. These conditions required the system to exhibit oscillations

about an equilibrium. An inequality (Equation (4.47)) was determined and used to govern the physical design of the stable platform.

$$\mu\left(M_s h_s + (M_d + 4M_g)h_d\right)g < 4(I)^2\left(\dot{\phi}_g\right)^2 \omega_0 \left(\frac{r_g + r_d}{r_g}\right) \qquad (4.47)$$

A prototype design (*Prototype A*) was established using the systematic approach of Pahl and Beitz (1984). The prototype did not perform as intended. A development process was undertaken to achieve the desired system behaviour. The inclusion of a drive motor to precess the disc meant that symmetric oscillatory motion was the desired response of the system.

Testing of the new prototype (*Prototype B*) revealed several conditions that must be satisfied in order for a similar gyroscopically stabilized system to maintain an unstable body in the upright position.

i) The ratio of the total angular momentum produced by the system versus the weight of overall system must be 0.8 or greater.

ii) It is important that an equal pivot angle for the diametrically opposite gyroscopes gimbal frames is maintained. Due to the oscillatory motion of the system, this will ensure that an equivalent restoring torque is transmitted to the external structure in all planes as the system pivots about the equilibrium.

iii) The distance between the pivot point of the disc and the centre of mass of the disc needs to be maximised to increase the gravitational stability of the disc.

iv) Maintaining a symmetrically balanced design of the disc/gyroscope assembly will also ensure that the system is not subjected to any mass imbalance torques.

v) The amplitude of the angular displacement of the disc should be approximately twice that of the external structure. This motion is desirable as it indicates that as the disc precesses through large angles the external structure only moves through angles half the size. These two responses must also be out of phase.

9.3 Recommendations for further work

It is recommended a new system is designed utilizing the findings from this research. One suggested solution to overcome several of the issues encountered in the existing gyroscopically stabilized platform is the reorientation of the gyroscope gimbal frame and flywheels to rotate in the same plane as the Brennan monorail. This arrangement will give a better force transmission path between the gyroscopes and the external structure.

Another potential arrangement for a new gyroscopically stabilized system is the design of a “double Brennan”. This is effectively two Brennan stabilizers positioned at right angles to one another. The Brennan stabilizer is a proven system that has

been shown to work. This coupled with modern technologies such as accelerometers, control systems and small electric motors to precess the gyroscopes gimbal frames when deviation from the horizontal occurs should produce a system that would achieve stabilization in all planes. A preliminary design for such a system is show in Figure 9.9.1.

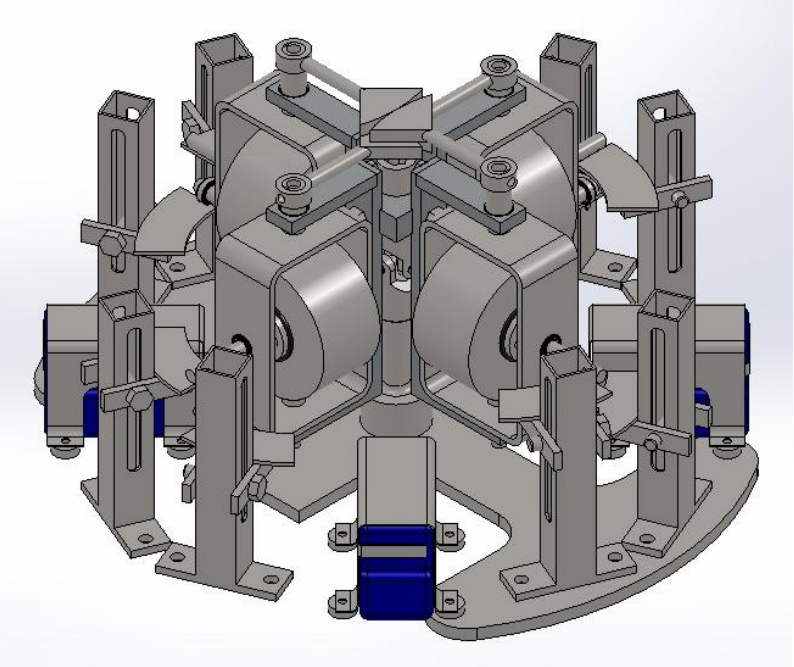

Figure 9.9.1 – Preliminary design of "double Brennan" stabilizer

The major downside to a "double Brennan" arrangement is that the size of the restoring torque produced by the system will vary in each plane. The largest torque will occur in line with the flywheel axes while the points 45 degrees between each of the gimbal frames will be subjected to a torque that is significantly lower. More investigation into how this will impact the stabilization process is required.

It is also recommended that a small scale working Brennan stabilizer model be constructed using modern machines, materials and control components. Testing of such a system will provide further insight into how coupled gyroscopes can be utilized to maintain an unstable structure upright. This recommended work could further enable the verification of several design constraints that could be used to further optimise the four flywheel gyroscopically stabilized platform successfully designed, developed, manufactured and functionally verified in the work reported in this thesis.

10

References

Arnold, R. N., Maunder, L., & Roberson, R. E. (1963). *Gyrodynamics* (Vol. 30).

Bauer, Robert J. (2002). Kinematics and dynamics of a double-gimbaled control moment gyroscope. *Mechanism and machine theory, 37* (12), 1513-1529.

Beitz, Wolfgang, & Pahl, G. (1984). *Engineering design*. London: Design Council ; Berlin : Springer.

Bennett, GG. (1970). An historical review of the development of the gyroscope. *Australian Surveyor, 23* (4), 244-252.

Beznos, AV, Formal'sky, AM, Gurfinkel, EV, Jicharev, DN, Lensky, AV, Savitsky, KV, & Tchesalin, LS. (1998). *Control of autonomous motion of two-wheel bicycle with gyroscopic stabilisation.* Paper presented at the IEEE International Conference on Robotics and Automation.

Blinn, James F. (2006). How to solve a cubic equation, Part 1: The shape of the discriminant. *IEEE Computer Graphics and Applications, 26* (3), 84-85

Brennan, Louis. (1905). US Patent No. 796893.

Brown, Daniel, & Peck, Mason A. (2008). Scissored-Pair Control-Moment Gyros: A Mechanical Constraint Saves Power. *Journal of guidance, control, and dynamics, 31* (6), 1823-1826.

Cousins, H. (1913). The stability of Gyroscopic single track vehicles. *Engineering*, 678–681, 711–712, 781–784.

Davidson, Martin. (1946). *The gyroscope and its applications: in three sections*. London: Hutchinson's scientific and technical publications.

Davyskib, A, & Samsonov, VA. (1995). The possibility of gyroscopic stabilization of the rotation of a system of rigid bodies. *Journal of Applied Mathematics and Mechanics, 59* (3), 363-367.

Denisov, G.G, & Novikov, V.V. (2006). A Problem of Gyroscopic Stabilization of Mechanical System. *Mechanics of Solids, 41* (3), 8-11.

Dickinson, A. F. (1910). The Brennan gyroscope. *Cassier's Magazine*.

Eddy, H.T. . (1910). Mechanical principles of Brennan's mono-rail car. *Journal of the Franklin Institute, v. 169*, 467-485.

Ferreira, Enrique D, Tsai, Shu-Jen, Paredis, Christiaan JJ, & Brown, H Benjamin. (2000). Control of the Gyrover: a single-wheel gyroscopically stabilized robot. *Advanced Robotics, 14* (6), 459-475.

Franklin, WS. (1912). An Important Practical Problem in Gyrostatic Action. *Physical Review (Series I), 34* (1), 48.

Gooch, S. (1998-1999). Project Feasability Study Documentation *University of Canterbury*. Christchurch, NZ.

Gutschmidt, S. (2005). *Mathematical-Mechanical Modelling of Wobbling Disc Piezoelectric Motors.* Forschen und Wissen - Mechatronik, Germany.

Hales, C. & **Gooch, S.** (2004). *Managing engineering design*. New York: Springer.

Huseyin, K, Hagedorn, P, & Teschner, W. (1983). On the stability of linear conservative gyroscopic systems. *Zeitschrift für angewandte Mathematik und Physik ZAMP, 34* (6), 807-815.

Joseph, James. (1967, September). 2 Wheeled Road Wonder! *Science & Mechanics,* 31-35.

Kamm, Lawrence J. (1993). *Designing cost-efficient mechanisms: minimum constraint design, designing with commercial components, and topics in design engineering*. Warrendale, PA, U.S.A: Society of Automotive Engineers.

Kane, T. R., Likins, P. W., & Levinson, D. A. (1983). *Spacecraft dynamics* (Vol. 1). New York: McGraw-Hill Book Co.

Karnopp, Dean. (2002). Tilt control for gyro-stabilized two-wheeled vehicles. *Vehicle System Dynamics, 37* (2), 145-156.

Klein, Richard E. (1990). Teaching linear systems theory using Cramer's rule. *Education, IEEE Transactions on, 33* (3), 258-267.

Kliem, Wolfhard, & Seyranian, Alexander P. (1997). Analysis of the gyroscopic stabilization of a system of rigid bodies. *Zeitschrift für angewandte Mathematik und Physik ZAMP, 48* (5), 840-847.

Kosov, AA. (2008). Gyroscopic stabilization of nonconservative systems. *Journal of Applied and Industrial Mathematics, 2* (4), 513-521.

Kuz'mina, L.K. (1972). On the Stability of Gyroscopic Stabilization Systems. *Journal of Applied Mathematics and Mechanics, 36* (4), 732-736.

Kuz'mina, L.K. (1980). On the Stability of Systems of Gyroscopic Stabilization in the Presence of Perturbation. *Journal of Applied Mathematics and Mechanics, 44* (1), 119-122.

Lam, Pom Yuan. (2011). *Gyroscopic stabilization of a kid-size bicycle.* Paper presented at the Cybernetics and Intelligent Systems (CIS), 2011 IEEE 5th International Conference

Matrosov, V. M. (1960). On the stability of gyroscopic stabilizers. *Journal of Applied Mathematics and Mechanics, 24* (5), 1214-1224.

McCallion, H. (1973). *Vibration of linear mechanical systems*. London: Longman.

Molian, S. (1997). *Mechanism design: the kinematics and dynamics of machinery*. New York: Elsevier.

Moots, Elmer Earl. (1911). *The design and testing of a monorail car model*: University of Wisconsin--Madison.

Photographer Unknown. (1927). Einschienenbahn von Brennan und Scherl from http://en.wikipedia.org/wiki/File:Einschienerp.jpg.

Roitenberg, I. N. (1960). On the theory of direct gyroscopic stabilizers. *Journal of Applied Mathematics and Mechanics, 24* (4), 1156-1163.

Savet, Paul H. (1961). *Gyroscopes: theory and design : with applications to instrumentation, guidance and control*. New York: McGraw-Hill.

Schilovski, P. (1909). Patent GB 12,021.

Schilovski, P. (1914). Patent GB 12,021.

Schilovski, P. (1924). *The Gyroscope: Its Practical Construction and Application, Etc*: E. & FN Spon.

Shigley, Joseph Edward. (2011). *Shigley's mechanical engineering design*. New York: McGraw-Hill.

Sperry, E. A. (1908). Patent US 907,907.

Spry, Stephen C, & Girard, Anouck R. (2008). Gyroscopic stabilisation of unstable vehicles: configurations, dynamics, and control. *Vehicle System Dynamics, 46* (S1), 247-260.

Townsend, Greg. (1983). Project Feasability Study Documentation *Technix Group Ltd*. New Plymouth, NZ.

Townsend, N. C., Murphy, A. J., & Shenoi, R. A. (2007). A new active gyrostabiliser system for ride control of marine vehicles. *Ocean Engineering, 34* (11-12), 1607-1617.

Ullman, David G. (1992). *The mechanical design process*. New York: McGraw-Hill.

Waldron, Manjula B., & Waldron, Kenneth J. (1996). *Mechanical design: theory and methodology*. New York: Springer.

Ward, Morgan. (1959). The vanishing of the homogeneous product sum of the roots of a cubic. *Duke Mathematical Journal, 26* (4), 553-562.

Wells, Dare A. (1967). *Schaum's outline of theory and problems of Lagrangian dynamics: with a treatment of Euler's equations of motion, Hamilton's equations and Hamilton's principle*. New York: Schaum Pub. Co.

Zhu, Zhen, Naing, Myint Phone, & Al-Mamun, Abdullah. (2009). *A 3-D simulator using ADAMS for design of an autonomous gyroscopically stabilized single wheel robot.* Paper presented at the 2009 IEEE International Conference on Systems, Man and Cybernetics

Appendix A

Mathematical Simplifications

The following appendix looks at the mathematical simplifications used in Chapter 4.

$$\left(\dot{\psi}_d \sin\theta_d \sin\phi_d + \dot{\theta}_d \cos\phi_d\right)^2 + \left(\dot{\psi}_d \sin\theta_d \cos\phi_d - \dot{\theta}_d \sin\phi_d\right)^2$$
$$= \left(\dot{\theta}_d{}^2 + \dot{\psi}_d{}^2 \sin^2\theta_d\right) \qquad \textit{(A1.1)}$$

and

$$\left[-\dot{\theta}_s \cos(\phi_d + \delta_m)\cos\left(\phi_{g_m}\right) + \dot{\theta}_s \sin(\phi_d + \delta_m)\cos\left(\theta_{g_m}\right)\sin\left(\phi_{g_m}\right)\right.$$
$$\left. + \dot{\phi}_d \sin\left(\theta_{g_m}\right)\sin\left(\phi_{g_m}\right) - \dot{\theta}_{g_m}\cos\left(\phi_{g_m}\right)\right]^2 + \left[\dot{\theta}_s \cos(\phi_d + \delta_m)\sin\left(\phi_{g_m}\right)\right.$$
$$\left. + \dot{\theta}_s \sin(\phi_d + \delta_m)\cos\left(\theta_{g_m}\right)\cos\left(\phi_{g_m}\right) + \dot{\phi}_d \sin\left(\theta_{g_m}\right)\cos\left(\phi_{g_m}\right) + \dot{\theta}_{g_m}\sin\left(\phi_{g_m}\right)\right]^2$$
$$= \left(\dot{\theta}_s \cos(\phi_d + \delta_m) + \dot{\theta}_{g_m}\right)^2 + \left(\dot{\theta}_s \sin(\phi_d + \delta_m)\cos\left(\theta_{g_m}\right) + \dot{\phi}_d \sin\left(\theta_{g_m}\right)\right)^2 \qquad \textit{(A1.2)}$$

A1 Proof of simplification of Equation A1.1

$$\left(\dot{\psi}_d \sin\theta_d \sin\phi_d + \dot{\theta}_d \cos\phi_d\right)^2 + \left(\dot{\psi}_d \sin\theta_d \cos\phi_d - \dot{\theta}_d \sin\phi_d\right)^2$$

$$= \dot{\psi}_d{}^2 \sin^2\theta_d \sin^2\phi_d + 2\dot{\psi}_d\, \dot{\theta}_d \sin\theta_d \sin\phi_d \cos\phi_d + \dot{\theta}_d{}^2 \cos^2\phi_d$$
$$+ \dot{\psi}_d{}^2 \sin^2\theta_d \cos^2\phi_d - 2\dot{\psi}_d\, \dot{\theta}_d \sin\theta_d \sin\phi_d \cos\phi_d + \dot{\theta}_d{}^2 \sin^2\phi_d$$

$$= \dot{\psi}_d{}^2 \sin^2\theta_d \sin^2\phi_d + \dot{\theta}_d{}^2 \cos^2\phi_d + \dot{\psi}_d{}^2 \sin^2\theta_d \cos^2\phi_d + \dot{\theta}_d{}^2 \sin^2\phi_d$$

$$= \dot{\theta}_d{}^2 (\cos^2\phi_d + \sin^2\phi_d) + \dot{\psi}_d{}^2 \sin^2\theta_d (\sin^2\phi_d + \cos^2\phi_d)$$

$$= \dot{\theta}_d{}^2 + \dot{\psi}_d{}^2 \sin^2\theta_d \qquad (A1.1)$$

A2 Proof of simplification Equation A1.2

It is easiest to break this simplification into two parts expand them separately and add like terms together cancelling out many of the repeated terms.

Let us first consider

$$\left[-\dot{\theta}_s \cos(\phi_d + \delta_m)\cos(\phi_{g_m}) + \dot{\theta}_s \sin(\phi_d + \delta_m)\cos(\theta_{g_m})\sin(\phi_{g_m}) + \dot{\phi}_d \sin(\theta_{g_m})\sin(\phi_{g_m}) - \dot{\theta}_{g_m}\cos(\phi_{g_m})\right]^2$$

$$\begin{aligned}
&= -\dot{\theta}_s{}^2 \cos^2(\phi_d + \delta_m)\cos^2(\phi_{g_m}) \\
&\quad - \dot{\theta}_s{}^2 \cos(\phi_d + \delta_m)\cos(\phi_{g_m})\sin(\phi_d + \delta_m)\cos(\theta_{g_m})\sin(\phi_{g_m}) \\
&\quad - \dot{\theta}_s\dot{\phi}_d \cos(\phi_d + \delta_m)\cos(\phi_{g_m})\sin(\theta_{g_m})\sin(\phi_{g_m}) \\
&\quad + \dot{\theta}_s\dot{\theta}_{g_m}\cos(\phi_d + \delta_m)\cos^2(\phi_{g_m}) \\
&\quad - \dot{\theta}_s{}^2 \cos(\phi_d + \delta_m)\cos(\phi_{g_m})\sin(\phi_d + \delta_m)\cos(\theta_{g_m})\sin(\phi_{g_m}) \\
&\quad + \dot{\theta}_s{}^2 \sin^2(\phi_d + \delta_m)\cos^2(\theta_{g_m})\sin^2(\phi_{g_m}) \\
&\quad + \dot{\theta}_s\dot{\phi}_d \sin(\phi_d + \delta_m)\cos(\theta_{g_m})\sin(\theta_{g_m})\sin^2(\phi_{g_m}) \\
&\quad - \dot{\theta}_s\dot{\theta}_{g_m}\sin(\phi_d + \delta_m)\cos(\theta_{g_m})\sin(\phi_{g_m})\cos(\phi_{g_m}) \\
&\quad - \dot{\theta}_s\dot{\phi}_d \sin(\theta_{g_m})\sin(\phi_{g_m})\cos(\phi_d + \delta_m)\cos(\phi_{g_m}) \\
&\quad + \dot{\theta}_s\dot{\phi}_d \sin(\theta_{g_m})\sin(\phi_d + \delta_m)\cos(\theta_{g_m})\sin^2(\phi_{g_m})
\end{aligned}$$

$$
\begin{aligned}
&+\dot{\phi}_d{}^2 \sin^2(\theta_{g_m}) \sin^2(\phi_{g_m}) \\
&-\dot{\phi}_d \dot{\theta}_{g_m} \sin(\theta_{g_m}) \sin(\phi_{g_m}) \cos(\phi_{g_m}) \\
&+\dot{\theta}_s \dot{\theta}_{g_m} \cos(\phi_d + \delta_m) \cos^2(\phi_{g_m}) \\
&-\dot{\theta}_s \dot{\theta}_{g_m} \cos(\phi_{g_m}) \sin(\phi_d + \delta_m) \cos(\theta_{g_m}) \sin(\phi_{g_m}) \\
&-\dot{\phi}_d \dot{\theta}_{g_m} \cos(\phi_{g_m}) \sin(\theta_{g_m}) \sin(\phi_{g_m}) \\
&+\dot{\theta}_{g_m}{}^2 \cos^2(\phi_{g_m})
\end{aligned}
\qquad \textit{(A1.3)}
$$

We now consider the second part of the equation

$$
\begin{aligned}
&\left[\dot{\theta}_s \cos(\phi_d + \delta_m) \sin(\phi_{g_m}) + \dot{\theta}_s \sin(\phi_d + \delta_m) \cos(\theta_{g_m}) \cos(\phi_{g_m}) \right. \\
&\left. +\dot{\phi}_d \sin(\theta_{g_m}) \cos(\phi_{g_m}) + \dot{\theta}_{g_m} \sin(\phi_{g_m}) \right]^2
\end{aligned}
$$

$$
\begin{aligned}
&= \dot{\theta}_s{}^2 \cos^2(\phi_d + \delta_m) \sin^2(\phi_{g_m}) \\
&+\dot{\theta}_s{}^2 \cos(\phi_d + \delta_m) \sin(\phi_{g_m}) \sin(\phi_d + \delta_m) \cos(\theta_{g_m}) \cos(\phi_{g_m}) \\
&+\dot{\theta}_s \dot{\phi}_d \cos(\phi_d + \delta_m) \sin(\phi_{g_m}) \sin(\theta_{g_m}) \cos(\phi_{g_m}) \\
&+\dot{\theta}_s \dot{\theta}_{g_m} \cos(\phi_d + \delta_m) \sin^2(\phi_{g_m}) \\
&+\dot{\theta}_s{}^2 \cos(\phi_d + \delta_m) \sin(\phi_{g_m}) \sin(\phi_d + \delta_m) \cos(\theta_{g_m}) \cos(\phi_{g_m}) \\
&+\dot{\theta}_s{}^2 \sin^2(\phi_d + \delta_m) \cos^2(\theta_{g_m}) \cos^2(\phi_{g_m}) \\
&+\dot{\theta}_s \dot{\phi}_d \sin(\phi_d + \delta_m) \cos(\theta_{g_m}) \sin(\theta_{g_m}) \cos^2(\phi_{g_m})
\end{aligned}
$$

$$+\dot{\theta}_s\dot{\theta}_{g_m}\sin(\phi_d + \delta_m)\cos(\theta_{g_m})\cos(\phi_{g_m})\sin(\phi_{g_m})$$

$$+\dot{\theta}_s\dot{\phi}_d\sin(\theta_{g_m})\cos(\phi_{g_m})\cos(\phi_d + \delta_m)\sin(\phi_{g_m})$$

$$+\dot{\theta}_s\dot{\phi}_d\sin(\theta_{g_m})\sin(\phi_d + \delta_m)\cos(\theta_{g_m})\cos^2(\phi_{g_m})$$

$$+\dot{\phi}_d{}^2\sin^2(\theta_{g_m})\cos^2(\phi_{g_m})$$

$$+\dot{\phi}_d\dot{\theta}_{g_m}\sin(\theta_{g_m})\cos(\phi_{g_m})\sin(\phi_{g_m})$$

$$+\dot{\theta}_s\dot{\theta}_{g_m}\cos(\phi_d + \delta_m)\sin^2(\phi_{g_m})$$

$$+\dot{\theta}_s\dot{\theta}_{g_m}\sin(\phi_{g_m})\sin(\phi_d + \delta_m)\cos(\theta_{g_m})\cos(\phi_{g_m})$$

$$+\dot{\phi}_d\dot{\theta}_{g_m}\sin(\phi_{g_m})\sin(\theta_{g_m})\cos(\phi_{g_m})$$

$$+\dot{\theta}_{g_m}{}^2\sin^2(\phi_{g_m}) \qquad \textit{(A1.4)}$$

Combining Equation A1.2 and A1.3 results in

$$= -\dot{\theta}_s{}^2\cos^2(\phi_d + \delta_m) + 2\dot{\theta}_s\dot{\theta}_{g_m}\cos(\phi_d + \delta_m) + \dot{\theta}_{g_m}{}^2$$

$$+\dot{\theta}_s{}^2\sin^2(\phi_d + \delta_m)\cos^2(\theta_{g_m}) + 2\dot{\theta}_s\dot{\phi}_d\sin(\phi_d + \delta_m)\cos(\theta_{g_m})\sin(\theta_{g_m})$$

$$+\dot{\phi}_d{}^2\sin^2(\theta_{g_m})$$

which can be factorised to give

$$= \left(\dot{\theta}_s\cos(\phi_d + \delta_m) + \dot{\theta}_{g_m}\right)^2 + \left(\dot{\theta}_s\sin(\phi_d + \delta_m)\cos(\theta_{g_m}) + \dot{\phi}_d\sin(\theta_{g_m})\right)^2 \qquad \textit{(A1.2)}$$

Appendix B

Design assessment

Concept Selection Chart

Sub-system 1: Gyroscopes

Concept No.	***Functional*** *(geometry, motion, load paths, compatibility, control*	***Manufacturing, quality, life cycle*** *(production, purchase, assembly, waste)*	***Ergonomic, ecological, aesthetic & safety*** *(user, environmental, appeal)*	***Can it be made to work*** *(potential, confidence, enthusiasm)*	***Economics & timing*** *(material, manufacturing, operational)*	***Information*** *(cooperation, expertise, experience)*	*Comments*	*Score*	*Develope further*	*Eliminate*	*Get information*
A1	✓	✓	✓	✓	✓		*Pros - easy to assemble, simple machining, room for wiring*				
		✓	✓		✓		*Cons - raises disc COM*	***8***	✓		
							Ideas - look at reducing weight				
A2	✓	×	✓	✓	✓	✓	*Pros - low COM, balanced design, easy to align with pivot point*				
			✓				*Con - difficult to manufacture and assemble*	*5*		✓	
							Ideas				
B1	✓	✓	×	✓	✓	✓	*Pros - easy to mauufacutre, no balancing required*				
		✓		✓			*Cons - extra components, difficult to assemble*	*7*		✓	
							Ideas				
B2	✓	✓	✓	✓	✓	✓	*Pros - COM in line with motor COM, easy to assemble*				
	✓		✓		✓		*Cons - flywheel must be well balanced*	**9**	✓		
							Ideas - look at accurate mounting solutions				
B3	✓	✓	✓	✓	×	×	*Pros - gearing options, large flywheel mass*				
	✓						*Cons - complex design, takes up a lot of space*	*3*		✓	
							Ideas				
C1	✓	✓	✓	✓	✓	✓	*Pros - simple to manufacture, inexpensive*				
		✓	✓	✓		✓	*Cons - fixed inertia, must be well balanced*	**10**	✓		
							Ideas - look at methods of manufacturing balanced wheel				
C2	✓	✓	×	✓	✓	✓	*Pros - promotes air flow, longer running times*				
	✓						*Cons - reduced inertia, complex machining*	*5*		✓	
							Ideas				
C3	✓	✓	✓	✓	✓	✓	*Pros - interchangable wheel,*				
	✓						*Cons - difficult to dynamically balance, increased cost*	*7*		✓	
							Ideas				

Key: (✓) yes +1, (×) no -1, ( ) neutral, (?) not enough information

Figure B1 - Concept selection chart for gyroscope sub system

Concept Selection Chart

Sub-system 2: Disc

Concept No.	***Functional*** *(geometry, motion, load paths, compatibility, control*	***Manufacturing, quality, life cycle*** *(production, purchase, assembly, waste)*	***Ergonomic, ecological, aesthetic & safety*** *(user, environmental, appeal)*	***Can it be made to work*** *(potential, confidence, enthusiasm)*	***Economics & timing*** *(material, manufacturing, operational)*	***Information*** *(cooperation, expertise, experience)*	*Comments*	*Score*	*Develope further*	*Eliminate*	*Get information*
D1	✓ ✓	✓	×	✓	✓	✓	*Pros - high strength, no assembly required* *Cons - expensive, no room for developments/extra attachments* *Ideas*	*5*		✓	
D2	✓ ✓	×	✓ ✓	✓	✓ ✓	✓	*Pros - rigid design, disc and cone and be machined individually* *Cons - distortion from heat, welding must be done off site* *Ideas*	*7*		✓	
D3	✓	✓	✓	✓ ✓	✓ ✓	✓	*Pros - components can be machined seperately, adaptable design* *Cons - accurate machining required, strength could be an issue* *Ideas - look at methods for reducing weight and lowering COM*	***9***	✓		
E1	✓	✓	✓	✓ ✓	✓ ✓	✓	*Pros - accessible for charging, simple path for connecting cables* *Cons - negative impact on COM, limited space for securing in place* *Ideas*	*8*		✓	
E2	✓ ✓	✓	✓ ✓	✓ ✓	✓	✓	*Pros - lowers disc COM, aesthetics* *Cons - diificult to assemble, reduces max disc tip angle* *Ideas- investigate methods for securing in place*	***9***	✓		
F1	✓ ✓	✓ ✓	✓	✓	✓	✓	*Pros - load paths, multiple mounting points,* *Cons - increased weight, high manufacturing cost, complex assembly* *Ideas - consider accurate positioning method and weight reduction*	***8***	✓		
F2	✓ ✓	×	✓	✓	✓	✓	*Pros - lightweight, inexpensive, simple to manufacture* *Cons - limited space for bearings, low strength, mounting options* *Ideas*	*5*		✓	
F3	×	✓ ✓	✓ ✓	✓	✓	✓	*Pros - inexpensive, eliminate need for assembly* *Cons - no disassembly, must be accurately positioned* *Ideas - can one leg be fabricated and one be assembled in place*	*6*		✓	
G1	✓	✓	✓ ✓	✓	✓	✓	*Pros - accurate locating method, cheap to machine holes in disc* *Cons - more complex assembly, difficult to align bearing surfaces* *Ideas - develope for quick assembly, assemble before machining*	***7***	✓		
G2	✓	✓	✓	✓	✓	✓	*Pros - quick to assemble, reduces disc weight, high accuracy* *Cons - expensive to machine slots, still requires fasteners* *Ideas*	*6*		✓	
G3	✓	×	×	✓	✓ ✓	✓ ✓	*Pros - allows for changes in design, simple to assemble, low cost* *Cons - machining time, does not align bearing surfaces accurately* *Ideas*	*4*		✓	

Key: (✓) yes +1, (×) no -1, ( ) neutral, (?) not enough information

Figure B2 - Concept selection chart for disc sub system

Concept Selection Chart

Sub-system 3: External structure

Concept No.	***Functional*** *(geometry, motion, load paths, compatibility, control*	***Manufacturing, quality, life cycle*** *(production, purchase, assembly, waste)*	***Ergonomic, ecological, aesthetic & safety*** *(user, environmental, appeal)*	***Can it be made to work*** *(potential, confidence, enthusiasm)*	***Economics & timing*** *(material, manufacturing, operational)*	***Information*** *(cooperation, expertise, experience)*	*Comments*	*Score*	*Develope further*	*Eliminate*	*Get information*
H1	✓ ✓	×	✓ ✓	✓ ✓	✓	✓	*Pros - pivot in all directions, easy to integrate into system* *Cons - difficult to control and measure response, expensive* *Ideas*	*7*		✓	
H2	✓ ✓	×	✓ ✓	✓	✓	✓ ✓	*Pros - cheap to manufacture, simple to measure restoring moment* *Cons - only one plane to pivot in, heavy, will require testing frame* *Ideas*	*7*		✓	
H3	✓ ✓	×	✓ ✓	✓ ✓	✓	✓ ✓	*Pros - inexpensive, excellent way to showcase design, low to ground* *Cons - difficult to verfiy size of torque produced by system* *Ideas - consider materials and manufacturing method*	***8***	✓		
I1	✓ ✓	✓ ✓	✓	✓	✓ ✓	✓	*Pros - height can be accurately set,* *Cons - high manufacutre cost, could be difficult to adjust* *Ideas - manufacture from aluminium, use coarse thread >M18*	***9***	✓		
I2	×	✓ ✓	✓	✓ ✓	✓	✓	*Pros - easy to adjust, simple to machine, low weight design* *Cons - must be machined and assembled accurately or will not work* *Ideas*	*6*		✓	
I3	×	✓	✓	✓	✓	✓	*Pros - very simple to make and assemble, can be hollow* *Cons - no adjustability* *Ideas*	*4*		✓	

Key: (✓) yes +1, (×) no -1, ( ) neutral, (?) not enough information

Figure B3 - Concept selection chart for external structure sub system

Concept Selection Chart

Sub-system 4: Disc drive mechanism

Concept No.	***Functional*** *(geometry, motion, load paths, compatibility, control*	***Manufacturing, quality, life cycle*** *(production, purchase, assembly, waste)*	***Ergonomic, ecological, aesthetic & safety*** *(user, environmental, appeal)*	***Can it be made to work*** *(potential, confidence, enthusiasm)*	***Economics & timing*** *(material, manufacturing, operational)*	***Information*** *(cooperation, expertise, experience)*	*Comments*	*Score*	*Develope further*	*Eliminate*	*Get information*
J1	✓ ✓	✓ ✓	✓	✓ ✓	✓ ✓	×	*Pros - high torque, low profile, simple to control, small, inexpensive* *Cons - difficult to mount in place, need to test for load capacity'* *Ideas - further testing required*	***8***	✓		✓
J2	✓	✓	✓	✓ ✓	✓	✓	*Pros - inline shaft arrangement, simple mount points, easy to control* *Cons - large in size, length raises overall assembly COM* *Ideas*	*7*		✓	
J3	✓ ✓	×	✓ ✓	✓	✓	×	*Pros - very accurate control, easy to assemble,* *Con - high cost, complex control system required, large size needed* *Ideas*	*4*		✓	
K1	✓	✓ ✓	✓ ✓	✓	✓	✓	*Pros - simple to manufacture, low cost, compact, low weight* *Cons - only motor gear reduction, possible alignment issues* *Ideas - can a coupling be used?*	***8***	✓		
K2	✓ ✓	×	✓	✓	✓	✓	*Pros - further increase in torque, high strength, reduced backlash* *Cons - expensive, large increase in assembly weight, maintenance* *Ideas*	*5*		✓	
K3	✓	×	✓	✓ ✓	✓	✓	*Pros - interchangeable motor pulley for varying gear ratio, high torque* *Cons - cost of manufacture, complex assembly, torsioner required* *Ideas*	*5*		✓	
L1	✓	✓ ✓	×	✓	✓	✓	*Pros - increased strength, reduced backlash, low cost* *Cons - no disassembly, alignment, failure destroys components* *Ideas*	*5*		✓	
L2	✓ ✓	✓ ✓	✓ ✓	✓	×	✓	*Pros - easy to assemble/disassemble, eliminates alignment issues* *Cons - expensive, loosening, restricted velocity/torque* *Ideas - investigate coupling options*	***7***	✓		
M1	✓ ✓	×	✓ ✓	✓	✓	✓	*Pros - acuurate alignment, easy to assemble, rigid connnection* *Cons - stress concentration, expensive to machine, difficult to modify* *Ideas*	*6*		✓	
M2	✓	✓	✓ ✓	✓	✓ ✓	✓	*Pros - simple disassebly/assembly, low cost, use off the shelf nut* *Cons - will loosen over time, extra components needed* *Ideas - use fine thread > M20, washer to increase clamping force?*	***8***	✓		

Key: (✓) yes +1, (×) no -1, ( ) neutral, (?) not enough information

Figure B4 - Concept selection chart for disc drive mechanism sub system

Concept Selection Chart

Sub-system 5: Gimbal frame linkage

Concept No.	***Functional*** *(geometry, motion, load paths, compatibility, control*	***Manufacturing, quality, life cycle*** *(production, purchase, assembly, waste)*	***Ergonomic, ecological, aesthetic & safety*** *(user, environmental, appeal)*	***Can it be made to work*** *(potential, confidence, enthusiasm)*	***Economics & timing*** *(material, manufacturing, operational)*	***Information*** *(cooperation, expertise, experience)*	*Comments*	*Score*	*Develope further*	*Eliminate*	*Get information*
N1	✓	×	✓	✓	✓	✓	*Pros - ensures equal angle pivot, aligns pivot axis,* *Cons - difficult to assemble, very expensive to manufacture gears* *Ideas*	*5*		✓	
N2	✓	✓	✓	✓ ✓	✓	✓	*Pros - maintains equal pivot angle, attach to gimbal frame shaft* *Cons - must be rigid, hard to assemble, high cost for UJ's* *Ideas*	*7*		✓	
N3	✓	✓ ✓	✓	✓ ✓	✓		*Pros - lightweight, simple to assemble, low cost* *Cons - requires central shaft, side loads on bearing cause pinching* *Ideas - look at making linkages adjustable, lengthen bearing*	***8***	✓		
O1	✓	✓	✓	✓	✓	✓	*Pros - low cost, easily accessible components, lightweight* *Cons - poor under side loads, accurate shaft contact required* *Ideas*	*6*		✓	
O2	✓	✓	✓	✓	✓	✓	*Pros - lengthened contact area, cheap, easy to maintain* *Cons - lubrication needed, high friction, not ideal for sliding* *Ideas - investigate more material options*	*6*		✓	
O3	✓ ✓	✓	✓ ✓	✓	✓	✓	*Pros - lengthened contact area, high tolerance, smooth motion* *Cons - high cost, high tolerance shaft needed, bearing retention* *Ideas - look at integrating shaft supplied with bearing as central shaft*	***8***	✓		
P1	✓ ✓	✓	×	✓	✓	✓	*Pros - rigid, simple to manufacture, lightweight, low cost* *Cons - fixed length, difficult to assemble and align gimbal frames* *Ideas*	*5*		✓	
P2	✓ ✓	✓	✓	✓ ✓	✓	✓	*Pros - adjustable, simple to assemble, equal gimbal angles* *Cons - low rigidity could under constrain assembly* *Ideas - consider including one rigid connection*	***8***	✓		

Figure B5 - Concept selection chart for gimbal frame linkage sub system

Concept Selection Chart

Sub-system 6: Central pivot

Concept No.	***Functional*** *(geometry, motion, load paths, compatibility, control*	***Manufacturing, quality, life cycle*** *(production, purchase, assembly, waste)*	***Ergonomic, ecological, aesthetic & safety*** *(user, environmental, appeal)*	***Can it be made to work*** *(potential, confidence, enthusiasm)*	***Economics & timing*** *(material, manufacturing, operational)*	***Information*** *(cooperation, expertise, experience)*	*Comments*	*Score*	*Develope further*	*Eliminate*	*Get information*
Q1	✓ ✓	✓	✓	✓	×	✓	*Pros - low friction, simple to integrate into system* *Cons - not constant velocity, high cost, requires extra bearings* *Ideas*	*5*		✓	
Q2	×	✓	✓	✓ ✓	×	✓	*Pros - only one bearing needed, low resistance to tipping of disc* *Cons - poor performance at angles > 5°, expensive* *Ideas*	*3*		✓	
Q3	✓ ✓	✓	✓ ✓	✓	✓	×	*Pros - velocity is constant at all angles, cheap, can be machined* *Cons - maintenance, extra components required to adapt into system* *Ideas - look at machining outer housing to fit bearings*	***6***	✓		

Key: (✓) yes +1, (×) no -1, ( ) neutral, (?) not enough information

Figure B6 - Concept selection chart for central pivot sub system

Conceptual Design Worksheet

Stable Platform System

Requirements	*Contributing factors*	*Current status*			*Required action*		
		Good	*Marginal*	*Poor*	*Proceed*	*Revise*	*N/A*
Functional	Overall geometry	■	□	□	□	■	□
	Motion of Parts	□	□	■	□	■	□
	Forces involved	□	■	□	□	■	□
	Energy needed	■	□	□	■	□	□
	Material to be used	□	■	□	□	■	□
	Control system	■	□	□	■	□	□
	Information flow	■	□	□	□	□	■
Safety	Operation	■	□	□	■	□	□
	Human	□	■	□	□	■	□
	Environmental	■	□	□	■	□	□
Quality	Qualtiy assurance	□	■	□	□	■	□
	Quality control	□	■	□	□	■	□
	Reliability	□	■	□	□	■	□
Manufacturing	Production of components	□	■	□	□	■	□
	Purchase of components	□	■	□	□	■	□
	Assembly	□	■	□	□	■	□
	Transport	□	□	□	□	□	■
Timing	Design schedule	■	□	□	□	■	□
	Development schedule	□	■	□	□	■	□
	Production schedule	□	□	■	□	■	□
	Delivery schedule	□	□	□	□	□	■
Economic	Marketing costs	□	□	□	□	□	■
	Design costs	■	□	□	□	■	□
	Development costs	■	□	□	□	■	□
	Manufacturing costs	□	■	□	□	■	□
	Distribution costs	□	□	□	□	□	■
Ergonomic	User needs	□	■	□	□	■	□
	Ergonomic design	■	□	□	□	■	□
	Cybernetic design	□	□	□	□	□	■
Ecological	Material selection	□	■	□	□	■	□
	Working fluid selection	□	□	□	□	□	■
Asesthetic	Customer appeal	□	□	□	□	□	■
	Fashion	□	□	□	□	□	■
	Future expectations	□	■	□	□	■	□
Life cycle	Distribution	□	□	□	□	□	■
	Operation	■	□	□	□	■	□
	Maintenance	□	■	□	□	■	□
	Disposal	□	□	■	□	■	□

Figure B7 - Conceptual design worksheet

Embodiment Design Worksheet

Stable Platform System

Requirements	*Contributing factors*	*Current status*			*Required action*		
		Good	*Marginal*	*Poor*	*Proceed*	*Revise*	*N/A*
Functional	Overall geometry	■	□	□	■	□	□
	Motion of Parts	□	■	□	□	■	□
	Forces involved	□	■	□	□	■	□
	Energy needed	■	□	□	■	□	□
	Material to be used	■	□	□	■	□	□
	Control system	■	□	□	■	□	□
	Information flow	■	□	□	□	□	■
Safety	Operation	■	□	□	■	□	□
	Human	■	□	□	■	□	□
	Environmental	■	□	□	■	□	□
Quality	Qualtiy assurance	■	□	□	■	□	□
	Quality control	■	□	□	□	■	□
	Reliability	□	■	□	□	■	□
Manufacturing	Production of components	□	■	□	□	■	□
	Purchase of components	■	□	□	□	□	□
	Assembly	■	□	□	□	■	□
	Transport	□	□	□	□	□	■
Timing	Design schedule	■	□	□	■	□	□
	Development schedule	■	□	□	■	□	□
	Production schedule	□	■	□	□	■	□
	Delivery schedule	□	□	□	□	□	■
Economic	Marketing costs	□	□	□	□	□	■
	Design costs	■	□	□	■	□	□
	Development costs	■	□	□	■	□	□
	Manufacturing costs	□	■	□	□	■	□
	Distribution costs	□	□	□	□	□	■
Ergonomic	User needs	■	□	□	□	■	□
	Ergonomic design	■	□	□	□	□	□
	Cybernetic design	□	□	□	□	□	■
Ecological	Material selection	□	■	□	□	■	□
	Working fluid selection	□	□	□	□	□	■
Asesthetic	Customer appeal	□	□	□	□	□	■
	Fashion	□	□	□	□	□	■
	Future expectations	■	□	□	□	■	□
Life cycle	Distribution	□	□	□	□	□	■
	Operation	■	□	□	■	□	□
	Maintenance	□	■	□	□	■	□
	Disposal	□	■	□	□	■	□

Figure B8 - Embodiment design worksheet

Detailed Design Worksheet

Stable Platform System

Requirements	*Contributing factors*	*Current status*			*Required action*		
		Good	*Marginal*	*Poor*	*Proceed*	*Revise*	*N/A*
Functional	Overall geometry	■	□	□	■	□	□
	Motion of Parts	■	□	□	■	□	□
	Forces involved	□	■	□	■	□	□
	Energy needed	■	□	□	■	□	□
	Material to be used	■	□	□	■	□	□
	Control system	■	□	□	■	□	□
	Information flow	■	□	□	■	□	□
Safety	Operation	■	□	□	■	□	□
	Human	■	□	□	■	□	□
	Environmental	■	□	□	■	□	□
Quality	Qualtiy assurance	■	□	□	■	□	□
	Quality control	■	□	□	■	□	□
	Reliability	■	□	□	■	□	□
Manufacturing	Production of components	□	■	□	■	□	□
	Purchase of components	■	□	□	□	□	□
	Assembly	■	□	□	□	□	□
	Transport	□	□	□	□	□	■
Timing	Design schedule	■	□	□	■	□	□
	Development schedule	■	□	□	■	□	□
	Production schedule	■	□	□	■	□	□
	Delivery schedule	□	□	□	□	□	■
Economic	Marketing costs	□	□	□	□	□	■
	Design costs	■	□	□	■	□	□
	Development costs	■	□	□	■	□	□
	Manufacturing costs	■	□	□	■	□	□
	Distribution costs	□	□	□	□	□	■
Ergonomic	User needs	■	□	□	■	□	□
	Ergonomic design	■	□	□	■	□	□
	Cybernetic design	□	□	□	□	□	□
Ecological	Material selection	■	□	□	■	□	□
	Working fluid selection	□	□	□	□	□	■
Asesthetic	Customer appeal	□	□	□	□	□	■
	Fashion	□	□	□	□	□	■
	Future expectations	■	□	□	■	□	□
Life cycle	Distribution	□	□	□	□	□	■
	Operation	■	□	□	■	□	□
	Maintenance	■	□	□	■	□	□
	Disposal	■	□	□	□	■	□

Figure B9 - Detailed design worksheet

Appendix C

Manufacturing drawings

C1 Prototype B Bill of Materials

The following set of tables outline the bill of materials relating to *Prototype B* divided into the sub systems that make up the overall system.

Prototype B Final Design (SP1-01-001)

Part Number	Description	Part/Assembly	Material	No. Required
SP2-01-001	Gyroscopes	Assembly	N/A	4
SP2-02-001	Disc	Assembly	N/A	1
SP2-03-001	External Structure	Assembly	N/A	1
SP2-04-001	Disc Drive Mechanism	Assembly	N/A	1
SP2-05-001	Gimbal Frame Linkage	Assembly	N/A	1
SP2-06-001	Central Pivot	Assembly	N/A	1

Table C1 - Prototype B final design bill of materials

Gyroscopes (SP2-01-001)

Part Number	Description	Part/Assembly	Material	No. Required
SP2-01-002	Gimbal frame	Assembly	N/A	1
SP2-01-003	Lightweight gimbal frame	Part	Mild Steel	1
SP2-01-004	Gimbal frame shaft	Part	4140	2
SP2-01-005	Flywheel	Part	4140	1
SP2-01-006	Gimbal frame contact arm	Part	4140	1
SP2-01-007	Contact arm end cap	Part	5083 Aluminium	1
SP2-01-008	Ø20mm ID, Ø32mm OD deep groove bearing	Part	N/A	1
SP2-01-009	MP160 Brushless DC Motor	Part	N/A	1
-	M16 Nut	-	N/A	1
-	M6 x 15 Countersunk screw	-	N/A	1
-	M4 x 15 Cap screw	-	N/A	12

Table C2 - Prototype B gyroscopes bill of materials

Disc (SP2-02-001)

Part Number	Description	Part/Assembly	Material	No. Required
SP2-02-002	Disc plate	Part	7075 Aluminium	1
SP2-02-003	Centre cone section	Part	7075 Aluminium	1
SP2-02-004	Gimbal frame leg	Part	7075 Aluminium	1
SP2-02-005	Gimbal frame leg - Right	Part	7075 Aluminium	1
SP2-02-006	Spacer washer	Part	7075 Aluminium	4
SP2-02-007	22.2V 2200mAh 6 Cell Li-Po Battery	Part	N/A	4
SP2-02-008	70A HV ESC	Part	N/A	4
SP2-02-009	Ø12mm ID, Ø21mm OD deep groove bearing	Part	N/A	8
-	M3 x 10 Cap screw	-	N/A	16
-	M8 x 20 Cap screw	-	N/A	4
-	M6 x 20 Cap screw	-	N/A	16
-	Ø4mm x 20 Dowel pin	-	N/A	16

Table C3 - Prototype B disc bill of materials

External Structure (SP2-03-001)

Part Number	Description	Part/Assembly	Material	No. Required
SP2-03-002	Tilt frame shaft	Part	5083 Aluminium	1
SP2-03-003	Main shaft end cap	Part	5083 Aluminium	2
SP2-03-004	Outer ring leg spacer	Part	7075 Aluminium	2
SP2-03-005	Leg mount plate	Part	7075 Aluminium	2
SP2-03-006	Outer ring mount legs	Part	5083 Aluminium	4
SP2-03-007	Outer contact ring	Part	7075 Aluminium	1
SP2-03-008	Tilt arm	Part	7075 Aluminium	1
-	M6 x 12 Cap screw	-	N/A	2
-	M4 x 12 Cap screw	-	N/A	16
-	M12 x 75 Cap screw	-	N/A	2
-	M20 Nut	-	N/A	8

Table C4 - Prototype B external structure bill of materials

Disc Drive Mechanism (SP2-04-001)

Part Number	Description	Part/Assembly	Material	No. Required
SP2-04-002	Bottom threaded structure connection	Part	5083 Aluminium	1
SP2-04-003	Bearing housing threaded boss	Part	5083 Aluminium	1
SP2-04-004	Bottom connecting boss	Part	5083 Aluminium	1
SP2-04-005	Boss mount block	Part	7075 Aluminium	1
SP2-04-006	Bearing housing	Assembly	N/A	1
SP2-04-007	Top bearing housing section	Part	5083 Aluminium	1
SP2-04-008	Centre pillar	Part	5083 Aluminium	1
SP2-04-009	Centre pillar mount	Part	7075 Aluminium	1
SP2-04-010	Central drive shaft	Assembly	N/A	1
SP2-04-011	Drive shaft	Part	4140 Steel	1
SP2-04-012	Drive shaft coupling	Part	4140 Steel	1
-	Ø4mm x 20 Dowel pin	-	N/A	1
-	M4 x 20 Countersunk screw	-	N/A	3
SP2-04-013	24V Worm drive DC motor	Part	N/A	1
-	Ø6mm x 20 Dowel pin	-	N/A	1
-	Ø4mm x 20 Dowel pin	-	N/A	1
SP2-04-014	Ø20mm ID, Ø32mm OD deep groove bearing	Part	N/A	1
SP2-04-015	Ø40mm ID, Ø52mm OD deep groove bearing	Part	N/A	1

Table C5 - Prototype B disc drive mechanism bill of materials

Gimbal Frame Linkage (SP2-05-001)

Part Number	Description	Part/Assembly	Material	No. Required
SP2-05-002	Overhead linear slide	Assembly	N/A	1
SP2-05-003	Overhead connecting arm	Part	7075 Aluminium	1
SP2-05-004	Linear bearing spacer	Part	5083 Aluminium	1
SP2-05-005	Ø16 x 86mm Linear bearing	Part	N/A	1
SP2-05-006	Ø26mm circlip	Part	N/A	2
SP2-05-007	Connecting rod	Part	7075 Aluminium	2
SP2-05-008	Universal joint clamping coupling	Part	N/A	1
SP2-05-009	Ø16mm Universal joint	Part	Mild Steel	4
-	M10 Half nut	-	N/A	4
-	M6 x 30 Cap screw	-	N/A	4
-	M5 x 25 Cap screw	-	N/A	4
-	M5 Nyloc nut	-	N/A	4

Table C6 - Prototype B gimbal frame linkage bill of materials

Central Pivot (SP2-06-001)

Part Number	Description	Part/Assembly	Material	No. Required
SP2-06-002	Universal joint coupling	Part	4140 Steel	1
SP2-06-003	Main shaft	Part	4140 Steel	1
SP2-06-004	Ø32mm Universal Joint	Part	Mild Steel	1
-	M24 half nut	-	N/A	1

Table C7 - Prototype B central pivot bill of materials

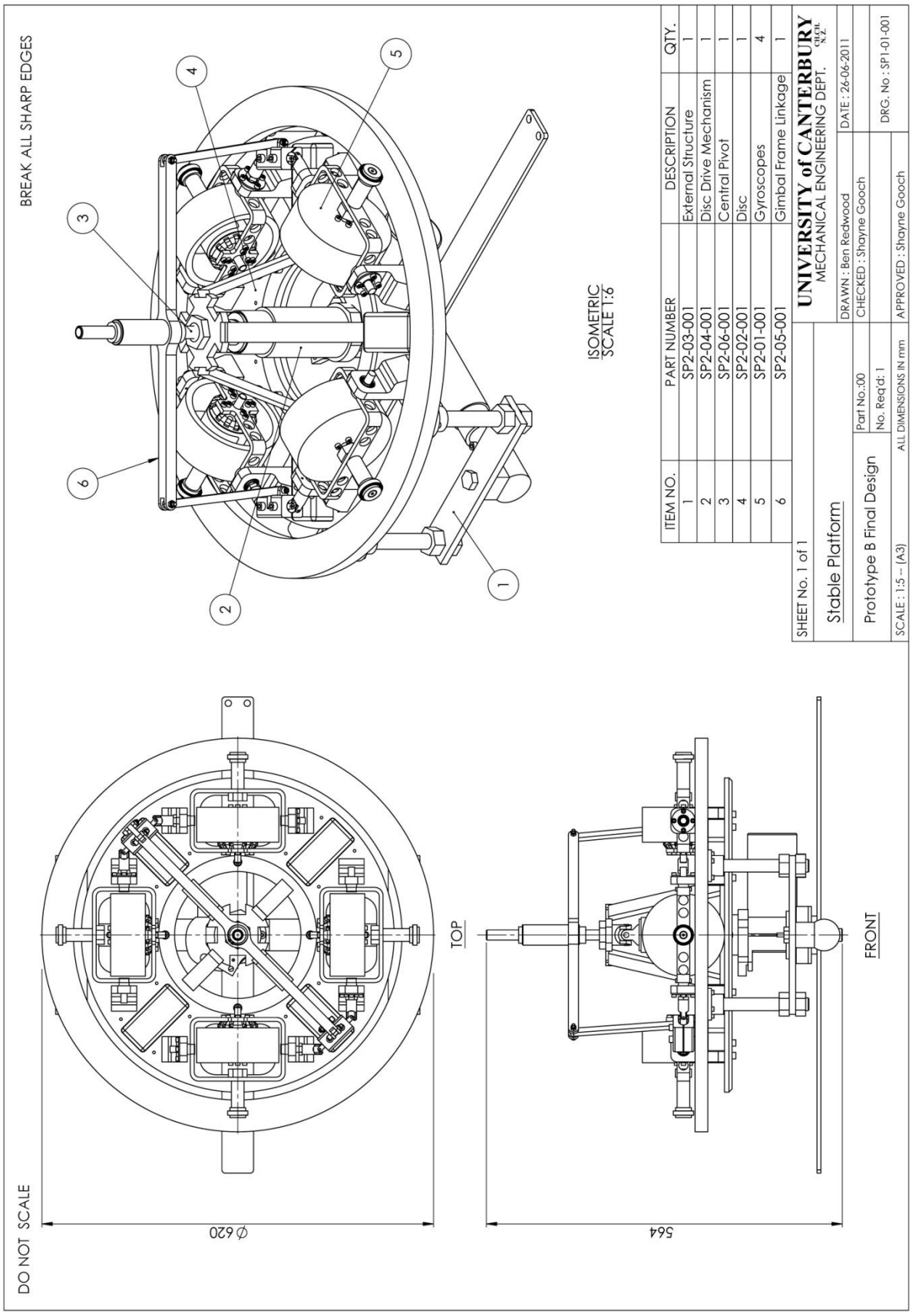

Figure C8 - Prototype B final design engineering drawing

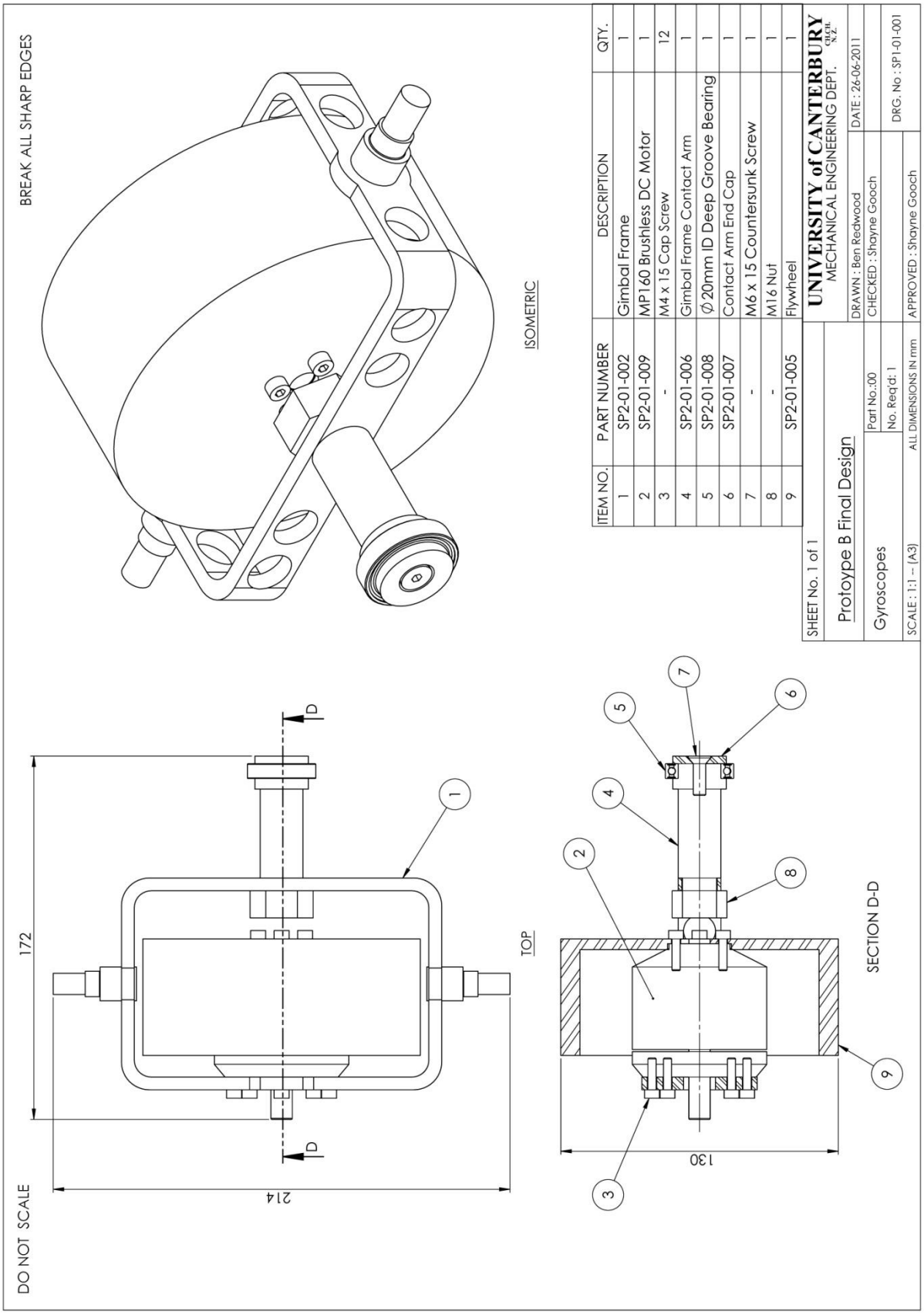

Figure C9 - Prototype B gyroscopes engineering drawing

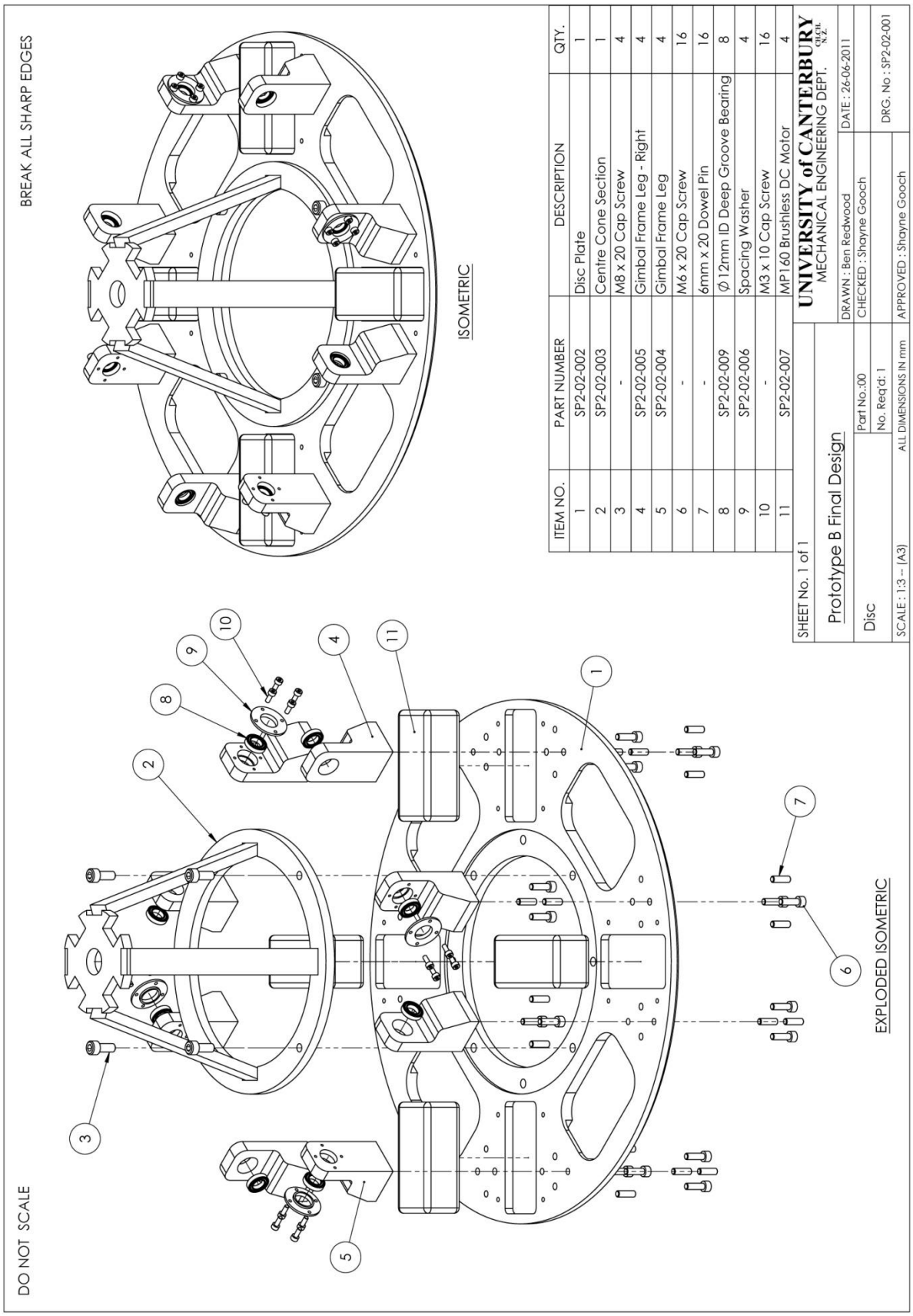

Figure C10 - Prototype B disc engineering drawing

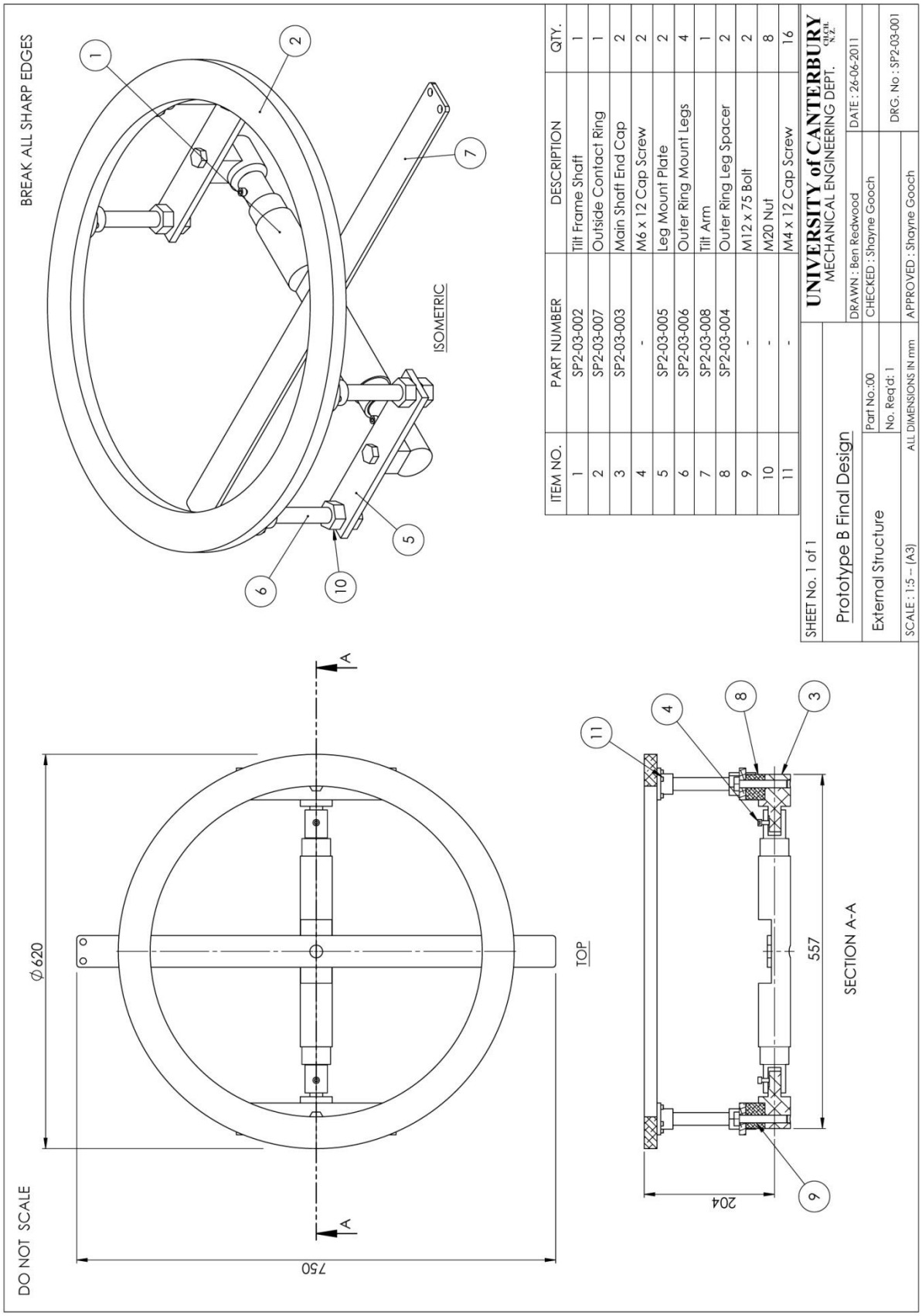

Figure C11 - Prototype B external structure engineering drawing

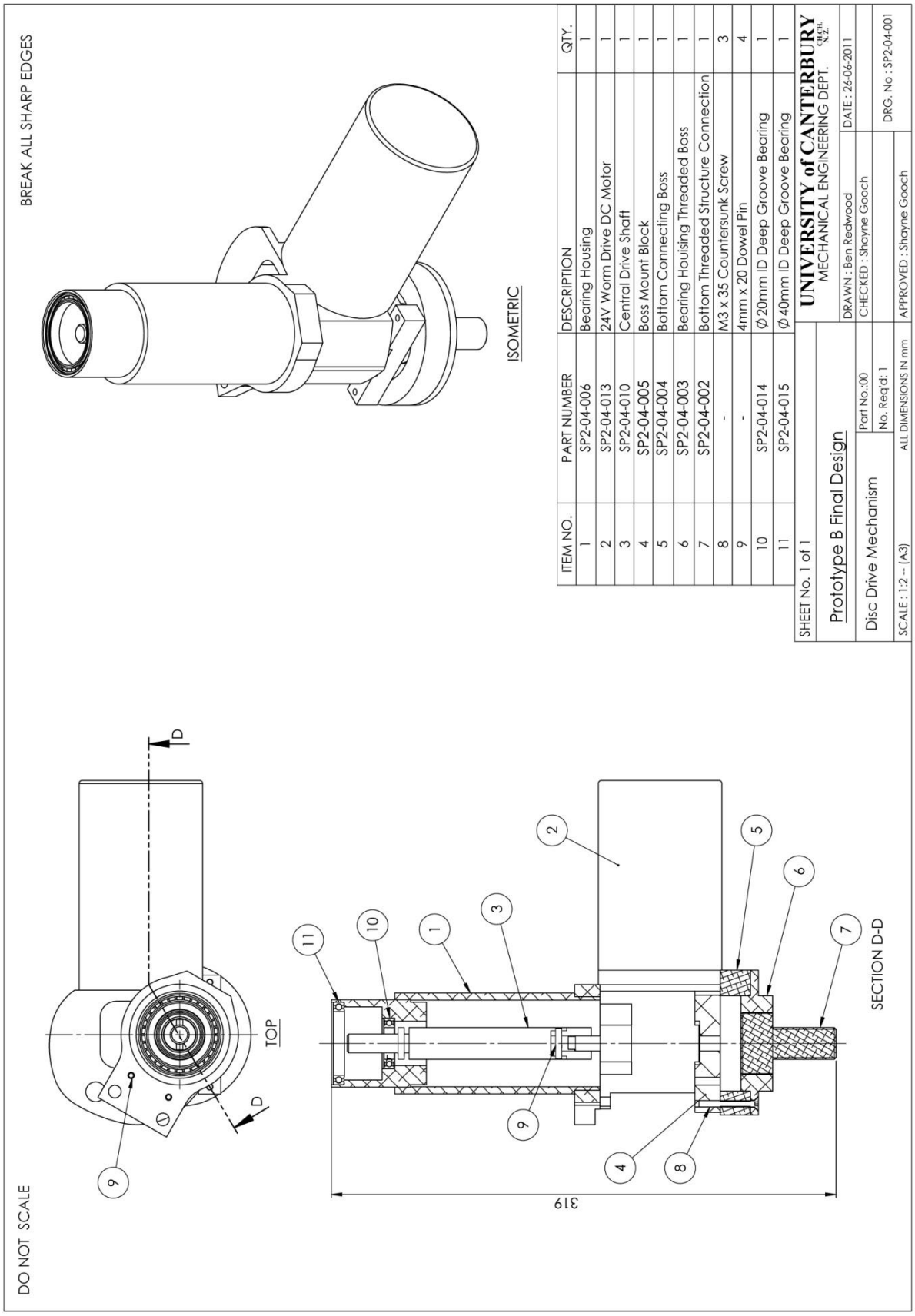

Figure C12 - Prototype B disc drive mechanism engineering drawing

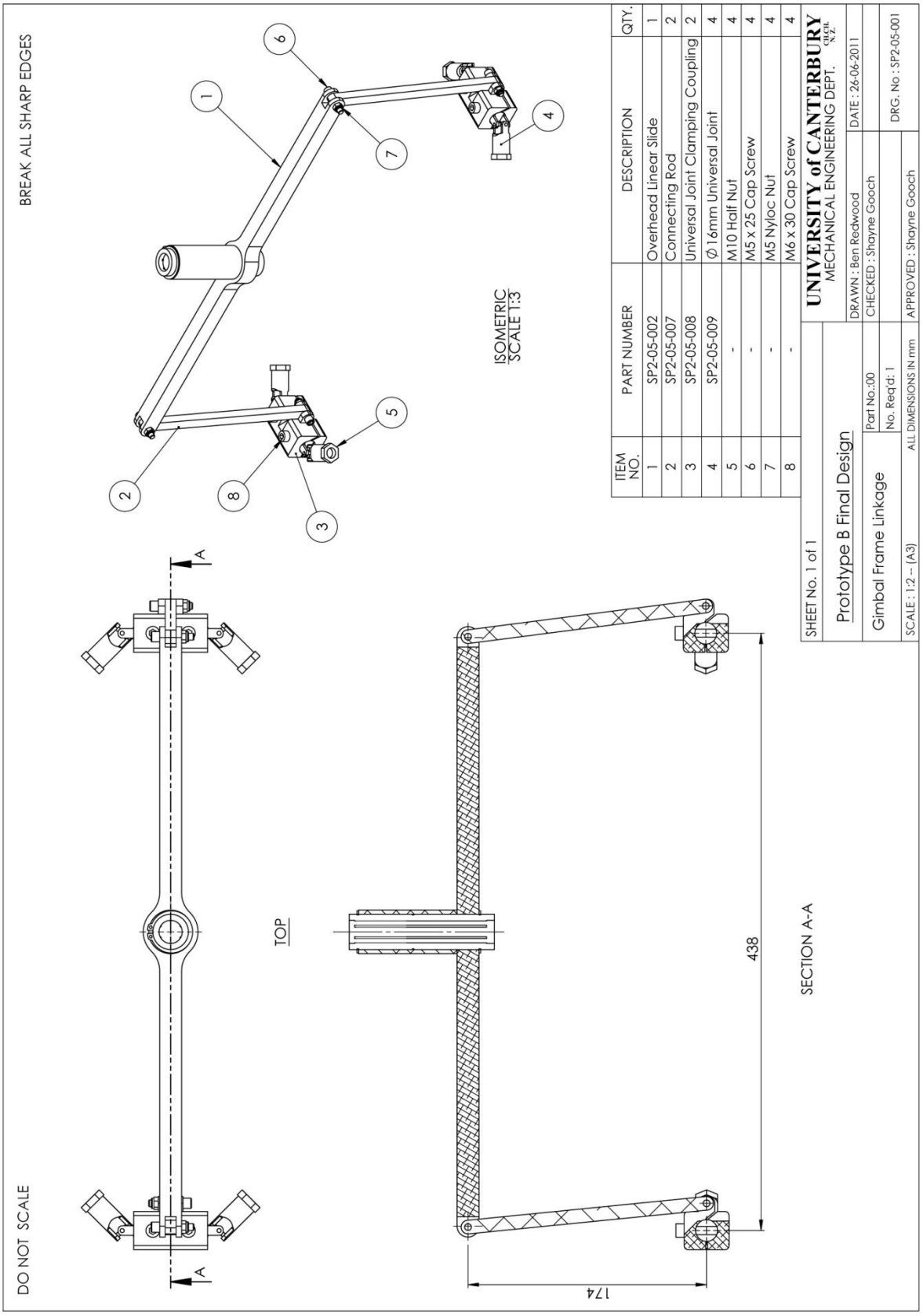

Figure C13 - Prototype B gimbal frame linkage engineering drawing

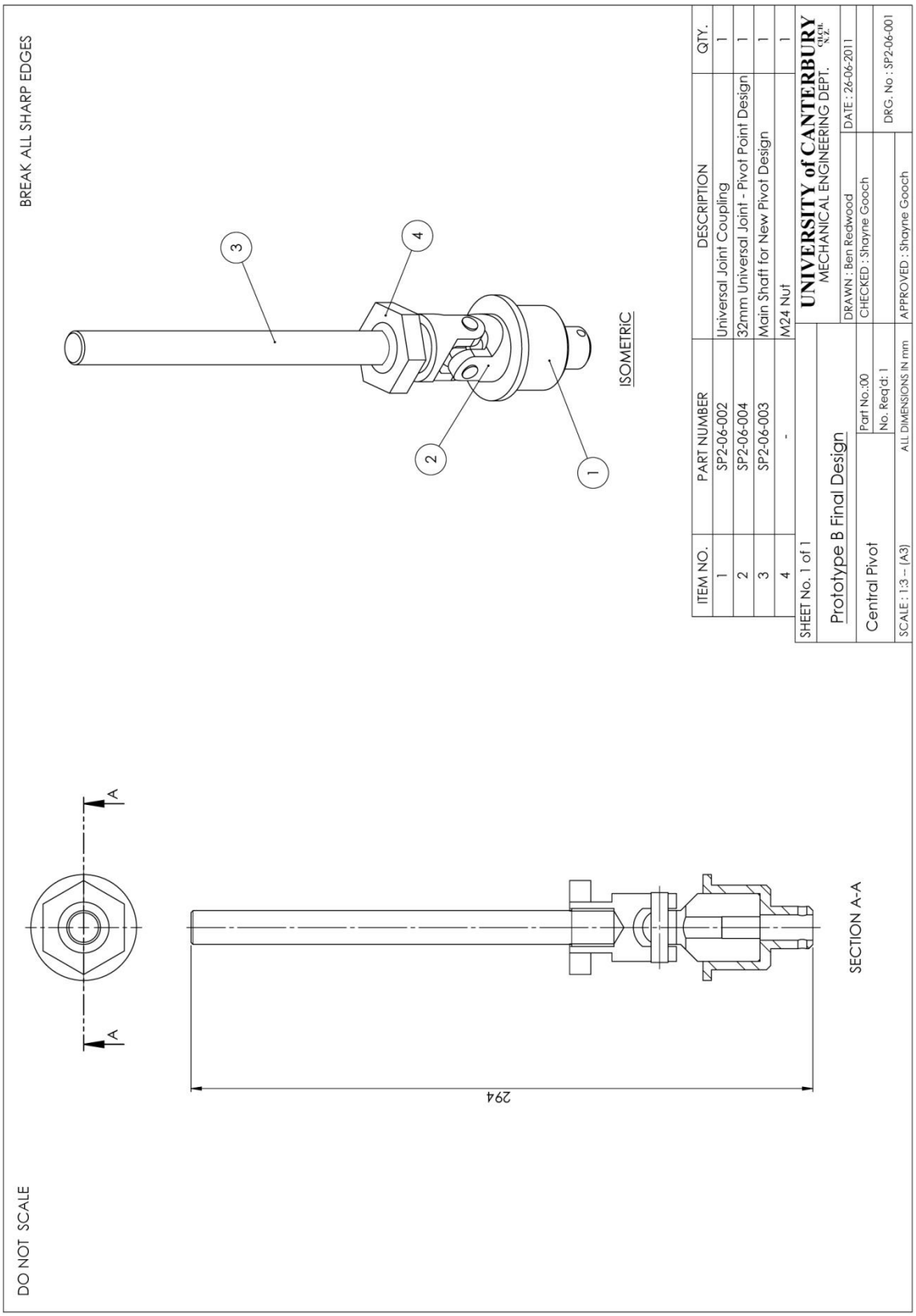

Figure C14 - Prototype B central pivot engineering drawing

Appendix D

Matlab code

D1 Homogeneous system

The following code relates to the response of the homogeneous system when the applicable physical parameters are substituted into the relevant constants

```
clear all
clc

I_z_d                   %inertia of the disc in the z direction, kgm^2
I                       %rotational inertia of one gyroscope, kgm^2

M_s                     %mass of external structure, kg
h_s                     %distance from the reference pivot point to the COM
                        of external structure, m
h_d                     %distance from the reference pivot point to the
                        disc pivot, m
g                       %acceleration due to gravity, ms^-2
M_g=1.94032             %mass of one gyroscope, kg
phi_dot                 %angular velocity of the gyroscopes, rads^-1
w_0                     %angular velocity of disc, rads^-1
r_g                     %distance from gyro pivot point to contact point, m
r_d                     %distance from disc centre axis to gyro pivot
                        point, m

M_d_and_4M_g            %mass of disc and gyroscope assembly, kg

mu=0.5;                 %coefficient of friction in drive motor
C_phi_g=4*I*phi_dot;
C=4*I*(phi_dot*((r_g+r_d)/r_g));

A=(I_z_d+4*M_g*r_d^2+4*I);
B=(M_s*h_s^2+(M_d_and_4M_g)*h_d^2+8*I);
D=(M_s*h_s+((M_d_and_4M_g)*h_d))*g;

if mu*D>C*w_0*C_phi_g;
    display('mu*D>C*w_0*C_phi_g')
end

if C_phi_g^2>A*D;
    display('C_phi_g^2>A*D')
end

a=A*B;
b=-mu*B;
c=-(A*D-C_phi_g^2);
d=mu*D-C*w_0*C_phi_g;

discriminant=18*a*b*c*d-4*(b^3)*d+(b^2)*(c^2)-4*a*(c^3)-27*(a^2)*(d^2);

if discriminant>0;
    display('discriminant>0')
end
```

```
delta_1=2*b^3-9*a*b*c+27*(a^2)*d;
delta_0=b^2-3*a*c;

C_eqn=((delta_1+sqrt((delta_1^2)-4*(delta_0^3)))/2)^1/3;

u_1=1;
u_2=(-1+1i*sqrt(3))/2;
u_3=(-1-1i*sqrt(3))/2;

lamda1=-(1/3*a)*(b+u_1*C_eqn+(delta_0/(u_1*C_eqn)));
lamda2=-(1/3*a)*(b+u_2*C_eqn+(delta_0/(u_2*C_eqn)));
lamda3=-(1/3*a)*(b+u_3*C_eqn+(delta_0/(u_3*C_eqn)));

beta=lamda1
alpha=real(lamda2)
delta=imag(lamda2)

root1=(C_phi_g*lamda2-C*w_0)/(A*lamda2^2-mu*lamda2)
root2=(C_phi_g*lamda3-C*w_0)/(A*lamda3^2-mu*lamda3)

%for phi_dot

a_phi=real(root1);
d_phi=imag(root1);

%for theta_dot

a_theta=real(root2);
d_theta=imag(root2);

r=sqrt((abs(a_theta))^2+(abs(d_theta))^2);
theta=atan(abs(d_theta)/abs(a_theta));

M=(root1+root2)/2;
N=(root1-root2)/2*1i;

t=-1000:0.001:-600;
delta_phi=exp(a_phi.*t).*(M*cos(d_phi.*t)+N*sin(d_phi.*t));
figure(1)
delta_theta=r*exp(a_phi.*t).*(M*cos(d_phi.*t+theta)+N*sin(d_phi.*t+theta));
subplot(2,1,1),plot(t,delta_phi,'b');
subplot(2,1,2),plot(t,delta_theta,'r');
```

D2 Driven system

The following code relates to the response of the driven system when the applicable physical parameters are substituted into the relevant constants

```
clear all
clc
```

```
I_z_d                   %inertia of the disc in the z direction, kgm^2
I                       %rotational inertia of one gyroscope, kgm^2

M_s                     %mass of external structure, kg
h_s                     %distance from the reference pivot point to the COM
                        of external structure, m
h_d                     %distance from the reference pivot point to the
                        disc pivot, m
g                       %acceleration due to gravity, ms^-2
M_g=1.94032             %mass of one gyroscope, kg
phi_dot                 %angular velocity of the gyroscopes, rads^-1
w_0                     %angular velocity of disc, rads^-1
r_g                     %distance from gyro pivot point to contact point, m
r_d                     %distance from disc centre axis to gyro pivot
                        point, m

M_d_and_4M_g            %mass of disc and gyroscope assembly, kg

mu=0.5;                 %coefficient of friction in drive motor
C_phi_g=4*I*phi_dot;
C=4*I*(phi_dot*((r_g+r_d)/r_g));

A=(I_z_d+4*M_g*r_d^2+4*I);
B=(M_s*h_s^2+(M_d_and_4M_g)*h_d^2+8*I);
D=(M_s*h_s+((M_d_and_4M_g)*h_d))*g;

if mu*D>C*w_0*C_phi_g;
    display('mu*D>C*w_0*C_phi_g')
end

if C_phi_g^2<A*D;
    display('C_phi_g^2<A*D')
end

a=A*B;
b=-mu*B;
c=-(A*D-C_phi_g^2);
d=mu*D-C*w_0*C_phi_g;

discriminant=18*a*b*c*d-4*(b^3)*d+(b^2)*(c^2)-4*a*(c^3)-27*(a^2)*(d^2);

if discriminant>0;
    display('discriminant>0')
end

delta_1=2*b^3-9*a*b*c+27*(a^2)*d;
delta_0=b^2-3*a*c;

C_eqn=((delta_1+sqrt((delta_1^2)-4*(delta_0^3)))/2)^1/3;

u_1=1;
u_2=(-1+1i*sqrt(3))/2;
u_3=(-1-1i*sqrt(3))/2;

lamda1=-(1/(3*a))*(b+u_1*C_eqn+(delta_0/(u_1*C_eqn)));
lamda2=-(1/(3*a))*(b+u_2*C_eqn+(delta_0/(u_2*C_eqn)));
```

```
lamda3=-(1/(3*a))*(b+u_3*C_eqn+(delta_0/(u_3*C_eqn)));

beta=lamda1
alpha=real(lamda3)
delta=imag(lamda3)

F=30;                %Force within motor during oscillations, N
gamma=5;

phi_d_1=-F*(-
B*gamma^2+D)/((A*gamma^2+1i*mu*gamma)*(B*gamma^2+D)+(C_phi_g*1i*gamma-
C*w_0))
theta_s_1=-
1i*F*C_phi_g*gamma/((A*gamma^2+1i*mu*gamma)*(B*gamma^2+D)+(C_phi_g*1i*gamma
-C*w_0))

a_phi=abs(real(phi_d_1));
b_phi=abs(imag(phi_d_1));

c_theta=abs(real(theta_s_1));
d_theta=abs(imag(theta_s_1));

b_d_1=sqrt((a_phi)^2+(b_phi)^2);
delta_phi_d=atan((b_phi)/(a_phi));

b_s_1=sqrt((c_theta)^2+(d_theta)^2);
delta_theta_s=atan((d_theta)/(c_theta));

t=0:0.01:20;
delta_phi=b_d_1*cos(gamma.*t+delta_phi_d);
delta_theta=b_s_1*cos(gamma.*t+delta_theta_s);

% figure(1)
% subplot(2,1,1),plot(t,delta_phi,'b');
% subplot(2,1,2),plot(t,delta_theta,'r');
plot(t,delta_phi,'b',t,delta_theta,'r')

[peak,peak_ind]=max(delta_phi);
peak_time=t(peak_ind);

[trough,trough_ind]=min(delta_phi);
trough_time=t(trough_ind);

Period_seconds_phi=(peak_time-trough_time)*2     %period of oscillations, s
Period_Hz=1/Period_seconds_phi;

[peak2,peak_ind2]=max(delta_theta);
peak_time2=t(peak_ind2);

[trough2,trough_ind2]=min(delta_theta);
trough_time2=t(trough_ind2);

Period_seconds_theta=(peak_time2-trough_time2)*-2     %period of
                                                          oscillations, s
Period_Hz_theta=1/Period_seconds_theta;
```

Appendix E

Slip ring wiring diagram

The following figure relates to the wiring arrangement used in the development of the slip ring design that precessed the disc when the outer contact arms and outer ring came in contact (Section 7.3.10).

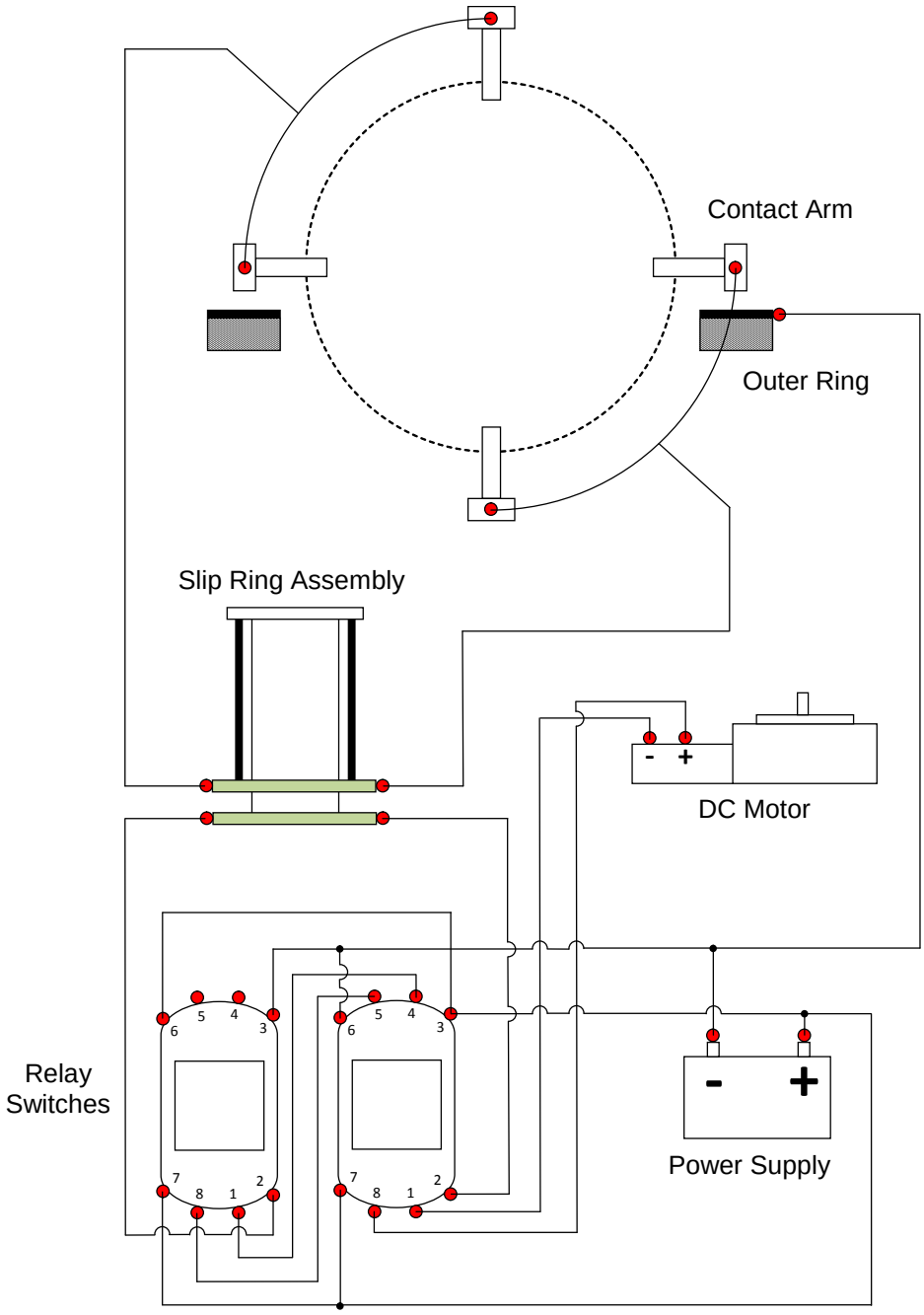

Figure E1 – Slip ring wiring diagram

Appendix F

Townsend's Platform Concept Sketches

The following appendix present the conceptual sketches produced by Townsend (1983) for the proposed configuration of the gyroscopically stabilized platform.

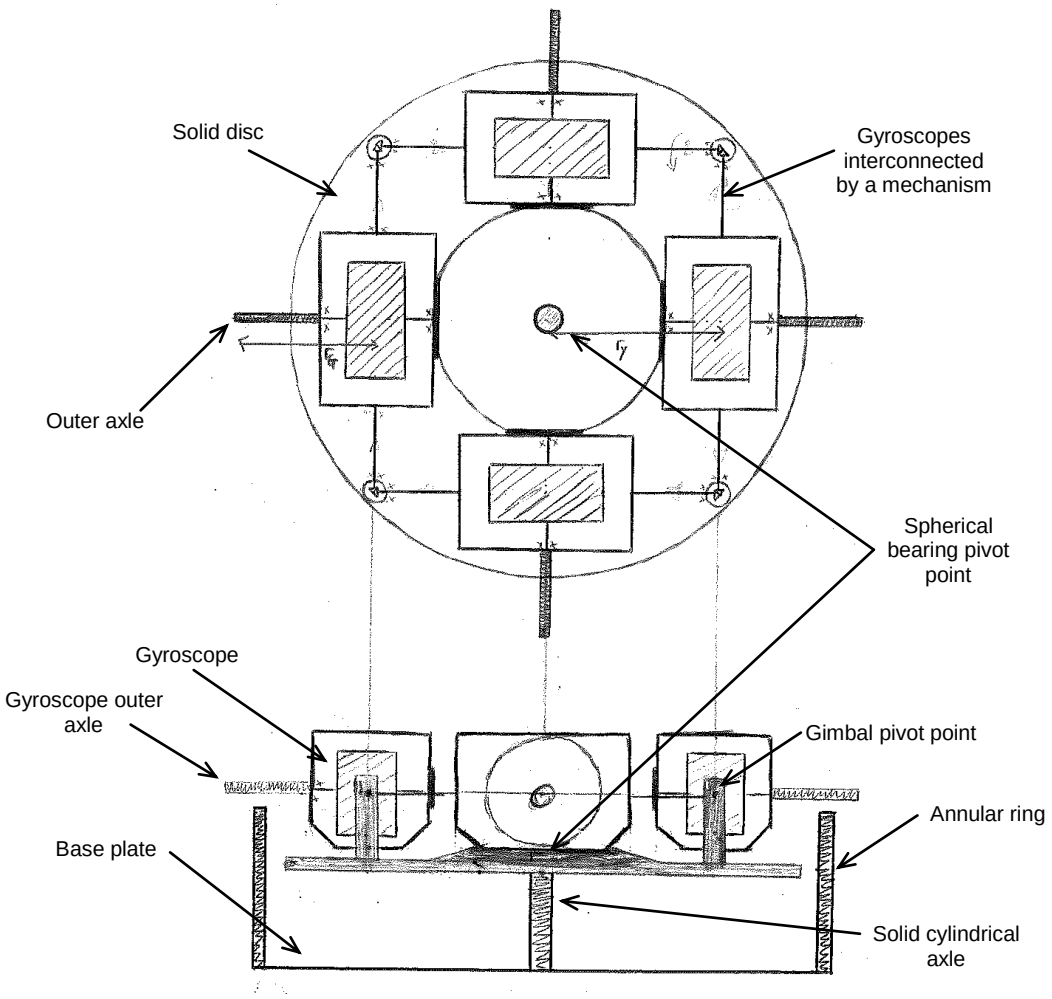

Figure F1 – Gyroscopically stabilized platform schematic sketch from Townsend (1983)

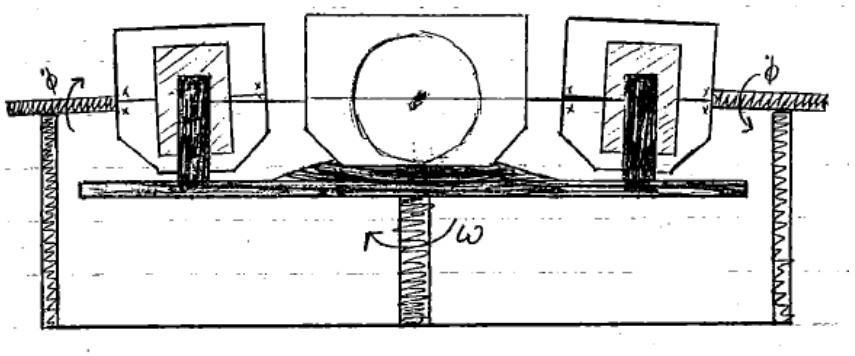

Figure F2 – Motion of components that comprise the system from Townsend (1983)

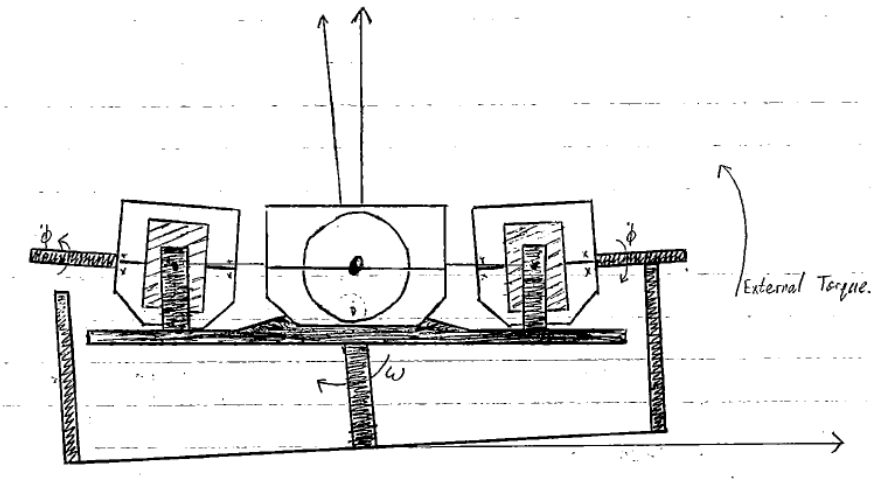

Figure F3 – Reactions of system after an external torque is applied to the system from Townsend (1983)

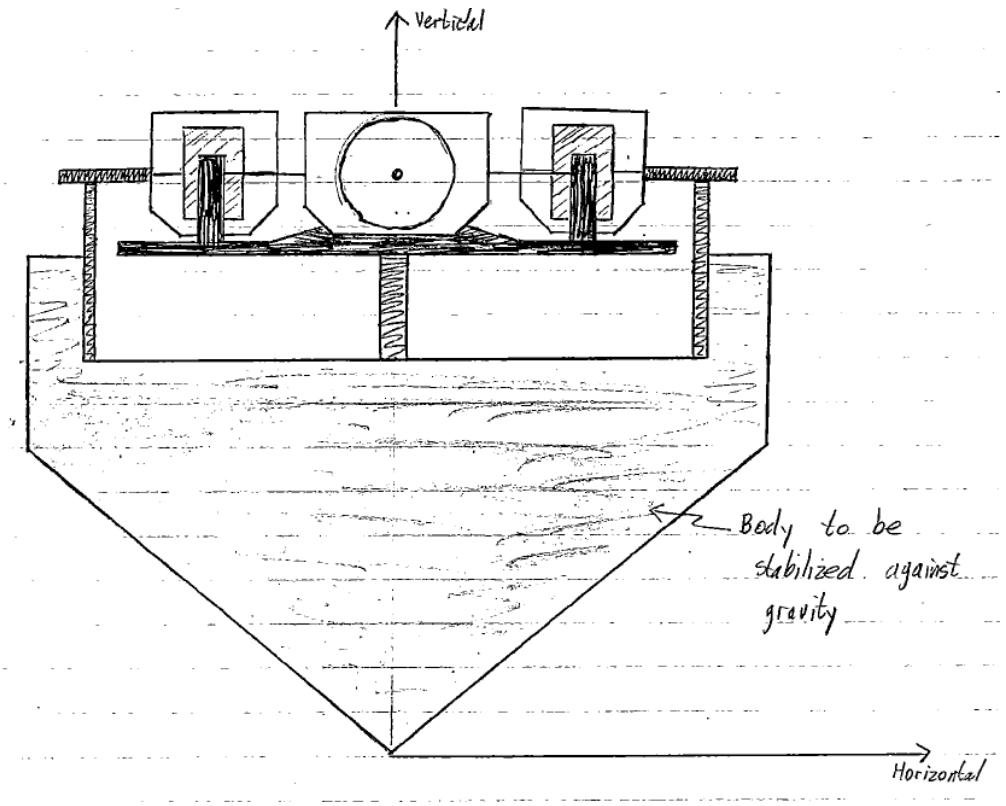

Figure F4 – Stabilizer system mounted upon external structure from Townsend (1983)

Appendix G

Operations Manual for Prototype B

CONFIDENTIAL

Operations Manual for Prototype B

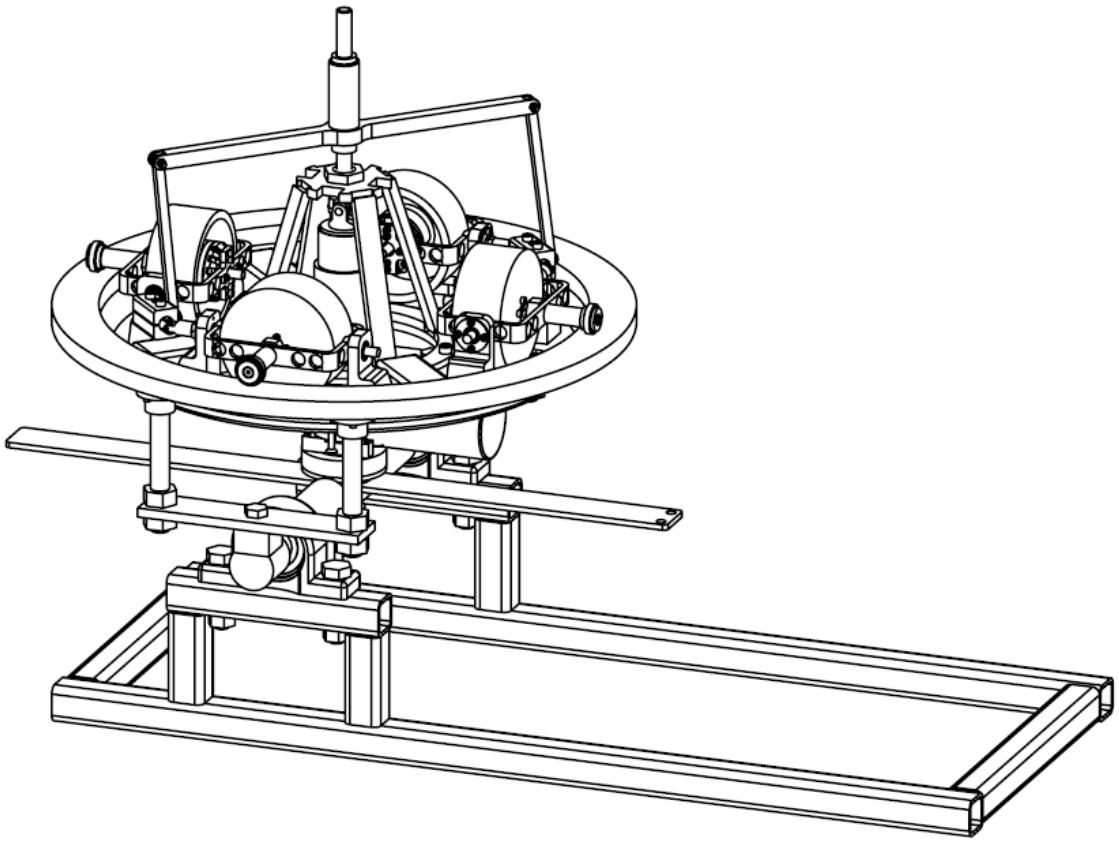

Written by Ben Redwood

For use by Technix Industries Limited

G1 Introduction

Prototype B is a gyroscopically stabilized platform designed, manufactured and tested by Ben Redwood as part of a PhD in Mechanical Engineering at the University of Canterbury, funded by Technix Industries Limited.

The purpose of this manual is to show the assembly methods for constructing Prototype B and the operational procedures required to achieve oscillatory stabilizing behaviour.

This manual will cover:

- The procedure required to assemble each of the 6 sub-systems that comprise Prototype B together to form the overall gyroscopically stabilized platform.

- A bill of materials and assembly drawings of each of the individual sub-systems of Prototype B.

- The connections and arrangement of the power systems that drive Prototype B and the procedures that must be followed to operate it.

- The critical safety issues that must be addressed when assembling and operating Prototype B.

G2 Assembly of Overall System

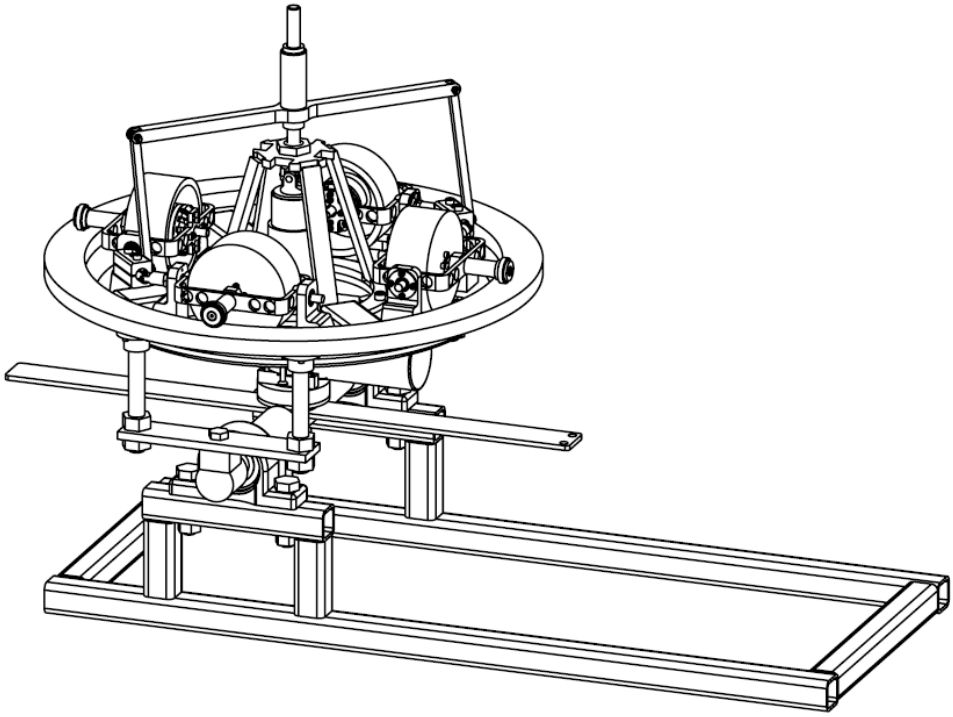

Figure G1 – Prototype B (SP1-01-001)

This section presents how to assemble each of the 6 subsystems that comprise Prototype B to form the overall gyroscopically stabilized platform. The assembly of each of the 6 sub-systems is shown in section G3 of this manual. The 6 sub-systems and their associated part numbers that Prototype B consists of are:

i) External structure (SP2-03-001)

ii) Disc Drive Mechanism (SP2-04-001)

iii) Central Pivot (SP2-06-001)

iv) Disc (SP2-02-001)

v) Gyroscopes (SP2-01-001)

vi) Gimbal Frame Linkage (SP2-05-001)

G2.1 Tools required

The following tools are needed for the assembly of Prototype B:

- Adjustable spanners to suit M10 – M40 bolts and nuts
- Allen keys to suit M4, M5, M6, and M8 cap screws
- 10m ring spanner
- Rubber mallet

G2.2 Assembly procedure

This section will assume that Prototype B will be assembled on a flat and level surface.

Step 1 – *Securing external structure frame*

Ensure the external structure mounting fame (SP2-03-009) is firmly secured to the floor. This will aid in reducing vibrations and significantly reduce the noise of the system during operation.

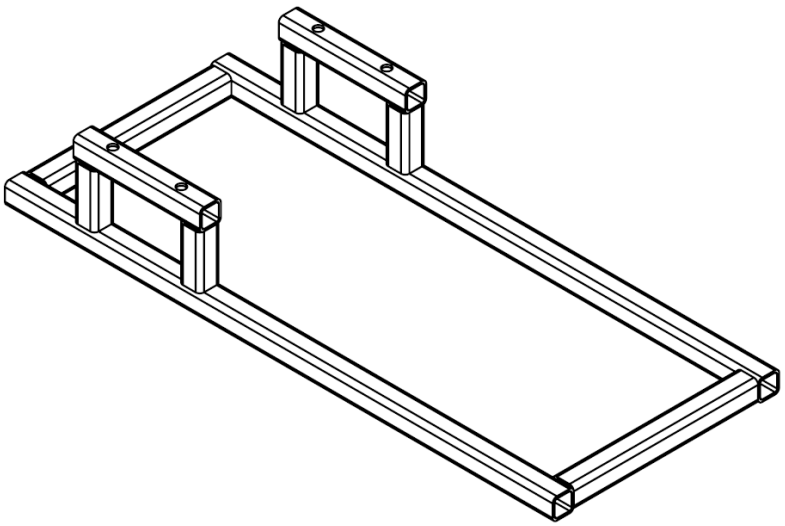

Figure G2 - External structure mount frame

Step 2 – *Attaching external structure to external structure frame*

Attach the external structure to the mount frame via four M16 x 75mm bolts, four M16 nuts and the two Ø35mm pillow blocks on the external structure tilt shaft (SP2-03-002). The mount holes of the pillow blocks align with the four holes drilled in the external structure mount frame (Figure G3).

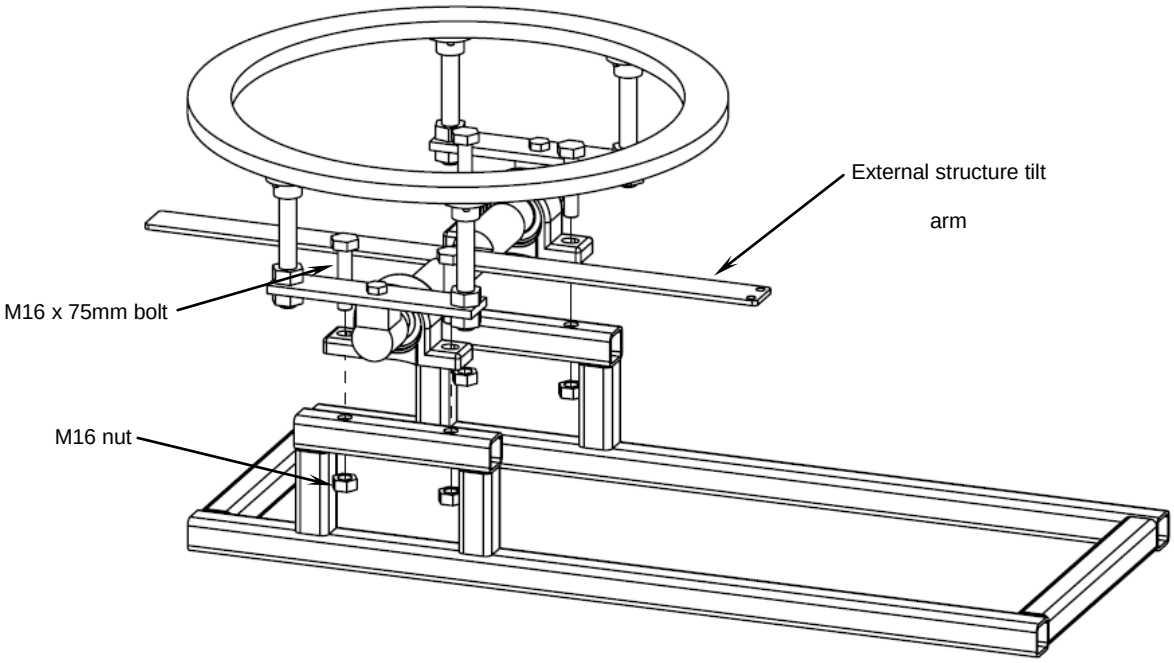

Figure G3 – External structure attaching to mount frame

The holes in the mount frame are slotted to aid in assembly. It is important that the external structure tilt frame shaft (SP2-03-002) is square relative to the mount frame. This will ensure more accurate readings when measuring the magnitude of the moment produced by Prototype B. Note that the external structure tilt arm (SP2-03-008) is currently not connected to the external structure. The assembly of the disc drive mechanism will ensure it is secured in place.

Step 3 – *Attaching disc drive mechanism to external structure*

Align the M20 bottom threaded structure connection (SP2-04-002) at the bottom of the disc drive mechanism with the M20 threaded hole in the centre of the external structure tilt shaft (SP2-03-002). It is critical that the external structures tilt arm (Figure G4) is perpendicular to the tilt frame shaft. This should be checked with a square before fully securing the disc dive mechanism in position.

It is safe to use the 24V DC drive motor (SP2-04-013) to gain more leverage when tightening down the drive mechanism to the external structure.

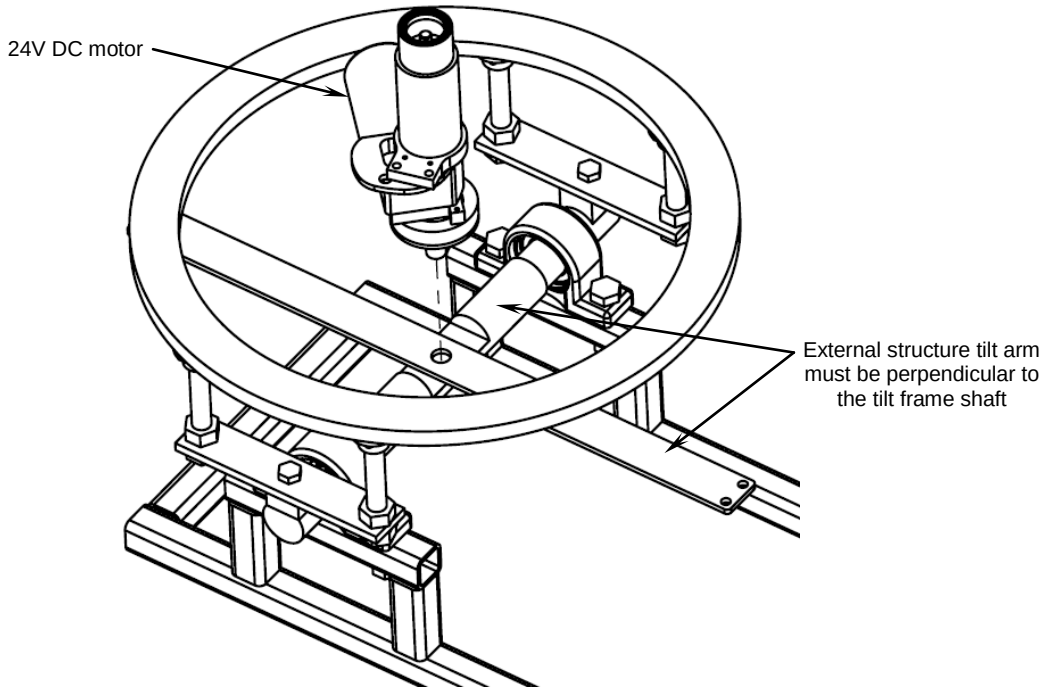

Figure G4 – Securing the disc drive mechanism to the external structure

Step 4 – *Attaching central pivot to disc drive mechanism*

The central pivot (SP2-06-001) can now be attached to the disc drive mechanism. An M12 threaded section of the main drive shaft (SP2-04-010) can be seen protruding from the top of the disc drive mechanism between two bearings. This

threaded shaft section is used to secure the central pivot to the disc drive mechanism.

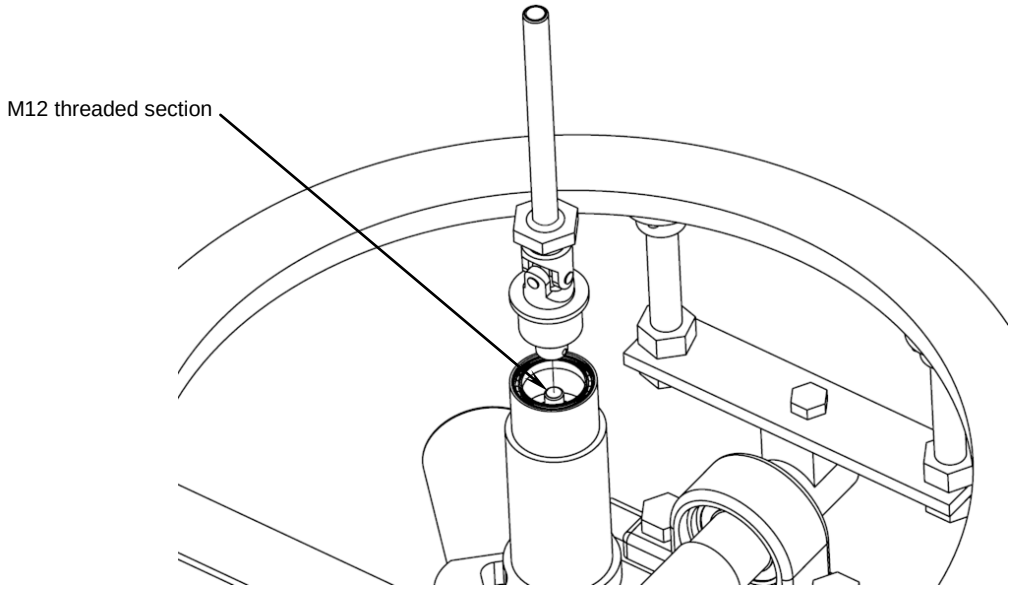

Figure G5 – Central pivot attaching to disc drive mechanism

The universal joint coupling (SP2-06-002) has been machined to a high tolerance to aid in the assembly of it with the 2 bearings. The central pivot assembly should be wound down upon the disc drive mechanism drive shaft as far as it will go. It is safe to tighten the thread by using the universal joint (SP2-06-004) for leverage ***(a force should not be applied to the main shaft (SP2-06-003) to tighten this connection).***

Step 5 – *Securing gyroscope assemblies to disc*

The gyroscope assemblies (SP2-01-001) are assembled onto the disc (SP2-02-001) (Note that this is a separate assembly that will be assembled into the overall system later).

The top of the disc has a large number of holes to suit sixteen Ø4mm dowel pins and sixteen Ø6mm clearance holes for M6 cap screws. These correlate to holes found in the bottom of the gyroscope assemblies mount legs (SP2-01-010 & SP2-01-011) (Figure G6).

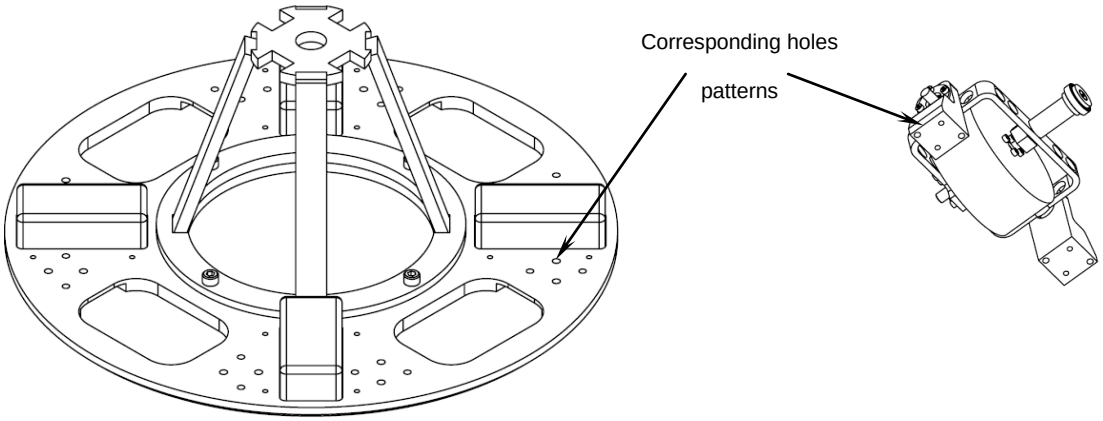

Figure G6 – Disc and gyroscopes mount hole patterns

The gyroscopes are secured to the disc by two M6 x 20mm cap screws and two 4mm dowel pins ***per leg***. The dowel pins are first placed in the gyroscope mount legs and aligned with the corresponding holes in the disc. The cap screws are then inserted from the bottom of the disc up into the corresponding threaded hole of the gyroscope mount legs and tightened, securing the gyroscopes in place (Figure G7).

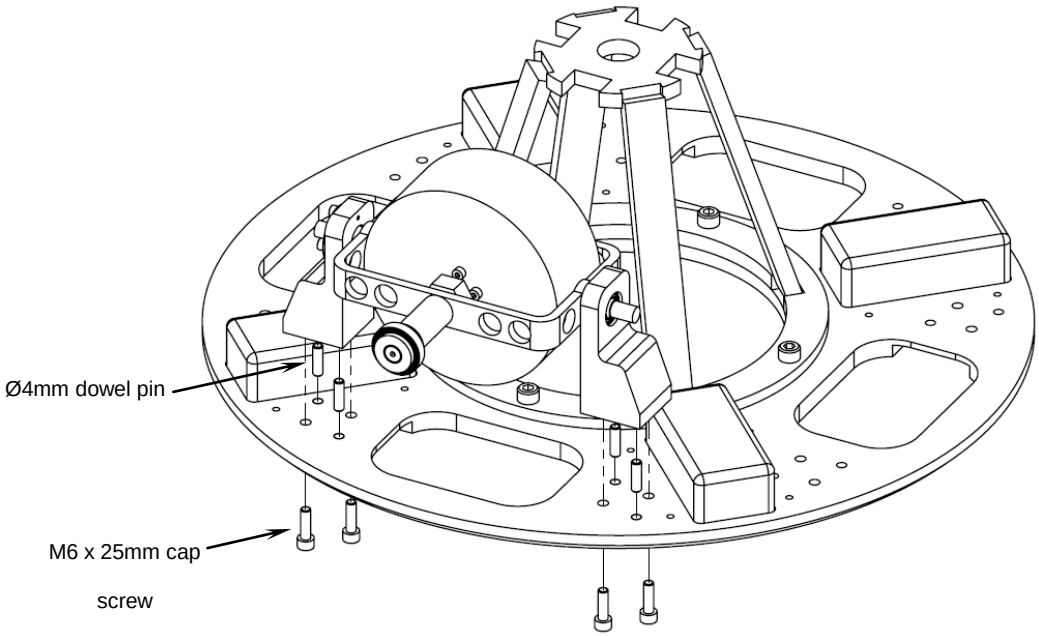

Figure G7 – Gyroscope assembled onto disc

The above step will need to be repeated for all four of the gyroscope assemblies.

Step 6 – *Attaching disc/gyroscope assembly to central pivot*

Once the gyroscopes are secured in place upon the disc the whole disc/gyroscopes assembly must be assembled into the overall system.

The M24 half nut attached to the central pivot assembly (SP2-06-001) must first be removed (Figure G8). This is used to tighten down upon the disc assembly securing it to the top of the universal joint shoulder (Figure G9).

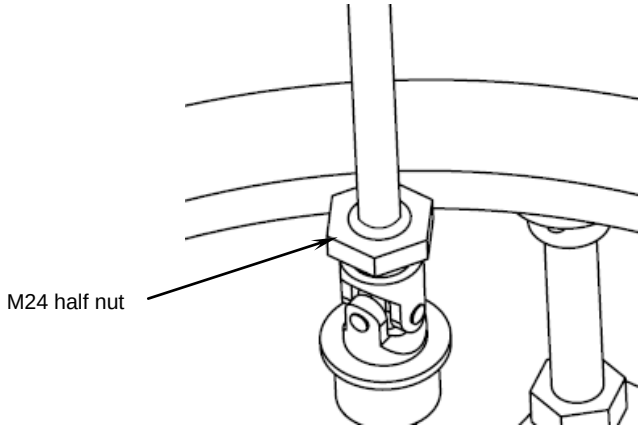

Figure G8 – M24 nut used to secure disc/gyro assembly

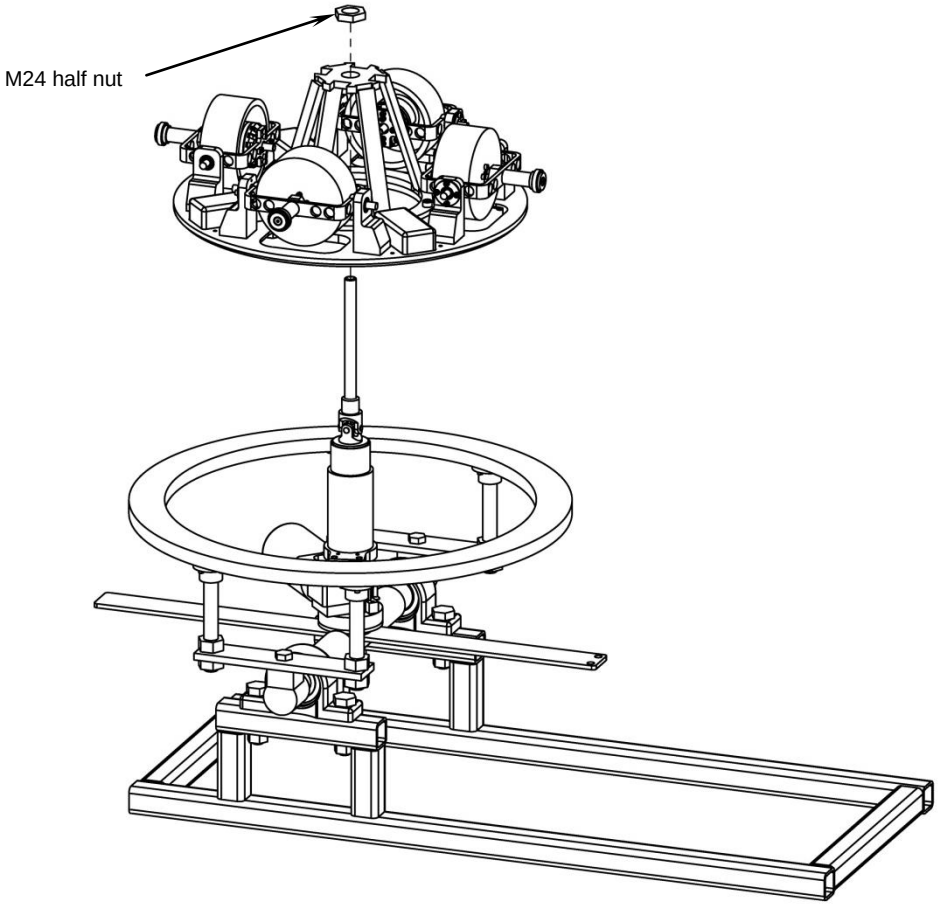

Figure G9 – Disc/gyro assembly secured to central pivot

This is one of the more complicated steps in the assembly of Prototype B and it is recommended that one person holds the central pivot main shaft (SP2-06-003) upright as another person lowers the disc/gyroscopes assembly over the shaft until it rests on the universal joint shoulder. The M24 half nut is then slid over the central pivot main shaft and tightened down as tight as possible securing the disc/gyroscopes assembly to the rest of the system.

Step 7 – *Attaching gimbal frame linkage to gyroscope gimbal frame*

The next step in the assembly of Prototype B involves attaching the gimbal frame connection (SP2-05-001) to the gimbal frame shafts (SP2-01-002). This process is completed in several steps.

Firstly, the machined universal joints (SP2-05-008) are screwed onto the gimbal frame shafts (SP2-01-004). The joints have been machined so that once they are 10mm from the end of the gimbal frame legs (SP2-01-010 & SP2-01-011) the slot machined in them is vertical (Figure G10). An M10 half nut is then tightened up against the universal joints to lock them in position. This step is repeated on the opposite side of the assembly for the other diametrically opposite gyroscope pair.

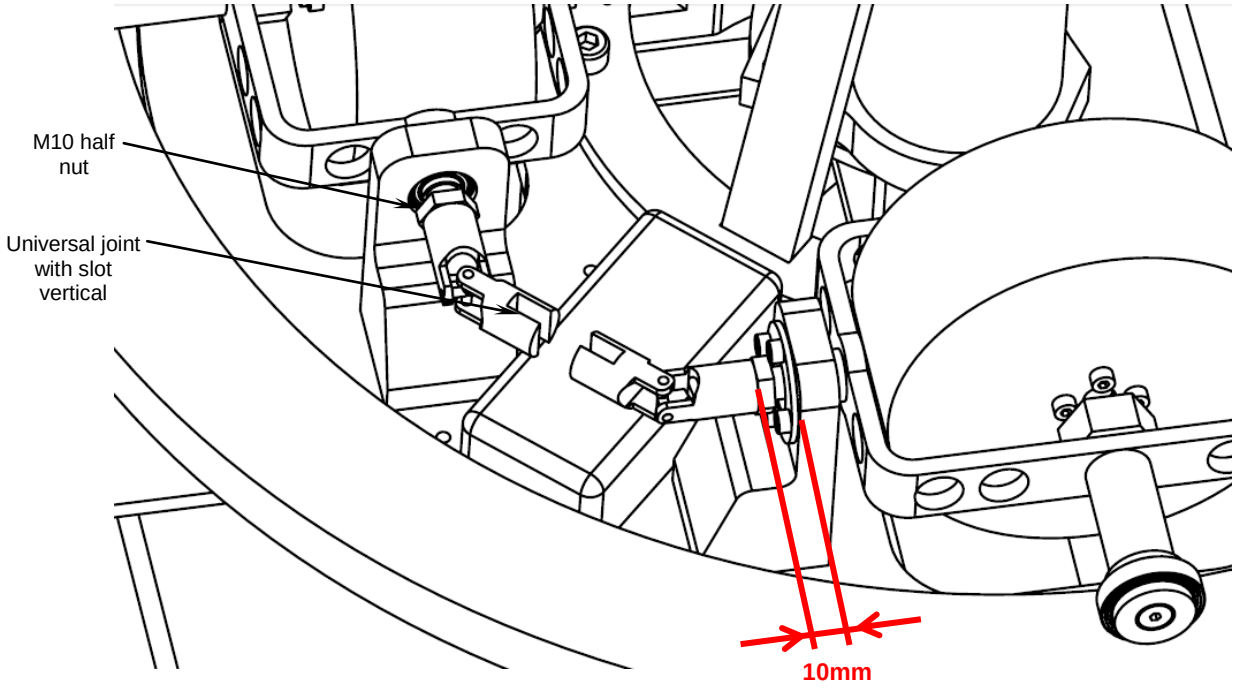

Figure G10 – Location of universal joints on gimbal frame shafts

Once the universal joints have been correctly positioned and locked in place the universal joint clamping coupling (SP2-05-007) is placed over the top (Figure G11) Again, this next step is repeated on both sides of the assembly.

The clamp consist of two sections; a top section that connects to the gimbal frame linkage connecting arm (SP2-05-006); and a bottom section that contains two tapped M6 holes that secure the top and bottom sections together.

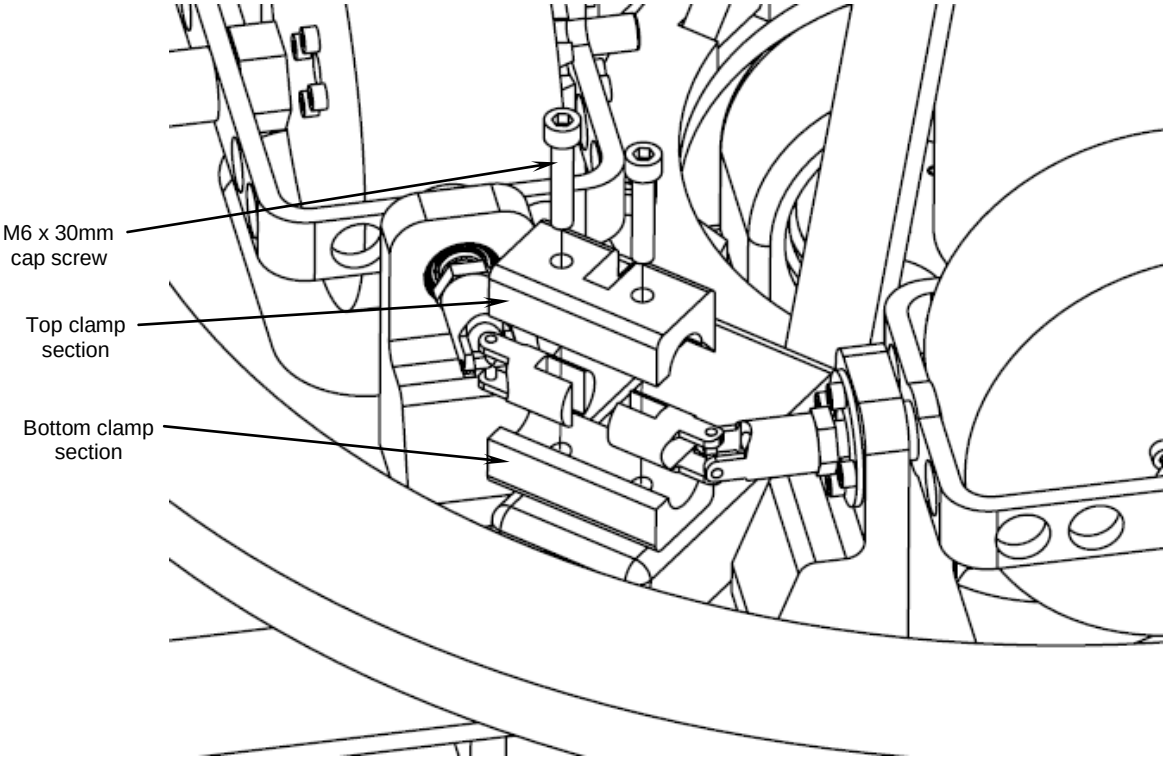

Figure G11 - Universal joint clamping coupling

The bottom section is held in place under the universal joint and the top section is placed over the top of the universal joint. Two M6 x 30mm cap screws are then used to clamp the two sections together (while also passing through the universal joint vertical slots, aligning them with the clamping sections). ***It is critical that one of the universal joint clamping couplings points away from the centre of the system, and one points to the centre*** (to match the diametrically opposite pairing of the gyroscopes). The example shown in Figure G11 demonstrates a clamping coupling pointing towards the centre of system. See Figure G13 for the example of an assembled clamping coupling pointing away from the centre of the system.

The overhead liner slide assembly (SP2-05-002) is now slid over the central pivot main shaft (SP2-06-003) as shown in Figure G12. Smooth motion of the linear slide assembly over the main shaft with no pinching or interference should occur. It is recommended this motion is checked before proceeding as any resistance or interference will have a large impact on the performance of the system during the stabilization process.

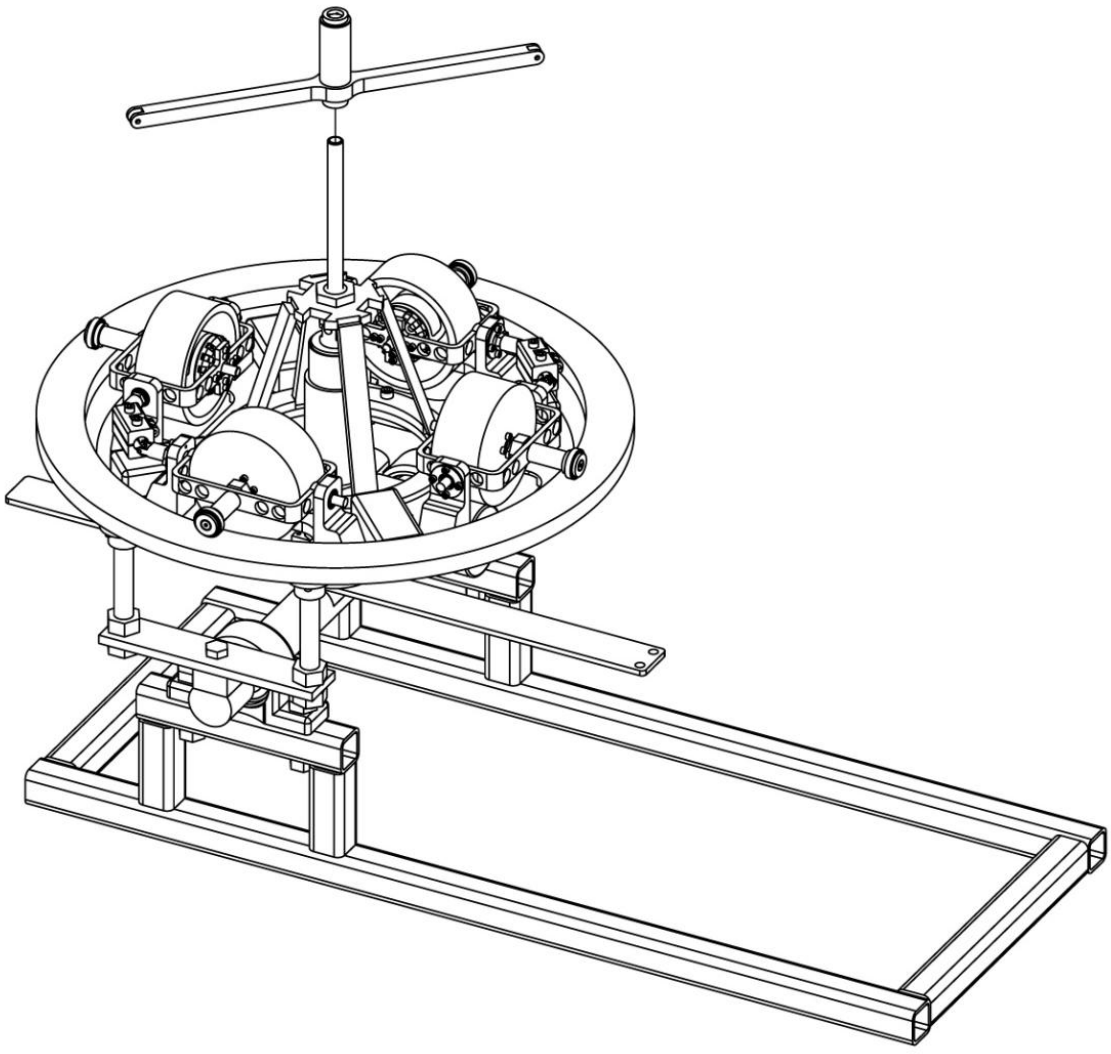

Figure G12 – Linear slide assembly into overall system

The final stage in the assembly of Prototype B is the attachment of the gimbal frame linkage connecting arms (SP2-05-006). The arms connect to the linear slide assembly and the universal joint clamping couplings via two M5 x 25mm cap screws and two M5 nyloc nuts ***per arm*** (Figure G13).

The overhead linear slide and gyroscope assemblies will need to be manipulated into the desired position in order to secure the connecting arms into the desired location. This step will also need to be repeated on the opposite side of the system.

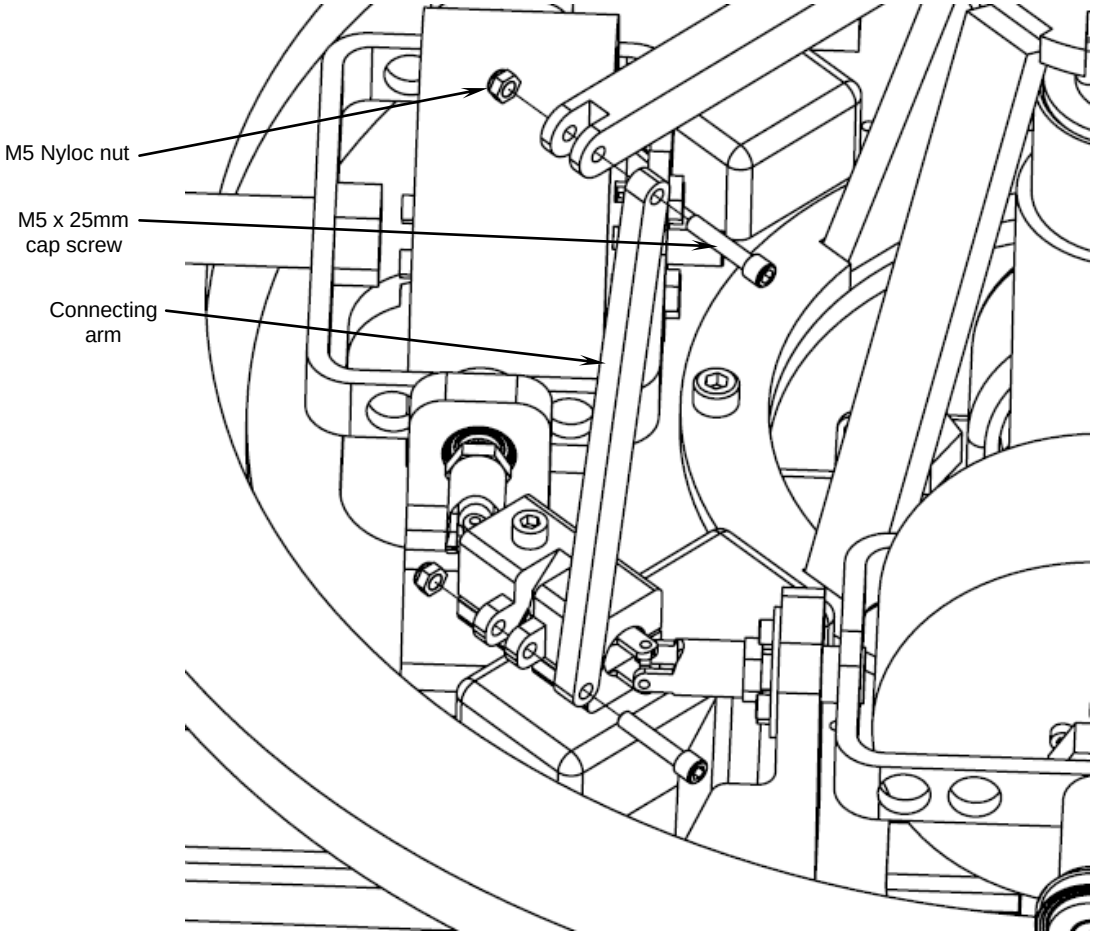

Figure G13 – Attaching connecting arms to clamping coupling and overhead linear slide

The nyloc nuts must not be tightened up against any surfaces. This will ensure the joints where they are included are free to move with no resistance.

G2.3 Conclusion of Prototype B assembly

Prototype B should now be completely assembled. It is recommended that all joints, connections, nuts, bolts and connections are secure and tight before operating the machine and attempting to achieve stabilization.

It is also recommended that all wires and cables are either cable tied to a surface via the available holes and cavities on the assembly or taped down to avoid any catching or tangling from occurring during operation of the machine.

G3 Assembly of Prototype B Sub-systems

The following section includes the assembly diagrams and bill of materials for each of the six sub-systems that form Prototype B. The 6 subsystems are:

- Gyroscopes (SP2-01-001)
- Disc (SP2-02-001)
- External structure (SP2-03-001)
- Disc Drive Mechanism (SP2-04-001)
- Gimbal Frame Linkage (SP2-05-001)
- Central Pivot (SP2-06-001)

The layout of this section will comprise of an assembly drawing of each sub-system with part balloons that relate to a bill of materials of that sub-system on the following page.

G3.1 Tools required

The following tools will be needed for the assembly of each of the Prototype B subsystems:

i) Adjustable spanners to suit M10 – M40 bolts and nuts
ii) Allen keys to suit M3, M4, M5, M6, and M8 cap screws
iii) 10m ring spanner
iv) Can of CRC
v) Velcro tape
vi) Duct tape

G3.2 Gyroscopes

The following section presents an exploded view of the gyroscopes and the associated bill of materials. Note it is critical when assembling the DC brushless motor into the gimbal frame that the motor power cables point down and to the left (when looking from the front of the assembly).

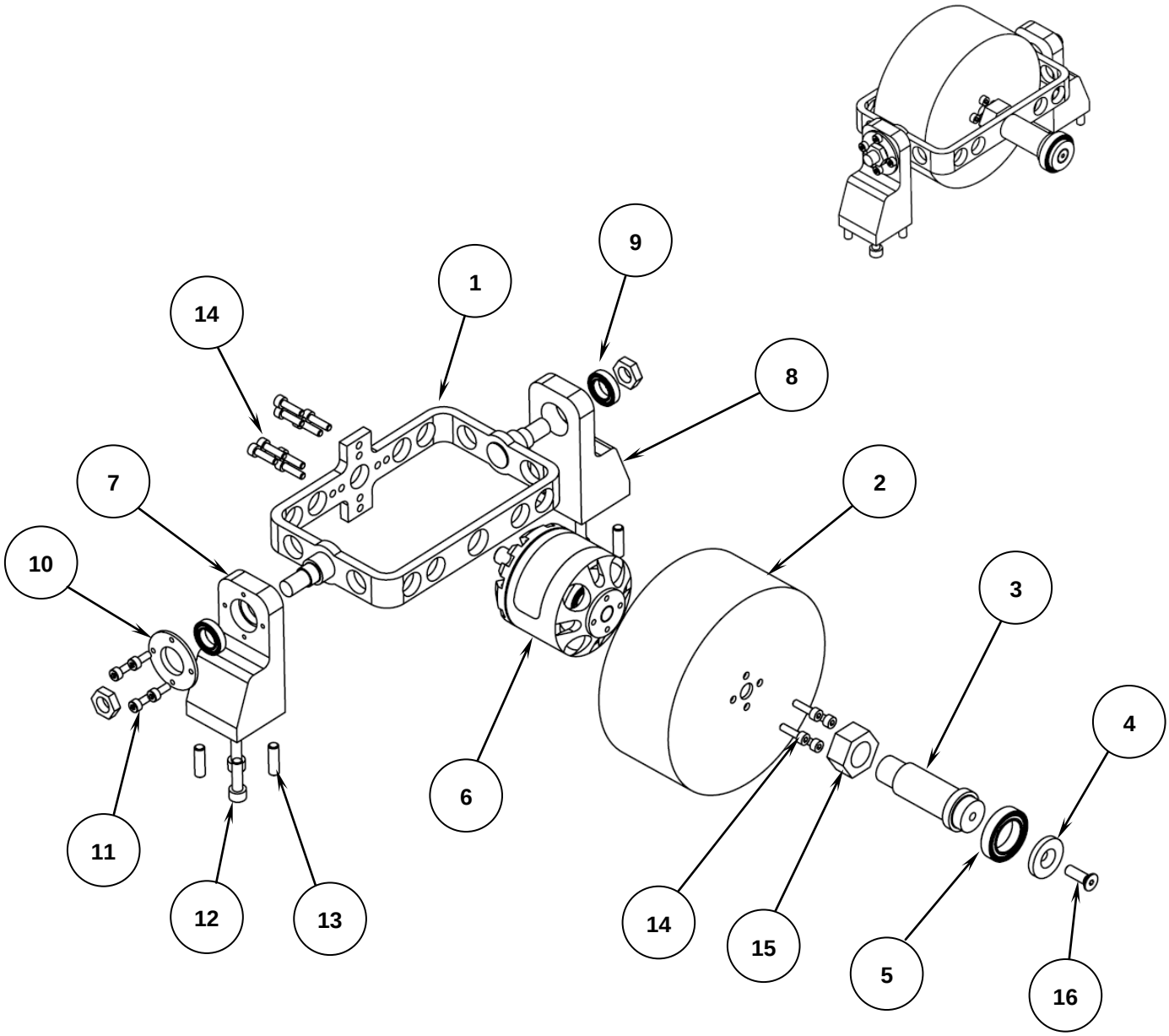

Figure G14 – Gyroscopes (SP2-01-001)

Table G1 – Bill of materials for gyroscopes relating to Figure G14

	Part No.	Description	Part/Assembly	Material	No. Required
1	SP2-01-002	Gimbal frame	Assembly	N/A	1
	SP2-01-003	Lightweight gimbal frame	Part	Mild Steel	1
	SP2-01-004	Gimbal frame shaft	Part	4140	2
2	SP2-01-005	Flywheel	Part	4140	1
3	SP2-01-006	Gimbal frame contact arm	Part	4140	1
4	SP2-01-007	Contact arm end cap	Part	5083 Aluminium	1
5	SP2-01-008	Ø20mm ID, Ø32mm OD deep groove bearing	Part	N/A	1
6	SP2-01-009	MP160 Brushless DC Motor	Part	N/A	1
7	SP2-01-010	Gimbal frame leg	Part	7075 Aluminium	1
8	SP2-01-011	Gimbal frame leg - Right	Part	7075 Aluminium	1
9	SP2-01-013	Ø12mm ID, Ø21mm OD deep groove bearing	Part	N/A	8
10	SP2-01-014	Spacer washer	Part	7075 Aluminium	4
11	-	M3 x 10 cap screw	-	N/A	16
12	-	M6 x 20 cap screw	-	N/A	16
13	-	Ø4mm x 20 dowel pin	-	N/A	16
14	-	M16 nut	-	N/A	1
15	-	M6 x 15 countersunk screw	-	N/A	1
16	-	M4 x 15 cap screw	-	N/A	12

G3.3 Disc

The following section presents an exploded view of the disc and the associated bill of materials. Note that the Li-Po batteries (3) are secured to the disc in the designated cavities via Velcro tape.

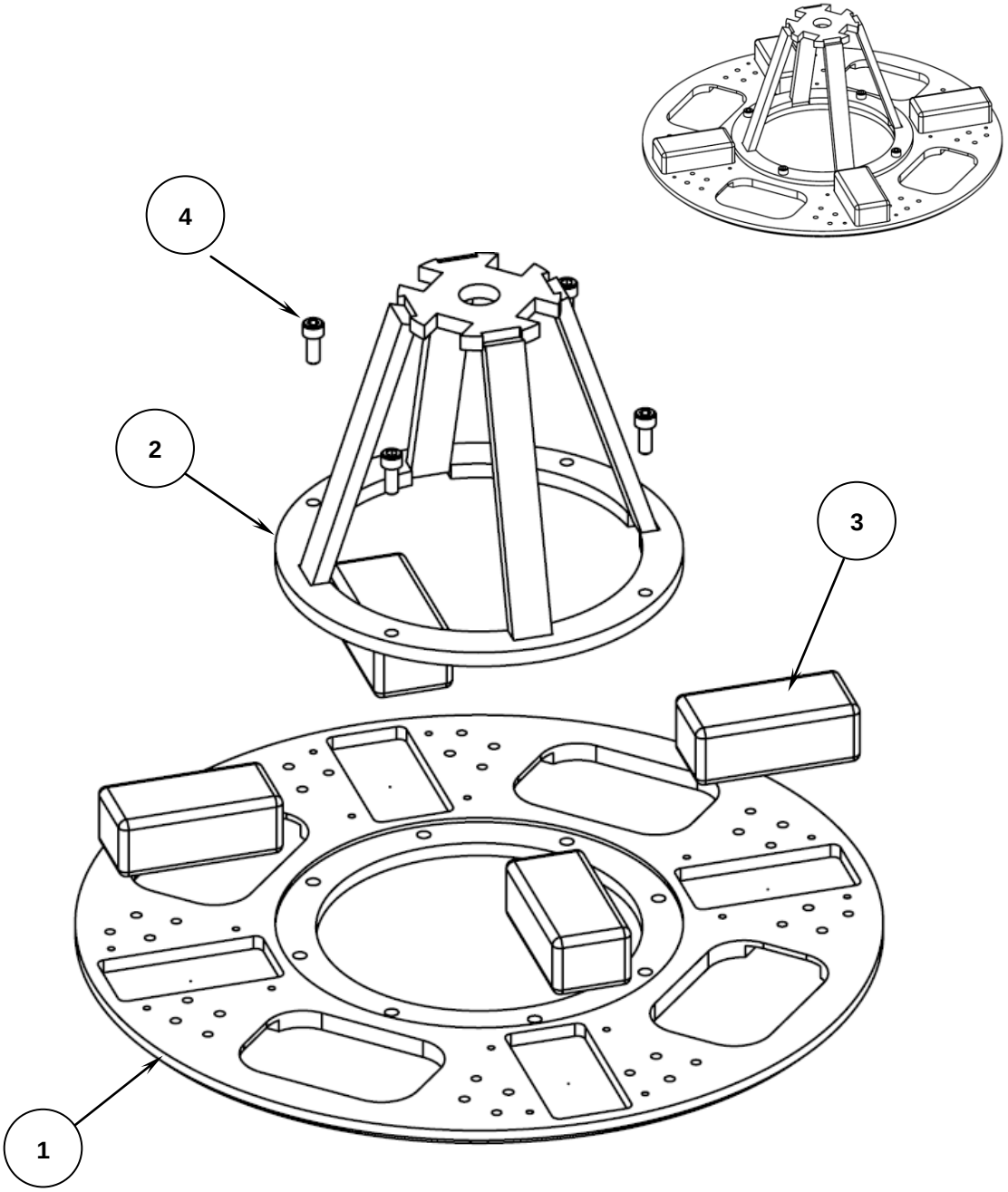

Figure G15 - Disc

Table G2 – Bill of materials for disc relating to Figure G15

	Part No.	Description	Part/Assembly	Material	No. Required
1	SP2-02-002	Disc plate	Part	7075 Aluminium	1
2	SP2-02-003	Centre cone section	Part	7075 Aluminium	1
3	SP2-02-004	22.2V 2200mAh 6 cell Li-Po battery	Part	N/A	4
4	-	M8 x 20 cap screw	-	N/A	4

3.4 External structure

The following section presents an exploded view of the external structure and the associated bill of materials. The external structure mount frame and associated fasteners are not included in this assembly. For information regarding these components see Step 1 and 2 of section G2.2.

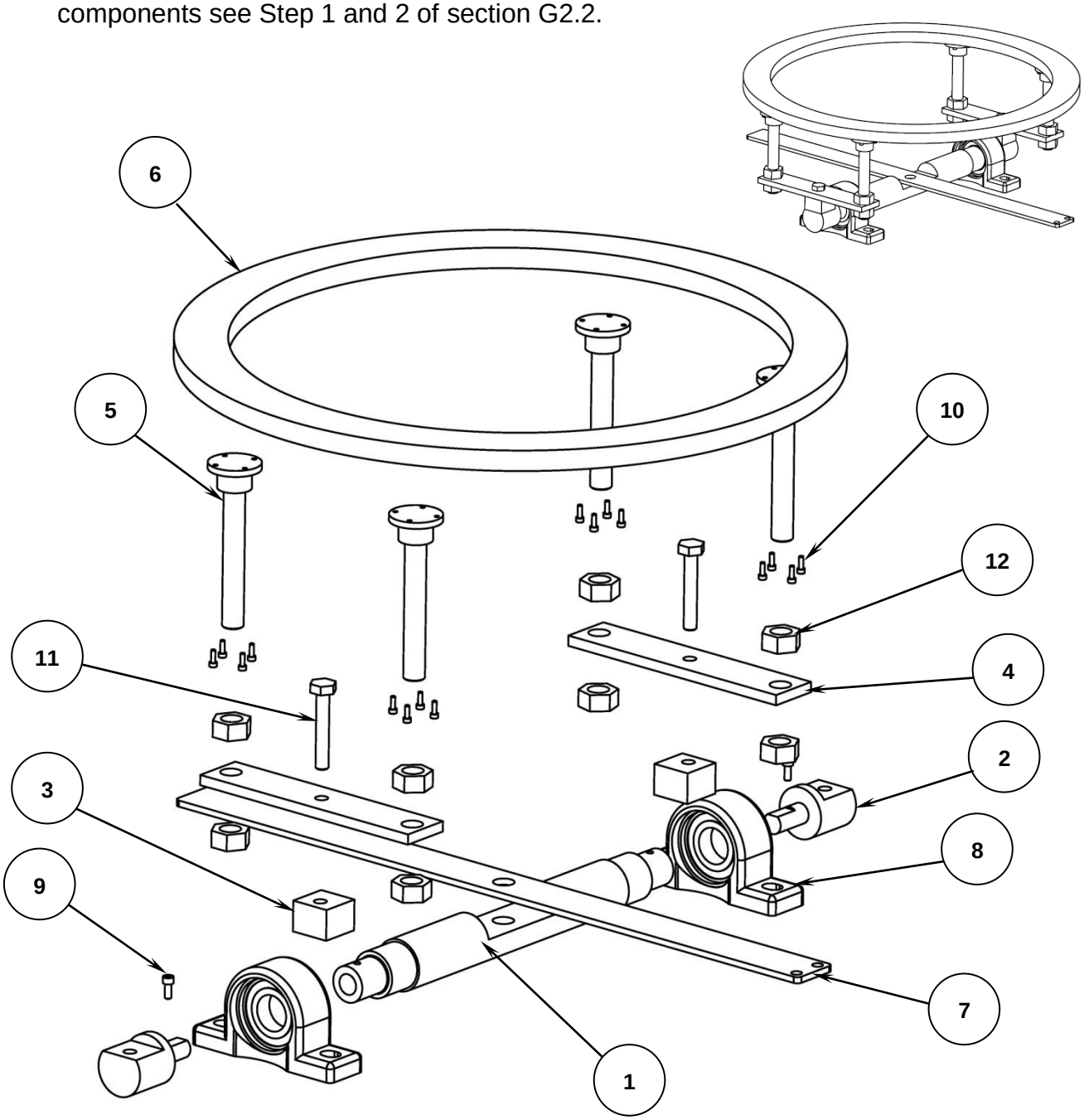

Figure G16 – External Structure

Table G3 – Bill of materials for external structure relating to Figure G16

	Part No.	Description	Part/Assembly	Material	No. Required
1	SP2-03-002	Tilt frame shaft	Part	5083 Aluminium	1
2	SP2-03-003	Main shaft end cap	Part	5083 Aluminium	2
3	SP2-03-004	Outer ring leg spacer	Part	7075 Aluminium	2
4	SP2-03-005	Leg mount plate	Part	7075 Aluminium	2
5	SP2-03-006	Outer ring mount legs	Part	5083 Aluminium	4
6	SP2-03-007	Outer contact ring	Part	7075 Aluminium	1
7	SP2-03-008	Tilt arm	Part	7075 Aluminium	1
8	-	Ø35mm Pillow Blocks	-	N/A	2
9	-	M6 x 12 cap screw	-	N/A	2
10	-	M4 x 12 cap screw	-	N/A	16
11	-	M12 x 75 bolt	-	N/A	2
12	-	M20 nut	-	N/A	8

G3.5 Disc drive mechanism

The following section presents an exploded view of the disc drive mechanism and the associated bill of materials.

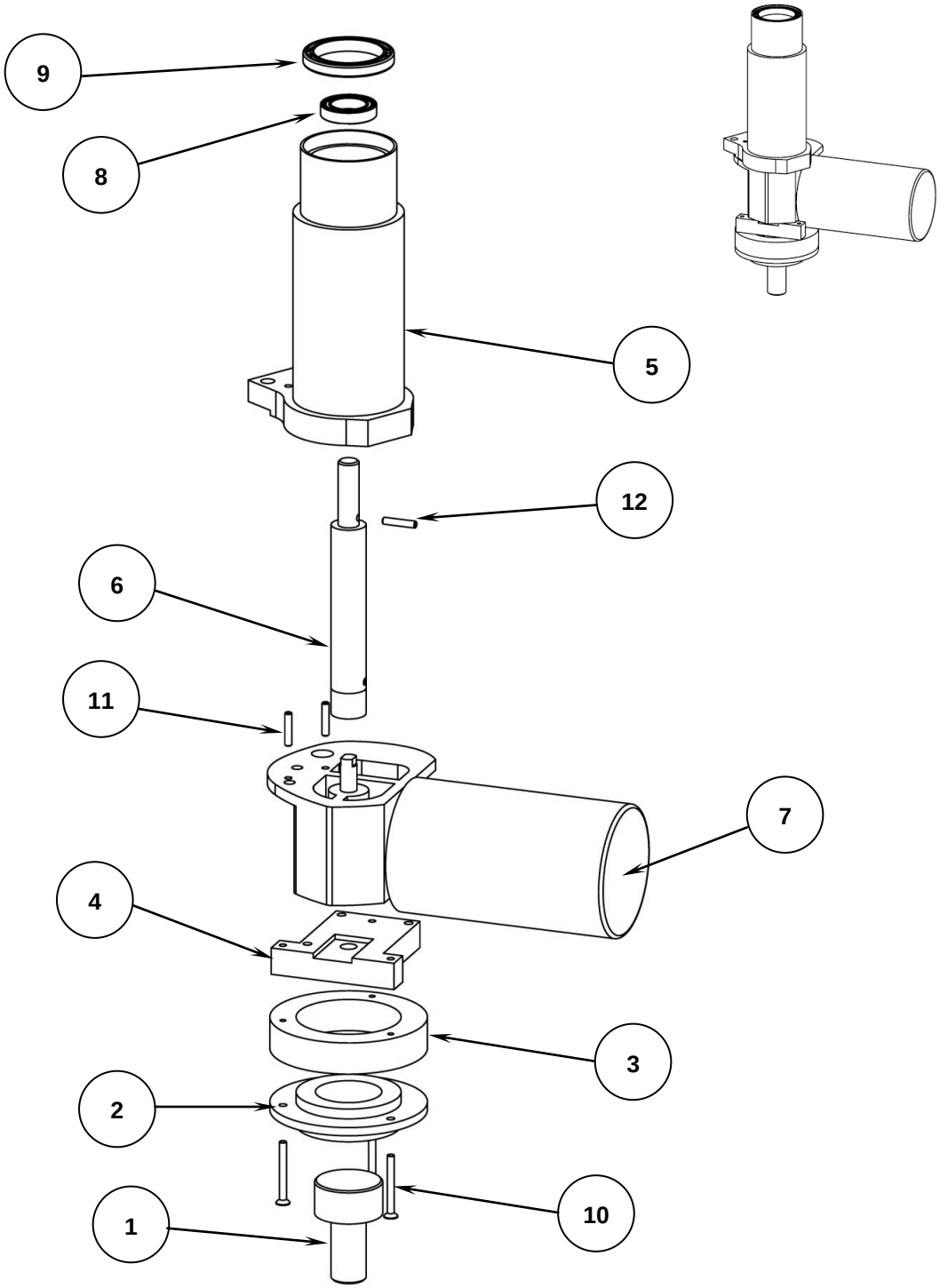

Figure G17 – Disc drive mechanism

Table G4 – Bill of materials for disc drive mechanism relating to Figure G17

	Part No.	Description	Part/Assembly	Material	No. Required
1	SP2-04-002	Bottom threaded structure connection	Part	5083 Aluminium	1
2	SP2-04-003	Bearing housing threaded boss	Part	5083 Aluminium	1
3	SP2-04-004	Bottom connecting boss	Part	5083 Aluminium	1
4	SP2-04-005	Boss mount block	Part	7075 Aluminium	1
5	SP2-04-006	Bearing housing	Assembly	N/A	1
	SP2-04-007	Top bearing housing section	Part	5083 Aluminium	1
	SP2-04-008	Centre pillar	Part	5083 Aluminium	1
	SP2-04-009	Centre pillar mount	Part	7075 Aluminium	1
6	SP2-04-010	Central drive shaft	Assembly	N/A	1
	SP2-04-011	Drive shaft	Part	4140 Steel	1
	SP2-04-012	Drive shaft coupling	Part	4140 Steel	1
	-	Ø4mm x 20 dowel pin	-	N/A	1
7	SP2-04-013	24V Worm drive DC motor	Part	N/A	1
8	SP2-04-014	Ø20mm ID, Ø32mm OD deep groove bearing	Part	N/A	1
9	SP2-04-015	Ø40mm ID, Ø52mm OD deep groove bearing	Part	N/A	1
10	-	M4 x 20 countersunk screw	-	N/A	3
11	-	Ø6mm x 20 dowel pin	-	N/A	2
12	-	Ø4mm x 20 dowel pin	-	N/A	1

G3.6 Gimbal frame linkage

The following section presents an exploded view of the gimbal frame linkage and the associated bill of materials. Only the overhead linear slide assembly will be shown. For the full assembly of all parts relating to the gimbal frame linkage see Step 7 of Section G2.2.

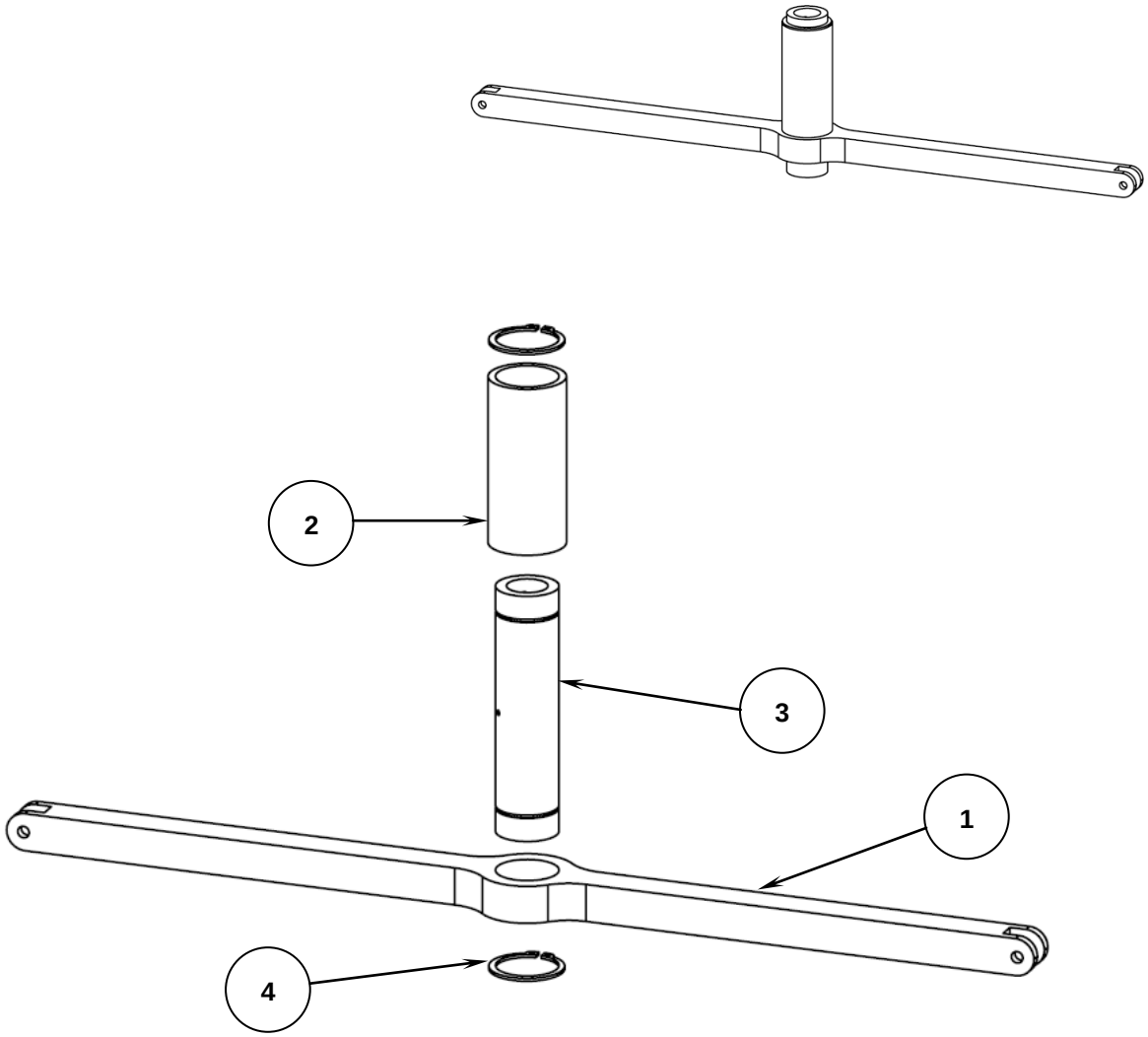

Figure G18 – Gimbal frame linkage

Table G5 – Bill of materials for gimbal frame linkage relating to Figure G18

	Part No.	Description	Part/Assembly	Material	No. Required
	SP2-05-002	Overhead linear slide	Assembly	N/A	1
1	SP2-05-003	Overhead connecting arm	Part	7075 Aluminium	1
2	SP2-05-004	Linear bearing spacer	Part	5083 Aluminium	1
3	SP2-05-005	Ø16 x 86mm Linear bearing	Part	N/A	1
4	-	Ø26mm circlip	Part	N/A	2

G3.7 Central pivot

The following section presents an exploded view of the central pivot and the associated bill of materials.

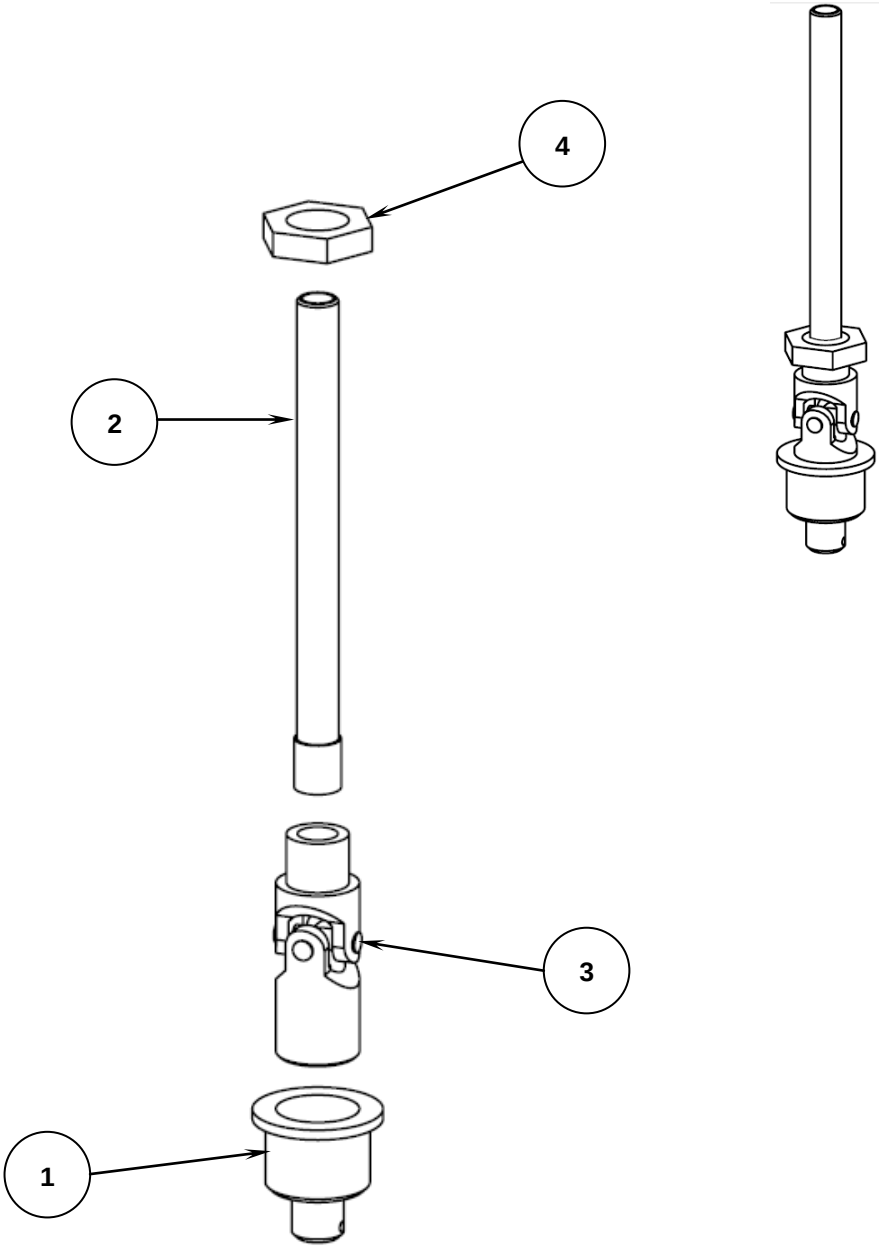

Figure G19 – Central pivot

Table G6 – Bill of materials for central pivot relating to Figure G19

	Part No.	Description	Part/Assembly	Material	No. Required
1	SP2-06-002	Universal joint coupling	Part	4140 Steel	1
2	SP2-06-003	Main shaft	Part	4140 Steel	1
3	SP2-06-004	Ø32mm Universal Joint	Part	Mild Steel	1
4	-	M24 half nut	-	N/A	1

G3.8 Conclusion of sub-systems assembly

This section has presented the assembly diagrams and bill of materials relating to the assembly of the sub-systems that comprise Prototype B.

Before assembling the sub-systems together to form the overall system it is recommended that all fasteners and connections are shown to be rigid and tight (where applicable).

G4 Operational Procedure for Prototype B

The following section outlines the testing procedures that will result in Prototype B exhibiting stabilizing oscillatory behaviour. It should be noted that the values stated in this section relating to the settings on various power supplies are obtained from extensive testing of the system. It is recommended the user varies and adjusts these values to gain a better understanding of the performance of the system. This may also be required to obtain the desired response from Prototype B.

G4.1 Power supplies and associated components

Prototype B uses four power supplies. Each power supply has a set of associated components. The purpose of this section is to familiarise the user with each of the power arrangements. Table G7 outlines each of the power supplies and the components they relate to.

Table G7 – Power supplies and associated components

Power Supply	Number	Function	Associated components
22.2V Li-Po battery	4	Supply power to flywheels	- Electronic speed controllers - MP160 brushless DC motors - 4-to-1 channel wire - Receiver - Transmitter
4.8V Ni-MH battery	1	Supply power to ESC	- Receiver
DC Variable Power Supply	1	Supply power to the relay switches to alternate the direction of precession of the disc	- Relay switch - Square wave generator - Relay circuit
DC Variable Power Supply	1	Supply power to the 24V drive motor to precess the disc	- Relay circuit

The above power supplies are identified in Figures G20 – G22 shown on the next page.

Figure G20 – 22.2V Li-Po battery

Figure G21 – 4.8V Ni-Mh battery

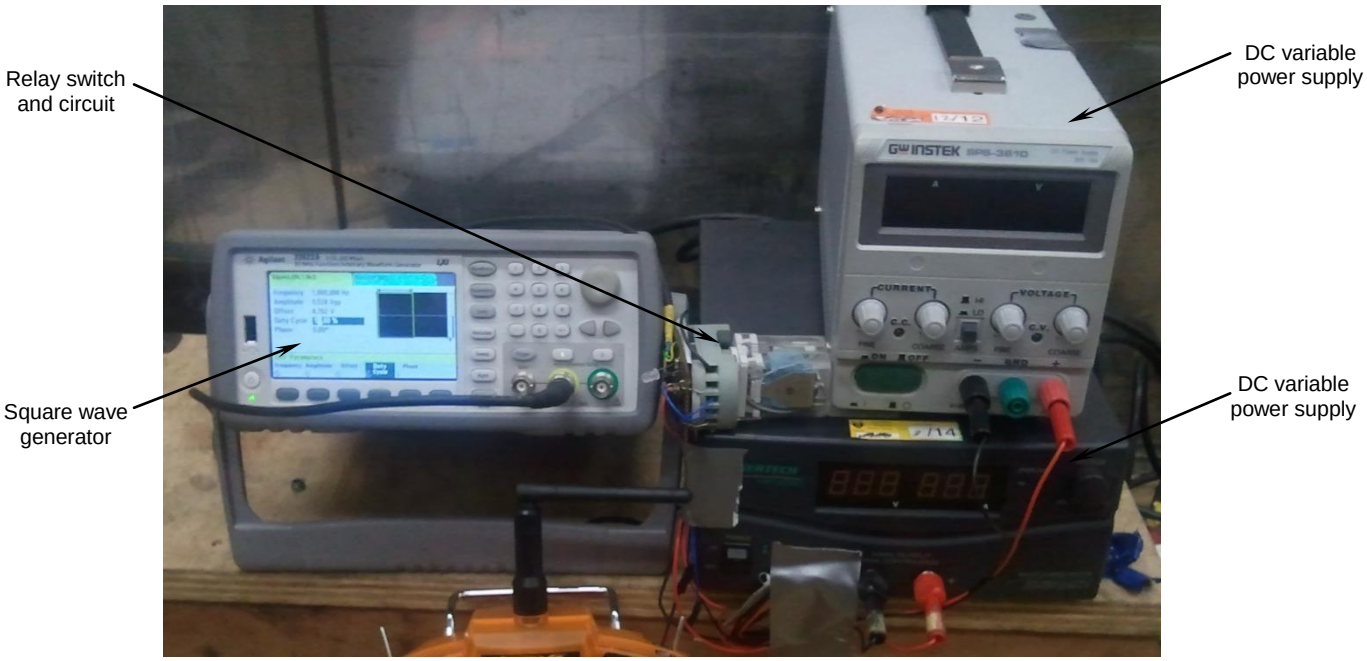

Figure G22 – Main power supply arrangement

G4.2 Flywheel motor power arrangement

The procedure for connecting the flywheel motor power system together is simple due to the use of hobby electrical components. All associated wire plugs and connections are specific to each component (that is that the brushless DC motor can only connect to the correct end of the electronic speed controller) making assembling the power arrangement quick and easy.

The functions of each of the components that comprise the flywheel motor power arrangement are shown below. Note that the number in brackets indicates the number of components that are used in Prototype B.

- Electronic speed controller (ESC) *(4)* – converts the signal from the receiver and draws power from the batteries to produce a signal to drive the brushless DC motor.
- Li-Po battery *(4)* – supplies power to the brushless DC motor.
- Brushless DC motor *(4)* – drives the gyroscope flywheels.
- 4-to-1 channel wire *(1)* – takes all four of the ESC's that comprise the total system and channels them into one wire that plugs into the receiver. This is included to ensure all four gyroscopes receive the same signal and are therefore rotating at equal speeds.
- Receiver *(1)* – receives the signal from the transmitter and supplies this signal to the ESC.
- Transmitter *(1)* – controller held by operator. Movement of drive switch controls flywheel motor speed.

- Ni-Mh battery *(1)* – due to the high spec ESC a separate power supply is required.

The power cables for the brushless DC motor should be pointing down and to the left (if assembled as per the instructions in section G3.2). These cables connect to the ESC which in turn connects to the Li-Po batteries. Some sparking may occur when connecting the ESC to the Li-Po batteries. Ensure fingers are not holding any of the wires (only the plug) when performing this step. The ESC also has a small set of wires coming off it that connect to the 4-to-1 channel wire which plugs into ***Channel 3*** of the receiver. The 4.8V Ni-Mh battery is then connected to the ***BATT*** channel of the receiver.

A schematic showing how the components are connected is shown in Figure G23.

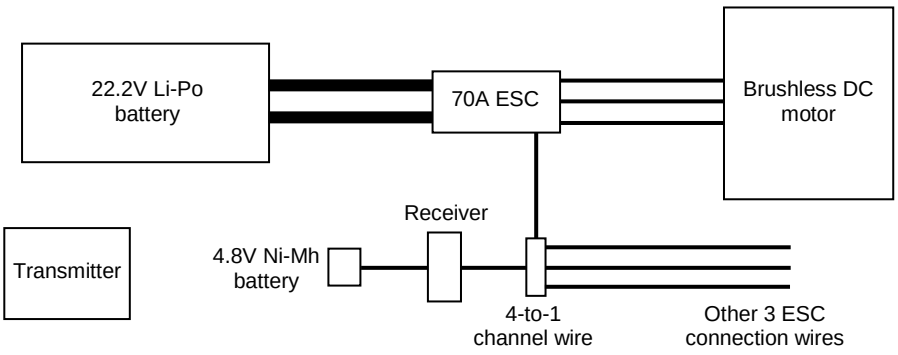

Figure G23 – Flywheel motor power arrangement

G4.3 Disc precession motor power arrangement

The disc precession motor power arrangement is used to oscillate the disc back and forth at a designated frequency. This is achieved by varying the input parameters of a square wave generator and a variable power supply.

The functions of each of the components that comprise the disc precession motor power arrangement are shown below. Note that the number in brackets indicates the number of components that are used in Prototype B.

- Relay switch and circuit *(1)* – the central connection hub for all components that comprise the disc precession motor power arrangement. The main function of the relay switch and circuit is to take the signal from the square wave generator and (coupled with the power from the two variable power supplies) transmit an oscillating signal to the 24V DC motor.
- Variable power supply 1 *(1)* – the function of power supply 1 is to provide power to the relay switch to allow it to alternate the voltage. This power supply is set to 14V (the relay switch needs 12V to operate).
- Variable power supply 2 *(1)* – the power supply that drives the 24V DC motor. The voltage of this power supply is varied to obtain the desired response from the system in conjunction with the square wave generator parameters.
- Square wave generator *(1)* – a unit that produces a specified voltage shape. A particular setting within the square wave generator is selected which has been programmed by an electrical technician (refer to generator manual). The square wave generator consists of 5 parameters that can all be varied to obtain the desired response. These are identified in Table 4.2.
- 24V DC motor *(1)* – motor with in-built worm drive used to precess the disc back and forth.

A schematic showing how the components of the disc precession drive arrangement are connected is shown in Figure G23.

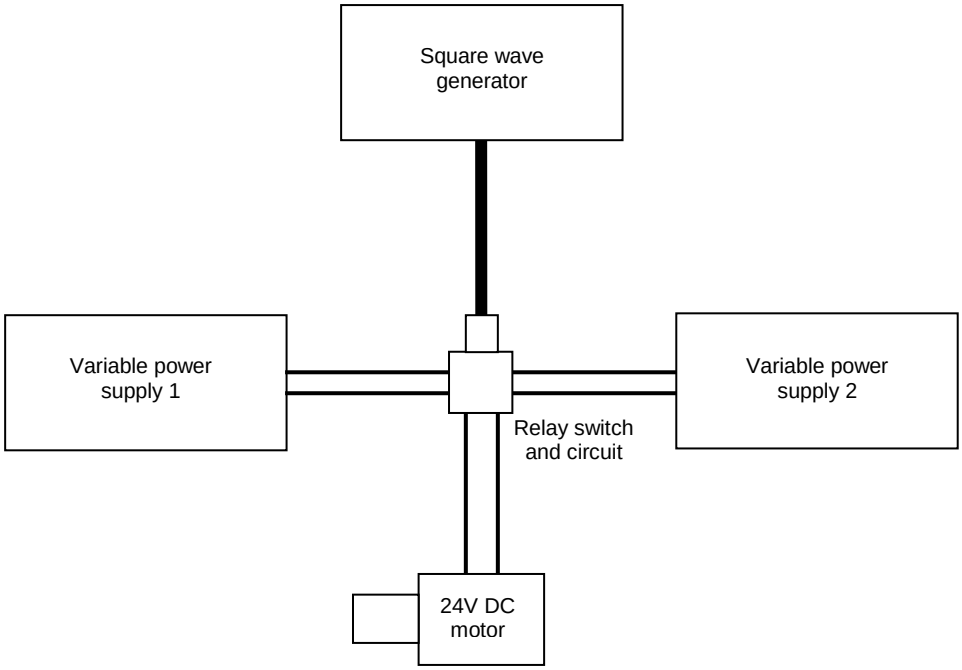

Figure G24 – Disc precession motor power arrangement

The relay switch and circuit should be secured in place on a non conductive surface. The positive and negative connections of each of the power supplies are connected to their associated connections on the circuit board. The positive and negative output cables of the circuit board can then be attached to the 24V motor.

The square wave generator output cable is a single wire that attaches to a special connection on the circuit board. It is recommended that the parameters of the square wave generator are set to the values in Table G8.

Table G8 – Square wave generator parameters

Parameter	Value
Frequency	1.00Hz
Amplitude	0.500Vpp
Offset	4.252V
Duty Cycle	50.00%
Phase	0.00°

Testing of the system revealed that the optimal voltage of the 24V DC power supply was approximately 16.5V.

G4.4 Operation of Prototype B

Once all power supply arrangements have been connected as per this manual the system may be switched on so that the stabilization process may begin. The safest order to turn on the system is:

i) Connect all flywheel motor power arrangements as per section G4.1.
ii) Turn on transmitter and wait for red LED on receiver to come on and remain solid (confirming it is paired to the transmitter). Brushless DC motor should sound a series of beeps and then a single beep every 2 seconds. ***Do not begin to drive flywheels at this stage!***
iii) Connect the disc precession motor power as per section G4.2.
iv) Turn on the square wave generator and set desired parameters
v) Turn on relay switch variable power supply and increase voltage until switch activates and a switching noise is heard (approximately 13V).

vi) Turn on 24V DC motor variable power supply and slowly increase voltage until desired disc precession occurs.

vii) ***Slowly*** move transmitter joystick to begin to drive flywheels until desired speed is obtained.

viii) Vary system parameters until desired response is achieved.

G4.5 Conclusions of operational procedure

This section has outlined the connection of the power arrangements that drive Prototype B. It has also outlined the steps that must be followed to operate the system.

While the values outlined in this manual were shown to work after extensive testing it is highly recommended that the user vary and alter them to gain a greater understanding in the operation of Prototype B. It is also likely that the user will need to vary the system parameters to obtain the desired oscillatory response from Prototype B.

It is recommended that the current system is not operated continuously for an extended period of time (> 5 minutes). This will help mitigate the issue of overheating components and allow for connections that may have vibrated loose to be inspected.

G5 Safety

Due to the high kinetic energy and large number of spinning components that comprise Prototype B, the user must be constantly aware of the large number of safety issues associated with operating the system. This section will highlight the critical safety issues that must be addressed during the assembly and operation of Prototype B. These are:

Testing area – the current location of Prototype B (testing container) is the optimal testing area for the system. It contains a partition that separates the operator and any other viewers from the machine should any failure occur during operation. A similar partition must always be used when testing the system. No person should ever be exposed to the machine when it is turned on without protection between themselves and Prototype B.

Safety glasses – safety glasses must be worn at all times when working on and operating Prototype B.

Brushless DC Motors – the flywheel motors draw a significant amount of current (up to 70A). It is highly recommended that all wiring and electrical connections on Prototype B are fully understood and the safety issues relating to working with such high currents are understood.

Pinching/jamming of fingers – due to the weight of some of the sub-assemblies that make up Prototype B, care must always be taken when assembling components together. The highest risk of injury occurs when placing the disc/gyroscopes

assembly onto the central pivot (see section G4.2, Step 6). This step must be completed by 2 people to avoid any injury.

External structure stop – the external structure is able to tip back and forth. A safety stop has been manufactured and must be inserted when the system is inactive.

Kill switch – it is recommended that all components that require mains power are connected to a single outlet via a multi-board. This will allow all power to be cut from the system at a single point. There is currently no rapid method of stopping the flywheels and the operator should always be aware of this and operate the machine accordingly.